GEOCHEMISTRY OF ARSENIC IN URANIUM MILL TAILINGS. SASKATCHEWAN, CANADA

A Thesis Submitted to the College of
Graduate Studies and Research
in Partial Fulfillment of the Requirements
for the Degree of Doctor of Philosophy
in the Department of Geological Science
University of Saskatchewan

Saskatoon

By

Robert Donahue

Fall 2000

PERMISSION TO USE

In presenting this thesis in partial fulfillment of the requirements for a Postgraduate degree from the University of Saskatchewan. I agree that the Libraries of this University may make it freely available for inspection. I further agree that permission for copying of this thesis in any manner, in whole or in part, for scholarly purposes may be granted by the professor or professors who supervised my thesis work or, in their absence, by the Head of the Department or the Dean of the College in which my thesis work was done. It is understood that any copying or publication or use of this thesis or parts thereof for financial gain shall not be allowed without my written permission. It is also understood that due recognition shall be given to me and to the University of Saskatchewan in any scholarly use which may be made of any material in my thesis.

Requests for permission to copy or to make other use of material in this thesis in whole or part should be addressed to:

Head of the Department of Geological Science

University of Saskatchewan

Saskatoon, Saskatchewan (S7N 5E2)

ABSTRACT

The Rabbit Lake uranium mine in-pit tailings body consists of alternating layers of ice, frozen tailings and unfrozen tailings. The tailings solids are predominately composed of quartz (16 to 36 wt%), calcium sulphate (0.3 to 54 wt%), illite (3 and 14 wt%) As-Ni sulphide 2 wt% and iron 2 wt%. Arsenic and Ni concentrations in the tailings showed similar patterns with depth, which were strongly related to historical changes in As and Ni concentrations in the mill feed. Mineralogy of the ore bodies indicated that As and Ni in the mill feed occurred primarily as 1:1 molar ratio arsenides such as niccolite and gersdorffite. EMP analysis suggested that solubilized arsenic is precipitated as Ca, Fe, and Ni arsenates during the neutralization process. Dissolved As concentrations in five monitoring wells installed within the tailing body ranged from 9.6 to 71 mg/L. Pore fluids in the wells had a pH between 9.3 and 10.3 and measured Eh between +58 and +213 mV. Sequential extraction analyses of tailings samples showed that As above 34 m depth was primarily associated with amorphous iron and metal hydroxides while the As below 34 m depth was associated with Ca, likely as amorphous calcium arsenate precipitates. The change in the dominant As solid phases at this depth was attributed to the differences in the molar ratio of Fe to As in the mill feed. Below 34 m it was <2 whereas above 34 m it was >4. The high Ca/As ratio during tailings neutralization would likely preferentially precipitate $Ca_4(OH)_2(AsO_4)_2{\cdot}4H_2O$. Geochemical modeling, using PHREEQC, suggested that if the pore fluids were brought to equilibrium with hydrated calcium arsenate, the long-term dissolved As concentrations would range between 13 and 81 mg/L. The predicted pH and speciation of arsenic in the filter sand was dependent on the redox conditions (oxidizing or reducing) assigned to the regional groundwater. Reducing conditions in the regional groundwater cause $HAsO_4^{2-}$ the dominant species in the tailings, to be reduced to $H_2AsO_3^{1-}$ as arsenic diffuses from the tailings into the filter sand. Under sulphate reducing conditions, iron as Fe^{2+} in the filter sand is oxidized to Fe(III) species as the sulphate (S(VI)) present in the tailings diffuses into the filter sand and is reduced to sulphide (S(-II)). The pH in the tailings will decrease as the high concentrations of protons in the filter sand diffuse into the tailings. As the solubility of calcium arsenate minerals present in the tailings are pH dependent, the decrease in pH in the tailings causes an increase in solubility of the calcium arsenate minerals resulting in the dissolution of calcium arsenate minerals.

DEDICATION

This Thesis is dedicated to Wanda

She provided me with the opportunity to pursue my goal as a scholar

She watched my back when I was alone

She provide funding when there was none

And most important

She believed in me

Without you this work would never have been completed

Thank you

ACKNOWLEDGEMENTS

Numerous people played a part in the research required for this thesis. Cameco Corporation, NSERC, the Cameco/NSERC chair and Wanda Goulden provided the financial support without which this thesis could not have been completed.

Thank you to Dr. Don Langmuir, Dr. C.A.J. Appelo, and Dr. David L. Parkhust for teaching me geochemistry.

A special thanks to Dr. Malcolm Reeves for the beers, the consulting work and for listening. As well, a special thanks to Dr. Garth van der Kamp for being a part of my thesis committee.

Thanks to the Crew of the S.S. Minnow: The very capable drillers Darryl, Mike and Karl, and the first mates Tyler, Ray, Gideon, and Sheldon.

Thank you to the staff of the Saskatchewan Research Council Analytical Services, particularly Brenda Stanek, for the excellent job they did on the analysis of the solids and fluids samples.

My thanks to the Rabbit Lake Environment Department, Mark, Rob, Cam and Tim for the help on site and Darryl McClarty and Michael Courtin of Envista Technologies for setting up the database.

Thanks to P.M. Huang in Soil Sciences for his help with the sequential extraction analysis and A. Mermout and A. Hossain for their help with the clay mineralogy.

Thanks to my supervisors Dr S. Lee Barbour and Dr. M. Jim Hendry.

I acknowledge the support of the staff and graduate students in Geology and especially Tom Bonli for his help with the electron microprobe work.

A special thanks to Wayne Clifton, P.Eng. for all his support and encouragement over the years.

A finally a big pet for my dog gromit for the hours of one sided discussions on reactive transport analysis.

TABLE OF CONTENTS

LIST OF TABLES

LIST OF FIGURES

CHAPTER 1.0 INTRODUCTION

1.1 URANIUM MILL TAILINGS MANAGEMENT

Thirty-three percent of the world production of uranium is mined in the Athabasca Basin in northern Saskatchewan, Canada (Natural Resources Canada, 1998) (Figure 1.1). As of 1996, uranium mining in Saskatchewan has resulted in the production of 31M tonnes of tailings (Scissons, 1997). Management practices for uranium tailings disposal have evolved since the first mill began operation near Beaverlodge in 1953 (Figure 1.1). Initially, tailings were disposed as a slurry into a topographic low or natural lake. As awareness of the potential environmental and health issues posed by uranium mill tailings increased, a second generation of engineered above ground tailings management facilities (TMFs) was developed. Above ground TMFs were designed to provide containment of mill tailings above the water table, built by constructing earth dams at the end of a valley (i.e., Rabbit Lake: Figure 1.1) or by the constructions of earth berms and liners (i.e., Cluff Lake and Key Lake; Figure1.1). As of 1996, 12.3M tonnes of tailings were contained in above ground TMFs at the Rabbit Lake, Cluff Lake, and Key Lake mines (Scissons, 1997)

Operational problems for above ground tailings storage facilities, such as freezing, grain size segregation and the need for larger storage facilities lead to the development of a third generation of disposal facilities: the engineered in-pit tailings management facilities. In-pit TMFs are designed such that tailings are permanently placed below the water table in an engineered facility constructed within mined-out open pits. The Rabbit Lake in-pit TMF (commissioned in 1984) was the first planned in-pit disposal of uranium tailings in Canada (Gulf, 1981). The technical basis of the design was that, upon decommissioning of the in-pit TMF, the hydraulic gradient between the tailings and the regional groundwater would be small enough that the migration of contaminants from the tailings to the regional groundwater

would be controlled by diffusion, not advection. A diffusion dominated system would minimize the flux of contaminants into the groundwater system (Gulf, 1981).

There are presently three in-pit tailings facilities in Saskatchewan: The Rabbit Lake TMF (pervious surround design), The Key Lake Deilmann TMF (side drain and subaqueous discharge design), and the McClean Lake Jeb pit TMF (natural surround and subaqueous discharge design) (Figure 1.1). The three in–pit facilities are designed differently, but all utilize a contrast in permeability between the consolidated tailings and adjacent materials to provide a diffusion dominated solute transport system. The Rabbit Lake TMF utilizes a pervious surround, which consists of a 1 m thick rock drain protected by a 5 m thick sand filter, constructed around the inside perimeter of the mined out open pit. The pervious surround is constructed in 3 to 5 m lifts as the pit is filled with tailings. The Key Lake Deilmann TMF utilizes a side drain constructed using a sand filter and rock drain along the side of the pit prior to tailings deposition. The McClean Lake Jeb pit natural surround design exploits the high permeability of the natural host sand sandstone in the design. Misfeldt et al. (1999) provides a description and analysis of the hydraulics of in-pit pervious surround and natural surround designs.

The design of in-pit facilities in Saskatchewan has focused on the geotechnical and hydrogeological aspects of the TMFs. The fate and transport of solutes from the in-pit facilities to the regional groundwater regimes has been studied using single species 2-dimensional and 3-dimensional, finite difference/finite element, advection-dispersion models (Cameco, 1994; Cogema, 1997; Geocon, 1984; Gulf, 1981). The source terms are either assumed to have fixed concentrations for the design life of the facility (10,000 years) or a finite mass. Adsorption and radioactive decay are the only two attenuation mechanisms considered in predictive contaminant transport modeling. Geochemical analysis of the tailings has been limited to the evaluation of source terms for target constituents (As, Ni, U, and Ra^{226}) and the empirical measurement of attenuation mechanisms, such as adsorption, using batch tests. No comprehensive geochemical studies have been performed on Saskatchewan uranium tailings to determine insitu geochemical conditions within the tailings mass or in the regional groundwater surrounding the tailings facilities or the potential for chemical interaction between the regional groundwater and the tailings.

The prediction of the long-term impact of the tailings on the surrounding environment, requires an understanding of the geochemical controls on contaminants present in the TMFs. There are, however, no detailed investigations of the geochemistry of subaqueously deposited uranium tailings in the Athabasca Basin on which to estimate the long-term source concentrations of contaminants to the environment. Existing geochemical studies were conducted on fresh or prototype tailings (Cogema, 1997; Cogema, 1998; Melis et al., 1987) and probabilistic modeling to estimate As and Ni loading to the environment (Snodgrass et al., 1986).

Geochemical studies from uranium tailings in other regions of the world are of limited use in understanding the geochemical controls on these contaminants because the ores mined and the milling technology used in the Athabasca Basin are unique. The ore typically contains very high grades of uranium (1 – 20 wt%), nickel (2 wt%), and arsenic (2 wt%). To reduce dissolved metal concentrations, tailings are neutralized with lime and deposited in an alkaline environment (pH≈10), which is 2 to 3 pH units higher then the regional groundwater (pH 7-8) surrounding the tailings facilities.

1.2 OBJECTIVES

The basis for this research program was the investigation of the active in-pit tailings management facility (TMF) at the Cameco Rabbit Lake mine. Of the three existing in-pit TMFs in northern Saskatchewan, the Rabbit Lake in-pit TMF was chosen for study because it has the longest history of use (1984-present), allowing investigation of the potential for changes in the chemistry of the tailings solids and fluids with time. Arsenic was chosen as the species of interest for this study because of its environmental and regulatory significance in assessing the performance of the tailings facility.

The research program was designed with the following objectives;

1. Characterize the source(s) of As in the Rabbit Lake in-pit tailings facility;
2. Measure insitu geochemical conditions in the Rabbit Lake in-pit tailings facility;
3. Determine primary and secondary As mineralization in the uranium tailings;
4. Determine the geochemical controls on dissolved As in the Rabbit Lake in-pit tailings;
5. Measure geochemical conditions in the regional groundwater surrounding the tailings facility; and

6. Investigate the potential for geochemical interaction between the tailings and the regional groundwater under diffusive mixing conditions.

1.3 METHODOLOGY

The research program included a review of tailings geochemistry for existing and proposed uranium mines in northern Saskatchewan, the design and implementation of a subsurface investigation in an active in-pit TMF, design of specialized pore-water sampling methods and insitu geochemistry monitoring, mineralogical analysis of tailings solids using x-ray diffraction and scanning electron microscopy, and the development of experimental procedures for several laboratory tailings studies.

This thesis is in the form of three papers submitted to peer reviewed scientific journals. (Chapters 2-4). All field work, laboratory studies, data analysis, and manuscript preparation were performed by the author. Manuscripts were edited by Jim Hendry, Patrick Landine, and Lee Barbour. Chapter 2: Distribution of Arsenic and Nickel in Uranium Mill Tailings, Rabbit Lake, Saskatchewan, Canada presents the results of the tailings solids analysis from the field investigation, identifies the primary and secondary arsenic minerals and presents the distribution of arsenic and nickel within the Rabbit Lake in-pit TMF. Chapter 3: Geochemistry of Arsenic in Uranium Mine Mill Tailings, Saskatchewan, Canada presents the insitu geochemical measurements, As pore fluid concentration measurements, sequential extraction analysis of the tailings solids and a quantitative assessment of the distribution of As minerals in the tailings. Chapter 4: Diffusive-Reactive Transport Analysis of Arsenic from an in-pit Uranium Tailings Management Facility, Saskatchewan Canada, presents the results of reactive transport modeling of the diffusive mixing of the Rabbit Lake tailings and regional groundwater. A summary of results and recommendations for future research are presented in Chapter 5.

1.4 REFERENCES

Cameco. (1994) Environmental Impact Statement Deilmann In-pit Tailings Management Facility. Cameco Corporation. Environmental Impact Statement. Report C101104. November 1993. Saskatoon.

Canada N. R. (1998) Canadian Uranium Statistics Fact Sheet. Natural Resources Canada, Uranium and Radioactive Waste Division. Energy Resources Branch. Ottawa.

Cogema. (1997) MaClean Lake Project - JEB Tailings Management Facility. Cogema Resources Inc. EIS. File 812B. December 4 1997. Saskatoon.

Cogema. (1998) Construction Licensing Application - Responses to Regulatory Agency Comments June 1998. Cogema Resources Inc. File No. 801A. June 1998. Saskatoon.

Geocon. (1984) Progress Report no. 1. Design of Pervious Envelope Disposal of Tailings in Rabbit Lake Pit. Geocon Inc. T10782-1. July 1984.

Gulf. (1981) Environmental Impact Statement Collins Bay B-zone Development. Second Addendum. Gulf Minerals Canada Limited. June 1981. Saskatoon.

Melis L. A., Steger H. F., Knapp R. A., Scharer J. M., and Smith C. W. (1987) Study of the State of Nickel and Arsenic in Uranium Mill Tailings. *International Symposium on Crystallizalization and Precipitation*, Saskatoon. 221-229.

Scissons K. (1997) Saskatchewan Uranium Mine Tailings - Quantity to end of 1996. Saskatchewan Environment and Resource Management. Memo. File -37 - 20 - 0 - 0.

Snodgrass W. J., McKee P. M., and R.V. N. (1986) Demonstration of the Probabilistic System Model for the Assessment of the long Term Effects of Arsenic and Nickel from Uranium Mill Tailings Deposits in Canada. National Uranium Tailings Program. Contract No. 05Q85-00207, August 1986. Ottawa.

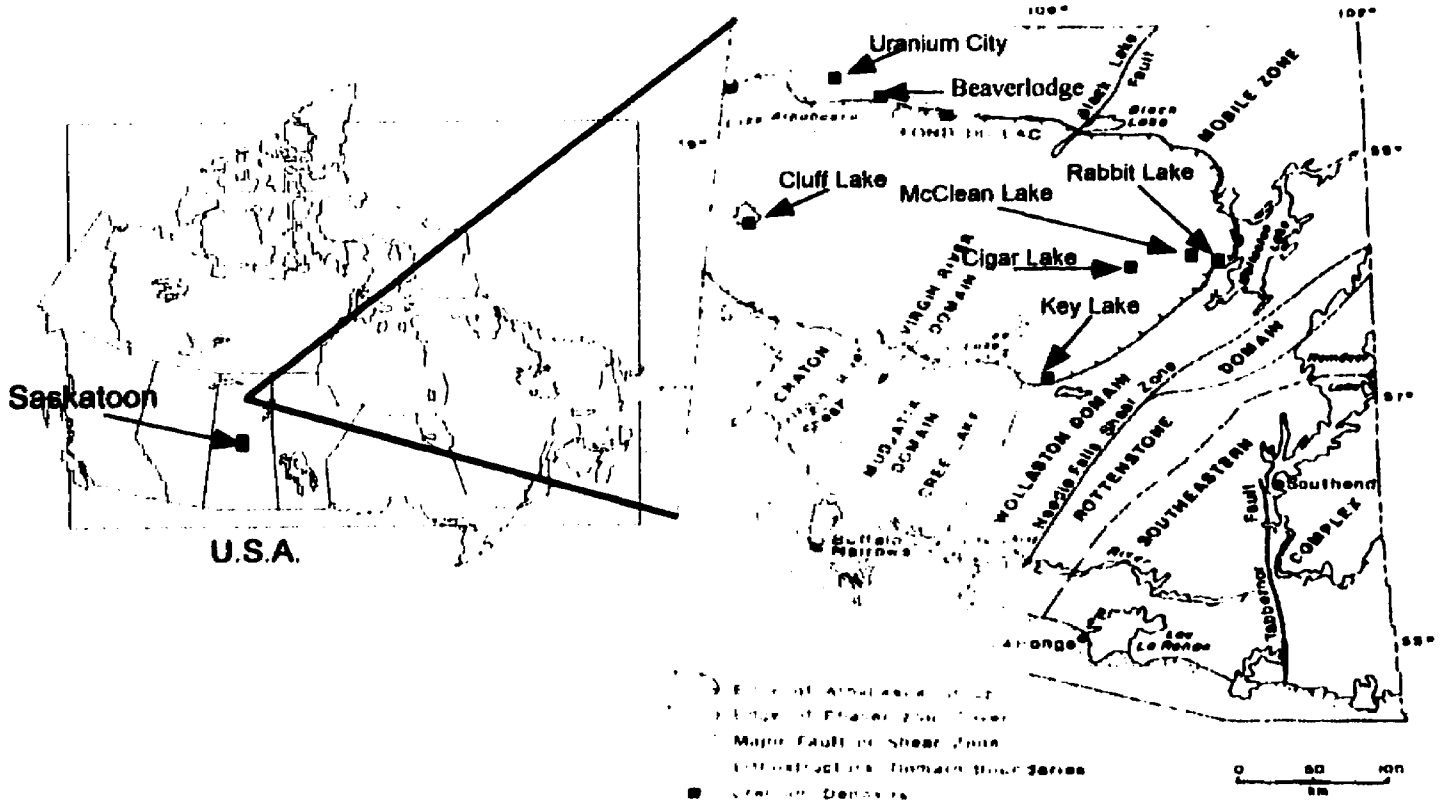

Figure 1.1 Map of Canada and geological map of northern Saskatchewan showing locations of uranium mines and tailings facilities.

CHAPTER 2.0 DISTRIBUTION OF ARSENIC AND NICKEL IN URANIUM MILL TAILINGS, RABBIT LAKE, SASKATCHEWAN, CANADA

ABSTRACT

The Rabbit Lake uranium mine in-pit tailings management facility (TMF) is located in northern Saskatchewan, Canada. In 1997, the tailings body was approximately 425 m long x 300 m wide and 91 m thick at its centre. An investigation of the TMF was performed to collect tailings samples from depth to quantify the distribution of As and Ni in the tailings with respect to ore type and assess the distribution of As and Ni with respect to tailings mineralogy. The tailings body consists of alternating layers of ice, frozen tailings and unfrozen tailings which varied in texture from a slurry to a firm silty sand. The tailings solids are predominately composed of quartz (16 to 36 wt%), hydrated calcium sulphate (0.3 to 54 wt%), and illite (3 and 14 wt%). Arsenic and Ni concentrations in the tailings show similar patterns with depth which was found to be strongly related to historical changes in As and Ni concentrations in the mill feed. Mineralogy of the ore bodies indicated that As and Ni in the mill feed occurred primarily as 1:1 molar ratio arsenides such as niccolite (NiAs) and gersdorffite (NiAsS). Arsenic and Ni concentrations in the tailings solids were also measured at a near 1:1 molar ratio. Mill process records showed that an average of 71 wt% of the arsenic in the mill feed was solubilized during leaching. EMP analysis suggested that solubilized arsenic is precipitated as Ca^{2+}, Fe^{+3} and Ni^{2+} arsenates during the neutralization process. Mill records indicated that 17,000 tonnes of As were discharged to the TMF of which approximately 88 wt% was as arsenates and 12 wt% as primary arsenides.

2.1 INTRODUCTION

Thirty-three percent of the world production of uranium is presently mined in the Athabasca Basin in northern Saskatchewan, Canada (Natural Resources Canada, 1998) (Figure 2.1). As of 1996, this mining has resulted in the production of 31M tonnes of uranium

tailings (Scissons, 1997). Management practices for disposal of uranium tailings have changed since the first mill began operation near Beaverlodge in 1953 (Figure 2.1). Initially, tailings were disposed of as a slurry into a topographic low or natural lake. A second generation of tailings management, engineered above ground tailings management facilities (TMFs), began at the Rabbit Lake mine in 1975 (Figure 2.1). Above ground TMFs were designed to provide containment of mill tailings above the water table. As of 1996, 12.3M tonnes of tailings were contained in above ground TMFs located at the Rabbit Lake, Cluff Lake, and Key Lake mines (Scissons, 1997) (Figure 2.1).

The third generation of disposal facilities, engineered in-pit TMFs, was initiated at the Rabbit Lake mine in October, 1984. In-pit TMFs place the tailings below the water table in an engineered facility constructed within mined-out open pits. The Rabbit Lake in-pit TMF marked the first planned in-pit disposal of uranium tailings in Canada (Gulf, 1981). The rationale for such placement was that upon decommissioning of the in-pit TMF the hydraulic gradient between the tailings and the regional groundwater would be small enough that the migration of contaminants from the tailings to the regional groundwater would be controlled by diffusion, not advection. The diffusion mechanism would minimize the flux of contaminants into the groundwater system (Gulf, 1981).

Until recently, the design of mine mill tailings management facilities in Saskatchewan has focused on the geotechnical, hydrogeological and simplified geochemical aspects of the TMFs. To understand the long-term impact of the tailings on the surrounding environment, more detailed information on the geochemical controls of contaminants present in the TMFs is required. Understanding the mineralogical controls on these contaminants is necessary to define the long-term evolution of the tailings mass and to derive a source term for evaluation of long-term environmental impacts (that would lead to refinement of mill processing to "design" a tailings mineralogy for a diminished source term)."

There are, however, no in-depth investigations of the geochemistry of subaqueously deposited uranium tailings in the Athabasca Basin on which to estimate the long-term source concentrations of contaminants to the environment. Existing geochemical studies were conducted on fresh or prototype tailings (Cameco, 1994; Cogema, 1997; Cogema, 1998; Langmuir et al., 1999; Melis et al., 1987) and probabilistic modelling to estimate As and Ni loading to the environment (Snodgrass et al., 1986).

Geochemical studies from uranium tailings in other regions of the world are of limited use in understanding the geochemical controls on these contaminants because the ore mined and the milling technology used in the Athabasca Basin is unique. The ore frequently contains relatively high grades of Ni (2 wt%) and As (2 wt%) and can be acid generating. Tailings are deposited in a very alkaline environment (pH≈10) to precipitate metals dissolved during processing. To further complicate the geochemistry, the ambient temperature in the tailings is near 0°C.

The goal of the current research is to characterize the source(s) of contaminants in uranium TMFs. This includes determining primary and secondary mineralization, determining the geochemical controls on dissolved As and Ni in TMFs and determining the rates of As and Ni transport with time. Accordingly, the objectives of the current study were to: (1) quantify the distribution and sources of As and Ni in the TMF with respect to the ore type; and (2) assess the distribution of As and Ni with respect to the mineralogy of the tailings.

Subsequent studies will provide more detailed information on the distribution of As and Ni in the tailings pore water and will evaluate the geochemical controls on the dissolved phase.

Current efforts focused on tailings in an in-pit TMF because this is the preferred disposal technology at mines in Northern Saskatchewan (e.g. Rabbit Lake in-pit TMF, Key Lake in-pit TMF and McClean Lake JEB pit TMF). Of the two existing in-pit TMFs, the Rabbit Lake in-pit TMF was chosen for study because it has the longest history of use (1984-present) of the two in-pit facilities. This allowed us to investigate the effects of the changes in dissolved and solid metal concentrations with time

The objectives of the current study were met by collecting and analysing solids samples from eight vertical bore holes drilled into the tailings. Analyses were conducted on selected samples. These analyses included grain-size distribution, moisture content, metals, nutrients, radionuclides, scanning electron microscopy, and powder X-ray diffraction.

2.2 BACKGROUND

2.2.1 Climatic Conditions

The Rabbit Lake mine is located along Collins Bay on the western shore of Wollaston Lake in northern Saskatchewan approximately 800 km northeast of Saskatoon, Canada (Figure 2.1 and 2.2). Climatic conditions at the mine are described in Cameco (1992). The area is classified as continental subarctic with a mean daily temperature of –4.0°C. The mean daily temperature for the summer months is below 20°C with only three months having mean daily temperatures over 10°C. Winters are cold and dry with a mean daily temperature below –20°C. Average annual precipitation is 546 mm, of which 65% is rain.

2.2.2 Uranium Ore Bodies Milled

Five separate ore bodies have been processed at the Rabbit Lake mill (Figure 2.2). These include Rabbit Lake ore (1975-1987), A-zone (1997-present), B-zone (1985-present), D-zone (1996-present) and Eagle point (1993–present). The five ore bodies are unconformity type uranium deposits that occur along regional faults (Heine, 1986; Jones, 1979; Ruzicka, 1986).

The Rabbit Lake ore body was situated along the Rabbit Lake Fault, a reverse fault, which strikes northeast through the pit and dips southeast 30° to 60° (Heine, 1986) (Figure 2.2). The A-, B-, and D-zone deposits are located along the Collins Bay Fault (Figure 2.2).. The Collins Bay Fault consists of one or two graphitic gouge zones up to one meter thick. The Eagle Point deposit is located along the Eagle Point Fault. This fault is a separate structure that parallels the Collins Bay Fault and lies approximately 45 m above the Collins Bay Fault. Graphitic gouge is present in the Eagle Point Fault but is not as common as in the Collins Bay Fault (Cameco, 1992).

Mineralization in the A-zone ore deposit consisted of high grade ore surrounded by a low grade clay envelope. Nickel mineralization in the A-zone deposit occurred below the zone of massive uranium mineralization. The B-zone deposit occurred mainly in clay altered sandstone of the Athabasca Group and to a lesser extent in the altered graphitic paragneiss of the Wollaston Group. D-zone uranium mineralization occurred totally within clay rich Athabasca sandstone

Uranium mineralization in the Rabbit Lake mine ore bodies was mainly pitchblende and coffinite. Gangue minerals were predominantly quartz, illite, kaolinite, chlorite and calcite (Eldorado, 1986). Nickel/arsenic minerals rammelsbergite ($NiAs_2$), pararammelsbergite, niccolite (NiAs), gersdorffite (NiAsS), and bravoite ($(Ni,Fe)S_2$) were present in the A-zone, B-zone and D-zone. Nickel/arsenic minerals are not found in the Eagle point ore deposit. Niccolite is the dominant arsenide mineral associated with the D-zone deposit while gersdorffite predominates in the A-zone deposit (van Huyssteen, 1986). Ore mineralization also included trace amounts of lead, gold, silver titanium, vanadium, zirconium, chromium, silver, barium and strontium (Ruzicka, 1986). Table 2.1 presents a summary of the Fe, As and Ni minerals in the Rabbit Lake pit, A-zone, B-zone, D-zone and Eagle point ores.

2.2.3 Milling Processes

The uranium milling process must be considered to develop an understanding of the temporal distribution of the geochemistry of the tailings solids in the Rabbit Lake in-pit TMF. The milling process at the Rabbit Lake Mine includes grinding, leaching, counter current decantation (CCD), solvent extraction, impurity precipitation, uranium precipitation, drying and packaging, effluent treatment, and neutralization. Initially, ore was ground and mixed with water to yield an admixture of 55% solids with 45% of the solids passing the 75 μm sieve (Bharadwaj et al., 1995). Next, the ground ore (leach feed) was leached with 93% sulfuric acid (pH<1) and oxidized with sodium chlorate (+450mV). Residence time in the leaching circuit was approximately 10 hours (Bharadwaj et al., 1995). Leaching dissolved minerals in the ore solubilizes uranium into a pregnant aqueous solution. The barren liquid from the solvent extraction circuit (raffinate) and solids from the CCD (leach residue) were combined in the neutralization circuit and slaked lime was added. The tailings were neutralized to pH 10 in three stages (pH 4, 8 and 10) over a three-hour period prior. The combined solids from the neutralization processes were brought to a density of 35 to 45% solids and spigot discharged to the TMF at one of two discharge points (Figure 2.3). Excess water from raffinate neutralization and mine water are sent to the effluent treat circuit prior to discharge to the effluent ponds. Isodecanol, kerosene, magnesia, and drainage from waste rock are periodically discharged to the in-pit TMF.

2.2.4 Tailings Management

The Rabbit Lake in-pit TMF was constructed in the mined out Rabbit Lake pit. The TMF design utilizes a pervious surround system which consists of an outer coarse grained rock and an inner sand filter pack installed between the pit wall and the tailings.(Eldorado. 1986)

Tailings are deposited subareally into the TMF surface from alternating discharge points at the north and south ends of the pit (Figure 2.3). Alternating discharge points are used to improve the distribution of tailings and to minimize grain-size segregation and depth of water ponded against the filter sand.

Groundwater conditions around the in-pit TMF are controlled through the dewatering of the filter sand by pumping from a raise well connected to the pit bottom drain via a horizontal dewatering drift. Groundwater levels are drawn down approximately 110 m below original level and the resulting drawdown cone extends 500 m to 800 m from the pit.

Currently, the Rabbit Lake in-pit TMF contains more than 3.6M tonnes of tailings solids. At the time of investigation (1997), the tailings surface was approximately 425 m long x 300 m wide and the tailings body was approximately 91 m thick at its centre. At present, the Rabbit Lake operation is scheduled to mill ore until 2002. At completion of operation, the in-pit TMF will be covered with a sand, rock, and water cover. Raise pumping will continue until the tailings are consolidated; at that time pumping will cease and natural groundwater levels will be re-established.

2.3 MATERIALS AND METHODS

Eight bore holes were drilled in the TMF between 11 August and 24 November 1997 (Figure 2.3) using a Sonic track mounted drill rig (Figure 2.3). The drill rig was placed on a pontoon barge and positioned on the TMF using a system of cables and anchors. Bore holes were continuously cored to depths of between 43 m and 70 m (Table 2.3). Core samples were collected using a 3.1 m long x 50 mm I.D. diameter core barrel. Once the core barrel was brought to surface, the sample was vibrated into plastic sleeves to facilitate geologic logging and sampling for moisture content and solids analysis. At depths where samples could not be collected using the core barrel, resampling was conducted using a 0.6 m long x 50 mm I.D. diameter piston sampler. To prevent sampling of disturbed media, the drill rig was moved

horizontally about 3 m prior to piston sampling. Piston samples were ejected onto a plastic tray for logging and sampling. All core samples were logged for colour, consistency, texture, layering, presence of ice crystals, and colour and size of any inclusions.

Tailings samples approximately 20 cm in length were collected for geochemical analysis and moisture content measurement in sealed 500 or 1000 mL plastic containers. Samples were stored in the dark at 4°C until submitted for analysis. Samples were typically stored 1 to 6 weeks prior to analysis.

Moisture contents were determined on 515 samples in the Rabbit Lake laboratory (Table 2.3). The entire content of the 1000 mL sample containers was dried at 105°C for approximately 48 hours. The mass of water in the samples was assumed to be the difference in mass due to drying. The moisture content was calculated as the weight of water divided by the mass of dry sample.

Grain size analyses were conducted on 72 samples (Table 2.3). These analyses were conducted in the Rabbit Lake laboratory. Between 100 and 200 g of well mixed, dried samples were weighed and washed through a 45 μm sieve. The retained solids were transferred to pans and dried for 6 hours at between 100 and 110°C. The dried samples were weighed, transferred to the top sieve of a sieve stack (420, 300, 212, 150, 75, and 45 μm sieves), and the samples shaken on a Fritsch™ (Analysette 3E) sieve shaker for 15 minutes. The material retained on each sieve was weighed. Three separate samples were analyzed for elemental distribution within grain-size fractions. Samples 474, 482 and 563 were submitted the Saskatchewan Research Council (SRC) geochemistry laboratory for grain size separation. The three samples were separated into four grain sizes (>125 μm, <120 μm, >45 μm, and <45 μm) and each size fraction was submitted for whole rock analysis. Tailings grain size samples were wet sieved using between 2,500 mL to 3,000 mL of distilled water. All solids retained on sieves were dried, weighed and submitted for ICP-AES, scanning electron microporbe, and powder XRD analysis. Sieve wash water was also filtered (0.45 μm) and submitted for ICP-AES analysis.

Solid samples from each bore hole underwent whole rock analysis (Table 2.3) at the Saskatchewan Research Council Analytical Laboratory (SRC), an accredited laboratory specializing in the analysis of environmental samples for the uranium mining industry in Saskatchewan. A summary of parameters analyzed and elemental detection limits is

presented in Table 2.4. Prior to analyses, all samples were oven dried at 105°C and ground to a fine powder (100 % passing a 48 μm sieve) using a Rocklab™ ring grinder.

For the analysis of B, P, Al, As, Ba, Be, Ca, Cd, Co, Cr, Cu, Fe, K, Mg, Mn, Ni, Pb, Sr, Ti, V, Zn, and Zr, 0.5 g of ground sample was digested in 5 mL concentrated nitric acid, 15 mL concentrated hydrochloric acid and 3 mL perchloric acid. Aliquots (≈5 mL) of the dissolved phases were analyzed for metals and sulphate on a Thermo Jarrell™ Inductively coupled Plasma Model ICAP-61E. Bismuth and antimony were analyzed by hydride generation atomic absorption. Total carbon and sulphur analyses were performed using a Horiba Model EMIA 520 Carbon/Sulphur analyzer. Inorganic carbon was analyzed by measuring the CO_2 evolved by the addition of acid to a sample. Chloride was analyzed using the mercuric thiocyanate colorimetric method and a Cobas Farall centrifugal analyzer. The silica content of the samples was determined by fusing the samples with sodium peroxide and sodium hydroxide.

Mineralogical analyses of three samples from bore hole 97-R3 were done using a JEOL JXA-8600 electron microprobe microanalyzer (EMP) and a Rigaku R200 X-ray diffractometer (XRD) in the Department Geological Sciences at the University of Saskatchewan. Samples RD482 (37.6 m), RD474 (29.6 m), and RD563 (46.7 m) were selected to represent the range in As concentrations measured on the solids samples. The samples were dried and lightly ground using a mortar and pestle to pass the 2 mm sieve. After grinding, three grab subsamples of between 81 and 104 g were separated into 3 grain sizes (+125 μm, -125 μm/+45 μm, and –45 μm) for EMP and XRD analysis. The samples of whole tailings and grain-size separated tailings were analyzed using EMP and XRD.

EMP samples were prepared in an epoxy resin diluted with ethanol to improve the penetration of epoxy around the fine-grained particles. The epoxy was allowed to set then the samples were dried, polished, and carbon coated. EMP samples were analyzed using electron backscatter imaging, energy dispersive spectrometry, and wavelength dispersive spectrometry. Energy dispersive spectrometry analysis provided a qualitative analysis of the elemental compositions of an area approximately 1.5 μm^2 to a depth of 0.5 μm. Wavelength dispersive spectrometry analysis provided As and Ni X-ray map images. The X-ray map images highlighted areas and particles where the characteristic X-rays of As or Ni were detected.

The XRD samples were ground to 4-5 μm. using an agate mortar and pestle and smear mounted using ethanol on petrographic slides. Samples were analysed from 3 to 75 degrees two-theta using monochromatic Cu K_α radiation operated at 40 kV and 80 mA. Interpretation was done by comparing XRD patterns of the samples to those of known minerals (JCPDS XRD patterns).

The clay mineralogy of 15 samples collected from bore hole 97-R3 was determined in the department of Soil Science. University of Saskatchewan (Table 2.5). Clay minerals were separated from tailings using dispersion techniques (Jackson. 1979). Carbonates were removed using 1 M sodium acetate buffered at pH 5 (in a solid solution ratio 1/100) and Fe-oxyhydroxides were removed using 0.3 M Na-citrate and 1 M $NaHCO_3$ solutions at 75-80°C (Sheldrick. 1984). Clay fractions were separated from the treated samples by centrifugation (Jackson. 1979).

Clay fractions were treated to prepare oriented slides of Mg-saturated. Mg-saturated and glycerol-solvated. K-saturated and K-saturated and heated at 550°C. Oriented slides were prepared by suspending 0.2 g of each treatment in 1 mL of deionized water. distributing on a regular petrographic slide and allowed to dry at room temperature. Slides were analyzed on a Rigaku D/MAX-RBX-XRD using monochromatic Fe K_α radiation operated at 40 kV and 140 mV. For identification of clay minerals. XRD patterns were superimposed and components of clay minerals were identified and estimated according to Eslinger and Pevear. (1988).

2.4 RESULTS AND DISCUSSION

2.4.1 STRATIGRAPHY OF THE TMF

The stratigraphy of the TMF consists of alternating frozen and non-frozen layers. Non-frozen tailings layers ranged in thickness from 0.1 to 20 m and were categorized as slurry, soft, or firm. Slurry tailings behaved as a liquid and typically had moisture contents (gravimetric) between 50 and 285 wt%. The soft tailings had a toothpaste-like consistency with moisture contents typically between 40 and 133 wt%. Firm tailings had the appearance and consistency of consolidated silty sand with moisture contents typically between 22 and 57 wt%.

Frozen layers ranged in thickness from 0.01 to 5 m and consisted of varying mixtures of tailings solids and ice. The presence of ice in some samples resulted in very high moisture contents (typically >500 wt%). The ice layers varied from massive ice to well defined ice crystals (5 to 30 mm dia.). Tailings and ice layers ranged in colour from light brown to dark red. Yellow inclusions of amines and white inclusions of magnesia (1 to 30 mm dia.) were observed in core samples. The distribution of tailings and ice in 97-R2 and 97-R3 is presented in Figure 2.4.

Frozen layers in the tailings were the result of deposition during the winter months. The distribution of frozen layers correlated with measured historical tailings surface elevations for all bore holes except 97-R5 and 97-R7. As a result, the elevation of the frozen layers, when used in conjunction with historic tailings surface elevation data, provided a well-constrained estimate of the timing of tailings deposition in the pit (Figure 2.4). From these data we were able to determine that 97-R2 and 97-R3 penetrated tailings deposited prior to June 1987. The gap in chronology at 34 m corresponded to a mill shut down from July 1989 to June 1991.

No ice layers were encountered between 15 and 37 m below tailings surface in 97-R5 and 97-R7. The absence of ice layering at these depths and in these bore holes was attributed to the injection of warm tailings (20–27°C) in this area at a depth of approximately 27 m in 1995 (Cameco, 1995). Warm tailings were injected to investigate methods of thawing the frozen tailings.

Results of grain size analysis on tailings samples from 97-R2 and 97-R3 indicated that all samples contained a mixture of very fine to medium grained sand (12-58 wt%) and silt+clay (42-88 wt%) size particles (Figure 2.5a,b). The percent passing the 45 μm sieve with depth for 97-R2 and 97-R3 is presented in Figure 2.6 and ranged from 38 to 80 wt%. Although no trends in grain size were evident with depth in 97-R2 nor between bore holes, the percent passing the 45 μm sieve in samples from 97-R3 generally increased with decreasing depth. The percent passing increased from 38 wt% at 63 m to 82 wt% at about 14 m.

The grain size distribution in the tailings can be attributed to specific ore characteristics such as natural clay content, grinding during milling and subsequent sedimentation in the TMF. Grinding resulted in >45 wt% of the tailings solids being <75 μm

(Bharadwaj et al., 1995). Tailings are discharged from the mill to the surface of the in-pit TMF, therefore the larger and heavy particles will tend to settle near the discharge pipe while the smaller particles are transported further from the discharge point before settling out. This method of deposition should produce grain size distributions that reflect the distance from the discharge points. The decreasing percentage of fines with increasing depth observed in 97-R3, which is located in the centre of the TMF, may be the result of this sedimentation process. As the discharge point is moved further from 97-R3 (i.e., as the pit fills with tailings), the coarser fractions of tailings will settle out further from the pit center (Bore hole 97-R3), resulting in an increased percentage of fine particles in the vicinity of the pit center.

2.4.2 ELEMENTAL ANALYSIS

A summary of the whole rock analyses is presented in Table 2.4 and a detailed list of results for 15 samples from bore hole 97-R3 is presented in Table 2.6. The most abundant analytes (typically >0.5% by weight) in order of abundance, were SiO_2, SO_4, Ca, Al, Fe, K, Mg, As, and Ni. The ^{226}Ra concentrations in the tailings ranged from <0.01 to 320 Bq/g. These abundances were similar to those reported for uranium tailings from Key Lake (Steffen et al., 1993).

With the exception of As, Ni, Fe, and ^{226}Ra, no well defined trends with depth were observed in the most abundant analytes. Concentrations of As versus depth for 97-R2 and 97-R3 are presented in Figure 2.7a. The As concentrations in 97-R3 increased from between 560 and 5,700 µg/g at the bottom of the bore hole (64 to 66 m) to 13,800 µg/g at 47 m. Between 47 and 37 m, the concentrations fluctuated from 5,200 to 13,000 µg/g. The maximum concentration (17,300 µg/g) was measured at 37.4 m. The As concentrations generally decreased from the peak concentration at 37 m to 32 µg/g at 11.2 m. From 11.2 to 3.8 m (the shallowest sample) the As concentrations increased to 13,000 µg/g. The distribution of As with depth in 97-R2 (Figure 2.7a) exhibited a similar trend with depth to that for 97-R3. The As concentration profile also showed that the As concentrations increased from 7,000 µg/g at 65 m to 13,000 µg/g at 71 m.

The Ni concentrations with depth in 97-R2 and 97-R3 are presented in Figure 2.7b. They displayed the same pattern as described above for arsenic. A Pearson correlation was used to quantify the apparent relationship between the As and Ni analyses, as well as

determine if a linear relationship exists between any of the elements presented in Table 2.4. In this analysis, only Ni and Sb exhibited a strong linear correlation to As at the 99.5% confidence limit. The correlation coefficients for As vs. Ni and for As vs. Sb were 0.995 and 0.898, respectively. A plot of the As vs. Ni data is presented in Figure 2.8. The near 1:1 molar ratio between Ni and As suggested that the abundance of As and Ni in the tailings is dominated by minerals in the ore feed which have a near 1:1 molar ratio of As and Ni. These minerals include niccolite (NiAs) and gersdorffite (NiAsS) (Table 2.1). The linear relationship between As and Sb was attributed to substitution of Sb for As in ore minerals.

The As and Ni concentrations in the tailings vary with depth and to a lesser extent, location in the TMF. Vertical variations were attributed to differences in the solids chemistry of the ore being processed as there have been no changes in the mill process since the in-pit TMF was commissioned.

The ores processed in the mill are presented in Figure 2.4. From 1985 (when the pit was commissioned) to the end of 1993, B-zone ore was the primary mill feed. In 1995 and 1996, Eagle Point ore was the dominant ore processed and in 1997 a blend of four ores were used in the mill. The monthly As and Ni concentrations in mill feed (Figure 2.9) reflect the ore processed. For example, the As and Ni concentrations in B-zone ore typically ranged from 0.25 to 1 wt%. In contrast, the concentrations of As and Ni in Eagle Point ore used in the mill feed in 1994 were below detection (<0.05%) reflecting the lack of As and Ni minerals in this ore (Cameco, 1992; Ruzicka, 1986).

The As and Ni concentrations with depth in the TMF (Figure 2.7) correlated to the ore processed in the mill (Figures 2.4 and 2.8). The elevated concentrations measured below 23 m in 97-R2 and 97-R3 correspond to tailings produced from milling B-zone ore whereas the lower arsenic and nickel concentrations in the tailings above 20 m depth correspond to the milling of Eagle Point ore. The increased concentrations at <4 m were attributed to elevated As and Ni concentrations in the mill feed in 1997 resulting from blending four ores.

The strong relationship between mill feed (e.g., B-zone ore vs. Eagle Point ore) and the distribution of As and Ni was also evident in the Fe and ^{226}Ra data. Figure 2.10 presents the Fe and ^{226}Ra concentrations versus depth at 97-R2 and 97-R3. Iron concentrations increased from about 1 wt% to 2 wt% below 35 m depth to between 3 and 4 wt% from 15 m to 35 m. This increase in concentration corresponds to an increase in Fe in the mill feed from

0.9 wt% in February 1987 to between 2.4 and 3.5 wt% in 1992 and 1993 (Figure 2.9). Above 15 m, the Fe concentrations in the tailings were generally <2 wt%. This agreed with the mill feed data, which indicated that from early 1994 to 1998 the Fe concentrations in the mill feed (Eagle Point ore) were generally below 1.5 wt% (Figure 2.9).

The ^{226}Ra concentrations in 97-R2 and 97 R3 (Figure 2.10b) were generally <100 Bq/g at depths greater than 15 m. Between 2 and 15 m, the concentrations ranged from 113 to 266 Bq/g. Because ^{226}Ra is a decay product of ^{238}U, concentrations of ^{226}Ra in the tailings are directly proportional to uranium content in the ore feed. The uranium concentration of the ore increased from 0.2 wt% in January 1985 to 0.9 wt% in November 1988 (Figure 2.9). The uranium concentrations in the ore fluctuated between 0.4 wt% and 1.0 wt% between November 1988 and January 1994. Since January of 1994, the uranium content of the ore was typically between 1.5 to 2.5 wt%, which corresponded to an increase in production of Eagle Point ore. Between 1993 and 1994, the yearly percentage of high grade uranium ore from the Eagle Point deposit increased from 11 wt% to 47 wt%. Tailings samples collected above 15 m depth, which correspond to tailings discharged after 1993 show a large increase in Ra^{226} concentration (Figure 2.10b).

As described above, segregation of grain size occurs in the TMF as a result of sedimentation of the tailings after discharge. The effect of grain-size segregation on the spatial variability of the As and Ni concentrations in the tailings (Figure 2.7) was investigated by analyzing the distribution of As, Al, Ca, Fe, Mg, Ni, K in three grain-size fractions of three tailings samples collected from 97-R3. Table 2.7 presents a summary of the elemental analyses of the grain-size fractions. With the exception of SiO_2, the results show that the majority of the elements were present in the <45 μm size fraction. Silica, which accounted for 26 to 40 wt% of the mass of the entire samples, was distributed evenly in all three grain-size fractions.

The lack of correlation between As vs. depth (Figure 2.7A) and grain size vs. depth (Figures 2.5 and 2.6) was due to most of the arsenic being present in the less than 45 μm grain size. Arsenic distribution with depth increases and decreases between 30 m and 60 m depth. Over this range the percent passing the 45 μm grain size only varies by 5 wt%. The lack of correlation between grain size and As depth is due to the relatively small change in % passing 45 micron sieve.

2.4.3 MINERALOGY

The prediction of long-term tailings pore fluid concentrations in the TMF is one of the primary objectives of this study. Identification and quantification of mineral phases in tailings solids is therefore essential. Minerals present in the tailings can be described as either primary minerals or secondary minerals. Primary minerals are those minerals in the ore that pass through the mill and neutralization process relatively unchanged. Secondary minerals are those minerals that form by the precipitation of solutes dissolved from the ore and reagents added during processing and neutralization. Insight into the mineralogy of the tailings solids was obtained by reviewing ore body mineralogy and mill process records and analyzing tailings solids using a combination of ICP-AES, EMP and XRD techniques. Descriptions of the dominant primary, secondary and As/Ni containing minerals are presented below.

Analyses indicated that SiO_2 is the most abundant constituent in the tailings with an average content of 28 wt% (Table 2.4). Quartz and clay minerals were determined to be the dominant source of SiO_2. The quartz and clay minerals originated from the sandstone and clay alteration halos associated with the uranium (Heine, 1986; Ruzicka, 1986).

Mineralogical analyses showed that the clay minerals typically constituted between 3 and 14 wt% of the tailings (Table 2.5). An exception was sample RD544 which contained 60 wt% clay. With the exception of one sample (RD590), the most common clay mineral was illite, comprising between 60 and 95 wt% of all clay minerals (Table 2.5; Figure 2.11a, c, d and e). In these samples, kaolinite and chlorite were less common than illite, both constituting <20 wt% of clay minerals (Table 2.5). The anomalous sample (RD590) from 62.5 m yielded low illite concentrations (30-40 wt%) and high chlorite concentrations (60-70 wt%). This sample was deposited prior to June 1987 and thus contained a component of Rabbit Lake ore (Figure 2.4) which may account for the high chlorite content. Mill records indicate that the mill feed in 1986 and 1987 contained approximately 15 and 3 wt% Rabbit Lake ore. Rabbit Lake ore contained chlorite (Heine, 1986; Ruzicka, 1986). Chlorite was also visible on the walls of the Rabbit Lake pit during the 1997 field investigation.

Mass balance calculations indicated that quartz is the dominant Si mineral in the tailings, constituting 16 to 36 wt% of the tailings. The calculated mass of quartz in the tailings was based on the range in SiO_2 present in the tailings samples (Table 2.4) and the

range in Si present in the clay minerals. The dominance of quartz in the tailings was supported by the observation that quartz was the most frequently observed mineral in EMP analyses (Figure 2.11 a, c, and e) and the dominant XRD peak in both composite tailings samples and individual grain-size fractions was that of quartz.

The most common analytes after SiO_2, were SO_4^{2-} and Ca^{2+} (Table 2.4). The high concentrations of these analytes was attributed of the addition of sulphuric acid in the leaching process and calcium oxide in the neutralization process. As a result, the dominant secondary minerals produced by these processes were Ca^{2+}-SO_4^{2-} salts (equation 9, Table 2.8). This is supported by elemental analyses, EMP , XRD, and mass balance calculations. Elemental analyses suggested that between 0.3 and 54 wt% of the tailings is in the form of Ca^{2+}-SO_4^{2-} salts. Assuming that all sulphate and an equimolar amount of calcium in Table 2.4 is in the form of $CaSO_4$, it constitutes, on average, 14 wt% of the tailings. Results of elemental analyses on individual grain-size fractions (Table 2.7) also supported the presence of soluble Ca^{2+} salts. In the three samples analyzed, between 7 and 14 wt% of the solids was soluble and these soluble salts were dominated by Ca^{2+}. In addition, EMP analyses commonly showed calcium sulphate in two forms: as individual acicular crystals (Figure 2.11b) and as a very fine grained material (<10μm) (Figure 2.11a,g).

Ca^{2+}-SO_4^{2-} salts were detected in XRD analysis of samples RD474, RD482 and RD563. XRD analysis indicated that both gypsum ($CaSO_4 \cdot 2H_2O$) and bassinite ($CaSO_4 \cdot 0.5H_2O$) are present in the tailings. The formation of bassinite was attributed to drying of the samples prior to XRD analysis.

The lack of other dissolved metals in Table 2.7 suggested that metal sulphates containing Al, K, Fe, Ni and to a lesser extent Mg are very minor constituents of the tailings. The lack of identifiable metal sulphates in EMP and XRD analyses confirmed this statement.

Analyses of grain-size fractions (2. 7) indicated that most of the Fe is in the <45 μm size fraction. EMP analyses of individual grain sizes supported this finding. EMP analyses showed that Fe was typically observed as finely disseminated particles within agglomerates of clay minerals (Figure 2.11a, c, and d). Iron was, however, also observed as small (<1μm) particles in association with Ni and S (Figure 2.11e).

Specific Fe minerals could not be identified using XRD. The dominant Fe mineral in the ore was hematite (Table 2.1). This mineral could not be identified in the tailings using

XRD and EMP techniques. The inability to identify iron minerals with XRD was attributed to the low Fe concentrations in the ore (typically <2 wt%; Figure 2.9) and the resulting low abundance in the small XRD samples. EMP analysis can not measure oxygen or hydrogen. The particles of Fe identified in figure 2.11a.c.d. and e maybe iron oxides or hydroxides.

The near 1:1 molar ratio between As and Ni (Figure 2.8) suggested that As and Ni in the mill feed was dominated by minerals such as gersdorffite (NiAsS) and niccolite (NiAs). which were major minerals in the A-, B-, and D-zone ores (Table 2.1). Trace amounts of these and other As and Ni minerals were present in the other ore bodies.

In the leaching process, arsenates and nickel were produced and released into solution by the dissolution of niccolite (equation 7, Table 2.8) and the oxidation of gersdorffite (equation 8, Table 2.8). Mill records were compiled and reviewed to estimate the amount of As in the tailings that occurs as arsenides and arsenates. Monthly mill feed assay records for As from 1989 to 1997 were compared to monthly As assays of leach residue solids (i.e., the solids residue from the leaching process). This comparison showed that an average of 71 wt% of the arsenic in the ore was leached into the pregnant aqueous solution. Using the monthly average arsenic solubilized, the tailings arsenide minerals would account for approximately 29 wt% of the arsenic present in the tailings solids and constitute less than 1 wt% of the tailings. The potential mass of arsenates deposited in the TMF was calculated from monthly arsenic concentrations in the mill feed, monthly tonnes of ore processed, and the calculated monthly percentage of arsenic solubilized. From 1985 to 1989, where no As leach residue data were available to calculate percentage As solubilized, the average As solubilized from 1989 to 1997 was used. This calculation suggested that of the 2.9M tonnes of ore processed between 1985 and 1997, approximately 17,000 tonnes of arsenic were discharged to the TMF. Of the total arsenic discharged, approximately 15,000 tonnes (88 wt%) was in the arsenate form and 2,000 tonnes (12 wt%) was in the form of primary arsenides.

EMP analysis of the tailings samples supported the presence of arsenide minerals in the tailings. In sample RD482, which had a very high total arsenic concentration (17,300 μg/g), EDS analysis of 50 particles identified 24 discrete mineral particles containing Ni, As and S. These particles, which ranged in size from <10 to 100 μm, were believed to be gersdorffite (Figure 2.11f). Because the As concentrations in the remaining two samples

(RD474 and RD563) were considerably less than in RD482 (6,700 and 5,200 μg/g). gersdorffite was more difficult to observe in these samples. Only one niccolite particle (20 x 30 μm in size) was identified. It was found in close association with a quartz grain in sample RD482 (Figure 2.11a).

Arsenic was also observed in association with Ca and S in very fine agglomerations of extremely fine-grained material less than 10 μm in size. They were often found as a halo around secondary $CaSO_4$ particles (Figure 2.11g and h). The form and association of the As with Ca and $CaSO_4$ particles suggested that this fine-grained agglomeration of material was calcium arsenates formed during the neutralization process (equation 12 : Table 2.8).

Because As and Ni occur predominantly as 1:1 molar ratio minerals, Ni would be solubilized to the same extent as As in the leaching process. During neutralization solubilized nickel (Ni^{2+}) was likely precipitated as nickel hydroxide ($Ni(OH)_2$) and to a lesser extent as nickel arsenate (equation 10 and 13, Table 2.8). Discrete particles of Ni-hydroxides were not specifically identified in the XRD or EMP analyses. Fine-grained masses containing Ni as well as Ca, As, Fe, and S were observed in EMP analysis. These masses could contain nickel and iron hydroxides and arsenates. As was the case for the Fe, the low concentrations of As and Ni in samples RD474 and RD563 and the resulting low abundance in the small XRD and EMP samples precluded the observation and quantification of discrete particles of arsenates and Ni-hydroxides using EMP and XRD methods.

The sieve washing process would tend to mobilize As that was in a water-soluble form or sorbed. Nickel was also dissolved during the sieving process but at lower concentrations. Arsenic was present in the sieve wash water at between 1.9 and 8.6% (Table 2.7) while nickel was present at between 0.02 and 1.6%. Sample RD482, which had the highest total As solids concentration, also had the highest dissolved As concentration and lowest dissolved Ni concentration. Sample RD474, which had the lowest dissolved As concentration, had the highest dissolved Ni concentration. The lack of similarity between dissolved concentrations of As and Ni between samples suggested that arsenic and nickel occurred in different secondary mineral forms.

Limitations in our analytical methods prevented us from commenting on the presence or absence of Fe arsenates and the adsorption or surface complexation of As on the iron oxides. In the neutralization process, reactions between the As(V) and Fe(III) in solution

could produce scorodite (equation 14; Table 2.8). Scorodite was identified in McClean Lake prototype tailings at concentrations up to 6.31 wt% (Cogema, 1998; Langmuir et al., 1999). Iron was detected in some of the suspected calcium arsenate particles but the relatively low Fe concentrations compared to high Ca concentrations suggests that scorodite would be a minor arsenate component in the Rabbit Lake tailings.

The adsorption and surface complexation of As onto iron oxides are well documented (Belzile and Tessier, 1990; Robins, 1985; Tahiija, 1985). Several iron particles and iron-clay agglomerations were X-ray mapped to determine the presence of As. In all cases, As concentrations were below detection limits (200 ppm). This suggested that surface complexation and adsorption of As with iron hydroxides may be a minor sink for arsenic.

In general, the mineralogy of the Rabbit Lake in-pit tailings was similar to uranium mill tailings from Key Lake and the McClean Lake prototype tailings. Quartz and gypsum were the most abundant minerals in the Rabbit Lake tailings and were present in similar proportions in the Key Lake and McClean Lake tailings. Clay minerals were predominantly illite and kaolinite. Primary arsenide minerals in the McClean Lake tailings accounted for between 40 and 60 % of the arsenic in the tailings solids (Cogema, 1997), which is similar to the 40% estimated for Key Lake tailings (Knight Piesold Ltd., 1986) but substantially more than the 29% estimated for Rabbit Lake tailings.

2.5 SUMMARY AND CONCLUSIONS

This ongoing research program is the first hydrogeochemical investigation to characterise the sources of arsenic and nickel in a long-term uranium in-pit tailings management system in northern Saskatchewan, Canada, the Rabbit Lake in-pit TMF. This paper presents the initial findings of this research program. It details the stratigraphy of the tailings, mineralogy of the ore bodies and tailings and the distribution of arsenic and nickel in the TMF.

The stratigraphy of the TMF consists of alternating layers of ice or frozen tailings, and tailings that varies in texture from a slurry to a firm silty sand. The age of tailings with depth in the Rabbit Lake TMF was estimated from historical tailings surface elevations and correlation with seasonal ice layer formation. Bore holes drilled as part of this investigation penetrated to a depth of 71 m corresponding to tailings deposited prior to June 1986.

As a result of the milling process, the bulk of the tailings was present in the <45 μm grain size. The tailings solids are predominately composed of quartz (16 to 36 wt%) and calcium sulphate (0.3 to 54 wt%). Clay minerals are primarily illite (70 to 95 wt%) and comprise between 3 and 14 wt% of the tailings mass.

Arsenic and Ni concentrations show similar patterns with depth. Both concentrations increased from a range of 500 to 8,000 μg/g below 55 m depth to a range of 5,000 and 13,000 μg/g from 35 to 55 m depth. At 10 m depth the concentrations approached zero, then increased to 8,000 to 10,000 μg/g near surface. These patterns are strongly related to historical changes in As and Ni concentrations in the mill feed. Mineralogy of the ore bodies indicated that As and Ni in the mill feed occurred primarily as 1:1 molar ratio arsenides such as niccolite and gersdorffite. This assumption is supported by the observation that As and Ni concentrations in the tailings were measured at a near 1:1 molar ratio.

Monthly mill feed assays for As were compared to monthly As assays of leach residue solids. This comparison showed that an average of 71 wt% of the arsenic in the mill feed was solubilized. EMP analysis suggested that solubilized arsenic is precipitated as Ca, Fe and Ni arsenates during the neutralization process. Calcium arsenate was the most commonly observed arsenate during EMP analyses but Fe, Ni and S were also detected in association with the Ca and As. Mill records indicated that 17,000 tonnes of As were discharged to the TMF of which approximately 15,000 tonnes (88 wt%) was in the arsenate form and 2,000 tonnes (12 wt%) was in the form of primary arsenides.

Nickel solubilized in the leaching process likely precipitated as nickel hydroxide during tailings neutralization, but may have also formed nickel arsenates as indicated by Ni being detected in association with Ca and As in tailings precipitates. Nickel hydroxides were not observed during EMP analyses nor were they detected in XRD analysis. Additional studies are being conducted to characterize the secondary arsenic and nickel minerals in the tailings. Mineral phases will be then used in conjunction with insitu Eh and pH measurements and pore fluid chemistry to develop a geochemical model of the tailings. The model will be used to predict long term As and Ni pore fluid concentrations in the tailings.

Acknowledgements: Cameco Corporation and the Cameco-NSERC Research Chair (MJH) provided funding. Field assistance was provided E. Yeates, R. Kirkland, T. Birkham, S. Gibb and Higgins Drilling. Mill records and metallurgical information provided by J. Jarvi and X. Li. T. Bonli assisted with the EMP analyses and A. Mermout and A. Hossain performed the clay mineralogy.

2.6 REFERENCES

Belzile N. and Tessier A. (1990) Interaction between arsenic and iron oxyhydroxides in lacustrine sediments. *Geochimica et Cosmochimica Acta.* **54**, 103-109.

Bharadwaj B. P., Jarvi J. W., and Lam E. K. (1995) The Rabbit Lake Mill - Twenty Years of Milling. Cameco Corporation. 1995. Saskatoon.

Cameco. (1992) Environmental Impact Statement: Collins Bay A-zone, D-zone and Eagle Point Development. Cameco Corporation Ltd. 1992.

Cameco. (1994) In-Pit Tailings Disposal System Performance Report 1985 to 1993. Cameco Corporation Ltd. May 1994.

Cameco. (1995) Deep injection of slurried tailings into the Rabbit Lake TMF January 1995. Cameco Corporation. March 1995. Saskatoon.

Canada N. R. (1998) Canadian Uranium Statistics Fact Sheet. Natural Resources Canada Uranium and Radioactive Waste Division, Energy Resources Branch. Ottawa.

Cogema. (1997) MaClean Lake Project - JEB Tailings Management Facility. Cogema Resources Inc. EIS. File 812B, December 4 1997. Saskatoon.

Cogema. (1998) Construction Licensing Application - Responses to Regulatory Agency Comments June 1998. Cogema Resources Inc. File No. 801A, June 1998. Saskatoon.

Eldorado. (1986) Project Review Collins Bay A-zone, D-zone, Eagle Pont Development. Eldorado. may 1986.

Eslinger E. and Pevear D. (1988) *Clay minerals for Petroleum Geologists and Engineers.* Society of Economic Paleontologists and Mineralogists.

Gulf. (1981) Environmental Impact Statement Collins Bay B-zone Development, Second Addendum. Gulf Minerals Canada Limited. June 1981. Saskatoon.

Heine T. H. (1986) The Geology of the Rabbit Lake Uranium Deposit. Saskatchewan. In *Uranium Deposits of Canada*, Vol. Special volume 33 (ed. E. L. Evans). pp. 324. Canadian Institute of Mining and Metallurgy.

Jackson M. L. (1979) *Soil chemical analysis-Advanced course.* by Author. 895 p

Jones B. E. (1979) The geology of the Collins Bay Uranium Deposit, Saskatchewan. C.I.M. District 4 Annual Meeting. Paper No. 10, 28 September. Winnipeg.

Knight and Ltd. P. (1986) Monitoring of layered Uranium Tailings - Phase II. The National Uranium Tailings Program. Canadian Center for Mineral and Energy Technology. Energy, Mines and Resources Canada. DSS File # 15SQ.23241-5-1705. March 1986. Ottawa.

Langmuir D., Mahoney J., MacDonald A., and Rowson J. (1999) Predicting the arsenic source term from buried uranium mill tailings. *Tailings and Mine waste 99.* Fort Collins. Colorado. .

Melis L. A., Steger H. F., Knapp R. A., Scharer J. M., and Smith C. W. (1987) Study of the State of Nickel and Arsenic in Uranium Mill Tailings. *International Symposium on Crystallizalization and Precipitation.* Saskatoon. 221-229.

Robins R. G. (1985) The Aqueous Chemistry of Arsenic in Relation to Hydrometallurgical Process. *Impurities Control & Disposal Proceedings of the CIM 15th Annual Hydrometallurgical Meeting*, Vancouver, Canada. 1-1 to 1-26.

Ruzicka V. (1986) Uranium Deposits in the Rabbit Lake-Collins Bay Area, Saskatchewan. In *Uranium Deposits of Canada*, Vol. Special volume 33 (ed. E. L. Evans). pp. 324. Canadian Institute of Mining and Metallurgy.

Scissons K. (1997) Saskatchewan Uranium Mine Tailings - Quantity to end of 1996. Saskatchewan Environment and Resource Management. Memo. File -37 - 20 - 0 - 0.

Sheldrick B. H. (1984) Analytical methods manual. Land Resource Research Institute, Vol. No. 84-30. Research Branch Agriculture Canada.

Snodgrass W. J., McKee P. M., and R.V. N. (1986) Demonstration of the Probabilistic System Model for the Assessment of the long Term Effects of Arsenic and Nickel from Uranium Mill Tailings Deposits in Canada. National Uranium Tailings Program. Contract No. 05Q85-00207, August 1986. Ottawa.

Steffen, Robertson, and Kirston. (1993) Key Lake Tailings Management Facility Water Chemistry. Cameco Corporation. Report C101104, November 1993. Vancouver.

Tahiija D. (1985) Hydrometallurgical Formation of Iron-Arsenic Compounds. *Impurities Control & Disposal Proceedings of the CIM 15th Annual Hydrometallurgical Meeting*, Vancouver, Canada. 4-1 to 4-14.

van Huyssteen E. (1986) Collins Bay D-zone - Ore Characteristics, Leaching and Settling Studies. Eldorado. PR85-25, May 1986. Ottawa.

Table 2.1 Arsenic, Nickel and Iron Minerals in the Rabbit Lake, Collins Bay B-Zone, A-Zone and D-Zone and Eagle Point Deposits (after Eldorado, 1986; Van Huyssteen, 1985, 1986)

	Rabbit Lake	B-Zone	A-Zone and D-Zone	Eagle Point
Major*		niccolite (NiAs) gersdorffite (NiAsS)	niccolite (NiAs) gersdorffite (NiAsS)	
Minor †	niccolite (NiAs) carollite [$Cu(CoNi)_2S_4$] pyrite (FeS_2) chalcopyrite ($CuFeS_2$) bornite ($CuFeS_4$)	rammelsbergite ($NiAs_2$) maucherite ($Ni_{11}As_8$) bravoite ($FeNiS_2$) violarite ($FeNi_2S_4$) polydimite ($CoNi_3S_4$) safflorite ($CoAs_2$) millerite (NiS) tennantite[$(Cu,Fe)_{12}As_4S_{13}$)] pyrite (FeS_2) chalcopyrite ($CuFeS_2$) bornite ($CuFeS_4$) hematite (Fe_2O_3)	rammelsbergite ($NiAs_2$) pararammelsbergite hematite (Fe_2O_3)	bravoite($FeNiS_2$) chalcopyrite ($CuFeS_2$) bornite ($CuFeS_4$) marcasite (FeS_2)

*The Major minerals are those which are estimated to make up more than 5% of the ore mineralogy.
†The Minor minerals each make up less than 5% of the ore, and are generally present in trace amounts.

Table 2.2 Mill process reactions for uranium (after van Huyssteen, 1985).

Oxidation of tetravalent uranium to hexavalent uranium using sodium chlorate

$$6Fe^{2+} NaClO_3 + 6H^{+} \Rightarrow 6Fe3+ NaCl + H_2O \quad [1]$$

$$UO_2^{2+} + 2Fe^{3+} \Rightarrow UO_2^{2+} + 2Fe^{2+} \quad [2]$$

Sulphuric acid dissolution of hexavalent uranium to form uranyl sulphate anions

$$UO_2^{2+} + SO_4^{2-} \Rightarrow UO_2SO_4^{\circ} \quad [3]$$

$$UO_2SO_4^{\circ} + SO_4^{2-} \Rightarrow UO_2(SO_4)_2^{2-} \quad [4]$$

$$UO_2(SO_4)_2^{2-} + SO_4^{2-} \Rightarrow UO_2(SO_4)_3^{4-} \quad [5]$$

Table 2.3 Summary of analysis on core samples.

		Numbers of core samples analysed For:		
Bore hole	Total depth (m)	Moisture Content	Grain size	Whole rock geochemistry
97-R1	55.7	57	12	8
97-R2	70.9	92	6	22
97-R3	66.6	106	13	56
97-R4	40.7	50	9	10
97-R5	47.3	46	6	3
97-R6	50.15	56	7	12
97-R7	52.9	52	9	6
97-R8	43	56	10	8
Total	NA	515	72	125

Figure 2.4 Summary of whole rock analysis of Rabbit Lake tailings samples.

Analyte	Number of Samples	Average µg/g	Maximum µg/g	Minimum µg/g	Standard Deviation µg/g	Detection Limit µg/g
SO4	125	101000	379000	2400	45112	10
Ca	125	51800	161000	3100	20660	1.0
Al	125	34100	79000	6600	12407	2
Fe	125	19200	63200	5700	8915	0.5
K	125	10900	33400	580	4916	40
Mg	125	7800	73800	1400	11286	2.0
As	125	5640	20400	16.0	4401	0.2
Ni	125	4010	15000	22	3275	0.5
Pb	125	749	5100	50	673	1.0
Na	125	707	2400	40	436	40
Cl	125	490	2000	100	318	10
P	125	246	1800	100	184	10
Cu	125	222	770	27.0	134	0.5
V	125	205	550	19.0	80	0.5
Mn	125	164	810	50	93	0.5
B	125	160	440.0	13.0	68	1.0
U	42	152	3630	N.D.	380	0.5
Ti	125	150	520	59.0	87	0.5
Sr	125	138	620	26.0	77	0.5
Mo	125	91	1200	9.80	110	0.5
Zr	110	81	240	N.D.	53	0.5
Ba	125	77	380	12.0	52	0.5
Co	125	49	160	6.5	28	0.5
Zn	125	44	400	8.40	50	0.5
Bi	125	30	76	2.7	15	0.2
SiO2 %	125	28	40.6	7.40	4.9	0.5
Cr	125	25	110	5.8	13	0.5
S (%)	125	3.2	12	0.140	1.4	0.01%
Be	125	1.2	4.2	N.D.	1.2	0.5
Sb	125	0.74	3.00	0.20	0.50	0.2
Cd	125		1.2	0.5	0.1	0.5
Ra-226	92	74	320	N.D.	72.9	0.01 Bq/g
Pb-210	27	18	360	N.D.	46.7	0.01 Bq/g
Po-210	27	14.0	266	N.D.	35.8	0.01 Bq/g
Th-230	27	19.5	286	N.D.	46.3	0.01 Bq/g
C	125	0.2	3.1	N.D.	0.3	0.01%
IC %	125	0.10	2.46	N.D.	0.23	.0005% as C
OC %	125	0.145	0.830	0.010	0.145	0.01%

N.D. below detection limits

Table 2.5 Clay Mineral Composition (particles < 2μm) of Samples from Borehole 97-R3.

Sample Number	Depth (m)	Illite*	Chlorite+	Kaolinite	Others (minor)	Sand wt%	Silt wt%	Clay wt%	Observations
RD508	7.0-7.2	80-90	10-15	0-5	Fl°	51	35	14	Moderately crystalline
RD518	15.1-15.3	80-90	10-15	0-5	Fl	64	27	9	Moderately crystalline
RD531	25.7-25.9	70-80	10-20	5-10	Fl	61	25	14	Well crystalline
RD474	29.5-29.7	85-95	-	0-15	-	60	31	9	Well crystalline
RD544	33.5-33.7	85-95	-	0-15	-	20	20	60	Well crystalline
RD482	37.3-37.5	80-90	10-15	0-5	-	69	20	11	Well crystalline
RD484	40.2-40.7	80-90	0-5	5-10	Fl	62	32	6	Well crystalline
RD546	42.5-42.7	80-90	5-10	5-10	Fl+Qz×	64	32	4	Well crystalline
RD561	45.5-45.7	80-90	5-10	5-10	Fl+Qz	61	32	7	Well crystalline
RD563	46.6-46.8	60-70	10-20	10-20	Fl+Qz	53	33	14	Well crystalline
RD496	50.0-50.2	70-80	10-20	5-10	Fl+Qz	64	30	6	Well crystalline
RD573	54.8-55.3	80-90	0-5	5-10	Fl+Qz	66	30	3	Well crystalline
RD584	59.3-59.5	80-90	5-15	0-5	Fl+Qz	57	37	6	Well crystalline
RD590	62.3-62.5	30-40	60-70	-	Qz	77	19	4	
RD500	65.2-65.3	70-80	10-15	5-10	Qz	55	34	11	Well crystalline

*Illite is dioctahedral (muscovite type).
+Low temperature, likely Fe-rich chlorite, may be interlayered with kaolinite.
°Feldspar
×Quartz

Table 2.6 Summary of whole rock analysis for 15 Rabbit Lake tailings samples from bore hole 97-R3

Analyte	97RD508 (7.1 m) µg/g	97RD474 (29.6 m) µg/g	97RD482 (37.4 m) µg/g	97RD484 (59.4 m) µg/g	97RD486 (50.1 m) µg/g	97RD500 (65.25 m) µg/g	97RD518 (15.2 m) µg/g	97RD531 (25.8 m) µg/g	97RD544 (33.6 m) µg/g	97RD546 (42.6 m) µg/g	97RD561 (45.6 m) µg/g	97RD563 (46.7 m) µg/g	97RD573 (55.1 m) µg/g	97RD584 (59.4 m) µg/g	97RD590 (62.4 m) µg/g	Detection Limit µg/g
SO4	114000	118000	178000	138000	93300	80100	206000	103000	2400	121000	114000	66700	94800	104000	135000	10
Ca	54200	51800	74900	60800	45800	34400	104000	47900	17800	54000	54400	31800	46500	48800	63700	1.0
Al	55200	35300	29300	26800	21500	18800	42700	27700	79000	23000	24900	20800	19200	41700	26900	2
Fe	12700	33500	15200	22700	13000	11400	13200	24800	63200	14100	14100	10300	12600	10000	13300	0 5
K	19300	13000	10800	9500	6800	5600	12400	9900	33400	8000	7100	6500	5600	16400	4300	40
Mg	13600	2800	2600	2600	1600	8400	12600	5400	8100	3600	5500	1400	5300	4200	39600	2.0
As	610	6700	17300	11800	10400	5700	570	7300	1500	13000	9500	5200	9600	4700	2600	0 2
Ni	430	4900	13500	8800	7700	3300	370	5400	1100	9900	6800	3800	6900	3600	1700	0 5
Pb	1400	480	810	390	500	600	2100	500	210	520	550	550	600	280	1000	1.0
Na	1200	880	770	740	720	200	990	1600	1000	460	920	770	640	560	230	40
Cl	1000	590	990	880	760	270	990	560	500	590	500	400	560	200	200	10
P	260	220	160	160	160	180	210	220	470	160	200	150	170	250	460	10
Cu	210	190	770	250	440	280	460	230	46	380	210	93	210	27	240	0 5
V	130	270	210	240	230	170	110	220	550	170	220	210	160	380	140	0.5
Mn	190	170	280	160	90	170	240	120	220	160	110	71	130	130	230	0 5
B	270	190	130	160	100	100	260	120	440	100	110	110	80	210	91	1 0
Ti	310	130	82	130	68	71	330	150	120	86	93	72	120	72	110	0 5
Sr	93	200	150	120	130	71	79	170	620	100	140	140	83	220	52	0.5
Mo	120	72	72	60	70	32	100	100	54	43	63	50	63	44	140	0 5
Ba	86	87	54	73	46	40	27	71	330	54	70	54	42	85	52	0 5
Co	16	72	160	63	32	120	24	63	65	84	47	28	54	18	47	0.5
Zn	16	49	120	55	25	72	15	30	52	76	48	25	30	14	50	0.5
Bi	15	38	19	25	46	26	21	40	15	35	30	20	35	17	15	0 2
SiO2 %	28.4	40.6	26.2	27.4	33.3	39.7	20,9	34.1	21 1	27 4	28 9	37 6	31.9	27 7	29.5	0.5
Cr	22	15	15	12	7.5	8.2	19	5 8	38	11	13	9 1	8 2	21	17	0 5
S (%)	3.06	3.07	4.44	3.75	2.76	2.53	6.13	2.66	0.14	3.43	3.37	2 02	2.95	2 92	4.36	0.01%
Be	0.0034	0.0023	0.0018	0.0017	0.0009	0.0014	0.0036	0 0017	0.0058	0 0015	0 0017	0.001	0 0011	0 002	0.0027	0.5
Sb	0.2	0.7	1.4	1	1	0.7	0.2	0.7	0 2	1 1	0 8	0 6	0.9	0 5	0.4	0.2
Cd	0.5	0.5	0 5	0 5	0.5	0.5	0 5	0 5	1.2	0 5	0 5	0 5	0.5	0.5	0.5	0 5
C	0.23	0.17	0.16	0.15	0.12	0.15	0 39	0 2	0 61	0.12	0 13	0.09	0.23	0 19	0 29	0.01%
IC %	0.039	0.063	0.034	0.041	0.034	0.017	0.24	0 14	0 45	0 036	0 037	0 028	0 044	0 049	0 11	0005% as C
OC %	0.19	0.11	0.13	0.11	0.09	0.13	0.15	0.06	0 16	0.08	0 09	0.06	0.19	0.14	0.18	0.01%

Table 2.7 Distribution of As, Al, Ca, Fe, Mg, Ni, K and Si by Grain Size.

	+120 Sieve (>125 µm)	-120/+325 Sieve (<120 µm >45 µm)	-325 Sieve (<45 µm)	Dissolved*
RD474 (29.4 m)				
% retained on sieve	**21%**	**17%**	**50%**	**11%**
Arsenic**	0.8%	2.5%	95%	1.9%
Aluminum	4.7%	7.3%	88%	0.01%
Calcium	0.2%	0.3%	48%	51%
Iron	5.0%	3.9%	91%	0%
Magnesium	3.9%	0.2%	94%	2.2%
Nickel	0.7%	2.5%	95%	1.6%
Potassium	4.2%	6.8%	88%	0.8%
Silica	37%	24%	39%	0.02%
RD482 (37.4 m)				
% retained on sieve	**23%**	**14%**	**49%**	**14%**
Arsenic	1.0%	6.9%	84%	8.6%
Aluminum	12%	16%	71%	0%
Calcium	0.08%	0.1%	50%	49%
Iron	4.8%	6.6%	89%	0.0%
Magnesium	7.2%	5.8%	84%	2.7%
Nickel	1.3%	7.5%	91%	0.1%
Potassium	7.2%	5.7%	86%	1.4%
Silica	27%	16%	57%	0.01%
RD563 (46.7 m)				
% retained on sieve	**54%**	**10%**	**29%**	**7%**
Arsenic	15%	10%	68%	7.9%
Aluminum	14%	4.6%	81%	0%
Calcium	0.4%	0.2%	45%	54%
Iron	28%	10%	62%	0%
Magnesium	16%	6.5%	76%	1.5%
Nickel	17%	9.2%	74%	0.02%
Potassium	13%	3.9%	82%	1.2%
Silica	76%	7.3%	16%	0.02%

* Dissolved -Mass of element dissolved in sieve wash water

**Percent retained = total mass of element on sieve / total mass on all sieve fractions

Table 2.8 Summary of mineral reaction during leaching and tailings neutralization.

Leach reactions

Dissolution of Hematite

$$Fe_2O_3 + 3H_2SO_4 \Rightarrow 2Fe^{3+} + 3SO_4^{2-} + 3H_2O \quad [6]$$

Dissolution of Niccolite

$$2NiAs + 2H_2SO_4 + 3.5O_2 + H_2O \Rightarrow 2Ni^{2+} + 2SO_4^{2-} + 2H_3AsO_4 \quad [7]$$

Oxidation of Gersdorffite

$$NiAsS + 3.25O_2 + 1.5H_20 \Rightarrow Ni^{2+} + SO_4^{2-} + H_3AsO_4 \quad [8]$$

Precipitation of secondary calcium sulphate

calcium sulphate.

$$Ca(OH)_2 + H_2SO_4 \Rightarrow CaSO_4 \bullet 2H_2O \quad [9]$$

Precipitation of secondary hydroxide minerals

Nickel hydroxide

$$Ni^{2+} + Ca(OH)_2 \Rightarrow Ni(OH)_2 + Ca^{2+} \quad [10]$$

Fe^{3+} Iron hydroxides

$$2Fe^{3+} + 3Ca(OH)_2 \Rightarrow 2Fe(OH)_3 + 3Ca^{2+} \quad [11]$$

Precipitation of secondary arsenate minerals

Calcium arsenate (Pharmacolite)

$$H_3AsO_4 + Ca(OH)_2 \Rightarrow CaHAsO_4 \bullet 2H_2O \quad [12]$$

Nickel Arsenate

$$3NiSO_4 + 2H_3AsO_4 + 3Ca(OH)_2 + 2H_2O \Rightarrow Ni_3(AsO_4)_2 \bullet 8H_2O + 3CaSO_4 \quad [13]$$

Iron Arsenate (Scorodite)

$$2Fe^{3+} + 3Ca(OH)_2 + 2H_3AsO_4 \Rightarrow 2FeAsO_4 \bullet 2H_2O + 3Ca^{2+} + 2H_2O \quad [14]$$

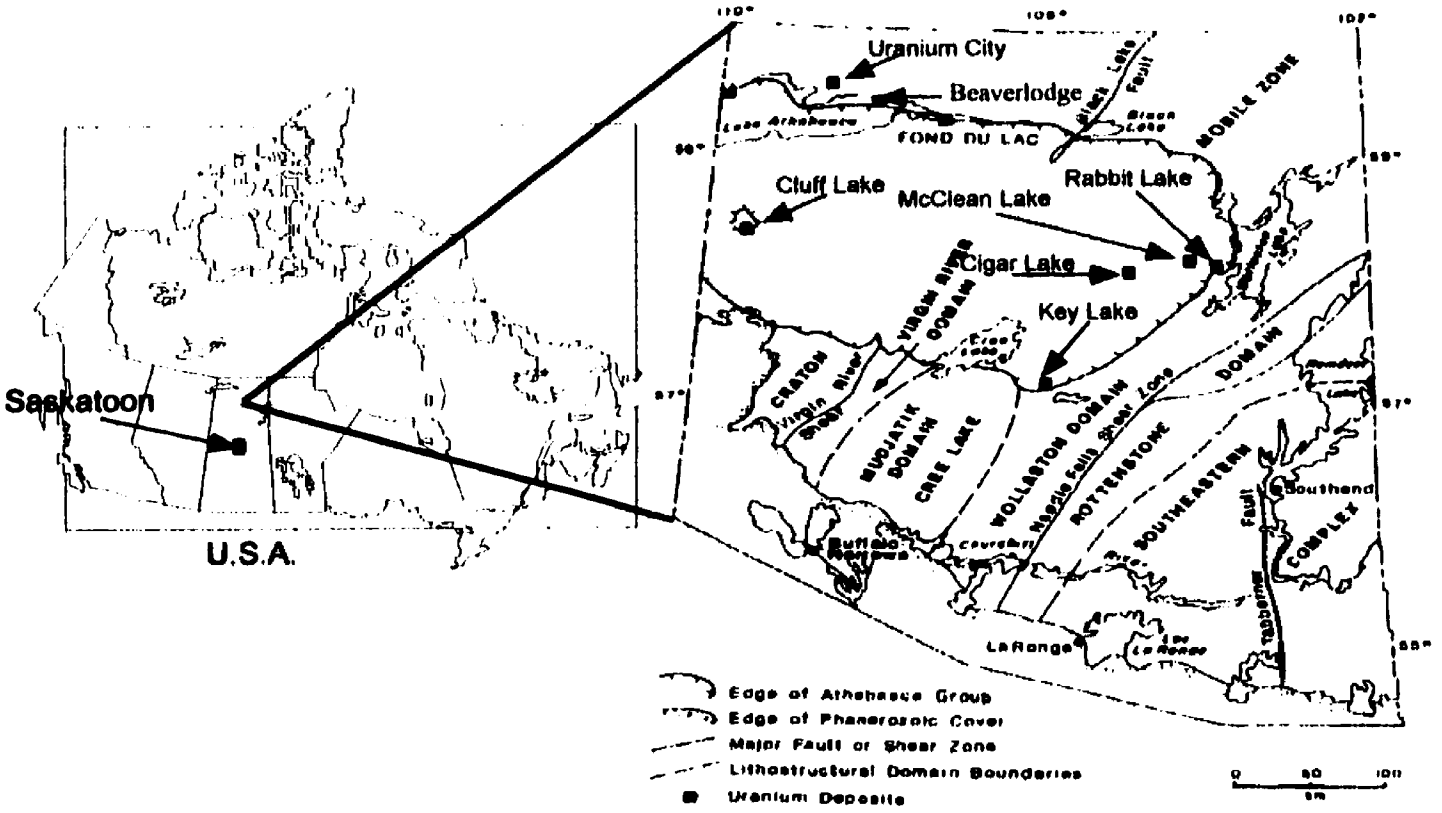

Figure 2.1 Map of Canada and geological map of northern Saskatchewan.

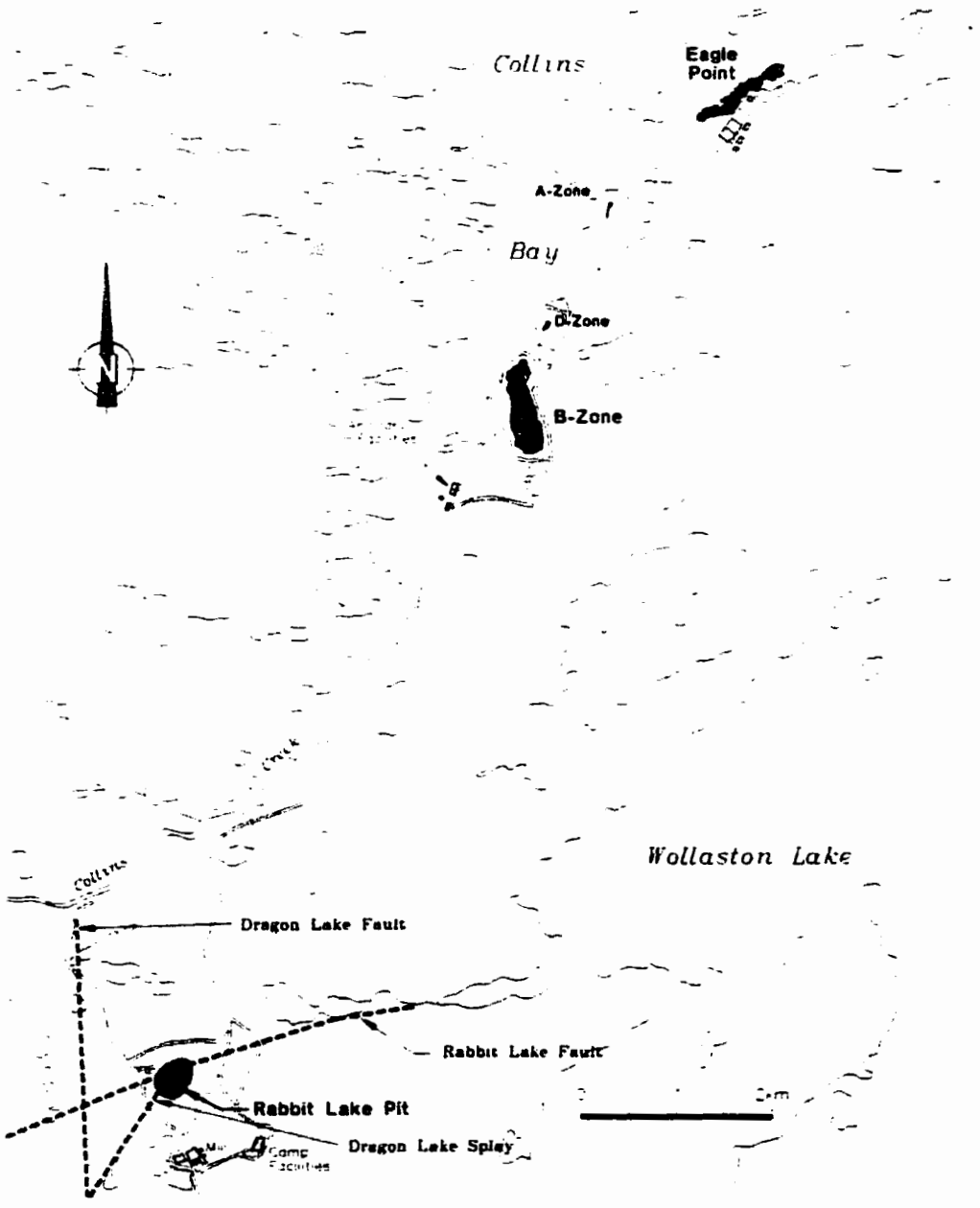

Figure 2.2 Rabbit Lake mine site showing location of Rabbit Lake pit, B-zone, D-zone, A-zone and Eagle point ore deposits.

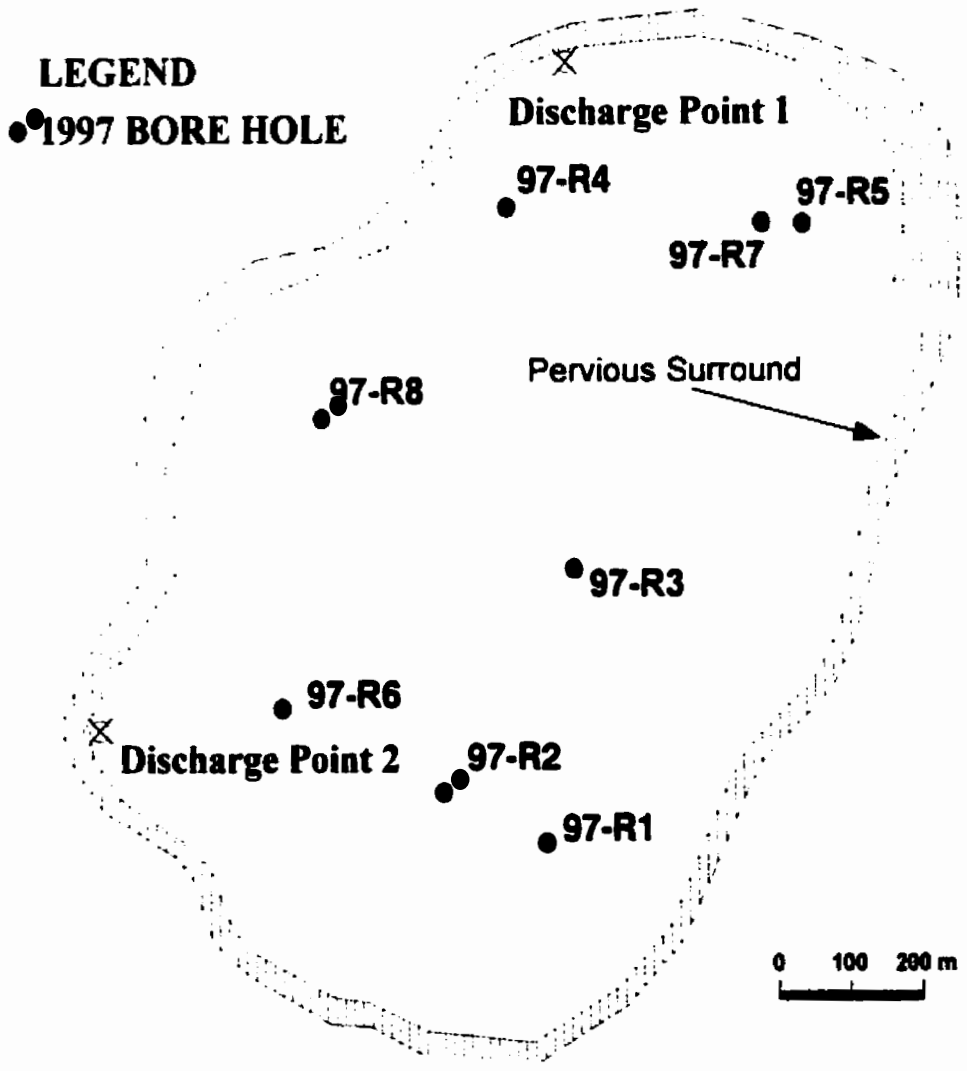

Figure 2.3 Plan view of Rabbit Lake pit showing bore hole locations, tailings discharge points and pervious surround (cross hatched).

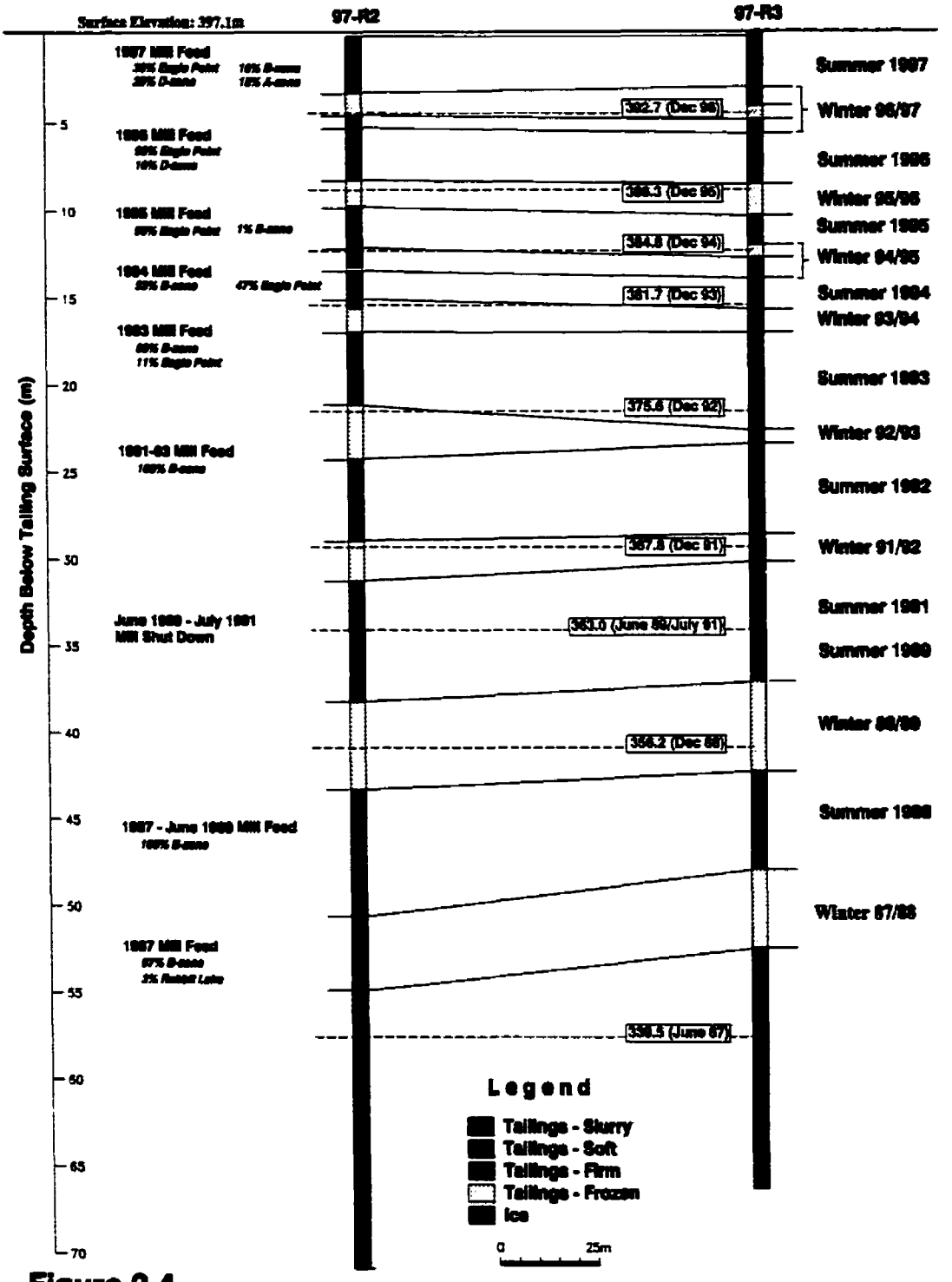

Figure 2.4

Stratigraphy of the tailings management facility between bore holes 97-R2 and 97-R3. The measured elevation of the surface of the tailings and the data measured are presented in the box to the left of bore hole 97-R3. The timing of deposition of tailings based on the distribution of frozen and unfrozen layers is presented to the right of bore hole 97-R3. Ore bodies processed in the mill with time are presented to the left of bore hole 97-R2

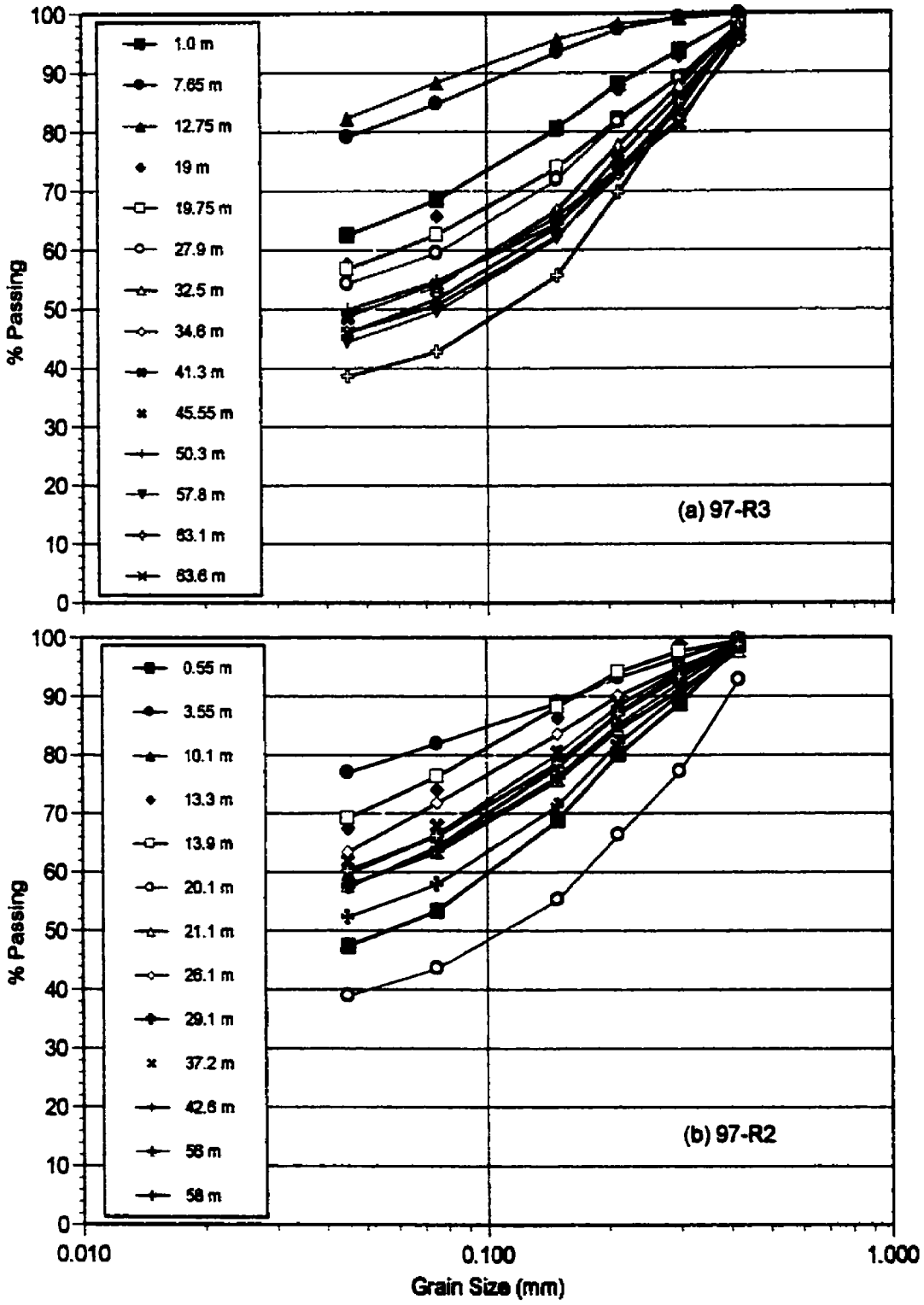

Figure 2.5 Grain size analysis for tailings samples from bore holes (a) 97-R3 and (b) 97-R2.

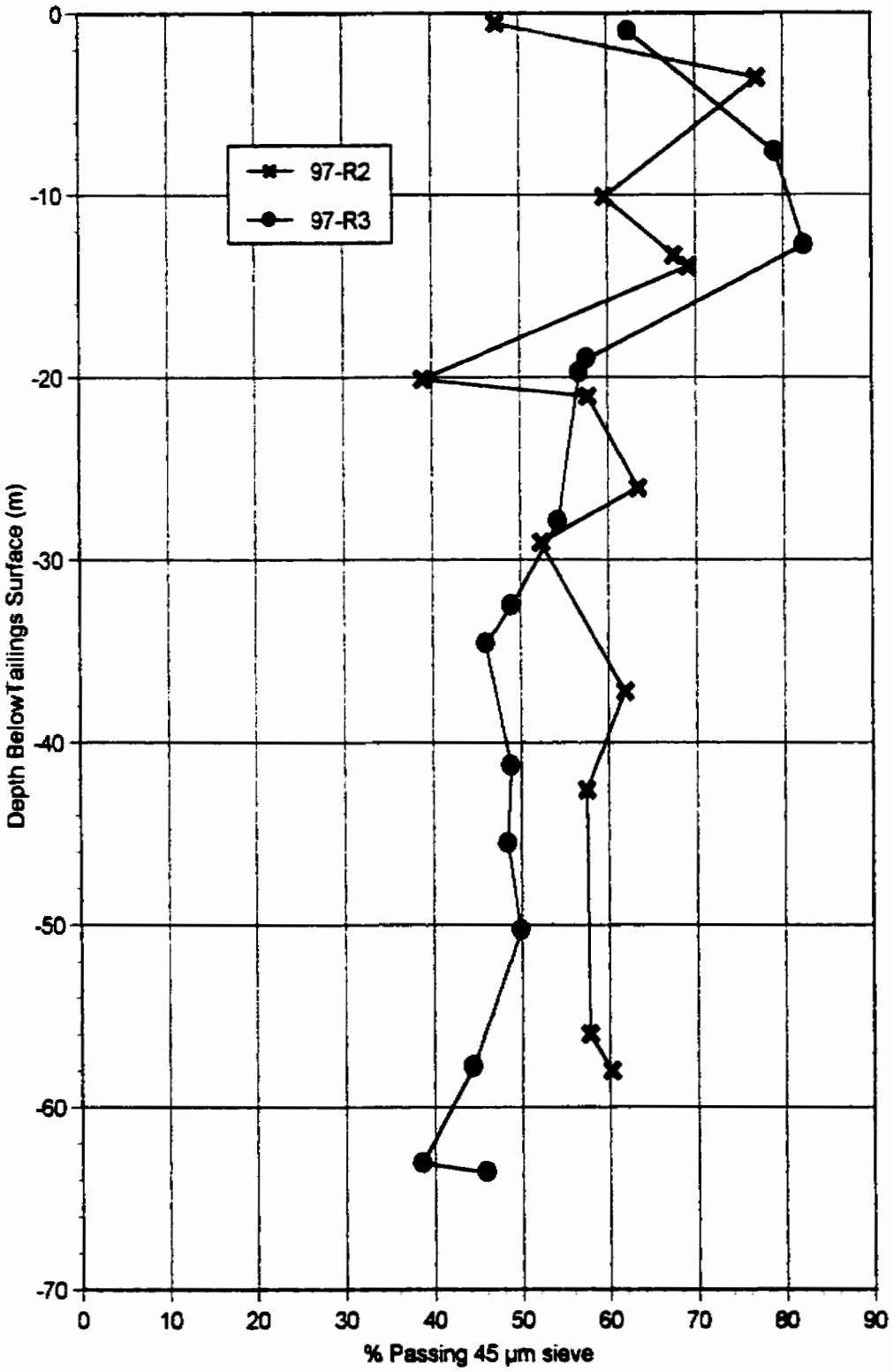

Figure 2.6 Percent passing the 45 µm sieve for tailings samples versus depth for bore holes 97-R2 and 97-R3.

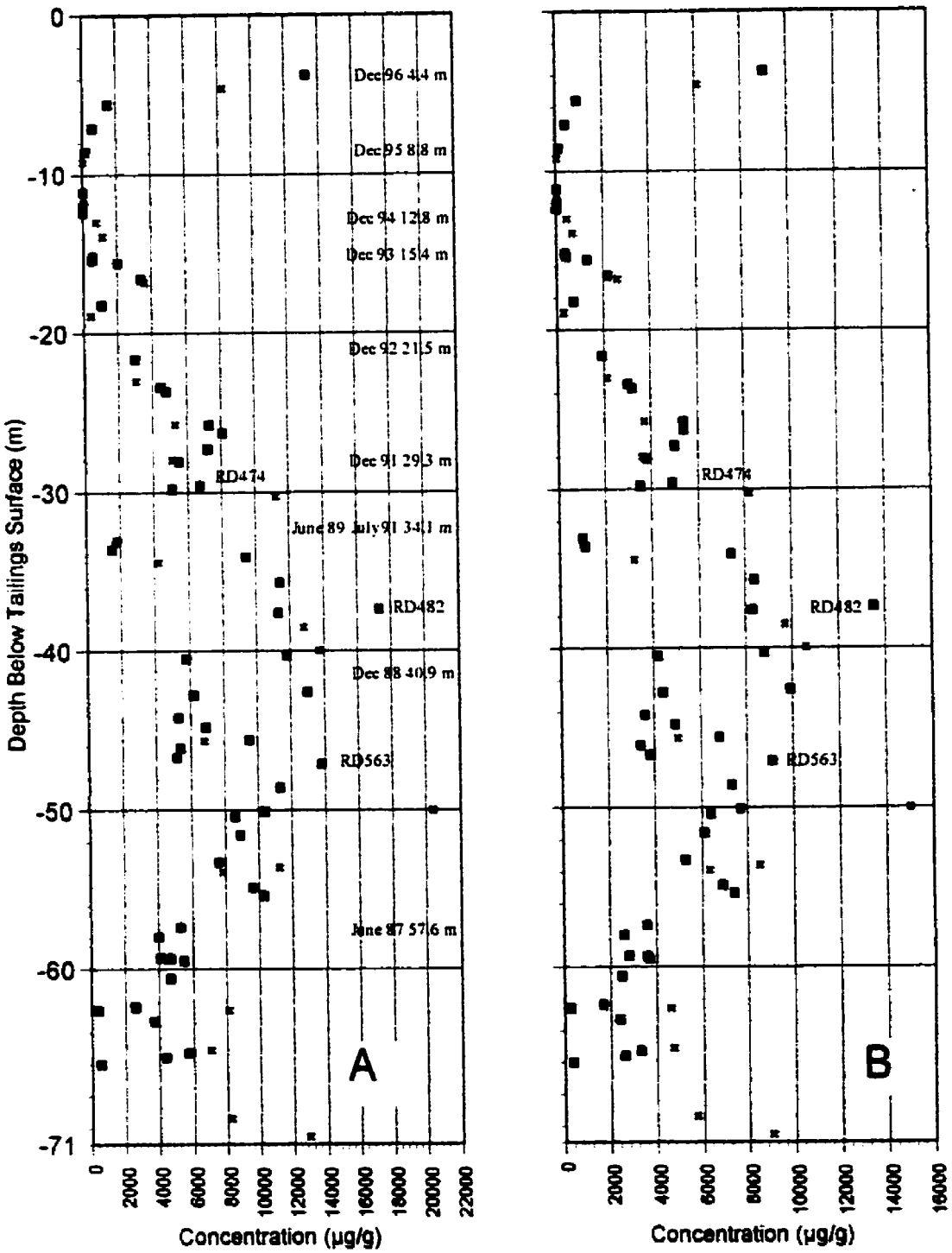

Figure 2.7 Distribution of (A) arsenic and (B) nickel concentrations in tailing samples with depth in bore holes 97-R2 (X) and 97-R3 (■). Timing of tailings depositions is presented in A (from Figure 2.4). Sample numbers from Table 2.6.

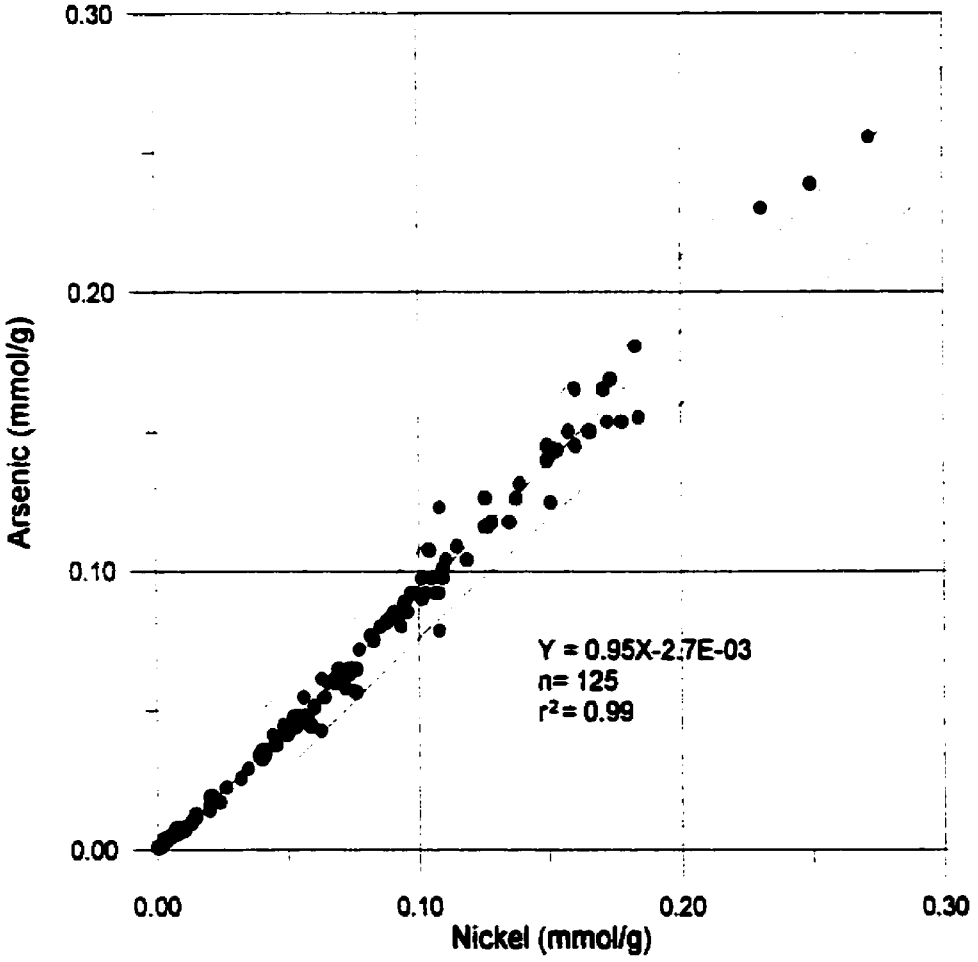

Figure 2.8 Linear relationship between the arsenic and nickel concentrations in tailings samples. The 95% confidence interval for the data is presented.

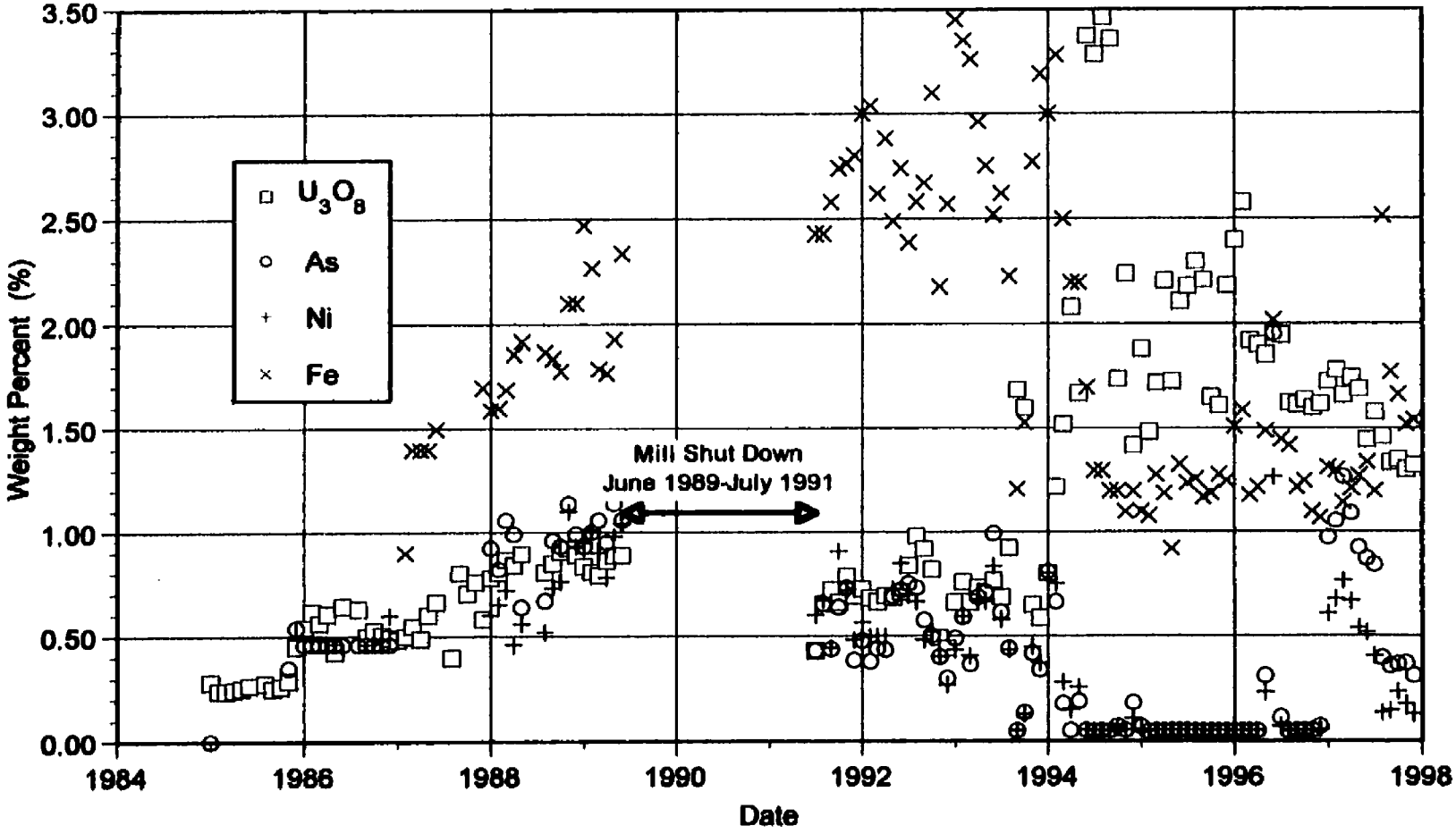

Figure 2.9 Monthly elemental analysis of ore entering the Rabbit Lake mill.

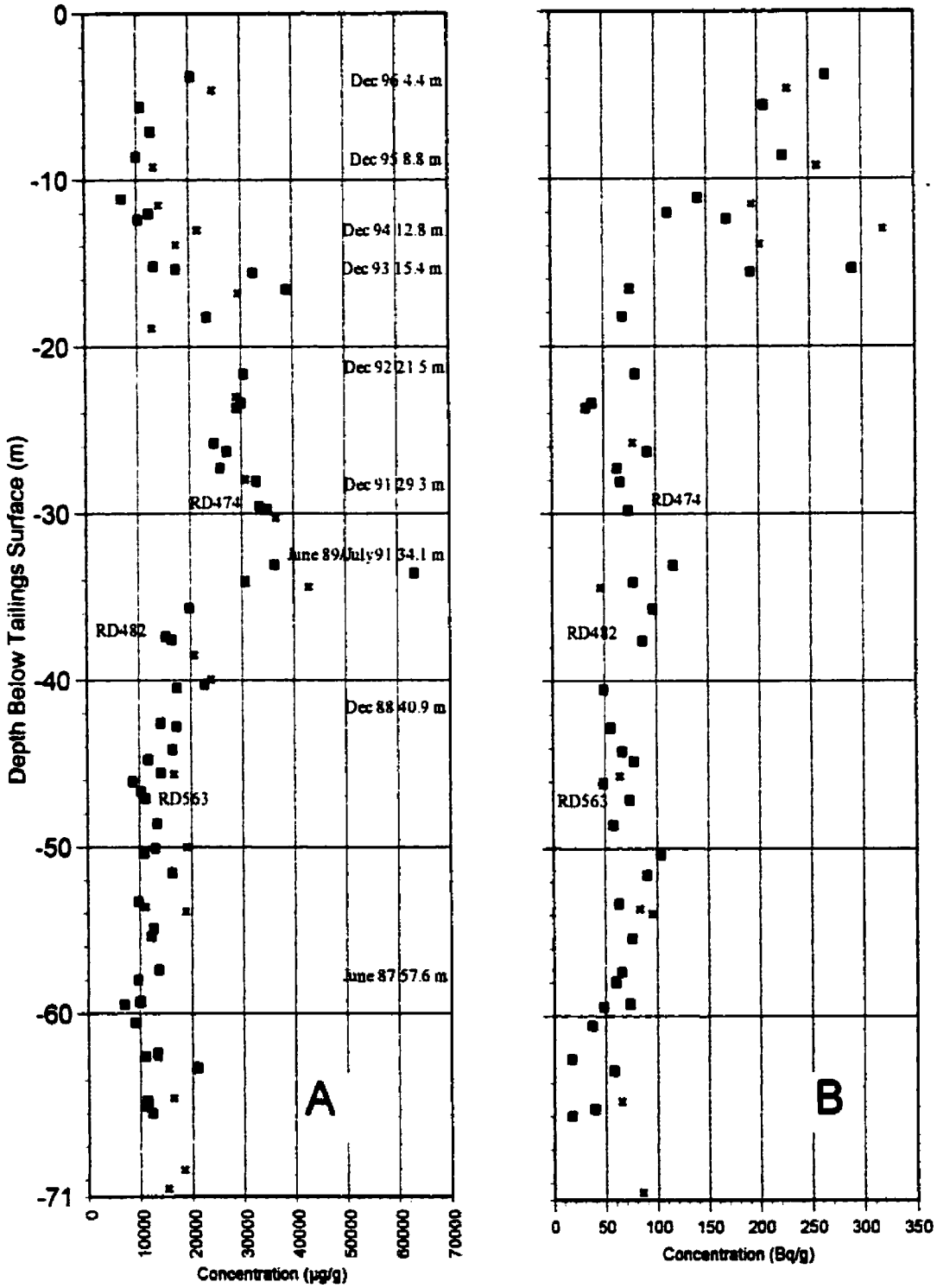

Figure 2.10 Distribution of (A) iron and (B) radium-226 concentrations in tailing samples with depth in bore holes 97-R2 (×) and 97-R3 (■). Timing of tailings depositions is presented in A (from Figure 2.4). Sample numbers from Table 2.6.

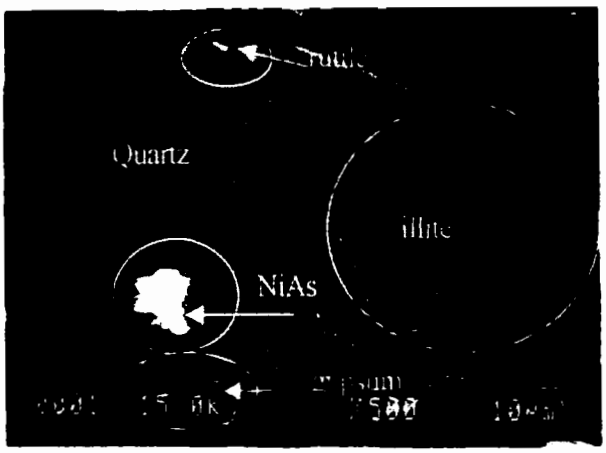

(a) RD482 - 37.4 m

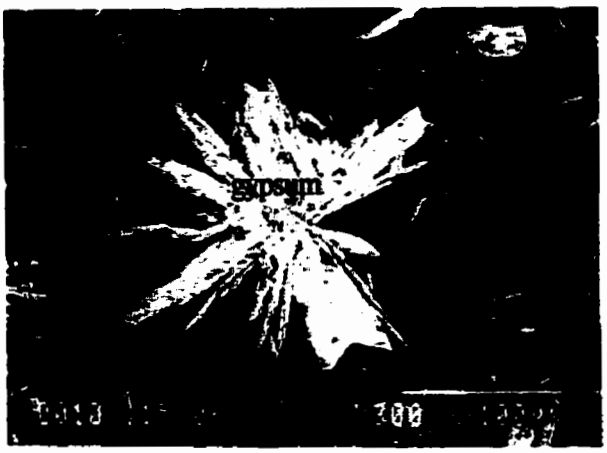

(b) RD482 - 37.4 m

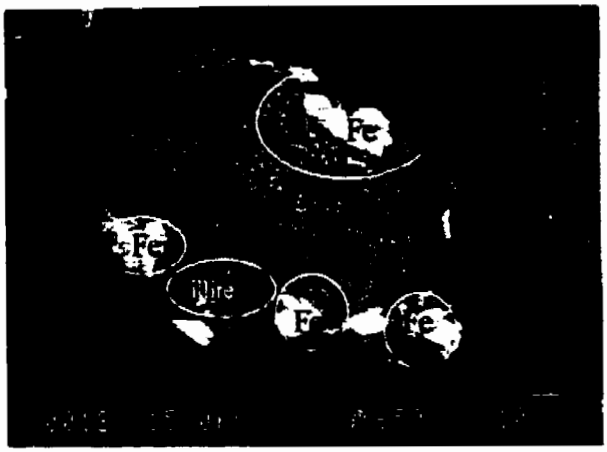

(c) RD482 - 37.4 m

Figure 2.11 Electron backscatter images of tailings samples. (a) RD482 37.4 m; (b) RD482 - 37.4 m; (c) RD482 - 37.4 m;

(d) RD482 - 37.4 m

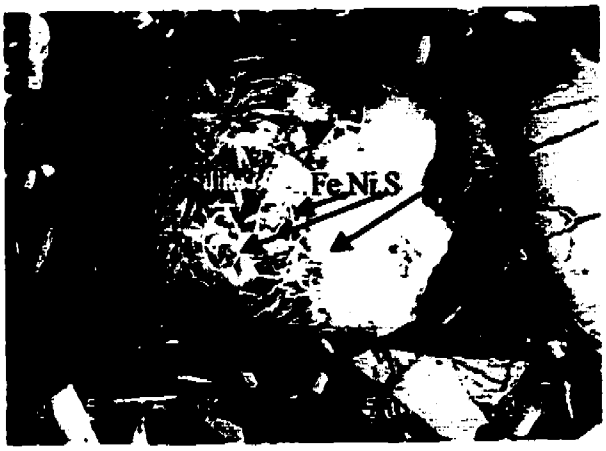

(e) RD482 - 37.4 m

(f) RD482 - 37.4 m

Figure 2.11 continued Electron backscatter images of tailings samples (d) RD482 - 37.4 m; (e) RD482 - 37.4 m; (f) RD482 - 37.4 m;

(g) RD474 - 29.4 m

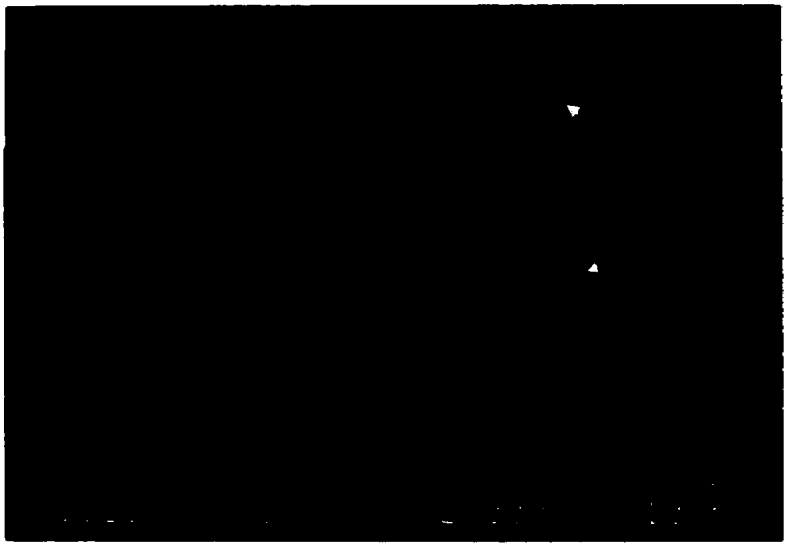

(h) RD474 – 29.4 As x-ray map of image

Figure 2.11 continued Electron backscatter images of tailings samples. (g) RD474 - 29.4 m (h) RD474 – 29.4 As x-ray map of image

CHAPTER 3.0 GEOCHEMISTRY OF ARSENIC IN URANIUM MINE MILL TAILINGS, SASKATCHEWAN, CANADA

ABSTRACT

The Rabbit Lake uranium mine in-pit tailings management facility (TMF) (425 m long x 300 m wide x 91 m deep) is located in northern Saskatchewan, Canada. The objectives of this study were to quantify the distribution of arsenic phases in the tailings and evaluate the present-day geochemical controls on dissolved As. These objectives were met by analyzing pore fluid samples collected from the tailings body for dissolved constituents, measuring Eh, pH, and temperature of tailings core and pore fluid samples, conducting sequential extractions on solids samples, conducting geochemical modeling of pore fluid chemistry using available thermodynamic data, and by reviewing historical chemical mill process records. Dissolved As concentrations in five monitoring wells installed within the tailing body ranged from 9.6 to 71 mg/L. Pore fluid in the wells had a pH between 9.3 and 10.3 and Eh between +58 and +213 mV. Sequential extraction analyses of tailings samples showed that the composition of the solid phase As changed at a depth of 34 m depth. The As above 34 m was primarily associated with amorphous iron and metal hydroxides while the As below 34 m was associated with calcium, likely as amorphous-poorly-ordered calcium arsenate precipitates. The change in the dominant As solid phases at this depth was attributed to the differences in the molar ratio of iron to arsenic in the mill tailings. Below 34 m it was <2 whereas above 34 m it was >4. The high Ca/As ratio during tailings neutralization would likely precipitate $Ca_4(OH)_2(AsO_4)_2{\cdot}4H_2O$. Geochemical modeling suggested that if the pore fluids were brought to equilibrium with this calcium arsenate, the long-term dissolved As concentrations would range between 13 and 81 mg/L.

3.0 INTRODUCTION

Uranium mines in the Athabasca basin, northern Saskatchewan, Canada produce 33% of the world's uranium (Natural Resources Canada, 1998). Uranium ore typically contains 1.2 wt% arsenic (As) (Natural Resources Canada, 1998) although as much as 10 wt% As has been reported (Langmuir et al., 1999). As a result, uranium mine tailings management facilities (TMF) can contain significant quantities of As (Donahue et al., 2000).

Arsenic can occur in four oxidation states (As^{+5}, As^{+3}, As^{0}, and As^{-3}), although arsenite (As^{+3}) and arsenate (As^{+5}) are the most common in aqueous environments. Arsenic toxicity to plants and animals is dependent on speciation, with As^{+3} being 25 to 60 times more toxic than As^{+5} (Korte and Fernando, 1991). Canadian water quality objectives do not distinguish between As oxidation states and recommend 50 µg/L total arsenic for both fresh water aquatic life and drinking water (CCREM, 1987). Phillips (1990) indicates that the relationship between As species in fresh water biota and human toxicity are inadequately characterized and as a result arsenic may represent a long-term toxicological hazard.

The presence of long-lived radioisotopes (^{226}Ra, ^{230}Th, and ^{210}Pb) in uranium tailings resulted in the adoption of a 10,000 year containment design criteria for uranium tailings facilities (Cogema, 1997). The potential for As toxicity in surface waters in the vicinity of uranium mines increases concern for the impact of As from uranium tailings on the environment and resulted in the recent adoption of a 10,000 year design criteria for arsenic containment (Cogema, 1997).

Long-term geochemical controls on dissolved As in uranium mine wastes are poorly defined, with the most detailed investigation conducted in laboratory studies on prototype tailings (Langmuir, 1999). In this study, the long-term geochemical controls on As in situ were investigated. Current efforts focused on tailings in the Rabbit Lake in-pit TMF. This TMF was chosen for study because it has the longest history of use (1984-present) of any in-pit facility in Saskatchewan. In addition, the record of long-term tailings discharge to the TMF provided a unique opportunity to investigate the distribution and changes in dissolved As concentrations with time.

The objectives of the current study were to quantify the distribution of As forms in the tailings, and evaluate the present-day geochemical controls on dissolved As. These

objectives were met by analyzing pore fluid samples collected from the tailings body for dissolved constituents, measuring Eh, pH, and temperature of tailings core and pore fluid samples, conducting sequential extractions on solids samples, conducting geochemical modeling of pore fluid chemistry using available thermodynamic data, and by reviewing historical chemical mill process records.

3.1 SITE DESCRIPTION

The Rabbit Lake in-pit TMF is located 800 km northeast of Saskatoon, Saskatchewan, Canada (58° 15' N latitude, 103° 40' W longitude). Construction of the TMF began in 1984 in the mined out Rabbit Lake pit. The TMF currently contains more than 3.6 million tonnes of tailings solids. At the time of the field investigation (1997), the tailings surface was approximately 425 m long x 300 m wide and the tailings body was approximately 91 m thick at its center.

The stratigraphy and age of the tailings with depth were determined by Donahue et al. (1999) using historical tailings surface elevations, correlated with the formation of seasonal ice layers, and through comparisons of the chemistry of ores milled and tailings at eight drill sites in the TMF (Figure 3.1). The texture of the tailings and timing of deposition are summarized in Figure 3.2 for bore holes 97-R2 and 97-R3. Five separate ore bodies, with characteristic As, Ni, and Fe concentrations, were processed at the mill: Rabbit Lake (1975-1987), A-zone (1997-present), B-zone (1985-present), D-zone (1996-1999), and Eagle point (1993–present). The chronology of tailings deposition of the five ore bodies milled with depth in the TMF is presented in Figure 3.2.

The milling process did not change during the operation time of the TMF. Ore was ground and mixed with water to yield a slurry of 55% solids with 45% of the solids passing the 75 μm sieve (Bharadwaj et al., 1995). The ground ore (leach feed) was leached with 93% sulfuric acid (pH<1) and oxidized with sodium chlorate (+450mV). Residence time in the leaching circuit was approximately 10 hours (Bharadwaj et al., 1995). Leaching dissolved minerals in the ore, solubilizes uranium into a pregnant aqueous solution. The barren liquid from the solvent extraction circuit (raffinate) and solids (leach residue) from the counter current decantation circuit (CCD) wash circuit were combined in the neutralization circuit and slaked lime was added. The tailings were neutralized to pH 10 in three stages (pH 4, 8

and 10) over a three-hour period. The combined solids from the neutralization processes were brought to a density of 35 to 45% solids and discharged from a single spigot to the TMF at one of two discharge points (Figure 3.1).

3.2 MATERIALS AND METHODS

3.2.1 Field Investigation

Eight bore holes were continuously cored to depths of 43-70 m in the TMF (Figure 3.1) in 1997. Details of the drilling, coring, sampling, and geological logging are presented in Donahue et al.,(1999).

Temperature, pH, and Eh of 545 tailings samples were measured immediately after recovery from the bore holes. Frozen samples were thawed prior to Eh and pH measurements. Measurements were made using an Orion model 250 pH/Ion meter, an Orion Triode 3 in 1 combination pH/ATC electrode, and a Cole-Parmer ORP platinum electrode. Electrodes were inserted into the center of the core samples. Measurements were recorded when the auto-hold function locked on a reading. Eh and pH instruments were calibrated twice daily using buffer solutions (pH 7 and pH 10) and a +435 mV Zobell's solution, respectively.

At the completion of the drilling program, five monitoring wells (SP-01 to SP-05), constructed of 50 mm diameter schedule 40 PVC pipe, were installed in the tailings within 15 m of bore hole 97-R3. The depths of the well intake zones ranged from 26 to 58 m as shown on Figure 3.2. To prevent potential contamination of the tailings pore fluids by drilling fluids, monitoring wells were installed "dry" using 300 mm steel casing and argon gas. Steel casing with a plastic end cap was installed in the tailings to the desired well depth. The end cap prevented tailings from entering the steel casing. The monitoring well was constructed inside the steel casing and an equal length of 25 mm diameter stainless steel pipe was placed inside the monitoring well to hold the well in place during installation. The steel casing was sealed and charged with argon gas (600 to 1200 kPa). The argon gas pressure pushed the end cap off and prevented tailings solids from entering the steel casing. Subsequently, the steel casing was withdrawn and the stainless steel pipe removed from inside the monitoring well.

Immediately after installation, pH, Eh, and temperature were measured down hole using a Hydrolab® Minisonde groundwater monitoring system. Each monitoring well was

pumped until the water levels in the wells were approximately 2 m above the top of the well screens. After pumping, the Hydrolab® was placed approximately 1 m above the top of the well screen to measure temperature, pH, and Eh. Measurements were recorded at 1-minute intervals over a 3 to12 hour period as the water level recovered. The Hydrolab® pH and Eh sensors were calibrated immediately prior to being deployed using pH 7 and 10 buffer solutions and +435 mV Zobell's solution.

With the exception of well SP-01 (56.5 m), three sets of water samples were collected from each well for chemical analysis within 24 hours of well installation. The first and third sets of water samples were collected using Watera® foot valves and plastic tubing. A second set of samples was collected using plastic bailers immediately after removal of the Hydrolab from the well. After the bailed water samples were recovered the third set of samples was collected using the Watera® system. Samples were collected from SP-01 on two occasions using the Watera® system. During sampling with the Watera® system, the foot valve was positioned about 1 m above the top of the screen and pumped using a gas powered Watera® pump. All water samples were filtered through 0.45 μm filters connected directly to the Watera® discharge tubing or to the bailer.

3.2.2 Analytical Methods

Tailings solids and pore fluid samples were analyzed at the Saskatchewan Research Council Analytical Laboratory (SRC) for Ca, K, Mg, Na, B, P, As, Al, Ba, Mn, Mo, Ni, Pb, Si, Sr, and SO_4 using inductively coupled plasma atomic emission spectroscopy (ICP-AES) methods. Chloride was analyzed using mercuric thiocyanate colormetric methods. Inorganic carbon was measured using standard titration methods. Organic carbon was analyzed using an Astro 2001 Carbon analyzer. Detailed analytical methods used for solid and pore fluid analyses are presented in Donahue et al. (1999).

Arsenic speciation ($As^{-3}$and As^{+5}) was determined on two 1 L pore fluid samples from each of the monitoring wells. One sample was collected using the Watera® pumping system and one collected using a bailer. Speciation analyses were performed at Brooks Rand Ltd., Seattle, U.S.A. Samples were shipped to the laboratory in coolers and received within 5 days of sampling. Arsenite was analyzed the day that the samples were received. Aliquots for As^{+3} analyses were buffered to pH 6 and then analyzed by hydride generation, purge and

cryogenic trapping, thermal desorption and atomic absorption spectroscopy. Arsenate was calculated as the difference between the total inorganic As and the As^{-3} (Brooks-Rand, 1997).

3.2.3 Sequential Extractions

Sequential extraction methods were used to determine the distribution of As, Fe, and Ca in samples of the tailings solids. The extraction scheme, based on that of Krishnamurti et al. (1995), is presented in Table 3.1. This scheme was selected over several others because it differentiated the oxide bound species initially described by Tessier et al. (1975) into four distinct extractions: easily reducible metal oxide bound; metal organic complex bound; amorphous mineral colloid bound; and crystalline oxide. This differentiation of the oxide bound As was considered important in the TMF because detailed information on adsorption and coprecipitation of As with oxides and hydroxides was needed.

In addition to the extractions detailed by Krishnamurti et al. (1995), distilled water soluble, sulphide (Olade and Fletcher, 1974), and residual extractions (Jenner et al., 1990) were included. The distilled water soluble extraction was included to provide information on elements associated with gypsum and elements that are easily mobilized at pH 5 under oxidizing conditions. The sulphide extraction was used to provide information on the sulphide minerals and the residual analysis was used to quantify the elemental mass balance for the extraction experiment.

Sequential extractions were performed on 10 samples of tailings collected from bore hole 97-R3. The sequential extractions were carried out in two sets. The first set consisted of three tailings samples run in triplicate. The second set contained one repeat sample from the first set and 7 other samples. Prior to testing, tailing samples were oven dried at 105 ° C for 24 hours and lightly ground using a ceramic mortar and pestle to pass a 2 mm sieve. For the first set of samples, approximately 4.5 g of dried tailing was weighed out and separated into three sub-samples, placed into 100 mL plastic centrifuge tubes, and weighed. For the second set of samples, approximately 1.5 g of dried tailing was weighed into 100 mL centrifuge tubes.

Reagents were added to the centrifuge tubes and mixed on a wrist shaker as per Table 3.1. After mixing, the samples were centrifuged and the supernatant removed using dedicated 30 or 60 mL plastic syringes with 16 gauge stainless needles. The supernatant was filtered through 0.45 μm cellulose acetate syringe filters and placed in polyethylene samples bottles.

After the supernatant was removed, 5 mL of distilled water was added to the centrifuge tubes to wash any remaining reagents from the samples. The sample and wash water were vortexed, centrifuged and the distilled water wash supernatant was removed and filtered using the same syringe and filter as used for the reagents. The wash water was combined with the reagent and submitted for chemical analysis.

Extracts were analyzed for As on the inductively coupled plasma-mass spectrometer (ICP-MS) in the Department of Geological Sciences, University of Saskatchewan and for Ca and Fe by ICP-AES at the SRC. Extraction reagents were also analyzed by ICP-MS/AES as blanks. After completion of the sulphide extraction step, the remaining solids were air dried at room temperature for 48 hours, and ground using an agate mortar and pestle. A 0.1 g sub-sample was submitted for residual analysis.

3.2.4 Saturation Indices and Equilibrium Modelling

The saturation indices (SI) of arsenates, iron hydroxides, sulphate minerals, primary As minerals and equilibrium arsenic concentrations were calculated with the PHREEQC-V2 geochemical model (Parkhurst and Appelo, 1999) using pore fluid analyses, and measured Eh, pH, and temperature data. The interpretation of mineral solubilities and equilibrium As concentrations using this program is dependent on the application of thermodynamic relationships. The PHREEQC program is designed to use the WATEQ4F database. This database contains thermodynamic data for only one calcium arsenate mineral ($Ca_3(AsO_4)_2{:}4H_2O$) and does not include arsenate complexing with Mg, Ca, Mn, Fe, and Al. Thermodynamic data for arsenate complexes were obtained from (Whiting, 1992) (Table 3.2) and were incorporated into the database.

In summary, the WATEQ4F thermodynamic database, provided with the PHREEQC model, was updated with thermodynamic data for As aqueous species (Table 3.2) and As minerals (Table 3.4). Mineral saturation was defined by $SI=0\pm0.05$ ($\log_{10}$ ($IAP/K_{mineral}$)) (Langmuir, 1997). To facilitate SI calculation for Fe minerals when Fe concentrations were below detection limits in a pore fluid sample the detection limit value (0.001 mg/L) was used.

3.2.5 Raffinate, Leach Residue Solids, and Tailings Discharge Monitoring Records

Samples of the mill ore feed, raffinate, leach residue solids, and tailings discharge were collected on a daily basis by the mine staff since 1984. These samples were analyzed for

As and Fe using X-ray fluorescence methods at the Rabbit Lake mine metallurgical laboratory. Mine staff also measured the pH of the tailings discharge on a daily basis from 1993 to 1997.

3.3 RESULTS AND DISCUSSION

3.3.1 Dissolved Arsenic

The As concentrations in the fluid samples collected from the wells are presented in Table 3.5. With the exception of SP-03 (46.8 m), As concentrations varied very little between sampling events and with the exception of SP-02 (55 m depth), the As concentrations in the tailings pore fluids typically ranged from 11 to 18 mg/L. In the case of SP-03, the first sample had an As concentration of 24 mg/L while the concentrations of the subsequent two samples were stable at 16 and 15 mg/L. In the case of SP-02, the average As concentration was higher (67 mg/L) than in the other wells.

The concentrations of dissolved As in the tailings can be attributed to either changes in the mineralogy of the ore feed with time and/or geochemical processes that occurred in the tailings since their deposition. The effects of geochemical processes and mill feed changes on the dissolved As concentrations were investigated by comparing the As concentrations in the tailings pore fluids to the daily As concentrations in the aqueous phase of the tailings at the time of discharge to the TMF (Figure 3.3). Arsenic concentrations in SP-04 and SP-05 approximated the average tailings discharge concentration while the As concentrations in SP-01 and SP-03 were slightly higher than the average tailings discharge but fell within one standard deviation of the daily As tailings discharge concentration. In contrast to these four samples, As concentrations in SP-02 were 30 mg/L higher than any daily As tailings discharge concentration in 1987 and 1988. The overall similarity between the As concentrations in pore fluid samples from wells SP-04 (35.5 m) and SP-05 (27.8 m) and the corresponding tailings discharge samples suggested that there has been no measurable change in dissolved As concentrations in the tailings since the mill restart in 1991. The slight increase in dissolved As concentrations in wells SP-01 and SP-03 and the large increase in well SP-02 suggested that the As concentrations in the tailings at these depth has increased since deposition (i.e., up to 12 years).

3.3.2 Geochemical Controls on the Arsenic in the Pore Fluids

Potential geochemical processes that could influence the distribution of As in the tailings include mineral-water reactions, oxidation/reduction reactions, and sorption. The study considered the insitu Eh and pH conditions, characterization of arsenic minerals, precipitates and sorbed phases and their corresponding thermodynamic stability as described below.

3.3.2.1 Eh, pH, and Temperature Controls

Eh, pH, and temperature measurements were made on 580 tailings samples collected from the eight bore holes. Measurements were within similar ranges within and between bore holes. The mean pH, Eh, and temperature of solid samples were 9.9 (standard deviation=0.71; range from 6.6 to 13), 174 mV (standard deviation = 104 mV, range of –400 to +400 mV), and 3.1°C (standard deviation=3.5°C, range of –0.72 to 20°C). Temperature measurements that exceeded 10°C were associated with surficial tailings samples collected on warm days and were not considered.

The results of monitoring well Eh, pH, and temperature measurements using the Hydrolab system are presented in Table 3.5. Pore fluid temperature ranged from 0.3 to –0.3°C. Solids samples from bore hole 97-R3 in the well screen intervals had temperature approximately 1.5°C higher than pore fluid temperatures from the wells. The lower pore fluid temperatures in the wells were attributed to the presence of thick frozen zones located immediately above or below the well screens.

Stable field pH readings on well-fluid samples ranged between 9.3 and 10.3. These values were within the standard deviation of the pH of the solids samples and the range and standard deviation of the pH in the tailing discharge recorded from 1987-1993 (mean=10.2; range from 8.6 to 12.2; n=270). The similarity between these three data sets suggested that the contact time between the atmosphere and tailings discharge prior to deposition had only a minor effect on the pH of the tailings pore fluid. In contrast to these pH measurements, the pH of the pore waters measured in the analytical laboratory (24 to 48 hr after sampling) were 0.5 to 0.8 pH units lower than the in situ measurements (Table 3.5). The decrease in pH measured in the laboratory suggested that these samples had reacted with atmospheric CO_2.

A plot of pH versus depth for data collected on solids samples from bore hole 97-R3 and well-water samples is presented in Figure 3.4. These results showed that the field pH determined on the solids samples and well-water samples were similar.

Stable Eh readings were obtained on well water from SP-03 to SP-05 after monitoring for 6 to 12 h. These Eh measurements ranged from +107 to +213mV. Eh readings for the two deepest wells, SP-01 and SP-02, were still decreasing at the completion of the monitoring period (3 and 6 h, respectively). Freezing conditions in SP-01 prevented the Hydrolab from being left in a static position. As a result, no stable Eh measurement was obtained for SP-01. A plot of Eh versus depth for data collected on solids samples and well-water samples showed that Eh determined on solids samples and well-water samples were not consistent and were not a function of depth. However, Eh readings on tailings solids and in the monitoring well did show that Eh measurements were more lower below 40 m depth.

The concentrations of As(III) and As(V) (Table 3.5) were used to estimate the redox potential for the tailings pore waters using PHREEQC. The calculated Eh for the As^{+3}/As^{+5} couples ranged from –193 mV in SP-02 to –291 mV in SP-05. These values were 250 to 420 mV more negative than the measured values. The poor agreement between the measured Eh and that calculated from the As redox couple was attributed to the As^{+3}/As^{+5} couple not being in redox equilibrium with other major redox couples. This observation was consistent with the findings of Bright (1989) who observed that there was no relationship between Eh calculated using the As^{+3}/As^{+5} redox couple and Eh measured with platinum electrodes.

The field pH and corresponding Eh values for tailings samples are plotted for the As-O-H system in Figure 3.5a. Eh and pH measurements plot within in the $HAsO_4^{2-}$ stability field. Monitoring well Eh and pH measurements also plot within the same stability filed. As(III)/As(V) speciation (Table 3.5) indicated that 98% of the As in the tailings pore water is As(V) and supported the stability field presented in the Eh-pH plot.

3.3.2.2 Saturation Indices of Solid Phases

A summary of calculated SI values of minerals that could influence the dissolved As concentrations in the pore fluids is presented in Table 3.6. The SI values for these minerals were calculated using (1) the original WATEQ4F database, (2) the WATEQ4F database plus arsenate complexing from Whiting (1992), and (3) the WATEQ4F database plus the arsenate

complexing data from Whiting (1992) plus the calcium arsenate complexing from Bothe and Brown (1999b) (Tables 3.2 and 3.4).

Some SI values in Table 3.6 were <5 (and in some cases <10). These values represent undersaturation by at least a factor of 10^5 and suggest that these minerals were considered to be either not present or nonreactive (Deutsch, 1997). Therefore, we assumed that minerals with SI values that were consistently <5 (e.g., niccolite) exerted a negligible influence on the pore fluid chemistry. Although gersdorffite (NiAsS) was identified as a primary arsenic mineral in the tailings, its thermodynamic data were not available and its SI values could not be estimated. However, because niccolite was considered to be nonreactive and both gersdorffite and niccolite are nickel arsenides, it too was considered nonreactive.

Gypsum was predicted to be saturated using all three databases (Table 3.6). This was expected given the masses of sulphuric acid and calcium hydroxide added during milling and neutralization, and its presence in the EMP analysis of tailings samples (Donahue et al., 2000).

Iron hydroxide was predicted to be saturated to oversaturated (SI = 0.0 to 3.2). The presence of $Fe(OH)_3$ was in keeping with it being the stable phase of Fe in the tailings. The oxidizing conditions under which the Fe was solubilized (+450 mV) suggested that Fe(III) was the dominant form of Fe in the raffinate. An Eh-pH stability diagram for Fe in the tailings pore waters (Figure 3.5b) confirmed that Fe(III) was the stable form of dissolved Fe in the tailings and that $Fe(OH)_3$ was the stable Fe phase.

The addition of complexing thermodynamics did not influence the calculated SI values for iron hydroxide (Table 3.6). This was attributed to the relatively weak complexing of Fe with arsenate ions under alkaline conditions. Iron complexes accounted for less than 1% of the As in the tailings pore fluids (Table 3.3).

Hydrous oxides play an important role in the adsorption of As (Walsh and Keeney, 1975; Livesey and Huang, 1981, from Huang 1996). The strongest adsorbent for As is freshly precipitated Fe(III) oxide, which is termed ferrihydrite or hydrous ferric oxide (HFO) (Fuller et al., 1993; Langmuir, 1999). The presence of oversaturated conditions with respect to iron hydroxide was attributed to excess OH in the tailings.

The rapid precipitation of HFO and As in the Rabbit Lake neutralization process was evident by the significant decrease in Fe and As concentrations from the raffinate to the

discharging tailings fluids (over a period of about 3 h). In the raffinate, the average Fe concentration was 29 mol/L whereas in the tailings discharge it was $1x10^{-7}$ mol/L. Similarly, As concentrations decreased from 17 mol/L in the raffinate to $1x10^{-3}$ mol/L in the discharging tailings. The adsorption of As to HFO is discussed further in Sections 4.2.3 and 4.2.4.

The SI values calculated for scorodite ($FeAsO_4:2H_2O$) indicated the mineral was undersaturated (SI = –9.7 to –1.3) and could dissolve if present. The most undersaturated values were determined using the WATEQ4F database (SI = -9.7 to -6.7). When high concentrations of Fe(III) and As(V) are present in acidic solutions, such as the raffinate, and the pH is increased gradually, ferric arsenates (scorodite) can precipitate before HFO (Demopoulos et al., 1987; Harris and Krause, 1993; Langmuir et al., 1999). Langmuir (1999) also indicated that scorodite was more likely to form if the partially neutralized raffinate was maintained at pH 1 for one hour prior to neutralization to pH 8. The relative quickness of the neutralization process at the Rabbit Lake mill and the low Fe content in the raffinate (Figure 3.4) suggested that it is unlikely that scorodite would be a major form of As in the Rabbit Lake tailings. That scorodite was not identified in EMP and XRD analyses of tailings samples (Donahue et al., 2000) further supported this conclusion. Further, at higher pH values, scorodite decomposes to HFO. For example, if scorodite is placed in a solution with pH>3, there is an almost immediate formation of a surface layer of HFO (Robbins, 1987). Nordstrom and Parks (1987) made similar observations.

EMP analysis suggested that calcium arsenate precipitates are present in the tailings (Donahue et al., 2000). These calcium arsenates were observed as amorphous precipitates, as solid solution/co-precipitates with gypsum, and as coatings on gypsum particles. From the available data we could not determine which calcium arsenate mineral(s) are present in the tailings.

The stability of calcium arsenate precipitates in aqueous systems was investigated by Bothe and Brown (1999a and b), Nishimura and Tozawa (1985), and Robins (1981). The literature generally identifies $Ca_3(AsO_4)_2$ as the sole calcium arsenate precipitate controlling arsenic solubility. Recently, however, Bothe and Brown (1999a) investigated aqueous arsenic immobilization resulting from the addition of lime and observed that $Ca_4(OH)_2(AsO_4)_2:H_2O$, $Ca_5(AsO_4)_3OH$, and $Ca_3(AsO_4)_2:4H_2O$ were the primary calcium arsenates formed.

The calculated distribution of calcium arsenate complexes in the pore fluids was dependant on the thermodynamic data used in the modeling simulations(Table 3.3). Using the WATEQ4F database, 98% of the As in the pore fluids are present as $HAsO_4^{-2}$. When the Whiting (1992) thermodynamic data were used, about 89% of the As in tailings pore fluids is predicted to be present as $CaAsO_4^-$ (Table 3.3). When the thermodynamic data from Bothe and Brown (1999b) are used, the As is predicted to be partitioned between $MgAsO_4^-$ (36%), $CaHAsO_4$ (23%), $HAsO_4^{-2}$(23%), and $CaAsO_4^-$(15%).

The differences in the As present in complexes was reflected in the calculated SI values for the calcium arsenates (Table 3.3). The main difference in calculated mineral SI values was that all calcium arsenate species are under saturated (SI<0) when the Whiting (1992) data are used. In contrast, when the calcium arsenate thermodynamic data from Bothe and Brown (1999b) are used, the $Ca_3(AsO_4)_2{:}H_2O$, $Ca_5(AsO_4)_3OH$, and $Ca_3(AsO_4)_2{:}4H_2O$ are oversaturated.

3.3.2.3 Partitioning of Arsenic, Iron, and Calcium in the Sequential Leaches

Sequential leaches are commonly used to obtain information on speciation of solids (Hall, 1998; Jones et al., 1997; Krishnamurti et al., 1995). Thus, to characterize the distribution of As in the tailings, a series of sequential leaches was conducted on dried tailings samples. Because the mineralogical controls on As appear to be related to HFO and possibly calcium arsenates (Section 4.2.2), leach data for Fe and Ca were also collected. Results of the sequential leaches are presented in Table 3.7.

The total recoveries of As and Ca from individual leaches were very similar to the bulk analyses (71 to 100% and 81 to 106% recovery, respectively). In both cases, the recoveries were similar to those reported by (Dhoum and Evans, 1995; Li et al., 1995). They report recoveries of between 85 and 110% for a number of elements. In contrast to As and Ca, the recoveries for Fe were poor, ranging from 86 to 202% and were attributed to inaccuracies in the analytical method. Results of sequential leaches conducted in triplicate on three samples yielded similar results (Table 3.7) and indicated that the sequential leach technique was reproducible.

The majority of the As in the tailings samples was extracted in two of the oxide bound phases (the metal organic and amorphous mineral colloid leaches) (16 to 80%). The

metal organic leach accounted for between 4 to 25 % of the As in the oxide bound phase while the amorphous mineral colloid extraction accounted for between 4 and 40% of the As. Lesser masses of As were extracted in the water (2.2 to 28%), exchangeable (2.6 to 22%), sulphide (5 to 20%), easily reducible metal oxide bound (1.3 to 8.3%), crystalline oxide (0.0 to 13.6%), and residual (0.7 to 3.4%) leaches.

The presence of large masses of As in both the metal organic and the amorphous mineral colloid leachates suggested that the As may be present at two sites in the precipitated HFO clusters. One adsorption site could occur near the surface of the precipitated clusters while the other site may be within the HFO clusters. The As at the surface sites may be easily desorbed from the $Fe(OH)_3$ while the As at the internal sites may require the destruction of the clusters to facilitate desorption. It is suggested that the alkaline pH used in the metal organic extraction would desorb As from the near-surface of the hydroxides without solublizing the HFO, while the amorphous oxide extraction would dissolve the amorphous minerals and solublize the As bound within the HFO precipitate. The fact that the As now associated with the HFO was present in solution with the Fe both during and after the precipitation of the HFO supported this mechanism.

The presence of two sites is further supported by Fuller et al. (1993) who observed that As(V) uptake from solution was greater when the arsenic was present in solution during the precipitation of the HFO than for sorption after the precipitation of HFO. The presence of As in solution during precipitation affects the precipitation and sorption by maximizing the number of sorption sites. As HFO precipitates, it forms clusters, as these clusters increase in size, the number of available adsorption sites decreases (Fuller et al., 1993). Spectroscopic analysis indicates that there was no structural difference in the way As was adsorbed in co-precipitation and post $Fe(OH)_3$ synthesis adsorption experiments (Fuller et al., 1993).

The greatest mass of water extractable As was obtained from samples collected below 34 m (prior to mill shut down, June 1989). The increase in water soluble As below 34 m is consistent with the greater As concentrations in the raffinate below this depth (Figure 3.3) and corresponded to the milling of As-rich, B-zone ore (Figure 3.2).

The water leach also released between 60 and 100% of the Ca present in the tailings (Table 3.7). The large mass of water extractable calcium was attributed to gypsum dissolution. As noted in Section 4.2.2, calcium and arsenic were found as amorphous

precipitates, co-precipitated/solid solution masses with gypsum, and as coatings on gypsum particles. The association of calcium sulphate and As in the EMP analysis and the large mass of water extractable As in some samples suggested that some As precipitated in association with the gypsum, possibly as a calcium arsenate.

The As in the exchangeable extraction was typically close to the average of 9% of the total As. The small mass of exchangeable As indicated that adsorption and surface complexation are not dominant reservoirs for As in the tailings. The lack of adsorption was attributed to the fact that, at the pH of the tailings, the primary As species in the tailings would be $HAsO_4^{2-}$. Under these conditions, the amorphous and crystalline Fe hydroxide surfaces would be negatively charged reducing the potential for anion sorption.

The presence of between 5 and 20% of the As as sulphide extractable leaches was attributed to the presence of primary gersdorffite and niccolite in the tailings (Donahue et al., 2000). The lack of As in the crystalline oxide leaches showed that As oxides are not a major reservoir of As in the tailing or in the mill.

Exchangeable As accounted for <10% of the total As in the samples that had high metal organic or amorphous mineral colloid extractable As. This suggested that the adsorption of As to metal hydroxide is not simply a surface complexation or adsorption process that occurred after the $Fe(OH)_3$ precipitated. This observation was supported by our inability to observe As in association with Fe and clay surfaces with the EMP analysis (Donahue et al., 2000).

With the exception of the water extractable leaches (discussed above) and the exchangeable leaches, little Ca was extracted in the other extraction steps. In the case of exchangeable Ca, it accounted for between 7 and 25% of the Ca in the tailings. The presence of Ca in the exchangeable phase was attributed to the saturation of the water extract solution with gypsum and subsequent carryover into the exchangeable leaches. This was supported by PHREEQC simulations that showed that the water extract leaches were at or above the solubility limit for gypsum.

The Fe analyses on the sequential leaches showed that the majority of Fe was present as oxides (49 to 138%, Table 3.7). Crystalline oxide Fe accounted for 14 to 123% of the Fe in the tailings with a slightly lesser amount as amorphous minerals (7 to 50%). The results of

the Fe sequential extraction analysis were supported by mill data that showed that <40% of the Fe in the ore was solubilized in the raffinate.

3.3.2.4 Quantification of Arsenic Solid Phases

The distribution of primary and secondary As minerals in contact with 1 L of pore fluid was estimated using the results of the sequential extractions and the moisture content and whole rock analyses presented by Donahue et al. (1999). The mass of minerals in contact with 1 L of pore fluid was used because it was required for geochemical modeling presented in Section 4.3. The sequential extraction results for crystalline oxide, sulphide, and residual extractions were used to approximate the As associated with oxides, sulphides, and residual nonreactive minerals, respectively. The mass of iron hydroxides indicated by the metal organic, easily reducible, and amorphous mineral leaches was assumed to be the mass of iron hydroxide associated with adsorbed and co-precipitated arsenic. We further assumed that 0.7 moles of arsenic was assumed to absorb or co-precipitate with each mole of iron as this was the highest value of iron adsorption observed by Pierce and Moore (1982). If the estimated mass of As absorbed to iron hydroxides was greater than the total mass of As, then the total mass of As minus the water extractable, exchangeable and metal organic As was used as the mass of As associated with iron hydroxides. This occurred for samples 544, 474, 508, and 518 all located above 34 m depth. The As mass associated with metal hydroxides was calculated from the results of the easily reducible extraction. Arsenic not associated with the metal hydroxides, iron hydroxides, crystalline oxides, sulphides, and residual solids was assumed to be present as a hydrated calcium arsenate phasr.

The results of these calculations are presented in Figure 3.6. Figure 3.6 shows that the As is predominately associated with iron hydroxide in samples located above 34 m depth. In contrast, arsenates are the dominant form of As in samples located below 34 m depth. The calculations also show that between 0.001 and 1.0 moles of As per L of pore fluid are present as a calcium arsenate.

In summary, sequential leach analyses showed that the majority of the As in the tailings above 34 m depth was present in association with HFO. In tailings samples located below 34 m depth, a considerable mass of As was present as primary As sulphide minerals

and associated with iron and metal hydroxides phases; however, the largest mass of As appeared to be present as secondary calcium arsenate.

3.3.2.5 Implications of Mill Chemistry Data on Arsenic Distribution

The strongest sorbent for As is HFO (c.f. Langmuir et al., 1999). As a result, considerable research has been conducted on the sorption of As(V) species on HFO (Fuller et al., 1993; Goldberg, 1986; Langmuir and Mahoney, 1998; Langmuir et al., 1999; Pierce and Moore, 1982; Robins, 1985; Waychunas et al., 1995; Waychunas et al., 1993). The rate of As(V) adsorption onto HFO is very rapid. Pierce and Moore (1982) show that adsorption was 90% complete after 1 hour in pH=4.0 to 9.9 and 99% complete after 4. Because neutralization of the Rabbit Lake tailings takes approximately 3 hours, adsorption of As by HFO should be complete by the time tailings are discharged from the Rabbit Lake mill to the TMF.

Studies by Waychunas (1993 and 1995); Pierce (1982) and Fuller (1993) show that increasing the Fe/As ratio results in an increase in the As adsorbed by HFO. Daily averaged As concentrations in the raffinate, tailings discharge, and pore water are plotted versus the molar Fe/As ratios of the associated raffinate in Figure 3.7. A decrease in As concentration with increasing Fe/As ratio was observed in these data. This trend is attributed to changes in the mill feed. Raffinate derived from B zone ore processed prior to the 1989 mill shut down (>34 m depth) had an Fe/As ratio <2. Raffinate derived from B-zone ore processed collected after the mill restated in 1991 (15 to 34 m depth) had Fe/As ratios typically >4. Raffinate from A-zone and Eagle Point blended ores (<15 m depth) had Fe/As ratios >8.

The trends in the tailings discharge and the limited pore fluid data are similar in shape to the raffinate trend, but the As concentrations are considerably reduced. Interpretation of these data sets suggests that As concentrations in pore fluids that exceeded 1 mg/L equated to a raffinate Fe/As ratio of <5. These results are in contrast to those of Langmuir et al. (1999) who, based on laboratory-aging tests on prototype uranium mill tailings, concluded that As concentrations could be maintained below 1 mg/L if the Fe/As ratio was >3. The difference between their observations and those reported here were attributed to differences in raffinate neutralization. In the Langmuir et al. (1999) study, raffinate was neutralized to between pH 7 and 8 whereas Rabbit Lake tailings were neutralized to pH 10.

In addition to the observed relationship between As concentrations in the tailings discharge and pore fluid and Fe/As ratios in the raffinate, these data further suggested that had the Fe/As ratio in the tailings collected from >34 m depth been >3, the majority of the As would have been adsorbed by HFO with the result that there would have been less water soluble As. This could have resulted in the As concentrations in the pore fluids being <10 mg/L.

3.4 IMPLICATIONS FOR LONG-TERM AS CONCENTRATIONS IN THE RABBIT LAKE TMF

In situ geochemical conditions and the presence of primary and secondary As-bearing solid phases in the tailings will control the long-term As pore fluid concentrations. Because sequential extraction and EMP analyses indicated that the dominant As-bearing phases in the tailings are iron hydroxides and calcium arsenate precipitates, this analysis focuses on the potential effects of these phases on the long-term As concentrations in the pore fluid. In this analysis, it was assumed that the long-term effects of the dissolution of primary minerals such as niccolite and gersdorffite will have a negligible effect on the As concentrations over the next 10ka (see above).

SI calculations indicated that HFO is stable in the tailings and it should continue to precipitate. Further precipitation could result in a decrease in the As concentrations in the pore fluids. The potential for long-term recrystallization of HFO to goethite or hematite (Atkinson et al., 1968) has been noted to result in lower As adsorption capacities (Belzile and Tessier, 1990; Goldberg, 1986), which would tend to desorb As. However, studies by Fuller et al., 1993; Manceau, 1995; Waychunas et al., 1995; and Waychunas et al., 1993 indicate that adsorption/co-precipitation of As inhibits the transformation of HFO to goethite or hematite. The recrystallization of HFO is also strongly inhibited by the presence of specifically adsorbed anions such as sulphate, arsenate, and silicate (pH $\geq$ 9.71, 25° C) (Langmuir and Mahoney, 1998) all of which are abundant in the tailings pore fluids. These findings suggested that the HFO in the tailings should be stable and further suggested that As concentrations in the pore fluids are unlikely to increase as a result of desorption or recrystallization of HFO.

The dissolution and/or precipitation of calcium arsenate minerals could also alter the long-term As concentrations in the tailings. Because the composition of the various amorphous calcium arsenate minerals in the tailings are not known, the potential long-term implications of calcium arsenate dissolution and precipitation on the As concentrations in the pore fluids was investigated by equilibrating the pore fluids with the calcium arsenate mineral(s) in Table 3.8.

Equilibrating the pore fluids with the various calcium arsenate minerals using PHREEQC yielded dissolved As concentrations that ranged from 2.9 to 1248 mg/L with all but one of the calcium arsenate minerals resulting in As concentration of <126 mg/L. The exception, $CaHAsO_4{:}H_2O$, resulted in very high concentrations of dissolved As (1124 to 1248 mg/L). Equilibrium pH conditions for these calcium arsenates ranged from 8.1 to 10.3. No relationship between the equilibrium As concentrations and the equilibrium pH was observed: an increase in As concentration occurred under both increasing and decreasing pH conditions.

Equilibrium modeling using only the WATEQ4F database resulted in slight increases in As concentration (12 to 67 mg/L) and in pH (9.4 to 10.4) relative to the pore fluids. Equilibrium modeling using the WATEQ4F database, arsenate complexing from Whiting (1992), and the Ksp for tricalcium arsenate calibrated for complexing generally yielded greater dissolved As concentrations than determined using the WATEQ4F database (54 to 67 mg/L). The equilibrium pH values were similar to those determined above (9.4 to 10.4). A broad range in equilibrium As concentrations was calculated when the individual calcium arsenate phases were used with the thermodynamic data reported by Bothe and Brown (1999b)(4 to 1248 mg/L). The equilibrium pH for these simulations ranged from 8.1 to 10.4.

The large mass of gypsum in the tailings and its existing equilibrium conditions in the tailings pore fluids suggested that equilibrium modeling of the pore fluids should incorporate both calcium arsenate minerals and gypsum. With the exception of the equilibrium As concentrations for monitoring wells SP-03 and SP-04 determined using the WATEQ4F database and those for all wells determined for $CaHAsO_4{:}H_2O$, the results of these simulations typically differed by less than 4 % from those presented in Table 3.8. The addition of gypsum equilibrium to the calculations resulted in a decrease in equilibrium As concentrations for pore fluid samples from monitoring wells SP-03 and SP-04 using the

WATEQ4F data base (20.3 and 15.9 mg/L, respectively) and an increase in the equilibrium As concentrations for all pore fluids brought to equilibrium with $CaHAsO_4:H_2O$ (1152 to 1345 mg/L). The equilibrium pH of simulations conducted under gypsum saturation were the same as those presented in Table 3.8.

If the long-term As pore fluid concentrations in the tailings are controlled by calcium arsenate mineral equilibrium, the dissolved As concentrations in the tailings are unlikely to exceed 126 mg/L unless $CaHAsO_4:H_2O$ is the dominant calcium arsenate mineral phase. Bothe and Brown (1999b) indicate that $CaHAsO_4:H_2O$ forms at pH of 5.76 to 6.22 and low Ca/As ratios (0.88 to 1.0). The low pH, low Ca/As ratio, and degree of undersaturation in the tailings pore fluids suggested that $CaHAsO_4:H_2O$ is not likely to precipitate in the tailings. A more likely calcium arsenate mineral phase to precipitate is $Ca_4(OH)_2(AsO_4)_2:4H_2O$ which forms at the highest Ca/As ratio and an equilibrium pH of 10. Equilibrium modeling showed that for $Ca_4(OH)_2(AsO_4)_2:4H_2O$ the As pore fluid concentration at equilibrium could increase slightly from those measured in the pore fluids to between 13 and 81 mg/L and the pH could increase to 10.

3.5 SUMMARY AND CONCLUSIONS

Dissolved arsenic concentrations in water samples collected from five monitoring wells installed within the tailing body ranged from 9.6 to 71 mg/L. The Eh, pH, and temperature measurements on tailings samples were within similar ranges in and between bore holes. The mean pH, Eh, and temperature of solid samples were 9.9, 174 mV and 3.1°C, respectively. The Eh, pH, and temperature measurements on monitoring well fluids were with similar ranges with pH between 9.3 and 10.3, Eh between +58 to +213 mV, and temperature between 0.3 to –0.3°C. Eh measurements were still decreasing when monitoring was discontinued indicating that Eh conditions are < +58 mV below 50 m depth in the tailings.

Sequential extraction analysis of tailings samples showed that the solid phase As changed composition at 34 m depth. Arsenic in tailings above 34 m depth was primarily associated with iron and other metal hydroxides. Arsenic in tailings below 34 m was primarily associated with amorphous poorly ordered calcium arsenate precipitates. The change in As solid phases at this depth correlated to a change in the ratio of dissolved Fe to

As in the associated raffinate. Tailings above 34 m depth had higher Fe to As ratios (>4) than tailings from below 34 m depths (<2).

The partitioning of As between the metal organic and amorphous mineral colloid leaches suggested that the iron hydroxides incorporate As in a co-precipitation process. The sequential leaching further suggested that the As is adsorbed to the surface of iron hydroxides that in turn form clusters. Arsenic is held within the iron hydroxide clusters and was unavailable for desorption during the high pH metal organic extractions. When the iron hydroxide clusters are solubilized in the amorphous mineral colloid leach, the As was released.

Saturation index calculations indicated that tailings pore fluids are in equilibrium with respect to gypsum and oversaturated with respect to iron hydroxide. Although Ca-arsenates were observed with the EMP as amorphous masses of calcium sulphates, iron hydroxides, and as coatings of Ca-sulphates and Ca-arsenates on gypsum crystals, their mineralogy could not be determined. Thus, the SI values of several potential calcium arsenate minerals were calculated using thermodynamic data obtained from the literature. These SI values ranged from undersaturated to saturated. Based on the most likely calcium arsenate minerals present in the tailings, equilibrium As concentrations in the pore fluids should range between 13 and 81 mg/L, values that are very similar to those measured in the pore fluid samples.

3.6 REFERENCES

Atkinson R. J., Bosner A. M., and Qirk J. B. (1968) Crystal nucleation in Fe(III) solutions and hydroxide gels. *Journal of Inorganic Nuclear Chemistry* **30**, 2371-2381.

Belzile N. and Tessier A. (1990) Interaction between arsenic and iron oxyhydroxides in lacustrine sediments. *Geochimica et Cosmochimica Acta* **54**, 103-109.

Bharadwaj B. P., Jarvi J. W., and Lam E. K. (1995) The Rabbit Lake Mill - Twenty Years of Milling. Cameco Corporation. 1995. Saskatoon.

Bothe J. V. and Brown P. W. (1999a) Arsenic Immobilization by Calcium Arsenate Formation. *Environment Science and Technology* (accepted for publication 1999).

Bothe J. V. and Brown P. W. (1999b) The Stabilities of Calcium Arsenates. *Journal of Hazardous Materials*(Accepted for publication 1999).

Bright D. A. (1989) Electrode response to the As(V)/As(III) redox couple and the use of arsenic speciation as an indicator of redox conditions in natural waters. M.Sc., University of Colorado.

Brooks-Rand. (1997) Arsenic(III), Arsenic(IV) Speciation Internal Method SOP#BR0021. Brooks Rand Ltd. letter report. #SSK001. November 6 1997. Seattle.

CCREM. (1987) Canadian Water Quality Guidelines. Task Force on Water Quality Guidelines of the Canadian Council Resource and Environment Ministers. March 1987. Ottawa.

Cogema. (1997) MaClean Lake Project - JEB Tailings Management Facility. Cogema Resources Inc. EIS. File 812B. December 4 1997. Saskatoon.

Demopoulos G. P., Kondoa P., and Papangelakis V. G. (1987) Prediction of Solubilities in Chemical Compound Precipitation Systems. *International Symposium on Crystallization and Precipitation*, Saskatoon. 231-246.

Dhoum R. T. and Evans G. T. (1995) Evaluation of uranium and arsenic retention by soil from a low level radioactive waste management site using sequential extraction. *Applied Geochemistry* **13**(4), 415-420.

Donahue R. D., Hendry J. H., and Landine P. (2000) Distribution of Arsenic and Nickel in Uranium Mill Tailings, Rabbit Lake, Saskatchewan, Canada. *Journal of Applied Geochemistry*. **5**, No.8 1097-1119.

Fuller C. C., Davis J. A., and Waychunas G. A. (1993) Surface chemistry of ferrihydrite: Part 2. Kinetics of arsenate adsorption and coprecipitation. *Geochimica et Cosmochimica Acta*. **57**, 2271-2282.

Goldberg S. (1986) Chemical Modeling of Arsenate Adsorption on Aluminum and Iron Oxide Minerals. *Soil Science Society of America Journal* **50**, 1154-1157.

Hall G. E. M. (1998) Analytical perspective on trace element species of interest in exploration. *Journal of Geochemical Exploration* **61**, 1-19.

Harris G. B. and Krause E. (1993) The disposal of arsenic from metallurgical processes: Its status regarding ferric arsenate. *The Paul E. Queneau International Symposium on Extractive Metallurgy of Nickel, Cobalt and Associated Metals*, Denver, Colorado..

Jenner G. A., Longerich H. P., Jackson S. E., and Fryer B. J. (1990) ICP-MS A Powerful tool for high precision trace element analysis in Earth Sciences: Evidence from analysis of selected U.S.G.S. reference samples. *Chemical Geology* **83**, 133-148.

Jones C. A., Inskeep W. P., and Neuman D. R. (1997) Arsenic Transport in Contaminated Mine Tailings Following Liming. *Journal of Environmental Quality* **26**(2), 433-439.

Korte N. E. and Fernando Q. (1991) A Review of Arsenic (III) in Groundwater. *Critical Review of Environmental Control* **21**, 1-36.

Krishnamurti G. S. R., Huang P. M., Van Rees K. C. J., Kozak L. M., and Rostad H. P. W. (1995) Speciation of Particulate-bound Cadmium of Soils and Its Bioavailability. *Analyst* **120**, 659-665.

Langmuir D. (1997) *Aqueous Environmental Geochemistry*. Prentice-Hall. 600

Langmuir D. and Mahoney J. (1998) Appendix 3 McClean Lake Project, JEB Tailings Management Facility, Construction License Additional Information, Geochemistry, Sub-Appendix F Thermodynamic Data for Selected Species and Solids of Arsenic and Nickel. Cogema Resources Inc. April 1998. Saskatoon.

Langmuir D., Mahoney J., MacDonald A., and Rowson J. (1999) Predicting the arsenic source term from buried uranium mill tailings. *Tailings and Mine waste 99*, Fort Collins, Colorado. .

Langmuir D. (1999) Formation of scorodite in McClean Lake prototype tailings. personal communication. January 1999.

Li X., Coles B. J., Ramsey M. H., and Thornton I. (1995) Sequential extraction of soils for multielement analysis by ICP-AES. *Chemical Geology* **124**, 109-123.

Manceau A. (1995) The mechanism of anion adsorption on iron oxides: Evidence for the bonding of arsenate tetrahedra on free $Fe(O,OH)_6$ edges. *Geochimica et Cosmochimica Acta*. **59**(17), 3647-3653.

Nishimura T. and Tozawa K. (1985) Removal of Arsenic from Waste Water by Addition of Calcium Hydroxide and Stabilization of Arsenic-Bearing Precipitates by Calcination. *Impurities Control & Disposal Proceedings of the CIM 15th Annual Hydrometallurgical Meeting*, Vancouver, Canada. 3-1 to 3-18.

Olade F. and Fletcher K. (1974) Potassium Chlorate- Hydrochloric Acid: A Sulphide Selective Leach for Bedrock Geochemistry. *Journal of Geochemical Exploration* **3.** 337-344.

Parkhurst D. L. and Appelo C. A. J. (1999) Users guide to PHREEQC - A computer program for speciation, reaction-path, 1D-transport and inverse geochemical calculations. U.S. Geological Survey Water Resources Inv.

Pierce M. L. and Moore C. B. (1982) Adsorption of Arsenite and Arsenate on Amorphous Iron Hydroxide. *Water Research* **16.** 1247-1253.

Robins R. G. (1981) The Solubility of Metal Arsenates. *Metallurgical Transactions B* **12B**(1). 103-109.

Robins R. G. (1985) The Aqueous Chemistry of Arsenic in Relation to Hydrometallurgical Process. *Impurities Control & Disposal Proceedings of the CIM 15th Annual Hydrometallurgical Meeting*. Vancouver, Canada. 1-1 to 1-26.

Waychunas G. A., Davis D. A., and Fuller C. C. (1995) Geometry of sorbed arsenate on ferrihydrite and crystalline FeOOH: Reevaluation of EXAFS results and topological factors in predicting sorbate geometry, and evidence for monodentate complexes. *Geochimica et Cosmochimica Acta.* **59**(17). 3655-3661.

Waychunas G. A., Rea B. A., Fuller C. C., and Davis J. A. (1993) Surface chemistry of ferrihydrite: Part 1. EXAFS studies of the geometry of coprecipitated and adsorbed arsenate. *Geochimica et Cosmochimica Acta.* **57**, 2251-2269.

Whiting K. S. (1992) The Thermodynamics and Geochemistry of Arsenic with the Application to Subsurface Waters at the Sharon Steel Superfund Site Midvale, Utah. Master of Science, Colorado School of Mines.

Table 3.1 Sequential Extraction Method for As, Ca, and Fe in Uranium Mill Tailings.

Extraction Step	Reagent /Mixture	Extraction Process
1. Water soluble	Ultrapure Water Two 50 mL distilled water leaches	1 hour shake centrifuge for 30 min at 5000 rpm
2. Exchangeable 5000 rpm (Hall, 1998; Krishnamurti et al., 1995)	Magnesium Nitrate 15 mL of 1 M $Mg(NO_3)_2$ (pH 7.0), 10 mL wash water	4 hour shake, centrifuge for 1 hour at
3. Metal Organic Complex Bound rpm (Hall, 1998; Krishnamurti et al., 1995)	Tetra-Sodium Pyrophosphate (pH 10) 45 mL 0.1 M $Na_4P_2O_7$ $10H_2O$ (pH 10), 5 mL wash water	20 hour, centrifuge for 1 hour at 5000
4. Easily reducible Metal Oxide-Bound (Hall, 1998; Krishnamurti et al., 1995)	Hydroxylamine Hydrochloride and Nitric Acid 30 mL 0.1 M NH_2OH• HCl in 0.01M HNO_3, 5 mL wash water	30 minutes shake, centrifuge for 15 min at 5000 rpm
5. Amorphous Mineral Colloid-Bound (Krishnamurti et al., 1995)	Ammonium Oxalate adjusted to pH 3 with Oxalic Acid 15 mL 0.2 M $(NH_4)_2C_2O_4$ – pH 3 with $H_2C_2O_4$ 5 mL wash water	4 hour shake in the (dark) centrifuge for 20 min at 5000 rpm
6. Crystalline Oxides (Krishnamurti et al., 1995)	Ammonium Oxalate, Ascorbic Acid pH 3 with Oxalic Acid 37.5 mL 0.2 M $(NH_4)_2C_2O_4$ -pH 3.0 in 0.1 M ascorbic acid, 5 mL wash water	30 minutes at 90° C centrifuge for 20 min at 5000 rpm
7. Sulphides (Olade and Fletcher, 1974)	Potassium Chlorate and Concentrated Hydrochloric Acid 1.0 g $KClO_3$,10 mL HCl, 40 mL distilled water, 5 mL wash water	let $KClO_3$ HCl stand for 30 min dilute with distilled water then centrifuge for 25 min at 5000 rpm
8. Residual in HF (Jenner et al., 1990)	HF-HNO_3	0.1 g solid sample digested for 48 hours and HNO_3

Table 3.2 Thermodynamic data for Mg, Ca, Mn, Fe, and Al complexes with arsenous acid added to WATEQ4F database in PHREEQC.

Species	Formation Reaction	Log K
From Whiting (1992)		
MgH_2AsO_4	$Mg^{+2} + H_2AsO_4^- = MgH_2AsO_4^+$	1.52
$MgHAsO_4$	$Mg^{+2} + HAsO_4^{-2} = MgHAsO_4$	2.86
$MgAsO_4^-$	$Mg^{+2} + AsO_4^{-3} = MgAsO_4^-$	6.34
$CaH_2AsO_4^+$	$Ca^{+2} + H_2AsO_4^- = CaH_2AsO_4^+$	1.06
$CaHAsO_4$	$Ca^{+2} + HAsO_4^{-2} = CaHAsO_4$	2.69
$CaAsO_4^-$	$Ca^{+2} + AsO_4^{-3} = CaAsO_4^-$	6.22
$MnHAsO_4$	$Mn^{+2} + HAsO_4^{-2} = MnHAsO_4$	3.74
$MnAsO_4^-$	$Mn^{+2} + AsO_4^{-3} = MnAsO_4^-$	6.13
$FeH_2AsO_4^+$	$Fe^{+2} + H_2AsO_4^- = FeH_2AsO_4^+$	2.68
$FeHAsO_4$	$Fe^{+2} + HAsO_4^{-2} = FeHAsO_4$	3.54
$FeAsO^+$	$Fe^{+2} + AsO_4^{-3} = FeAsO_4^-$	7.06
$NiHAsO_4$	$Ni^{+2} + HAsO_4^{-2} = NiHAsO_4$	2.90
$FeH_2AsO_4^{+2}$	$Fe^{+3} + H_2AsO_4^- = FeH_2AsO_4^{+2}$	4.04
$FeHAsO_4^+$	$Fe^{+3} + HAsO_4^{-2} = FeHAsO_4^+$	9.86
$FeAsO_4$	$Fe^{+3} + AsO_4^{-3} = FeAsO_4$	18.9
$AlH_2AsO_4^{+2}$	$Al^{+3} + H_2AsO_4^- = AlH_2AsO_4^{+2}$	4.04
$AlHAsO_4^+$	$Al^{+3} + HAsO_4^{-2} = AlHAsO_4^+$	9.86
$AlAsO_4$	$Al^{+3} + AsO_4^{-3} = AlAsO_4$	18.9
From Bothe and Brown (1999b)		
$CaH_2AsO_4^+$	$Ca^{+2} + H_2AsO_4^- = CaH_2AsO_4^+$	1.30
$CaHAsO_4$	$Ca^{+2} + HAsO_4^{-2} = CaHAsO_4$	2.66
$CaAsO_4^-$	$Ca^{+2} + AsO_4^{-3} = CaAsO_4^-$	4.36

Table 3.3 *Example of arsenic (V)speciation using three different thermodynamic databases for a tailings pore fluid samples from monitoring well SP-01.*

Arsenic speciation using the WATEQ4F database

Species	Molality	Activity	% of total
As(V)	2.50E-04		
HAsO4-2	2.46E-04	1.03E-04	98%
AsO4-3	3.93E-06	5.53E-07	2%
H2AsO4-	1.98E-07	1.59E-07	0%
H3AsO4	5.04E-15	5.13E-15	0%
		Total	100%

Arsenic speciation using the WATEQ4Fdatabase and arsenate complexing thermodynamics from Whiting (1992).

Species	Molality	Activity	% of total
As(V)	2.50E-04		
CaAsO4-	2.21E-04	1.78E-04	89%
MgAsO4-	1.39E-05	1.12E-05	6%
HAsO4-2	7.46E-06	3.13E-06	3%
CaHAsO4	6.08E-06	6.17E-06	2%
MgHAsO4	4.26E-07	4.36E-07	0%
AlAsO4	2.53E-07	2.57E-07	0%
AsO4-3	1.88E-07	2.66E-08	0%
FeAsO4-	1.62E-07	1.47E-07	0%
H2AsO4-	9.51E-09	7.65E-09	0%
FeHAsO4	5.11E-09	5.20E-09	0%
MnAsO4-	3.33E-09	2.68E-09	0%
NiHAsO4	2.45E-09	2.49E-09	0%
MnHAsO4	1.26E-09	1.28E-09	0%
CaH2AsO4-	4.40E-10	3.54E-10	0%
FeAsO4	3.15E-10	3.21E-10	0%
MgH2AsO4-	6.06E-11	4.87E-11	0%
FeH2AsO4+	2.18E-12	1.76E-12	0%
AlHAsO4+	3.42E-14	2.75E-14	0%
H3AsO4	2.43E-16	2.47E-16	0%
FeHAsO4+	4.27E-17	3.44E-17	0%
AlH2AsO4+2	2.44E-22	1.02E-22	0%
FeH2AsO4+	3.04E-25	1.27E-25	0%
		Total	100%

Arsenic speciation using the WATEQ4Fdatabase and arsenate complexing thermodynamics from Whiting (1992) and calcium arsenate complexing from Bothe and Brown (1999b)

Species	Molality	Activity	% of total
As(V)	2.50E-04		
MgAsO4-	9.03E-05	7.26E-05	36%
CaHAsO4	5.79E-05	5.89E-05	23%
HAsO4-2	5.83E-05	2.36E-05	23%
CaAsO4-	3.82E-05	3.08E-05	15%
MgHAsO4	2.78E-06	2.82E-06	1%
AlAsO4	1.70E-06	1.73E-06	1%
AsO4-3	1.42E-06	2.01E-07	1%
FeAsO4-	1.01E-06	8.13E-07	0%
H2AsO4-	7.07E-08	5.69E-08	0%
FeHAsO4	2.83E-08	2.88E-08	0%
MnAsO4-	2.23E-08	1.79E-08	0%
NiHAsO4	1.84E-08	1.87E-08	0%
MnHAsO4	8.44E-09	6.58E-09	0%
CaH2AsO4-	4.41E-09	3.55E-09	0%
FeAsO4	1.75E-09	1.78E-09	0%
MgH2AsO4-	3.87E-10	3.12E-10	0%
FeH2AsO4+	1.19E-11	9.61E-12	0%
AlHAsO4+	2.30E-13	1.85E-13	0%
H3AsO4	1.83E-15	1.86E-15	0%
FeHAsO4+	2.37E-16	1.91E-16	0%
AlH2AsO4+2	1.61E-21	6.75E-22	0%
FeH2AsO4+	1.66E-24	6.97E-25	0%
		Total	100%

Table 3.4 Thermodynamic data for arsenic minerals added to WATEQ4F database in PHREEQC.

Mineral	Dissociation Reaction	Log K_{sp}	ΔH
(Langmuir and Mahoney, 1998)			
Niccolite	$NiAs + 4H_2O = Ni^{+2} + H_3AsO_4 + 5H^+ + 7e^-$	-35.76	62.14 kcal/mol
Arsenopyrite	$FeAsS + 8H_2O = Fe^{+2} + AsO_4^{-3} + SO_4^{-2} + 16H^+ + 13e^-$	-93.75	120.8 kcal/mol
Millerite	$NiS + H^+ = Ni^{+2} + HS^-$	-9.05	3.9 kcal/mol
Annabergite	$Ni_3(AsO_4)_2{:}8H_2O = 3Ni^{+2} + 2AsO_4^{-3} + 8H_2O$	-28.38	-11.0 kcal/mol
(Robins, 1981)			
Tricalcium arsenate	$Ca_3(AsO_4)_2{:}4H_2O = 3Ca^{+2} + 2AsO4^{-3} + 4H_2O$	4.72	
(PHREEQCV2 WATEQ4F database, Parkhurst and Appelo, 1999)			
Tricalcium arsenate	$Ca_3(AsO_4)_2{:}4H_2O = 3Ca^{+2} + 2AsO_4^{-3} + 4H_2O$	-21.257	
(Bothe and Brown, 1999b)			
Calcium Arsenate Hydrate	$Ca_4(OH)_2(AsO_4)_2{:}4H_2O = 4Ca^{+2} + 2H_3AsO_4 + 6H_2O - 8H^+$	40.2	
Calcium Arsenate Hydrate	$Ca_5(AsO_4)_3(OH) = 5Ca^{+2} + 3H_3AsO_4 + H_2O - 10H^+$	37.8	
Calcium Arsenate Hydrate	$Ca_3(AsO_4)_2{:}4H_2O = 3Ca^{+2} + 2H_3AsO_4 + 4H_2O - 6H^+$	20.22	
Calcium Arsenate Hydrate	$CaHAsO_4{:}H_2O = Ca^{+2} + H_3AsO_4 + H_2O - 2H^+$	4.22	
Ferrarisite	$Ca_5(HAsO_4)_2(AsO_4)_2{:}9H_2O = 5Ca^{+2} + 4H_3AsO_4 + 9H_2O - 10H^+$	27.75	
Guerinite	$Ca_5(HAsO_4)_2(AsO_4)_2{:}9H_2O = 5Ca^{+2} + 4H_3AsO_4 + 9H_2O - 10H^+$	28.55	

Table 3 5 Summary of chemical analysis of tailings pore fluid samples from 1997 Rabbit Lake in-pit monitoring wells

Analyte	SP-01** Average	St. Deviation	SP-02 Average	St. Deviation	SP-03 Average	St. Deviation	SP-04 Average	St. Deviation	SP-05 Average	St. Deviation	Units	Detection Limits
Well Screen Depth	56.5		54 5		46 8		35 5		27 8		m	
Temperature	-0 08		0 27		-0 32		-0 31		-0 31		°C	0 01
pH (lab)	6 60	0 05	8 45	0 05	9 02	0 31	9 19	0 10	9 53	0 26		
pH (field)	9.62		9 29	0 09	9 69	0 12	9 46	0 10	10 28	0 07	pH	0 1
Eh * (field)	< 145		< 58		107		213		148		mV	±20
Eh (As^{+3}/As^{+5})	-214	1 2	-193	2 9	-226	0 0	-209	0 6	-291	1	mV	
Dissolved Oxygen *	0 21		0 15		0 09		0 2		0 28		mg/L	0 1
Specific Conductivity*	4758		5083	211	5184	75	4348 99	152	6436	142	µS/cm	1
Calcium	532	2	542	32	532	11 8	580	25	500	4 5	mg/l	0 1
Chloride	390	57	646	49	718	27 5	483	14	735	22	mg/l	1
Potassium	8.0	0 0	9 8	1.4	6 4	0 4	6 2	0 76	11	0 58	mg/l	0 2
Magnesium	9.3	0 0	17	2.1	4 2	1 1	8 9	0 38	1 7	0 15	mg/l	0 1
Sodium	463	98	649	102	737	61	326	15	882	40	mg/l	0.1
Sulphate	1840	57	1723	170	1823	110	1453	42	2090	139	mg/l	0 1
Boron	0 08	0 04	0 08	0 002	0 07	0 02	0 12	0 025	0 13	0 077	mg/l	0 002
Phosphorus	0.08	0 014	0 07	0 02	0 05	0	0 11	0 015	0 16	0 021	mg/l	0 05
Arsenic	21	1 6	67	6 4	18	4 9	13	1 5	11	1 7	mg/l	100
Arsenic[1] Inorganic	17	2 1	57	2 2	12	0	13	0 38	9 5	0 40	mg/l	1
Arsenic[1] (III)	0.13	0 006	0.56	0.070	0 13	0 005	0 33	0 02	0 10	0 005	mg/l	1
Arsenic[1] (V)	17	2 1	57	2 3	12	0 32	13	0 36	9 4	0 40	mg/l	1
Aluminum	0.20	0.09	0 35	0.10	0 25	0 1	0 21	0 065	0 28	0 18	mg/l	0 005
Barium	0.018	0.008	0 032	0.004	0.023	0 004	0 031	0 004	0 014	0 01	mg/l	0 001
Iron	0.13	0.01	0 16	0 28	0 065	0 06	0 10	0 16	0 016	0.027	mg/l	0.001
Manganese	0.007	0.004	0 013	0 01	0 007	0 002	0 009	0 005	0 004	0 003	mg/l	0 001
Molybdenum	31	1.4	38	4 2	43	6 1	24	4 5	43	24	mg/l	0 001
Nickel	0.19	0.03	0 32	0 36	0.086	0 05	0 09	0 10	0 034	0 025	mg/l	0 001
Lead	0.018	0.013	0.017	0.026	0.002	0	0.003	0 001	0.004	0 004	mg/l	0 002
Silicon	1.9	0.1	4.1	0.4	2.7	0 29	2 9	0 53	3.2	1 3	mg/l	0.01
Strontium	0.4	0.1	1.0	0 08	0.95	0 04	0 63	0 13	0.56	0.37	mg/l	0 001
Inorganic carbon	9	2.1	20	1.5	10	1.5	8	0 6	9	0 6	mg/l	1
Organic carbon	21	1	25	5 7	22	1 0	19	0 6	31	4 6	mg/l	0 2
Charge Balance	5.4%	1.0%	7.3%	1.6%	3.8%	0 6%	1 9%	1.6%	2 1%	1.0%	%	

Notes: Population is two for SP-01 and three for SP-02 through SP-05

* Eh, temperature dissolved oxygen and specific conductivity are not averaged

** SP-01 was freezing during monitoring so well could not be monotrinf long enough for Eh and DO to stabilize

Table 3.6 Summary of saturation indices calculated using PHREEQC for pore fluid samples from monitoring wells.

Mineral phase	Monitoring Well SP-01	SP-02	SP-03	SP-04	SP-05	SI Sensitivity
	average	average	average	average	average	±
WATEQ4F thermodynamic database						
Ca3(AsO4)2:4H2O	-0.6	0.03	-0.7	-1.1	-0.1	0.2
Scorodite	-6.4	-6.7	-7.7	-7.4	-9.7	0.7
Ni3(AsO4)2	-7.3	-4.4	-7.0	-7.2	-10.3	0.3
Gypsum	0.0	0.0	0.0	0.0	0.0	0.1
Fe(OH)3(a)	3.5	2.3	2.5	2.4	1.8	0.4
Ni(OH)2	3.7	4.0	4.0	3.6	3.8	0.3
Arsenate complexing thermodynamics from Whiting (1992) added to WATEQ4F database						
Ca3(AsO4)2:4H2O	-1.0	0.0	-1.1	-1.3	-1.5	0.2
Ca4(OH)2(AsO4)2:4H2O	-3.7	-3.2	-3.7	-4.3	-3.0	0.3
Ca5(AsO4)3OH	-0.2	1.0	-0.3	-0.8	-0.4	0.2
Ca3(AsO4)2:4H2O	-0.8	0.2	-0.9	-1.1	-1.3	0.2
Ca5H2(AsO4)4:9H2O-Ferrarsite	-5.7	-3.4	-6.1	-6.1	-8.0	0.2
Ca5H2(AsO4)4:9H2O-Guerinite	-6.5	-4.2	-6.9	-6.9	-8.8	0.2
CaHAsO4:H2O	-2.9	-2.2	-3.0	-3.0	-3.8	0.1
Scorodite	-1.8	-1.8	-3.0	-2.6	-5.6	0.7
Ni3(AsO4)2	-9.7	-6.7	-9.7	-9.7	-14	0.3
Annabergite	-7.5	-4.6	-7.6	-7.6	-12	0.3
Gypsum	0.0	0.0	0.0	0.0	0.0	0.1
Niccolite	-49	-35	-45	-57	-56	0.9
Fe(OH)3(a)	3.5	2.3	2.5	2.4	1.8	0.4
Ni(OH)2	3.8	4.0	4.0	3.6	3.8	0.3
Arsenate complexing thermodynamics from Whiting (1992) and Bothe and Brown (1999b) added to WATEQ4F database						
Ca3(AsO4)2:4H2O	1.1	2.0	1.4	0.8	1.7	0.2
Ca4(OH)2(AsO4)2:4H2O	-2.3	-1.8	-1.9	-2.8	-0.5	0.3
Ca5(AsO4)3OH	1.9	3.0	2.4	1.4	3.4	0.2
Ca3(AsO4)2:4H2O	0.6	1.5	0.9	0.4	1.2	0.2
Ca5H2(AsO4)4:9H2O-Ferrarsite	-2.9	-0.8	-2.4	-3.2	-3.1	0.2
Ca5H2(AsO4)4:9H2O-Guerinite	-3.7	-1.6	-3.2	-4.0	-3.9	0.2
CaHAsO4:H2O	-2.2	-1.6	-2.1	-2.2	-2.6	0.1
Scorodite	-0.7	-1.0	-1.8	-1.6	-4.0	0.7
Ni3(AsO4)2	-7.8	-4.9	-7.2	-7.6	-11	0.3
Annabergite	-5.6	-2.7	-5.1	-5.5	-8.7	0.3
Gypsum	0.0	0.0	0.0	0.0	0.0	0.1
Niccolite	-49	-35	-44	-56	-55	0.9
Fe(OH)3(a)	3.5	2.2	2.5	2.4	1.8	0.4
Ni(OH)2	3.7	4.0	4.0	3.6	3.8	0.3

Table 3.7 Summary of sequential extraction results for (a) arsenic, (b) iron, and (c) calcium

(a) Arsenic

Sample No.	Depth (m)	Total Moles	Water Extraction	Exchangable	Metal Organic	Easily Reducible	Amorphous Mineral	Crystaline Oxide	Sulphides	Residual Solids	Total
508	7.1	1.26E-05	6.0%	5.9%	9.3%	3.2%	45%	0.4%	13%	2.2%	86%
518	15.2	1.17E-05	7.8%	8.4%	10.7%	4.3%	41%	-1.0%	5.6%	1.4%	79%
474-1	29.6	1.50E-04	4.3%	2.6%	48%	2.1%	29%	2.6%	4.6%	1.5%	94%
474-2	29.6	1.54E-04	4.2%	3.0%	43%	4.2%	30%	2.6%	5.1%	1.8%	95%
474-3	29.6	1.69E-04	4.0%	2.9%	52%	4.1%	28%	2.8%	5.0%	1.4%	100%
474	29.6	1.35E-04	4.4%	5.1%	29%	1.3%	34%	2.2%	19%	2.3%	97%
544	33.6	3.10E-05	16%	5.8%	5.1%	6.3%	17%	13.6%	5.3%	16%	87%
482-1	37.4	3.74E-04	13.9%	9.2%	29%	5.0%	13%	0.8%	15%	0.7%	86%
482-2	37.4	3.50E-04	14.6%	10%	31%	4.5%	15%	0.9%	15%	0.8%	93%
482-3	37.4	4.29E-04	10.8%	9.4%	29%	4.0%	16%	0.9%	16%	0.7%	87%
546	42.6	2.64E-04	11%	9.7%	20%	2.2%	20%	0.9%	21%	1.1%	85%
563-1	46.7	1.20E-04	23%	9.9%	23%	5.8%	4.4%	2.1%	17%	1.5%	88%
563-2	46.7	1.11E-04	25%	8.0%	19%	3.8%	4.3%	2.0%	20%	1.3%	84%
563-3	46.7	1.37E-04	21%	6.3%	23%	3.8%	4.2%	2.1%	20%	2.6%	83%
496	50.1	2.13E-04	25%	18%	16%	4.7%	11%	1.2%	5.3%	1.2%	82%
584	59.35	9.74E-05	24%	22%	18%	5.8%	12.4%	3.5%	20%	3.4%	110%
500	65.3	1.16E-04	19%	15.0%	7.7%	2.8%	9.2%	2.2%	12%	2.9%	71%

(b) Iron

Sample No.	Depth (m)	Total Moles	Water Extraction	Exchangable	Metal Organic	Easily Reducible	Amorphous Mineral	Crystaline Oxide	Sulphides	Residual Solids	Total
508	7.1	3.51E-04	0%	0%	1.7%	0.87%	22%	26%	5.7%	45%	102%
518	15.2	3.63E-04	0%	0%	1%	0.30%	50%	17%	1.2%	26%	95%
474-1	29.6	8.25E-04	2.7%	0.043%	5.3%	0.64%	25%	65%	2.3%	11%	111%
474-2	29.6	8.48E-04	2.6%	0.038%	4.0%	0.38%	26%	64%	2.2%	12%	111%
474-3	29.6	9.34E-04	2.2%	0.031%	7.1%	0.28%	24%	59%	2.2%	10%	105%
474	29.6	9.05E-04	0.0%	0.0%	2%	0.9%	26%	46%	36%	20%	131%
544	33.6	1.75E-03	0.0%	0.00%	0.3%	0.16%	15%	93%	2.8%	30%	142%
482-1	37.4	4.60E-04	6.7%	0.10%	1.8%	0.26%	22%	43%	2.2%	10%	86%
482-2	37.4	4.29E-04	7.5%	0.10%	2.3%	0.49%	22%	52%	2.4%	12%	99%
482-3	37.4	5.27E-04	6.2%	0.15%	2.3%	0.27%	20%	50%	1.7%	11%	91%
546	42.6	3.84E-04	0%	0.0%	3%	1.0%	32%	53%	39%	20%	148%
563-1	46.7	3.09E-04	5.9%	0.17%	1.2%	0.78%	7.5%	64%	1.9%	12%	93%
563-2	46.7	2.84E-04	5.4%	0.21%	1.3%	0.88%	7.2%	67%	2.3%	12%	97%
563-3	46.7	3.52E-04	5.2%	0.36%	1.1%	0.63%	6.7%	66%	3.4%	13%	96%
496	50.1	3.57E-04	0%	0.0%	1.0%	0.20%	13%	79%	0.8%	19%	113%
584	59.35	2.78E-04	0%	0.0%	2%	0.64%	14%	123%	34%	27%	202%
500	65.3	3.11E-04	0%	0.0%	3.4%	2.2%	14%	56%	2.4%	21%	99%

Table 3.7 continued
(c) Calcium

Sample No.	Depth (m)	Total Moles	Water Extraction	Exchangable	Metal Organic	Easily Reducible	Amorphous Mineral	Crystaline Oxide	Sulphides	Residual Solids	Total
508	7.1	2.09E-03	87%	12%	1.2%	0.34%	0.029%	0.011%	0.19%	1.3%	102%
518	15.2	3.99E-03	50%	25%	1.1%	2.2%	0.012%	0.0084%	6.7%	0.55%	86%
474-1	29.6	1.86E-03	81%	10%	2.8%	1.1%	0.019%	0.018%	0.062%	0.58%	96%
474-2	29.6	1.91E-03	82%	8%	2.3%	1.0%	0.023%	0.018%	0.13%	0.46%	93%
474-3	29.6	2.11E-03	79%	6.6%	2.4%	0.66%	0.017%	0.016%	0.67%	0.73%	91%
474	29.6	1.95E-03	65%	33%	3.8%	0.9%	0.038%	0.04%	0.19%	0.34%	103%
544	33.6	6.88E-04	9%	20%	14%	14%	0.05%	0.11%	39%	2.2%	98%
482-1	37.4	2.82E-03	80%	9.1%	1.3%	0.36%	0.015%	0.0032%	0.018%	0.44%	91%
482-2	37.4	2.64E-03	78%	8.8%	1.3%	0.45%	0.020%	0.013%	0.018%	0.42%	89%
482-3	37.4	3.23E-03	63%	15%	2.6%	0.59%	0.011%	0.0039%	0.095%	0.36%	81%
546	42.6	2.05E-03	90%	12%	1.6%	0.68%	0.039%	0.032%	0.13%	0.82%	106%
563-1	46.7	1.20E-03	82%	8.3%	2.4%	0.63%	0.058%	0.047%	0.028%	1.3%	95%
563-2	46.7	1.10E-03	81%	6.4%	1.8%	0.34%	0.063%	0.050%	0.017%	1.6%	91%
563-3	46.7	1.36E-03	79%	7.4%	2.3%	0.44%	0.058%	0.048%	0.11%	0.81%	90%
496	50.1	1.75E-03	93%	12%	0.69%	0.14%	0.057%	0.076%	0.009%	0.71%	106%
584	59.35	1.89E-03	74%	27%	1.6%	0.24%	0.042%	0.06%	0.056%	0.65%	104%
500	65.3	1.31E-03	103%	8%	1.0%	0.23%	0.057%	0.082%	0.26%	1.3%	114%

Table 3.8 Concentrations of dissolved arsenic and pH in equilibrium with various calcium arsenates using PHREEQC.

Monitoring Well	SP-01	SP-02	SP-03	SP-04	SP-05
Field pH	9.62	9.42	9.69	9.46	10.28
Measured total As (mg/L)	21.3	67.3	18.3	13.3	11.2
Equilibrium phase	**Equilibrium As Concentration (mg/L)**				
WATEQ4F thermodynamic database					
Ca3(AsO4)2:4H2O	25	67	20	16	12
Equilibrium pH	9.9	9.4	10.0	9.9	10.3
Arsenate complexing thermodynamics from Whiting (1992) added to WATEQ4F database					
Ca3(AsO4)2:4H2O	62	67	59	54	61
Equilibrium pH	9.8	9.4	9.9	9.8	10.4
Arsenate complexing thermodynamics from Whiting (1992) and Bothe and Brown (1999b) added to WATEQ4F database					
Ca3(AsO4)2:4H2O	9.7	40.3	10.1	8.7	2.9
Equilibrium pH	9.3	8.5	9.1	9.1	9.6
Ca4(OH)2(AsO4)2:4H2O	33.7	80.6	23.8	21.3	12.6
Equilibrium pH	10.3	9.9	10.2	10.3	10.4
Ca5(AsO4)3OH	12.1	49.5	12.4	10.0	4.0
Equilibrium pH	9.2	8.7	9.1	9.1	9.6
Ca3(AsO4)2:4.00H2O	13.7	43.7	11.9	11.0	4.3
Equilibrium pH	9.4	8.7	9.3	9.3	10.0
Ca5H2(AsO4)4:9H2O-Ferrarsite	80.9	92.5	58.7	62.5	55.7
Equilibrium pH	9.7	9.5	9.9	9.7	10.2
Ca5H2(AsO4)4:9H2O-Guerinite	112	126	86.7	89.1	85.3
Equilibrium pH	9.8	9.6	10.0	9.8	10.2
CaHAsO4:H2O	1214	1217	1203	1124	1248
Equilibrium pH	8.2	8.3	8.2	8.1	8.3

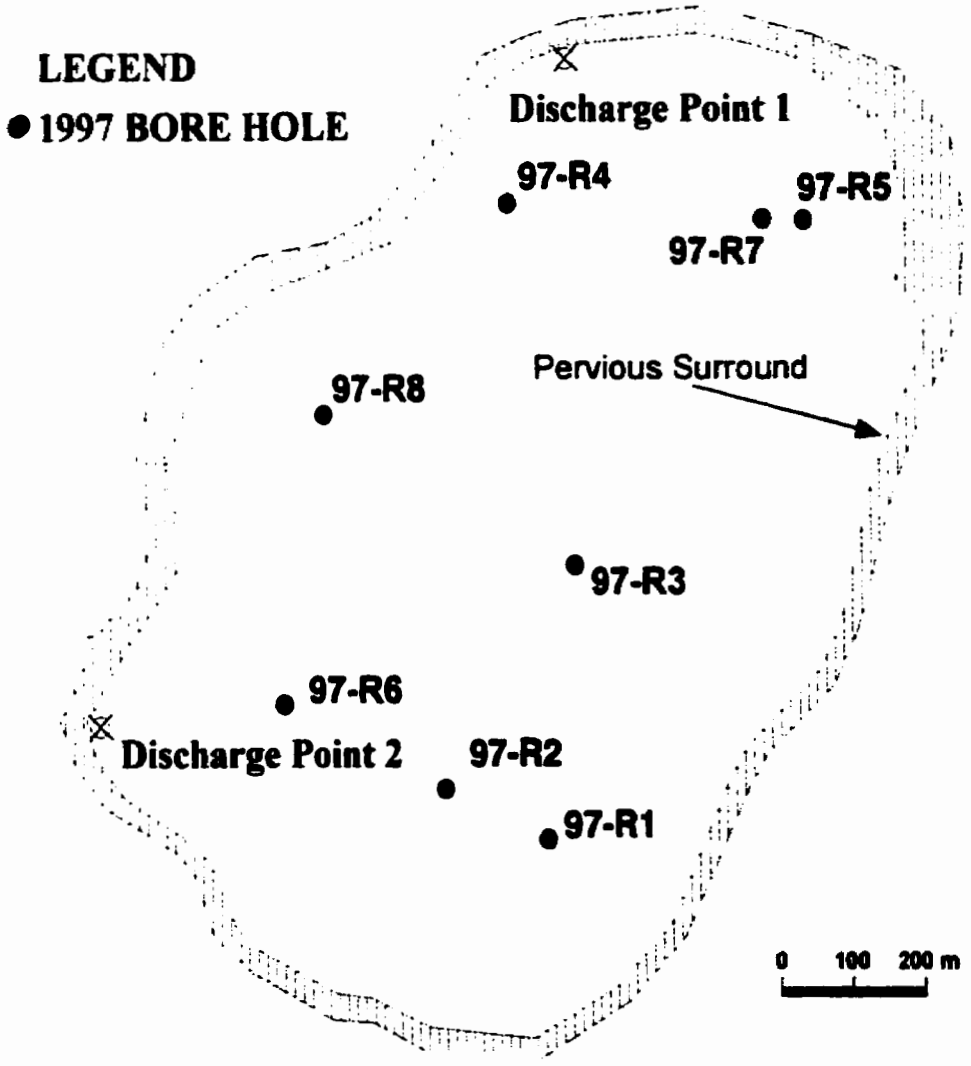

Figure 3.1 Plan view of Rabbit Lake pit showing bore hole locations, tailings discharge points and pervious surround (cross hatched).

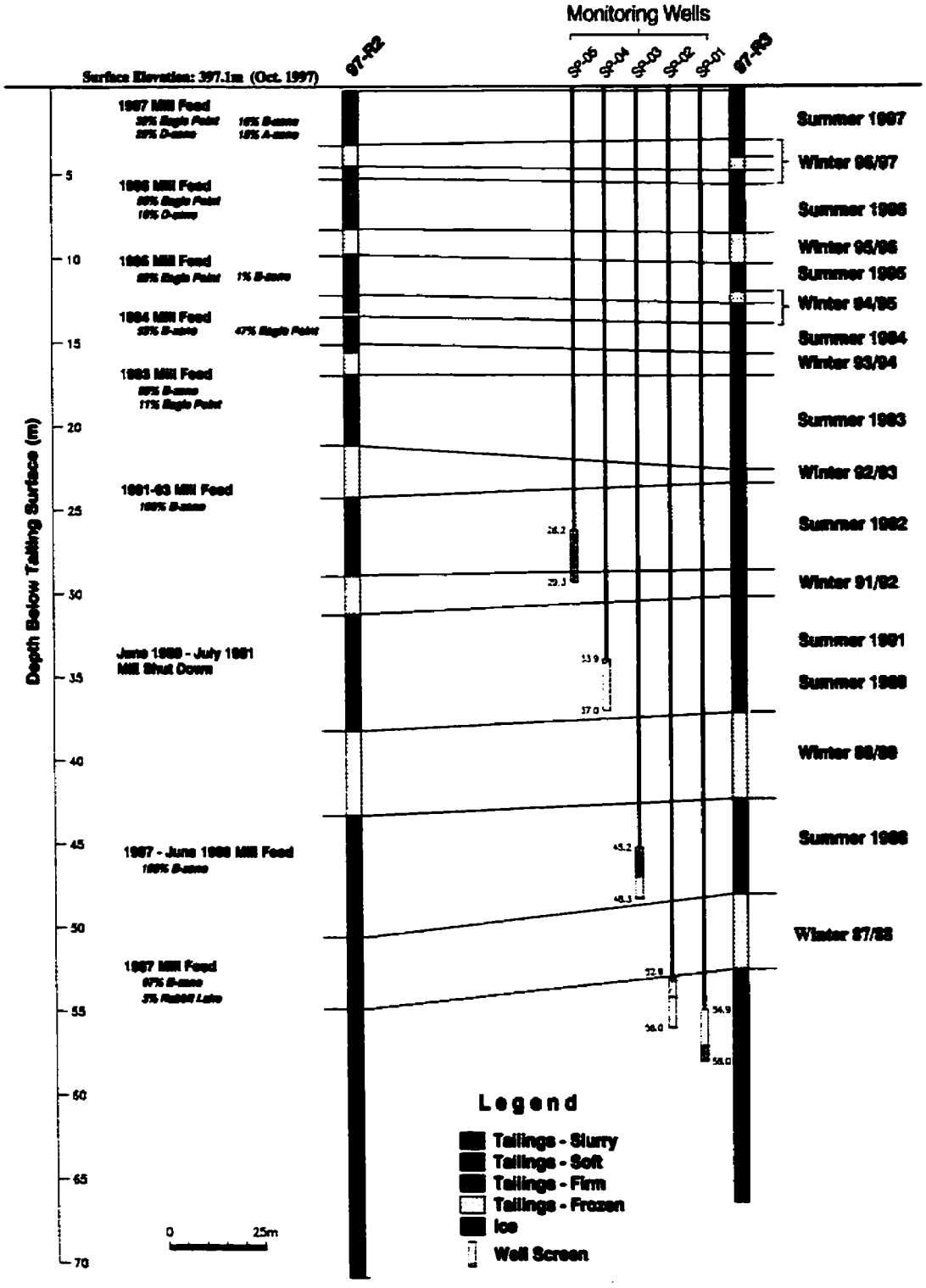

Figure 3.2

Stratigraphy of the tailings between bore holes 97-R2 and 97-R3. Timing of tailings deposition is presented on the right side of figure, ores used in the mill feed are presented on the left side of the figure, and the screened depths of the monitoring wells are presented to the left of 97-R3.

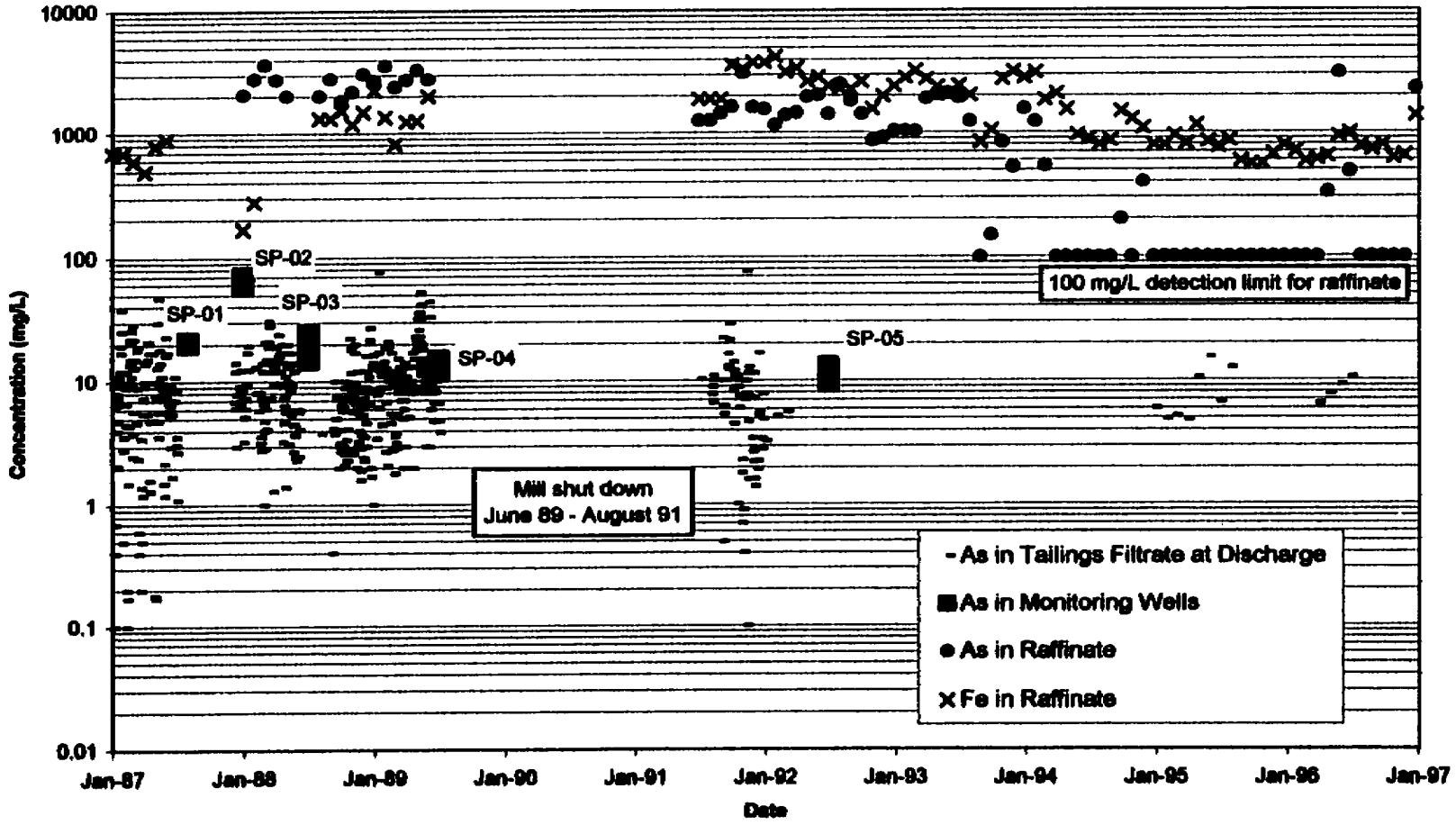

Figure 3.3 Arsenic concentrations in samples of tailings porewaters, tailings discharge, and raffinate with time in the tailings management facility using monthly raffinate discharge data from 1987 to present day and daily tailings discharge data from June 1988 to June 1989.

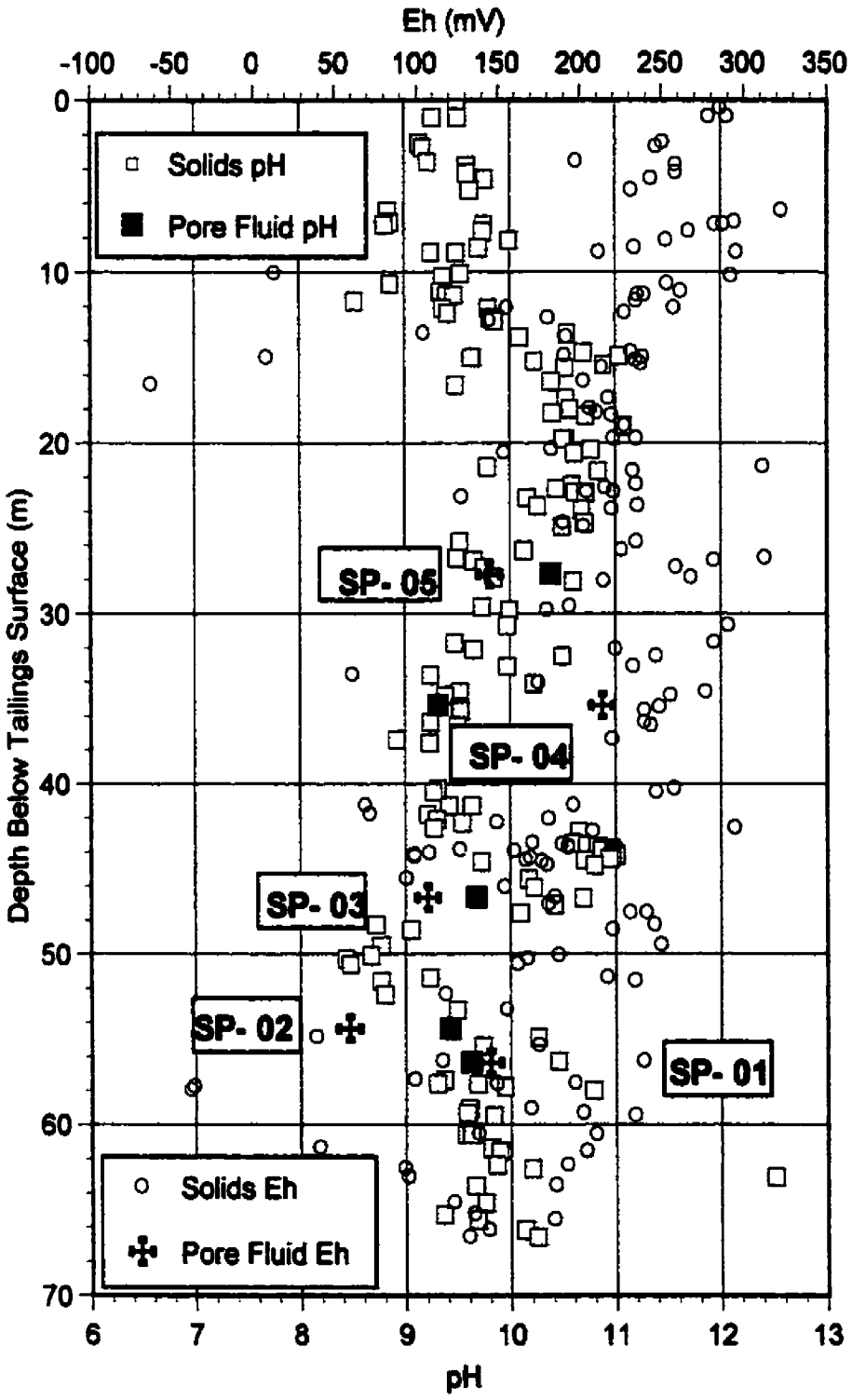

Figure 3.4 Plots of Eh for tailings and monitoring wells versus depth

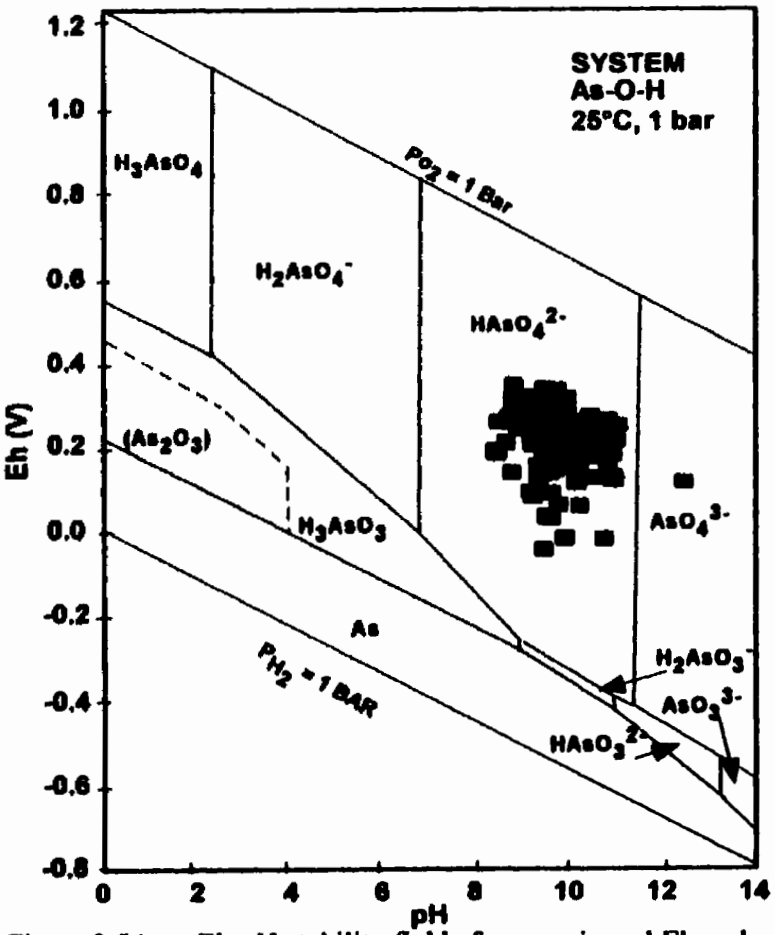

Figure 3.5A Eh-pH stability fields for arsenic and Eh and pH measurements from 97-R3 tailings solids Brookins, 1988 activity of As=10^{-6}.

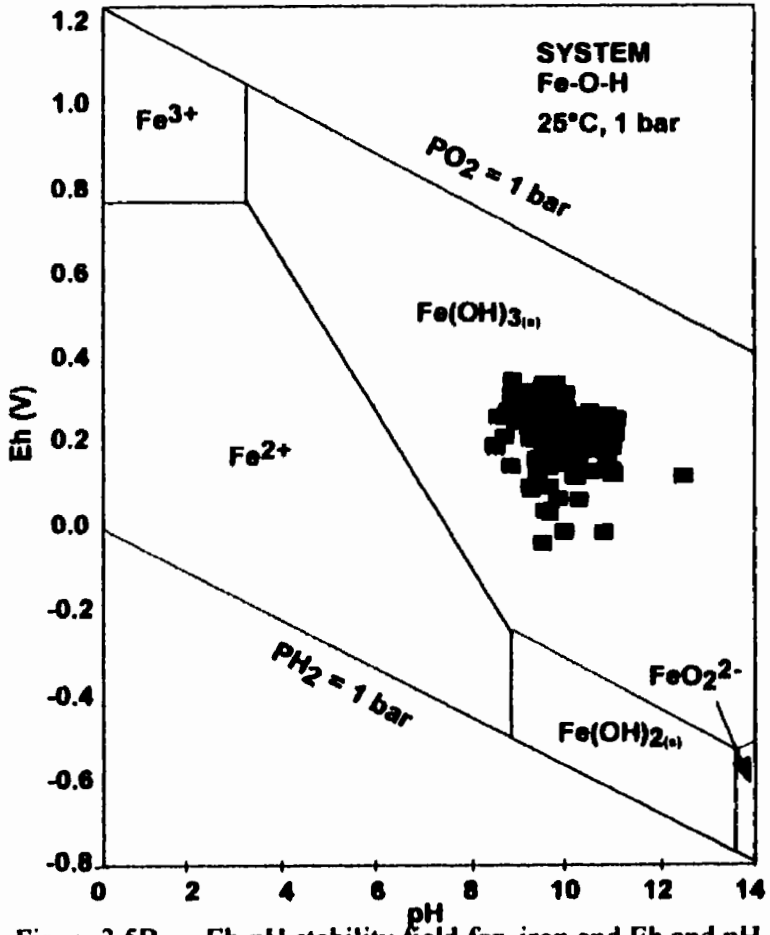

Figure 3.5B Eh-pH stability field for iron and Eh and pH measurements from 97-R3 tailings solids. Brookins, 1988 activity of Fe=10^{-6}.

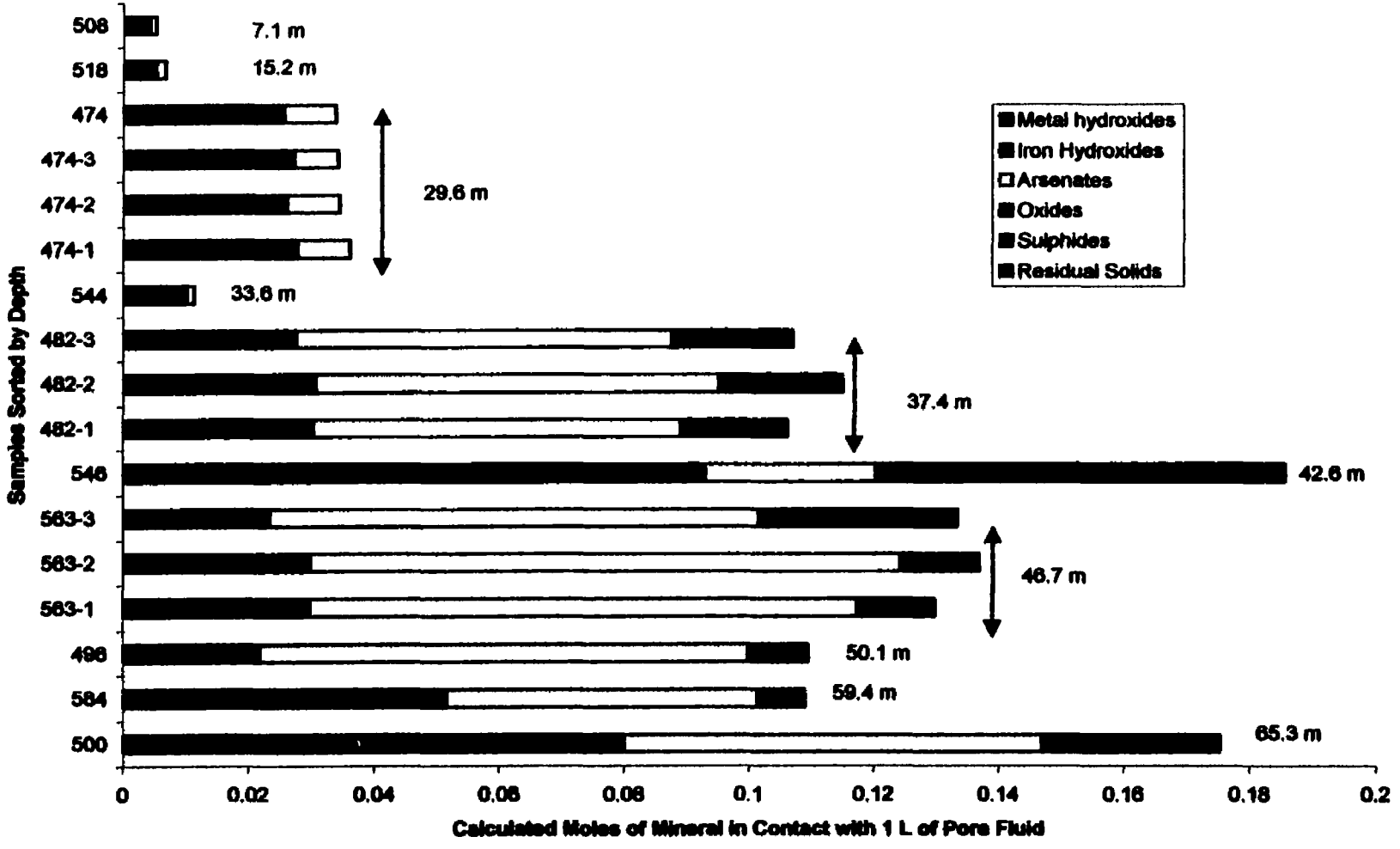

Figure 3.6 Distribution of As phases in tailings samples calculated from sequential extraction and whole rock analysis results.

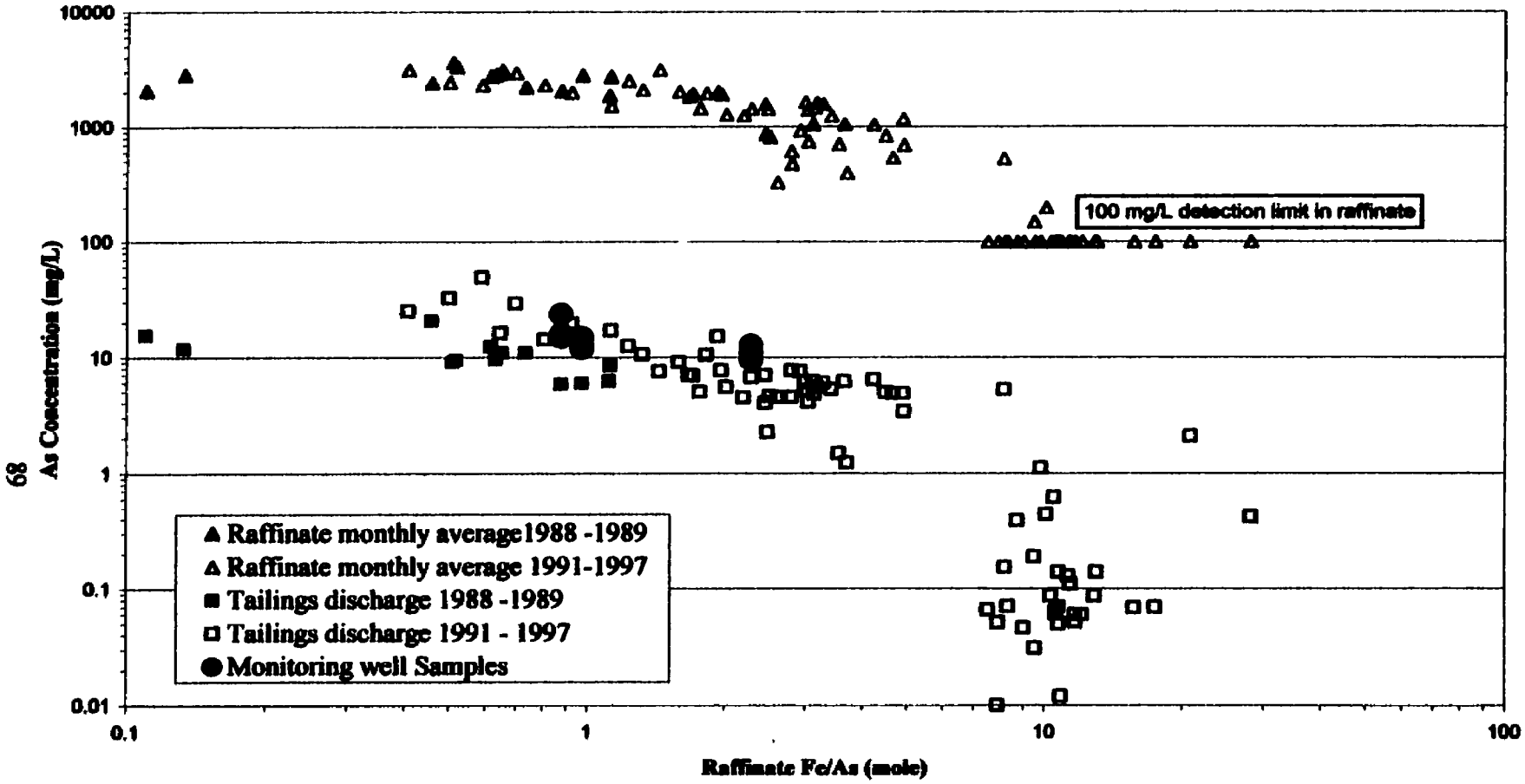

Figure 3.7 Dissolved arsenic concentrations versus molar Fe/As ratios of associated raffinate for monthly raffinate, tailings discharge, and monitoring well pore fluid samples.

CHAPTER 4.0 DIFFUSIVE-REACTIVE TRANSPORT ANALYSIS OF ARSENIC FROM AN IN-PIT URANIUM TAILINGS MANAGEMENT FACILITY, SASKATCHEWAN CANADA.

ABSTRACT

The Rabbit Lake uranium mine, located in northern Saskatchewan, Canada, uses an in-pit tailings management facility (TMF) to dispose of mill wastes. The in-pit TMF at Rabbit lake was constructed by placing a high hydraulic conductivity (0.01 m/s) layer, called a pervious surround, around the outside of the mined out pit. The pervious surround consists of a 5 m thick filter sand adjacent to the tailings and 1 m coarse rock drain adjacent to the pit wall. The rationale for in-pit disposal is that the presence of a more permeable zone surrounding the tailings mass minimizes the hydraulic gradient across the tailings, thereby limiting the contaminant flux from the tailings to a diffusion process. The objective of this research was to study the diffusive transport of arsenic from the tailings pore fluids into regional groundwater present within the filter sand using both a multi species reactive transport model and a single species diffusion model. The analyses were based on measurements of tailings and regional groundwater chemistry made at the Rabbit Lake in-pit TMF.

Redox conditions in the regional groundwater were found to be crucial to the prediction of geochemical conditions, arsenic transport and arsenic speciation in the filter sand. Using oxidizing or reducing conditions in the pervious surround had different effects on the predicted pH and speciation of arsenic. Under reducing conditions in the filter sand, arsenate in the tailings is be reduced to arsenite as arsenic diffuses into the filter sand. Iron as Fe^{2+} in the filter sand is oxidized to Fe(III) as the sulphate S(VI) diffuses into the filter sand and is reduced to sulphide S(-II). The pH in the tailings will decrease as the high concentrations (10^{-8} M) of protons (lower pH) in the filter sand diffuse into the tailings. As

the solubility of calcium arsenate minerals present in the tailings are pH dependent. the decrease in pH in the tailings causes an increase in solubility of the calcium arsenate minerals resulting in the dissolution of these minerals.

4.1 INTRODUCTION

Approximately a third of the world production of uranium is currently mined in the Athabasca Basin in northern Saskatchewan, Canada (Natural Resources Canada, 1998). Processing of this uranium ore in northen Saskatchewan has produced in excess of 31M tonnes of mill tailings (Scissons, 1997). Uranium tailings management practices in Canada have evolved from the deposition of tailings into topographic lows or natural lakes for mines in production in the 1950's (Beaverlodge, Gunner and Laredo) to engineered above ground tailings facilities for mines in production in the 1960's and 1970's (Cluff Lake and Rabbit Lake). The need for larger storage facilities and operational problems for above ground tailings storage facilities such as freezing and grain size segregation, led to the development of a third generation of disposal facilities, the engineered in-pit tailings management facilities (TMF). In-pit tailings management is the preferred method of tailings management in northern Saskatchewan. Recently commissioned facilities at Key lake and McClean Lake use in-pit disposal technology.

An in-pit TMF is an engineered facility constructed within a mined-out open pit (Figure 4.1). The rationale for in-pit disposal is that the presence of a more permeable zone surrounding the tailings minimizes the hydraulic gradient across the tailings thereby limiting the advective transport of contaminants from the tailings. The mass flux from the tailings into the regional groundwater is then controlled by diffusion from the tailings rather than advection through the tailings. Limiting the mechanism of mass flux to diffusion was thought to minimize the flux of contaminants into the groundwater system (Gulf, 1981). The in-pit TMF at Rabbit lake was constructed by placing a high hydraulic conductivity (0.01 m/s) layer of rock in combination with a sand filter, called a pervious surround, around the outside of the mined out pit. In the JEB pit at the McClean lake mine, where the hydraulic conductivity of the host rock for the pit is high, a natural pervious surround is already present thereby eliminating the need for a constructed surround. Misfeldt et al. (1999) provides a

description and analysis of the hydraulics of in-pit pervious surround and natural surround designs.

The design of in-pit facilities in Saskatchewan has focused on the geotechnical and hydrogeological aspects of TMF performance. The fate and transport of solutes from the in-pit facilities to regional groundwater regimes has been studied using two or three dimensional, finite difference and finite element, advection-dispersion models of single species (Cameco, 1994; Cogema, 1997; Geocon, 1984; Gulf, 1981). Geochemical analyses of the tailings has been limited to the evaluation of the concentration of the source terms for target constituents (e.g. As, Ni, U, and Ra^{226}) and the definition of attenuation mechanisms through the use of empirical measurements of adsorption coefficients. Source term solute concentrations have been determined from prototype tailings produced from bench-scale pilot plants and maximum solute concentrations at downstream receptors were predicted using constant source concentrations over the design life of the TMF (approximately 10,000 years).

The geochemistry of the tailings fluids is very different from that of the regional groundwater surrounding the tailings facility. Tailings pore fluids at Rabbit Lake have a high pH (9-11) and high concentrations of dissolved salts, metals, and nutrients (Donahue and Hendry, 1999; Donahue et al., 1999). The tailings solids contain significant masses of arsenic, nickel, and calcium sulphate minerals, which have the potential to chemically interact with the pore fluid. The regional groundwater surrounding the Rabbit Lake pit has a pH between 7.5 and 8, low total dissolved solids and strong reducing conditions (Donahue, 2000). The reduced groundwater conditions are part of the mechanism for the formation of the uranium deposit. Uranium deposits in northern Saskatchewan are primarily unconformity type deposits which formed as a result of oxidizing water containing uranium, mixing with reducing waters resulting in the precipitation of uranium (Marmont, 1988).

The Rabbit Lake site was chosen for the analysis because it is the longest operating in-pit tailings facility in northern Saskatchewan. In addition, the detailed geochemical information required for reactive transport analysis is also available (Donahue and Hendry, 1999; Donahue et al., 1999). The objective of this study was to compare the diffusive transport of arsenic from the tailings pore fluids into the regional groundwater within the filter sand as predicted by a multiple species reactive transport model and a single species

non-reactive transport model. These analyses are based on the insitu geochemical conditions present within the Rabbit Lake in-pit tailings facility and in the regional groundwater surrounding the TMF. The fate and transport of arsenic from the TMF is of particular interest in these analyses due to its environmental and regulatory significance. The simulations have a number of significant limitations and assumptions but illustrative the potential for geochemical interaction between the tailings pore fluids and regional groundwater.

Two numerical models were used to investigate solute transport and speciation. The POLLUTE numerical model (Rowe and Booker. 1990) was used to simulate single species. one-dimensional. non-reactive diffusive transport. PHREEQC (Parkhurst and Appelo. 1999) was used to simulate multi species diffusive-reactive transport.

4.2 NUMERICAL MODELS

The following sections present a brief explanation of the theory for the two numerical models.

4.2.1 POLLUTE

POLLUTE is a one dimensional model that simulates the migration of a single dissolved species through saturated, heterogeneous soil. The model was originally developed by Rowe and Booker (1985) to simulate contaminant transport from a landfill into a natural hydrogeologic system. The model is based on a semi-analytical solution of the one dimensional advection-dispersion equation, subject to the appropriate boundary conditions for a given problem. This semi-analytical model was chosen over finite difference models to avoid problems of numerical dispersion that may result from inappropriate discretization. The problem is divided into layers, each layer being defined in terms of thickness (th), effective molecular diffusion coefficient (De), Darcy velocity (v), porosity (n), dry density (ρd) and adsorption coefficient (Kd). Because POLLUTE was used to simulate non-reactive transport an adsorption coefficient was not used.

4.2.2 PHREEQC

PHREEQC was developed by the U.S. Geological Survey to perform a variety of aqueous geochemical calculations. PHREEQC is based on an ion-association aqueous model and can be used to calculate aqueous solute speciation, mineral saturation indices, reaction

path modeling and one dimensional solute transport calculations. Transport simulations can incorporate reversible reactions utilizing minerals, gases, solid-solutions, surface-complexation and ion exchange. One dimensional transport calculations are done using the advection-dispersion-reaction equation (Parkhurst and Appelo, 1999):

$$\frac{\partial C}{\partial t} = -v\frac{\partial C}{\partial x} + D_L\frac{\partial^2 C}{\partial x^2} - \frac{\partial q}{\partial t} \qquad 4.1$$

where C is concentration in water (mol/kg H_2O), t is time, v is pore water velocity, x is distance, q is concentration in the solid phase (expressed as mol/kg H_2O in the pores), and D_L is the longitudinal hydrodynamic dispersion coefficient (m^2/s). Hydrodynamic dispersion is defined as $D_L = De + \alpha_L v$, where D_e is the effective diffusion coefficient (m^2/s) and α_L the dispersivity (m). The term $-v\frac{\partial C}{\partial x}$ represents advective transport. $D_L\frac{\partial^2 C}{\partial x^2}$ represents dispersive transport and $\frac{\partial q}{\partial t}$ is the change in concentration in the solid phase. The PHREEQC program assumes that v and D_L are the same for all species. For diffusive transport the velocity is zero and Equation 4.1 simplifies to:

$$\frac{\partial C}{\partial t} = De\frac{\partial^2 C}{\partial x^2} - \frac{\partial q}{\partial t} \qquad 4.2$$

The transport part of equation 4.2 is solved with an explicit finite difference scheme that is forward in time, central in space and upstream for advective transport. The chemical interaction term $\frac{\partial q}{\partial t}$ is calculated separately for all solutes and for all reactions with solids after each time step. In each time step, advective transport is calculated first, followed by calculations for equilibrium and kinetically control reactions. Dispersive transport is then calculated followed again by calculations of equilibrium and kinetically controlled reactions. Calculating equilibrium and kinetically controlled reactions both before and after each advection step and after each dispersive step reduces numerical dispersion (Parkhurst and Appelo, 1999)

4.3 METHODOLOGY

The first series of numerical simulations examined only diffusive transport between the tailings and the filter sand. The second series of simulations examined diffusion from the

tailings to the filter sand with a calcium arsenate and calcium sulphate mineral phase present in the tailings solids.

A number of assumptions were made to simplify the models, to reduce computer time and to more clearly observe the effects of reactive transport. The flow velocity in the filter sand is assumed to be equal to zero and the filter sand is assumed to contain regional groundwater. The coefficient of diffusion is the same for all species and the porosity of the tailings and filter sand were assumed to be equal. The filter sand is composed predominantly quartz minerals and is assumed to be inert. The arsenic adsorbed/coprecipitated with iron hydroxides was assumed to be stable in the tailings and unlikely to desorb. Chemical kinetics are not used.

The geometry used in the simulations was for a 10 m cross-section comprised of 5 m of tailings and 5 m of filter sand. The 10 m section was divided into 50, 0.2 m cells, for the PHREEQC model and 50 layers for the POLLUTE model. All simulations were run for 100 years, a long enough period to observe geochemical interactions without encroaching on boundary conditions. The time step was set to a half a year (15768000 s). Simulations using a quarter of a year (7884000 s) time steps provided identical results. The model parameters are presented in Table 4.1.

The initial pore fluid chemistry of the tailings was defined based on analysis and measurements from pore fluids collected from a tailings monitoring well. The pore fluid chemistry is from high arsenic low iron B-zone tailings representative of tailings with highest arsenic pore fluid and solids concentration (Donahue and Hendry, 1999). The chemistry of the pore fluids in the filter sand was based on measurements from a regional groundwater monitoring well. Results of chemical analysis for both wells is presented in Table 4.2.

The redox condition for the tailings and filter sand were defined using either redox couples or pE values. To define redox conditions using a redox couple in PHREEQC, the concentrations of each redox species must be defined. The arsenite (As(III)) and arsenate (As(V)) redox couple was used to define redox conditions in the tailings pore fluids and the sulphide (S(-II)) sulphate (S(VI)) redox couple was used to define redox conditions in the filter sand.

As mentioned above, redox conditions in PHREEQC can also be defined using a pE value. Two methods were used to calculate a pE value. The first method was to calculated a

pE from insitu Eh measurements made with a platinum silver/silver chloride electrode. The second method was to calculate a pE from the arsenite (As^{+3}) and arsenate (As^{+5}) concentrations in the tailings and the sulphide (S^{-2}) sulphate (S^{+6}) concentrations in the filter sand (Table 4.2). To speciate pore fluids according to a calculated pE, total dissolved elemental concentrations need to be defined, rather than a redox species (ie. sulphate S^{+6}). If sulphate is defined in PHREEQC then sulfur is speciated to sulphate regardless of whether the defined pE value indicates sulphide might be present. A summary of calculated pE values is presented in Table 4.2.

Simulations were run using different initial redox conditions and analyzed by interpreting predicted redox conditions, pH, and arsenic concentrations. For the analysis of predicted redox conditions, simulations were run using four different initial redox conditions. In simulation 1, redox conditions were defined by a pE calculated from Eh values measured with a silver/silver chloride platinum electrode in the tailings and regional groundwater. In simulation 2, redox conditions were defined by the arsenite (As^{+3}) and arsenate (As^{+5}) concentrations in the tailings and the sulphide (S^{-2}) and sulphate (S^{+6}) concentrations in the filter sand. In simulation 3, redox conditions in the tailings were defined by a pE calculated from the measured Eh and redox conditions in the filter sand were defined by the sulphide (S^{-2}) sulphate (S^{+6}) concentrations. Simulation 3 was required to determine whether initial redox conditions in the filter sand or the tailings had the more significant effect on the simulations results. In simulation 4, redox conditions were defined by pE values calculated from the arsenite (As^{+3}) and arsenate (As^{+5}) concentrations in the tailings and the sulphide (S^{-2}) and sulphate (S^{+6}) concentrations in the filter sand. Simulation 4 was used to examine the difference between speciation based on a defined pE or redox couple (simulation 2). To determine the governing redox couple in the simulations results pE values were also calculated for the sulphide redox couple using the sulphide (S^{-2}) sulphate (S^{+6}) concentration results of the simulations.

In the analysis of predicted pH, arsenic concentrations, and equilibrium mineral phase simulations only simulations using initial redox conditions 1 and 2 were presented. A summary of PHREEQC simulations are presented in Table 4.3

Simulations were also performed where calcium arsenate and gypsum mineral phases were defined for the tailings cells (Table 4.3). Simulations 5 and 6 were run with a calcium

arsenate mineral phase defined for the tailings cells. Simulations 7 and 8 were run with calcium arsenate and calcium sulphate mineral phases defined for tailings cells. If the mineral phase was calculated to be undersaturated with respect to the fluids in the cell, the mineral would be allowed to dissolve until mineral-water equilibrium conditions were satisfied. If the mineral phase was oversaturated with respect to the fluids in a cell then the mineral is precipitated until mineral-water equilibrium conditions were satisfied. PHREEQC performs calculations on a per litre of fluid basis therefor equilibrium minerals phases need to be defined in terms of the moles of mineral phase in contact with one litre of pore fluid. Sequential extraction analysis of tailings solids and field moisture content measurements indicated that 0.02 moles of calcium arsenate minerals per litre of pore fluid were available for dissolution in the tailings (Donahue and Hendry, 1999). Mineralogical analysis of the tailings sample indicates that calcium sulphate constitutes 0.3 to 54 wt% of the tailings solids (Donahue et al., 2000). For gypsum equilibrium phase simulations, 10 moles of gypsum per litre of pore fluid were available for dissolution in the tailings.

4.4 RESULTS AND DISCUSSION

The simulations were run for a 100 year period and the results for predicted solute concentrations, pH and pE profiles were interpreted. PHREEQC and POLLUTE simulations for conservative species (unreactive or unattenuated) provide identical results for diffusive transport of single species. This agreement can be observed for total arsenic, as discussed latter.

4.4.1 Diffusion Only Simulations

Determining representative redox conditions in the regional groundwater is critical to the results of the reactive-transport simulations. Available field measurement and analytical testing data yields a range in pE values for the regional groundwater. The pE calculated from the Eh measured with a silver/silver chloride electrode in the regional groundwater was –2.29 at 7.97° C(Eh = –128 mV absolute). The pE calculated using the measured sulphide-sulphate redox couple was –4.47 (–248 mV). The effect of the different initial redox conditions on the

results of the simulations are evident in the predicted values of pE and pH and in the speciation of arsenic.

Figure 4.2 presents the predicted redox conditions for diffusive transport between the tailings and filter sand under a variety of initial redox conditions. Using the redox conditions defined by the measured Eh in the tailings and filter sand (simulation 1 and chart symbol ■) results in oxidizing conditions developing in the filter sand. Using redox conditions defined by the concentrations of sulphide and sulphate in the filter sand and arsenite and arsenate concentrations (simulation 2 and chart symbol •) in the tailings results in a slight increase in pE in the tailings (-2.97 to –2.63), a decrease in pE at the leading edge of the diffusive plume (3.5 m to 4.0 m) and an increase in pE in the filter sand adjacent to the tailings (4.3 m to 5.0 m). The simulation using the measured redox conditions in the tailings and the sulphide-sulphate redox couple in the regional groundwater (simulation 3 and chart symbol ▲) predicts pE conditions near the tailings interface that are almost identical to those of simulation 2. Oxidizing conditions are initially present in the tailings but the pE decreases rapidly in the tailings to the As^{+3}/As^{+5} redox couple as the species diffuse.

Simulations were also run using redox conditions defined by a pE calculated from As^{+3}, As^{+5}, S^{-2} and S^{+6} concentrations in the pore fluids (simulation 4 and chart symbol △). In these simulations initial pE conditions were set to the calculated pE for the sulphate and sulphide concentrations in the filter sand and the arsenate and arsenite concentrations in the tailings. Total dissolved arsenic and sulfur concentrations were specified so that PHREEQC would use the defined pE for speciation. The results of this simulation are similar to the results for the simulation for redox conditions defined by the concentrations of sulphate, sulphide, arsenate, and arsenite in the pore fluids (simulation 2, •). The results are similar because PHREEQC uses a similar method to calculate pE but uses all redox couples present in solution. Simulation 4 does, however, show a more pronounced increase in pE (greater than initial conditions) at the interface of the two fluids than simulation 2. For both simulation 2 and simulation 4, the increase in pE at the interface is the result of decreasing sulphide concentrations at the interface. At the interface, sulphides are diffusing into the tailings and oxidizing to sulphate and sulphate is diffusing into the filter sand and reducing to sulphide. The net result of the counter diffusion of sulphate and sulphide species is low sulphide concentration in the mixing zone (Figure 4.3) which produces a higher pE (Figure

4.2). The difference between these two simulations is attributed to slightly different initial sulphide concentrations. Defining a pE and total dissolved sulfur concentration (simulation 4) speciated slightly less sulphide ($1.12x10^{-5}$ mole/L) than was measured in the regional groundwater ($4.98x10^{-5}$ mole/L used in simulation 2). It should be noted that detection limits for sulphide are in the $1.0x10^{-7}$ to $1.0x10^{-6}$ mole/L range so it would be impossible to measure sulphide concentrations in the $1.0x10^{-26}$ to $1.0x10^{-18}$ mole/L range predicted in the mixing zone and tailings by these simulations.

Figure 4.2 shows pE values calculated using the concentrations of sulphide and sulphate predicted in the PHREEQC for simulations 2 and 4. In both simulations the pE calculated from the sulphide-sulphate redox couple is very close to the pE predicted for the simulations suggesting that the sulphide-sulphate redox couple is the governing redox reaction in the simulations.

Redox reactions require both a reducing half cell reaction and an oxidizing half cell reaction. Iron is present in the filter sand pore fluids ($6.67x10^{-7}$ mole/L). Under low pE conditions iron is present as Fe(II). As the solutes diffuse, iron in the filter sand is oxidized to Fe^{+3}. The governing redox reactions are as follows:

$$SO_4^{2-} + 9H^+ + 8e^- = HS^- + 4H_2O \qquad 4.3$$

$$Fe^{2+} = Fe^{3+} + e^- \qquad 4.4$$

As sulphate diffuses into the filter sand it is reduced by the oxidation of Fe^{2+}. Equations 4.3 and 4.4 show that eight moles of Fe^{2+} are required to reduce sulphate to sulphide. Figures 4.3 and 4.4 show the results of different redox conditions on the sulfur and iron species, respectively. They show that as sulphate diffuses into the filter sand iron is oxidized from Fe^{2+} to Fe^{+3} and sulphate is reduced to sulphide at the leading edge of the sulphate plume (Figure 4.3) thus creating an oxidizing plume that is migrating into the filter sand (Figure 4.4).

Figure 4.5 presents the predicted pH profile for diffusion simulations using different initial redox conditions (discussed above). The pH is initially 9.4 in the tailings and 8.0 in the regional groundwater system. This represents a 1.5 order magnitude difference in H^+ concentrations between the two fluids. As the solutes diffuse, the pH decreases in the tailings and increases within the filter sand. Using both the As^{+3}/As^{+5} and S^{-2}/S^{6+} redox couples for

the filter sand and tailings (simulation 2), respectively, or the S^{-2}/S^{6+} redox couple in the filter sand and measured pE in the tailings (simulation 3) results in very similar predicted pH profiles. The pH in the tailings decreases and the pH in the filter sand increases to about pH 9.0. The pH in the filter sand adjacent to the tailings increases rapidly by one pH unit, equivalent to an order of magnitude decrease in H^+ concentration. This rapid rise is attributed to the complexation of protons with the large numbers of dissolved species diffusing from the tailings fluids. The diffusion of solutes under these conditions is complex. Solutes are diffusing in both direction across the tailings filter sand interface. Protons are diffusing from the filter sand to the tailings and other solutes (As, Ni, SO_4^{2-}, etc.) are diffusing from the tailings into the filter sand.

When measured Eh values are used to define initial redox conditions (simulation 1), the pH profile has a shape similar to the simple single species diffusion case. The POLLUTE simulation of H^+ concentration shows a classic diffusion profile (Figure 4.5) which is not the same as the pH profile predicted by the PHREEQC for either simulation 1 or 2. As pH is a function of the interaction of all species in solution, it is not surprising that a single solute model could not predict the changes in pH for the diffusion of two solutions of different pH.

The pH profile for the PHREEQC simulations that use the S^{-2}/S^{+6} redox couple in the filter sand (simulations 2, 3 and 4) have a "Ski Jump" shape. The slight increase in pH at the interface of the two solutions (pH 9.0 at 5m to pH 9.05 at 4.3 m) is a result of a rapid decrease in $HAsO_4^{-2}$ and a gradual increase in H_3AsO_3 and $H_2AsO_3^{-1}$ concentrations up to a distance of 4.3 m where they begin to decrease (Figure 4.5). Under reducing conditions in the filter sand, arsenate species (AsO_4^{-3}) are reduced to arsenite species (AsO_3^{-3}) as they diffuse into the filter sand from the tailings. Arsenite species are polyprotic acids similar to the arsenate species but have a slightly different complex stability field (Figure 4.6). For arsenite complexes, the H_3AsO_3 complex is the dominant species up to pH 9. Above pH 9, H_3AsO_3 deprotonates to $H_2AsO_3^{-1}$ (Figure 4.6). As the arsenate diffuses into the filter sand it is reduced to an arsenite species and the dominant species changes from $HAsO_4^{-2}$ to H_3AsO_3 (Figure 4.7) increasing the pH (Figure 4.5) . While the arsenate species are diffusing into the filter sand the high concentration of H^+ (pH 8.0) in the filter sand are diffusing into the low H^+ concentrations (pH 9.4) in the tailings. The net effect of the counter diffusions and speciation change is an increase in pH at the mixing front in the filter sand (Figure 4.5).

The pH profile predicted using the measured redox conditions has a similar shape to that of the pH profile predicted using POLLUTE but shows very little increase in pH in the filter sand (Figure 4.5). Measured Eh conditions in the filter sand are not sufficiently reducing enough (Figure 4.2) to reduce sulphate to sulphide or arsenate to arsenite and the dominant species remains $HAsO_4^{-2}$ (Figure 4.8). As a result, there are not enough S^{-2} or As^{+3} species present in the filter sand to complex with the H^+ and increase the pH in the filter sand.

The use of the As^{+3}/As^{+5} redox couple or the measured Eh to define initial redox conditions in tailings has little effect on the results of the PHREEQC simulations in the prediction of As speciation, pH, or redox conditions in the filter sand (Figure 4.5).

Figure 4.9 presents the arsenic concentrations within the tailings and filter sand versus distance for diffusive transport. The total dissolved arsenic, as measured by the commercial laboratory that did the As^{+3} and As^{+5} speciation (Total As = 58 mg/L) was lower than the total arsenic measured by the local analytical laboratory (71 mg/L). Description of the analytical methods for arsenic determination are presented in (Donahue and Hendry, 1999). Consequently, the simulation concentrations were normalized to initial arsenic concentrations (C/Co) to allow for comparison of reactive transport simulations using total arsenic concentrations measured redox conditions, and the As^{+3} and As^{+5} redox couple.

The POLLUTE simulation results match the total arsenic curve for simulations 1 and 2. No attenuation processes were used in either simulation so the concentration profiles from both simulations show a classic diffusion profile. In the PHREEQC simulations using the S(-II/VI) redox couple to define redox conditions in the filter sand (simulation 2), As^{+5} is reduced to As^{+3} as it diffuses into the reducing conditions present in filter sand. Simulation 1 using measured redox conditions predict no reduction of As^{+5} to As^{+3} and As^{+5} is stable in the regional groundwater (Figure 4.6). Changing redox conditions in the tailings from the As^{+5}/As^{+3}redox couple to measured redox conditions (simulation 3) produced results identical to simulation 2.

The low dissolved oxygen concentration and the presence of sulphide in the regional groundwater indicates strongly reducing conditions (Donahue, 2000). These measurements along with the inherent unreliability of measuring redox conditions in natural systems with a platinum electrode (Thorstenson, 1984) suggests that the sulphide-sulphate redox couple is a

better measure of the redox conditions in the filter sand. Simulations using the sulphide-sulphate redox couple are likely a better indication of the interaction of the filter sand and tailings pore fluids.

The simulations indicate that as the solutes in the tailings pore fluids and regional groundwater mix the pH will decrease in the tailings and increase in the regional groundwater. A change in pH in the tailings should influence the solubility of the calcium arsenate minerals present in the tailings because the solubility of calcium arsenate minerals is pH dependent (Bothe and Brown, 1999a; Bothe and Brown, 1999b). A decrease in pH in the tailings should increase the solubility of calcium arsenate minerals. Analysis of the tailings pore fluids indicates that total dissolved arsenic concentrations are close to equilibrium concentrations for the calcium arsenate minerals ($Ca_4(OH)_2(AsO_4)_2{:}4H_2O$) thought to be present in the tailings (Donahue and Hendry, 1999).

4.4.2 Diffusion with Equilibrium Mineral Phases in Tailings Simulations

Figure 4.10 presents PHREEQC simulations of diffusive transport of arsenic with equilibrium mineral phases present in the tailings (simulation 5,6,7 and 8). Predicted equilibrium arsenic concentrations in the presence of the calcium arsenate mineral, $Ca_4(OH)_2(AsO_4)_2{:}4H_2O$, in the tailings is 84 mg/L, slightly higher than the measured arsenic concentration of 71 mg/L. These two values represent essentially equal source terms for the transport modeling of arsenic from the in-pit TMF. The results of the PHREEQC simulations lie between the POLLUTE curves for a fixed concentration source and the finite mass source. The fixed concentration POLLUTE simulation produces a high mass flux and arsenic diffuses approximately 0.5 m farther into the filter sand. The POLLUTE simulation using a finite mass source has a lower mass flux because it can not account for the arsenic released by the dissolution of the arsenate mineral phase. The PHREEQC simulation predicts a calcium arsenate mineral dissolution rate of 1.25×10^{-5} mole/year for the cell directly adjacent to the filter sand. Assuming there is approximately 0.02 moles of calcium arsenate mineral per litre of pore fluid available (Donahue and Hendry, 1999) it would take approximately 1500 years to consume the available calcium arsenate in a 0.2 m thick layer in the tailings directly adjacent to the filter sand.

The pH profile for diffusive transport with equilibrium phase calcium arsenate (simulations 5 and 6) is presented in Figure 4.11. Equilibrating the tailings fluids with the

arsenate mineral causes an increase in pH to a value of 10. The dissolution of 1 mole $Ca_4(OH)_2(AsO_4)_2{\cdot}4H_2O$ produces 2 moles AsO_4^{-3}, which in the tailings solutions, protonates to $HAsO_4^{-2}$. The formation of the $HAsO_4^{-2}$ complex decreases the H^+ concentration and raises the pH in the tailings solution. Single solute diffusion models do not account for pH changes as a result of mineral dissolution (Figure 4.11). Simulation 6 run with the S(-II/VI) redox couple and equilibrium calcium arsenate in the tailings show slightly higher As concentrations with time and a lower pH (Figure 4.10 and 11). The lower pH conditions increase the calcium arsenate solubility which results in higher As concentrations with time.

Calcium sulphate ($CaSO_4$) precipitates in the tailings as a results of the tailings neutralization process. Mineralogical analysis of the tailings sample indicates that calcium sulphate constitutes 0.3 to 54% of the tailings solids (Donahue et al., 2000). Geochemical analysis of the tailings pore fluids indicate that the pore fluids are in thermodynamic equilibrium with gypsum (Donahue and Hendry, 1999). The diffusive profile for both calcium arsenate and calcium sulphate equilibrium mineral phases (simulations 7 and 8) results a slight decrease in arsenic concentration and pH compared to simulations 5 and 6 which use only a calcium arsenate mineral phase (Figure 4.10 and 11). This decrease is attributed to the common ion effect from Ca^{2+}, which is present in both the calcium sulphate and calcium arsenate minerals.

4.5 CONCLUSIONS

The diffusive transport simulation results indicate that single solute diffusion models (POLLUTE) can not predict changes in pH, Eh, and As speciation as result of diffusive mixing of solutes from tailings pore fluids and the regional groundwater in the filter sand.

The selection of redox conditions in the regional groundwater was critical to the prediction of redox conditions in the filter sand. The redox conditions in the filter sand had a dominant influence on the predicted pH and speciation of arsenic within the filter sand. The presence of sulphide in the regional groundwater samples indicates that reducing conditions are present in the regional groundwater around the Rabbit Lake in-pit TMF. Reducing conditions in the regional groundwater cause As(V), the dominant species in the tailings, to be reduced to As(III) as arsenic diffuses from the tailings into the filter sand. Arsenite is

thought to be more mobile and more toxic to certain species (Cogema, 1997, Korte and Fernando, 1991).

The interaction of fluids within the filter sand and the tailings appear to be dominated by an iron-sulfur oxidation-reduction reaction under reducing conditions in the filter sand . Iron is speciated as Fe^{2+} in the filter sand and is oxidized to Fe(III) as the sulphate (S(VI)) diffuses into the filter sand and is reduced to sulphide (S(-II)). The iron-sulfur redox couple was the dominant redox reaction for initial redox conditions defined by sulphide-sulphate redox couple or a by a low pE.

Because the pH is lower in the filter sand (pH 8.0) than in tailings (pH 10), the pH will decrease in the tailings as the high concentrations of protons (lower pH) in the filter sand diffuse into the tailings. Because the solubilities of calcium arsenate minerals present in the tailings are pH dependent, the decrease in pH causes an increase in the solubilities of the calcium arsenate minerals. This results in the dissolution of calcium arsenate minerals causing an increase As concentration.

Diffusive transport analysis using a fixed concentration source term results in a higher mass flux of arsenic with time as compared to that due to reactive transport using an equilibrium arsenic mineral phase in the tailings. Using both a calcium arsenate and calcium sulphate equilibrium mineral phase in the tailings results in lower predicted As concentrations in both the tailings and filter sand than for the case where only calcium arsenate equilibrium mineral phases are used. Less calcium arsenate can dissolve because of the common (Ca^{2+}) ion effect.

Acknowledgements

Thanks to Tony Appelo for his help with the PHREEQC models and to Donald Langmuir for his help with arsenic thermodynamics.

4.6 REFERENCES

Bothe J. V. and Brown P. W. (1999a) Arsenic Immobilization by Calcium Arsenate Formation. *Environment Science and Technology* (accepted for publication 1999).

Bothe J. V. and Brown P. W. (1999b) The Stabilities of Calcium Arsenates. *Journal of Hazardous Materials* (Accepted for publication 1999).

Brookins D. G. (1988) *Eh-pH Diagrams for Geochemistry*. Springer-Verlag. 176

Cameco. (1994) Environmental Impact Statement Deilmann In-pit Tailings Management Facility. Cameco Corporation. Environmental Impact Statement. Report C101104. November 1993. Saskatoon.

Canada N. R. (1998) Canadian Uranium Statistics Fact Sheet. Natural Resources Canada. Uranium and Radioactive Waste Division, Energy Resources Branch. Ottawa.

Cogema. (1997) MaClean Lake Project - JEB Tailings Management Facility. Cogema Resources Inc. EIS. File 812B. December 4 1997. Saskatoon.

Donahue R. B. (2000) Appendix D Regional groundwater analysis. Geochemistry of Arsenic in the Rabbit Lake In-pit Uranium Tailing Management Facility, Saskatchewan Canada. Ph.D.. University of Saskatchewan.

Donahue R. D. and Hendry M. J. (2000) Geochemistry of Arsenic in Uranium Mill Tailings. Rabbit Lake. Saskatchewan. Canada Canada. *Journal of Applied Geochemistry*. **5**. No.8 1097-1119.

Donahue R. D., Hendry M. J., and Landine P. (1999) Distribution of Arsenic and Nickel in Uranium Mill Tailings. Rabbit Lake, Saskatchewan. Canada. *Journal of Applied Geochemistry* Accepted for publication April 1999.

Geocon. (1984) Progress Report no. 1. Design of Pervious Envelope Disposal of Tailings in Rabbit Lake Pit. Geocon Inc. T10782-1, July 1984.

Gulf. (1981) Environmental Impact Statement Collins Bay B-zone Development, Second Addendum. Gulf Minerals Canada Limited. June 1981. Saskatoon.

Korte N. E. and Fernando Q. (1991) A Review of Arsenic (III) in Groundwater. *Critical Review of Environmental Control* **21**, 1-36.

Marmont S. (1988) Unconformity -type Uranium Deposits. In *Ore Deposit Models* (ed. R. G. Robert and P. A. Sheahan), pp. Pages 103-131. Geological Association of Canada.

Misfeldt G. A., Loi J. I., Herasymuik G. M., and Clifton A. W. (1999) Comparison of tailings containment strategies for in-pit and above ground tailings management facilities. *52nd Canadian Geotechnical Conference*, Regina, Canada. Parkhurst D. L. and Appelo C. A. J. (1999) Users guide to PHREEQC - A computer program for speciation, reaction-path, 1D-transport and inverse geochemical calculations. U.S. Geological Survey Water Resources Inv.

Parkhurst D. L. and Appelo C. A. J. (1999) Users guide to PHREEQC - A computer program for speciation, reaction-path, 1D-transport and inverse geochemical calculations. U.S. Geological Survey Water Resources Inv.

Rowe R. K. and Booker J. R. (1985) 1-D pollutant migration in soils of finite depth. *ASCE Journal of Geotechnical Engineering* **111**(GT4), 13-42.

Rowe R. K. and Booker J. R. (1990) POLLUTE: 1-D Pollutant Migration Through A Non Homogeneous Soil. Geotechnical Research Centre, Faculty of Engineering Science. University of Western Ontario.

Scissons K. (1997) Saskatchewan Uranium Mine Tailings - Quantity to end of 1996. Saskatchewan Environment and Resource Management. Memo. File -37 - 20 - 0 - 0.

Thorstenson D. C. (1984) The Concept of Electron Activity and its Relation to Redox Potentials in Aqueous Geochemical Systems. U.S. Geological Survey. Open-File Report 84-072. 1984. Denver.

Table 4.1 Summary of Diffusion Model Parameters

PHREEQC Diffusion Model Parmeters	
Number of Cells	50
Cell length	0.2 m
Time step	15768000 s
Number of Steps	200
Diffusion Coefficient	1.0E-10 m^2/s
Cells 0-25 defined as pervious surround solutions	
Cells 26-50 defined as tailings pore fluid	
Equilibrium phase simulations	
Equilibrium phase defined for cells 26-50	
Ca4(OH)2(AsO4)2:4H2O	0.02 mole/L
Gypsum	10 mole/L

POLLUTE Diffusion Model Parameters	
Darcy velocity	0
Diffusion Coefficient	1.0E-10 m^2/s
Number of Layers	2
Layer 1 - 0 to 5 m	Tailings
thickness	5 m
Number of Sublayers	25 m
Porosity	0.3
Layer 2 - 5 to 10 m	Filter Sand
thickness	5 m
Number of Sublayers	25 m
Porosity	0.3
Initial Concentration Profile	0 to 5 m 71 mg/L

Table 4.2 Summary of Solution Chemistry Used in Numerical Simulations

Analysis	Monitoring Well SP-02 Tailings Pore Fluid	Assumed ‡ Filter Sand Pore Fluid	
Temperature	0.27 C	7.97 C	
pH	9.42	8.03	
Eh	+58 mV	-128 mV	
pE from measured Eh	1.07	-2.29	
Eh from As(3+/5+) redox couple	-161 mV		
Eh from S(2-/6+) redox couple		-248 mV	
pE from As(3+/5+) redox couple	-2.97		
pE from S(2-/6+) redox couple		-4.44	
Density	1	1	
Alkalinity		110 mg/L	as CaCO3
Ca	547 mg/L	13 mg/L	
Cl	610 mg/L	5.2 mg/L	
K	10 mg/L	4.5 mg/L	
Mg	19 mg/L	10 mg/L	
Na	553 mg/L	30 mg/L	
Sulfate	1630 mg/L	11 mg/L	
Sulfide	N.M.	1.7 mg/L	as H2S
Total sulfur	544 mg/L	3.7 mg/L	
B	0.082 mg/L	0.21 mg/L	
P	0.07 mg/L	N.D.	
Al	0.31 mg/L	0.014 mg/L	
Ba	0.032 mg/L	0.018 mg/L	
Cu	0.022 mg/L	N.D.	
Fe	0.001 mg/L	0.037 mg/L	
Mn	0.011 mg/L	0.039 mg/L	
Ni	0.087 mg/L	0.001 mg/L	
Pb	0.001 mg/L	N.D.	
Si	4 mg/L	4.6 mg/L	
Sr	1 mg/L	0.24 mg/L	
U	224 ug/l	N.D.	
Zn	0.007 mg/L	N.D.	
Total As	71 mg/L	2.5 ug/L	
As(III)	512 ug/l	N.M.	
As(V)	58183 ug/l	N.M.	

N.M. - not measured

N.D. - below detection limits

‡ Based on regional groundwater well 8.6.2 Rabbit Lake Mine

Table 4.3 A summary of PHREEQC simulations

Simulation	Initial redox conditions in filter sand	Initial redox conditions In tailings	Calcium Arsenate Mineral Phase	Calcium Sulphate Mineral Phase
1	pE calculated from measured Eh	pE calculated from measured Eh	No	No
2	Sulphate /sulphide concentrations	Arsenate/arsenite concentrations	No	No
3	Sulphate /sulphide concentrations	pE calculated from measured Eh	No	No
4	pE calculated from sulphate /sulphide concentrations	pE calculated from arsenate/arsenite concentrations	No	No
5	pE calculated from measured Eh	pE calculated from measured Eh	yes	No
6	Sulphate /sulphide concentrations	Arsenate/arsenite concentrations	yes	No
7	pE calculated from measured Eh	pE calculated from measured Eh	yes	yes
8	Sulphate /sulphide concentrations	Arsenate/arsenite concentrations	yes	yes

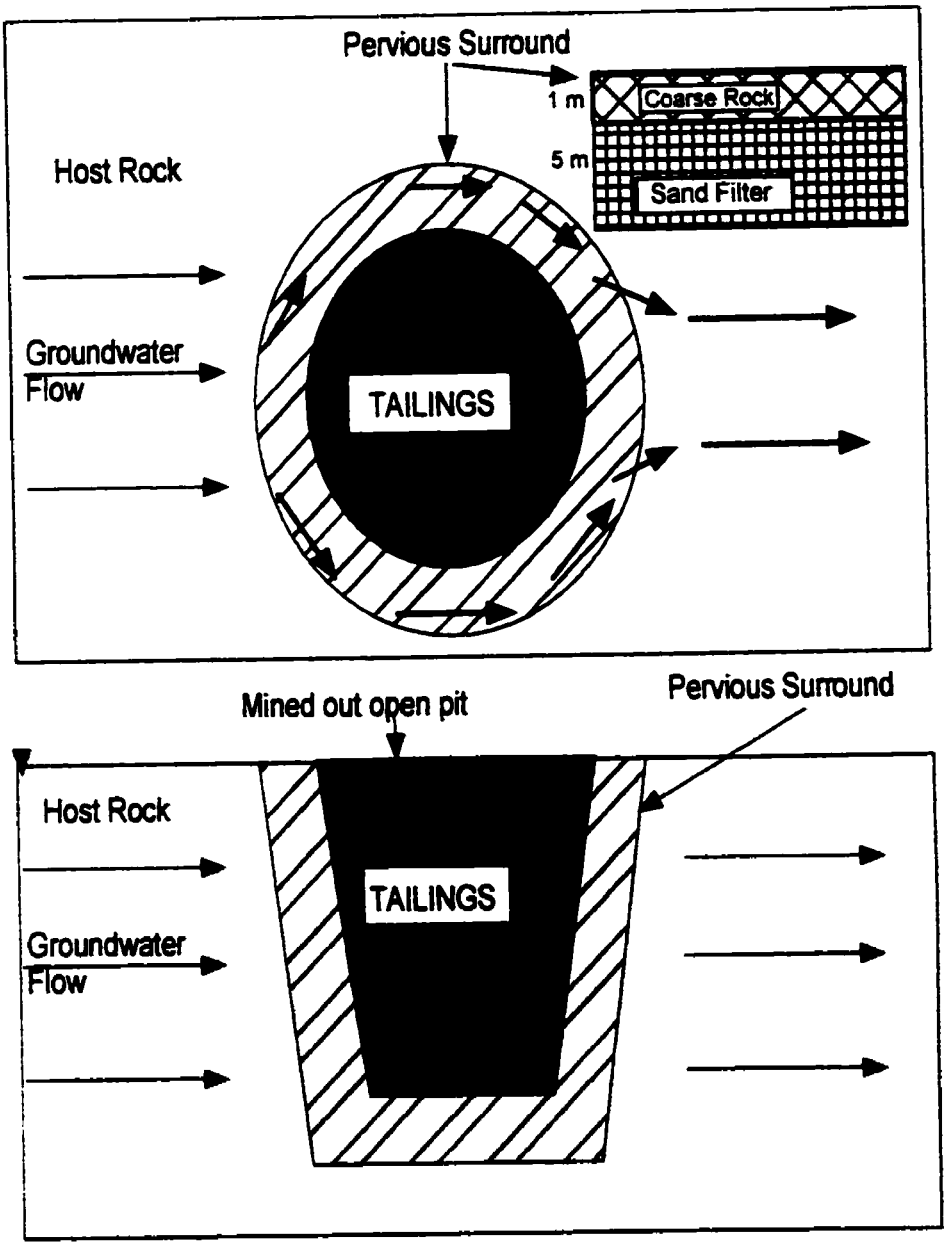

Figure 4.1 Sketch of pervious surround in-pit tailings management system.

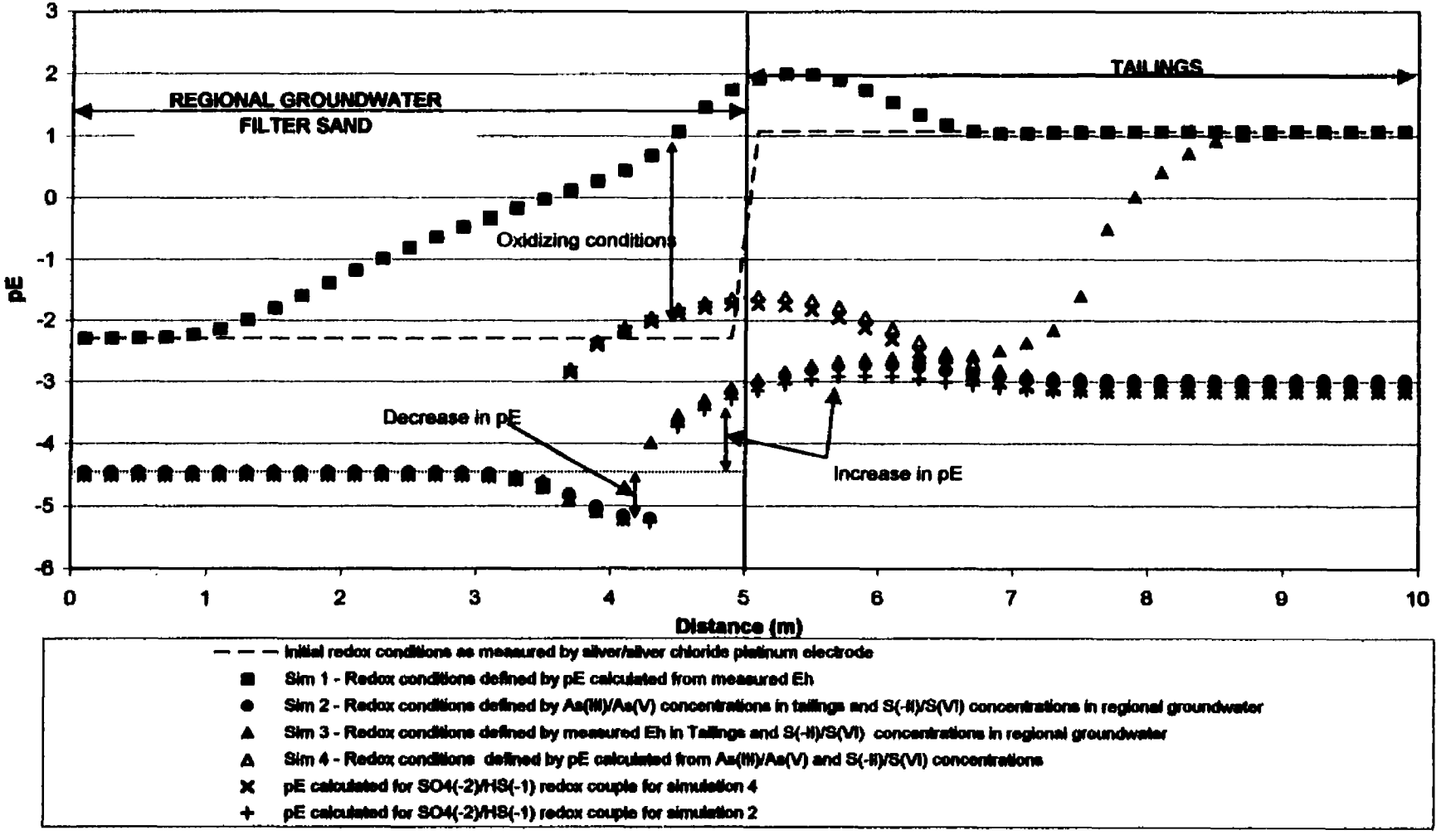

Figure 4.2 Predicted pE conditions from PHREEQC simulations after 100 years of diffusion.

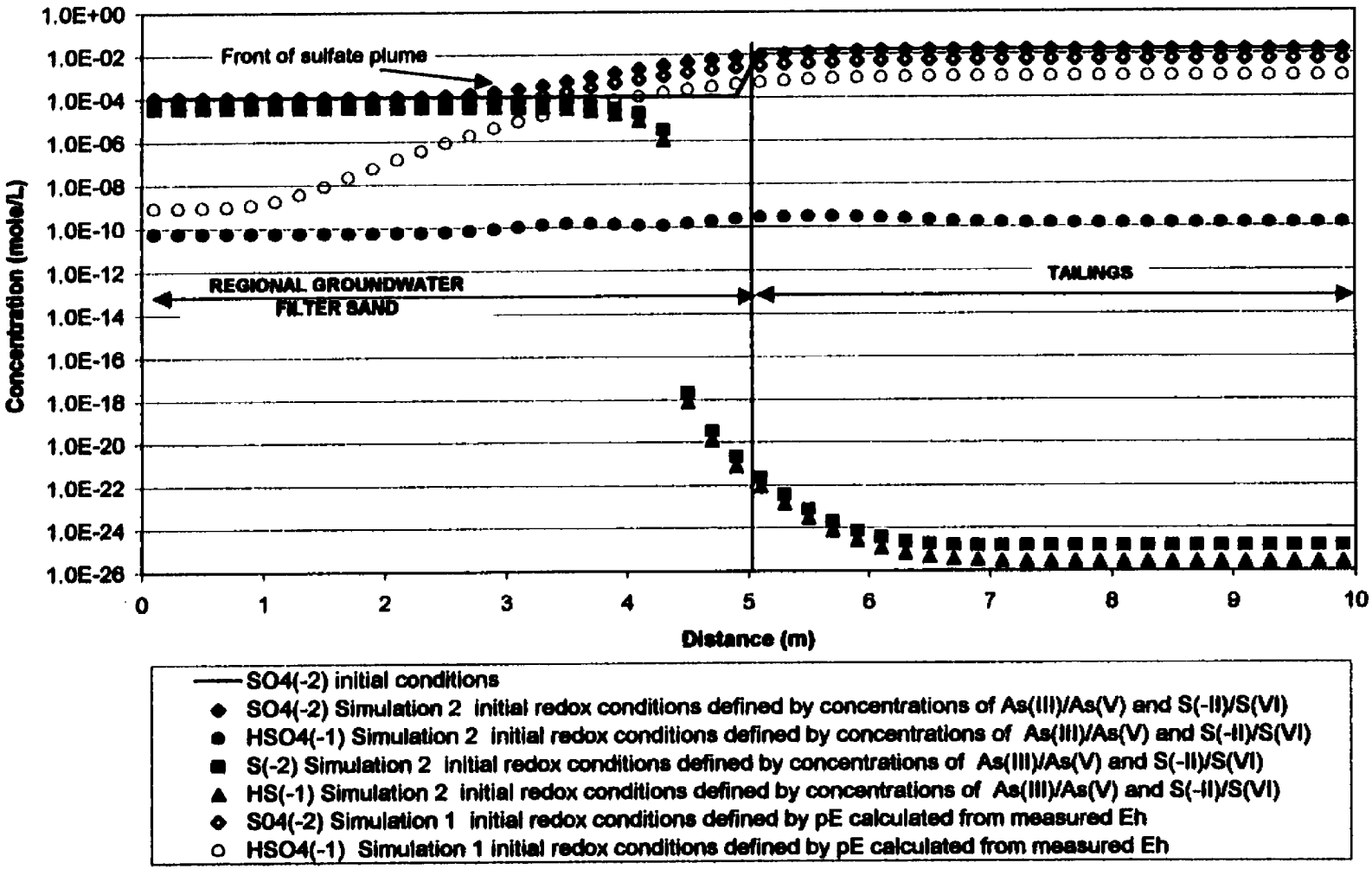

Figure 4.3 Sulphur speciation from PHREEQC simulations after 100 years of diffusion.

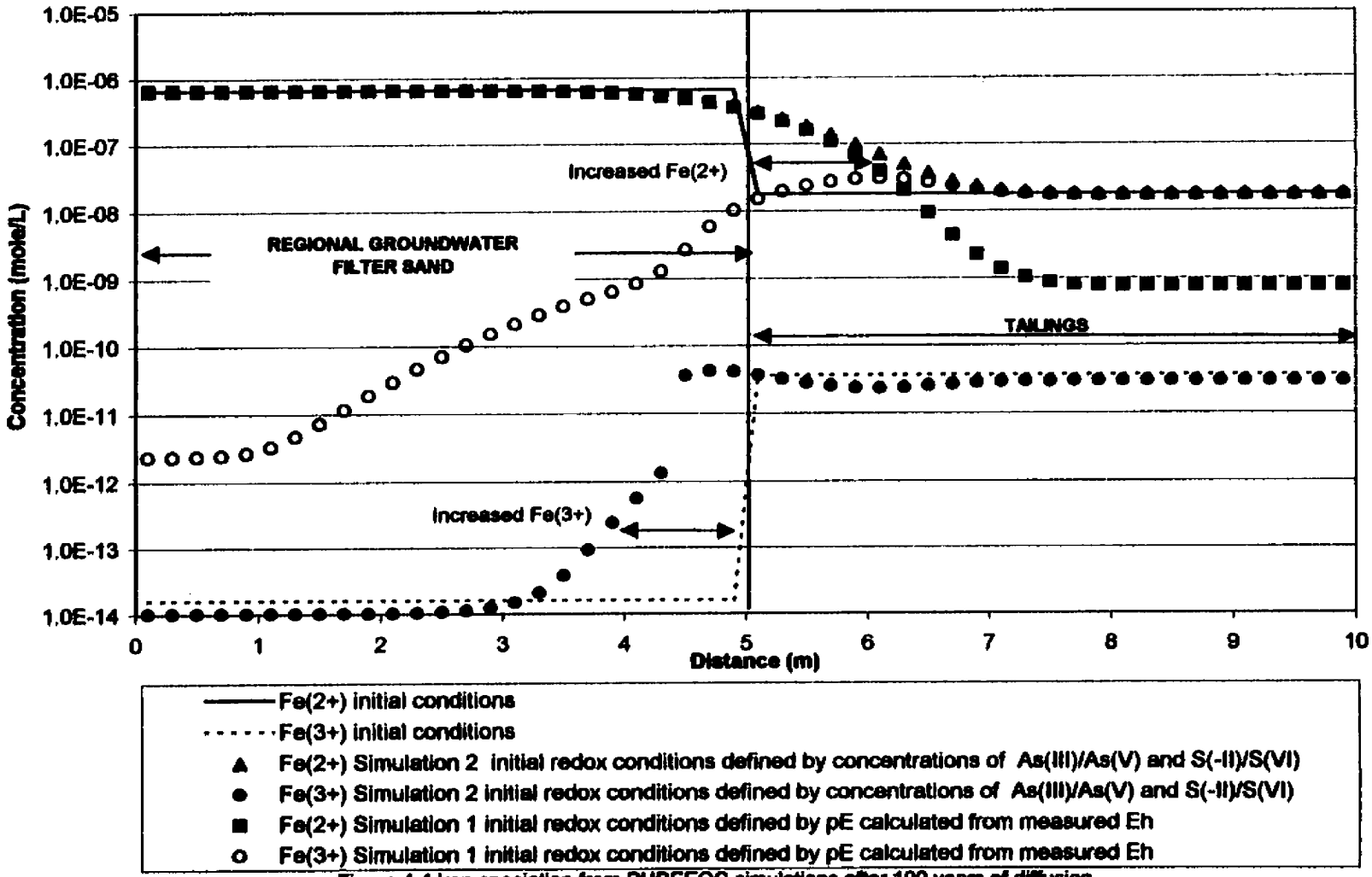

Figure 4.4 Iron speciation from PHREEQC simulations after 100 years of diffusion.

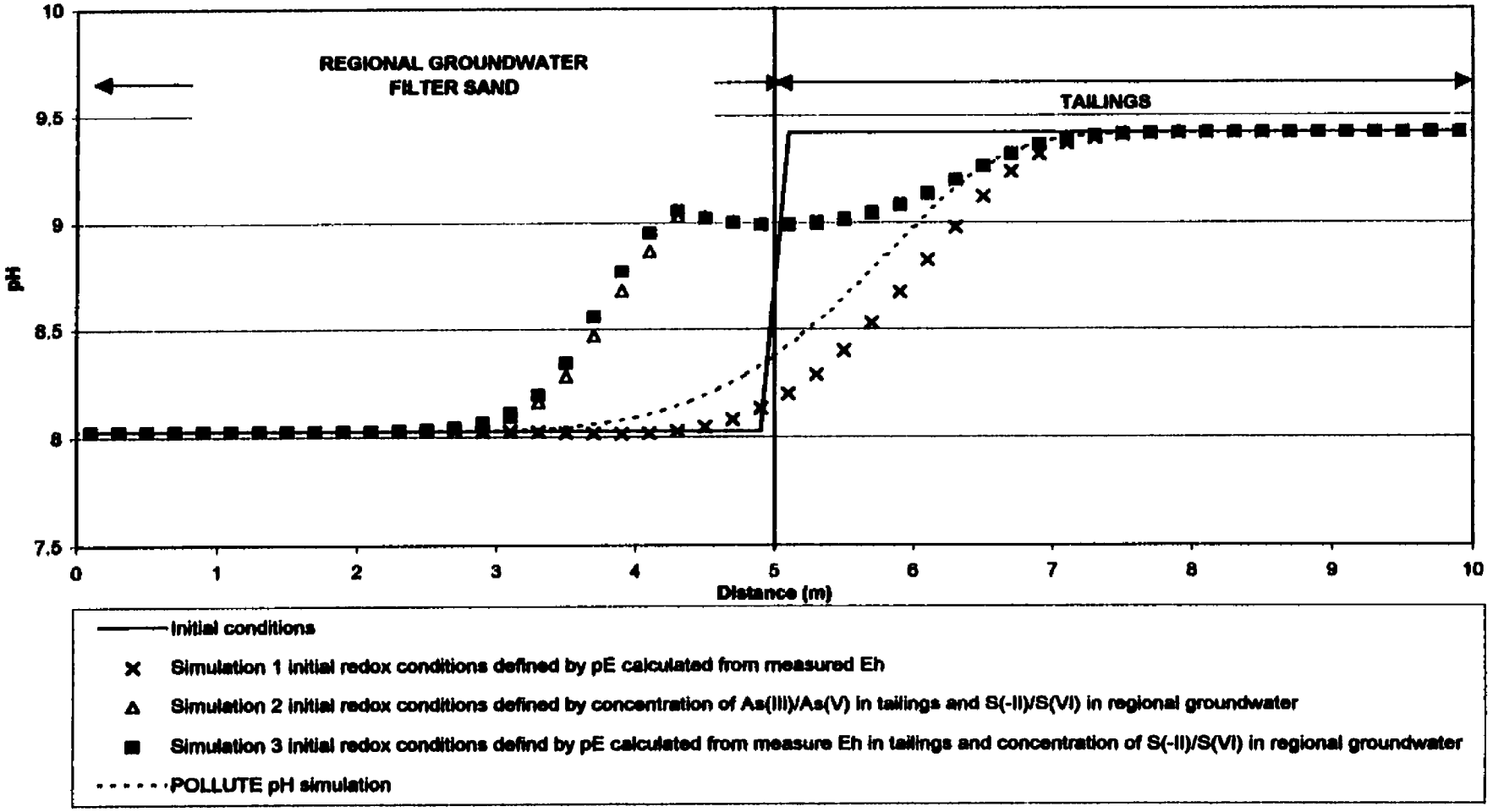

Figure 4.5 Predicted pH conditions from PHREEQC simulations after 100 years of diffusion.

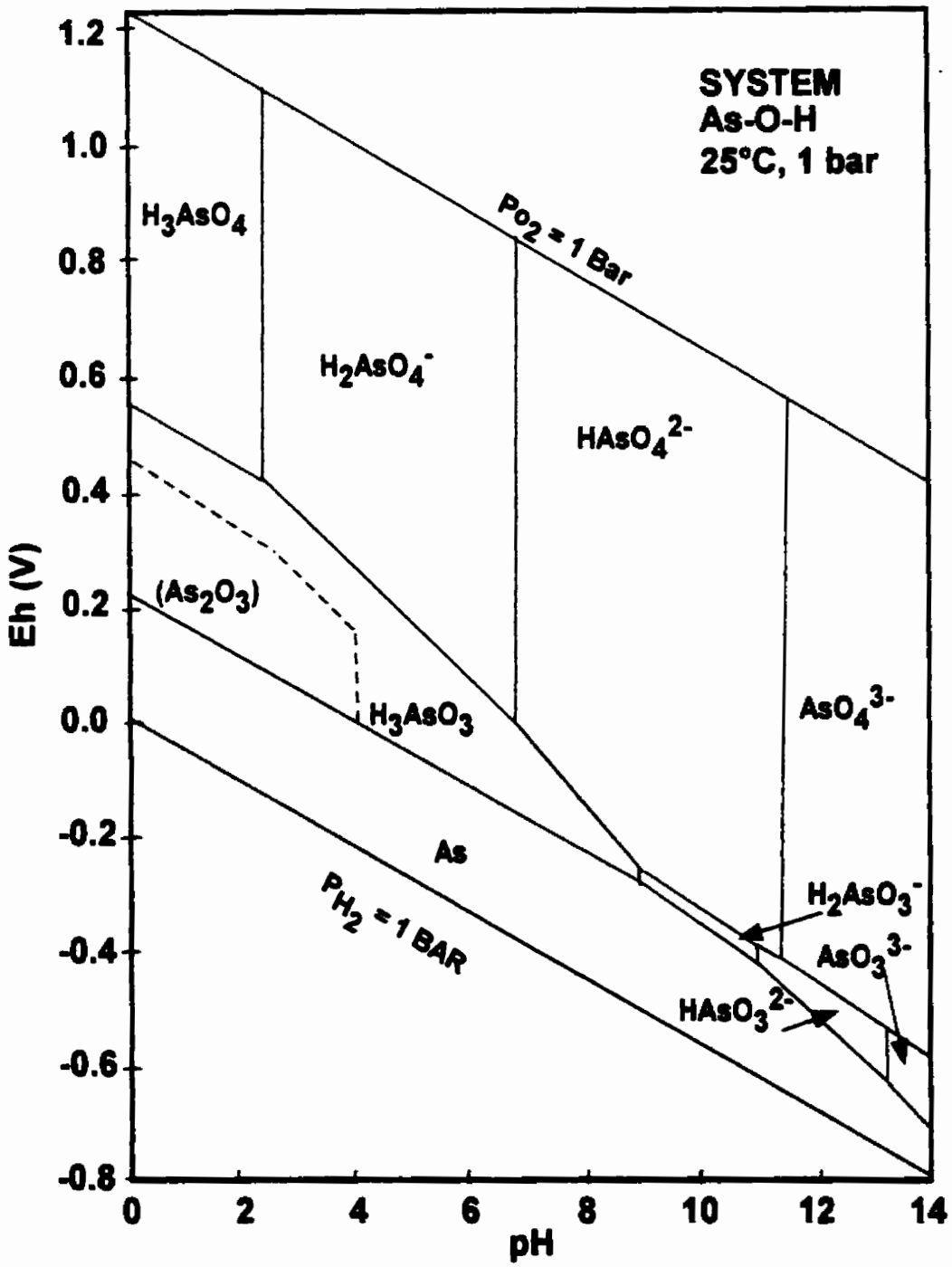

Figure 4.6 Eh-pH Diagram for Arsenic (Brookins, 1988)
activity of As = 10^{-6}

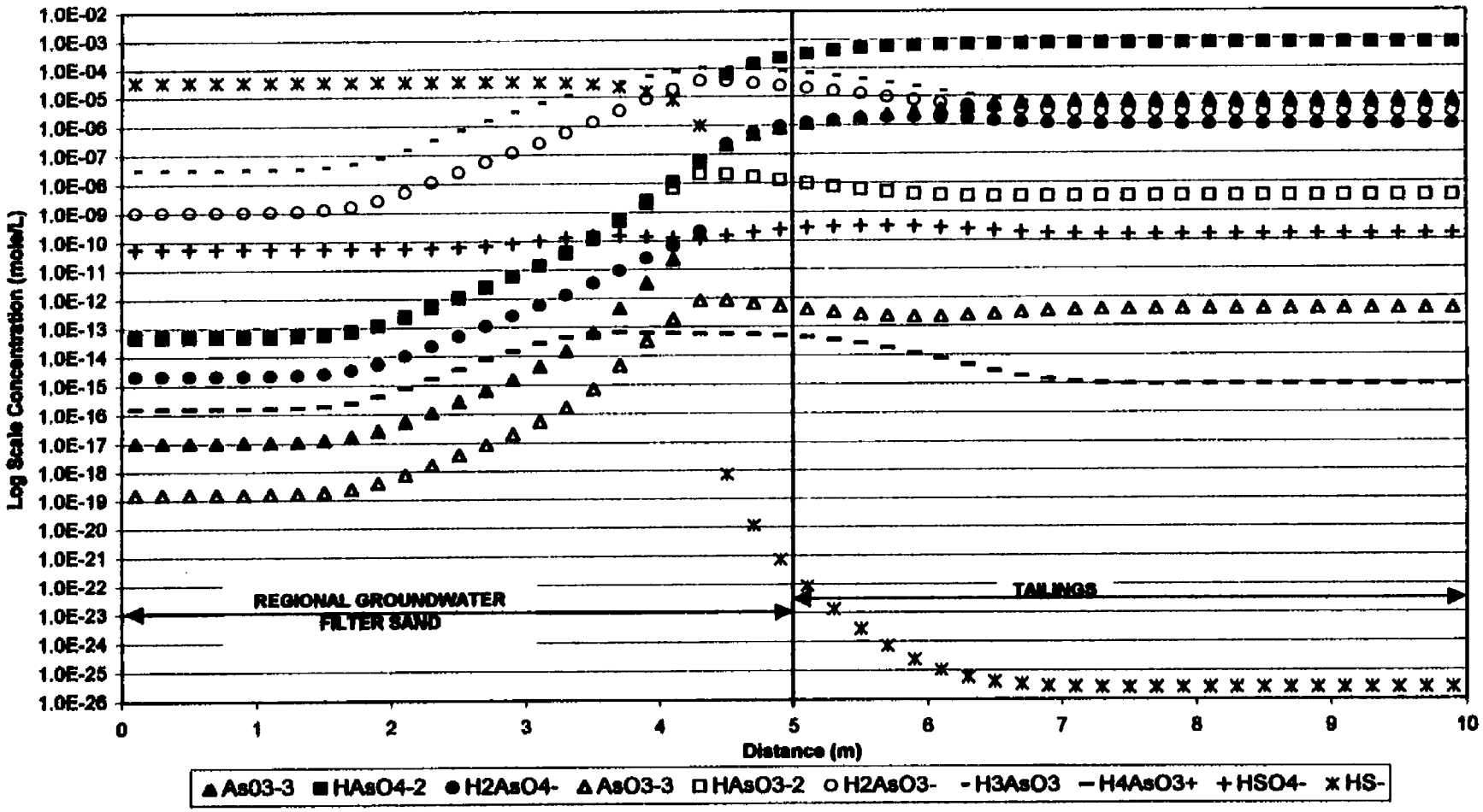

Figure 4.7 Predicted arsenic and sulphur complexes after 100 years of diffusion from PHREEQC simulation 2 using As(III)/As(V) redox couple in the tailings and the S(-II)/S(VI) redox couple in the pervious surround for initial redox conditions .

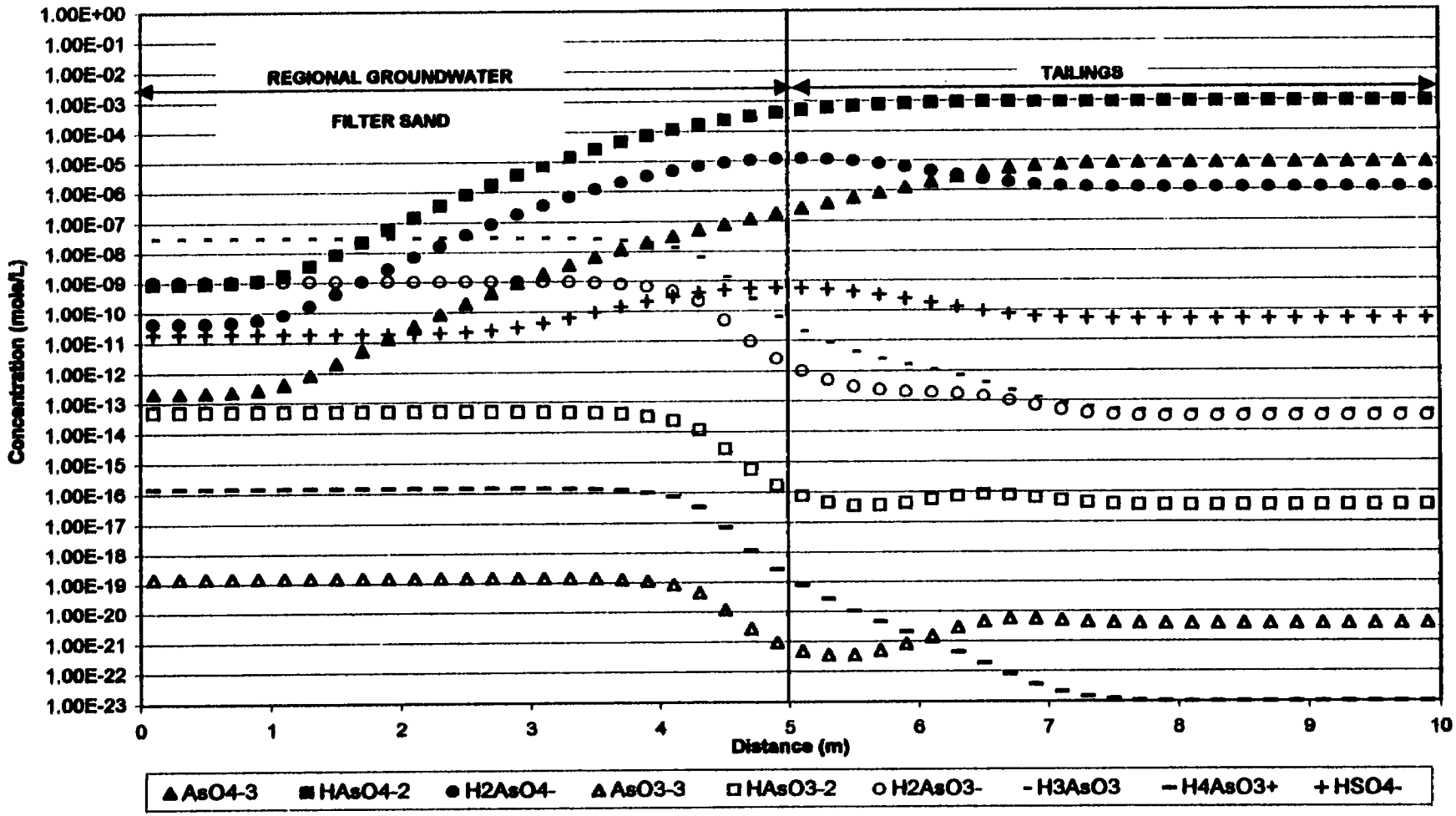

Figure 4.8 Predicted arsenic and sulfur complexes after 100 years of diffusion from PHREEQC simulation 1 using measured Eh conditions in the tailings and pervious surround for initial redox conditions.

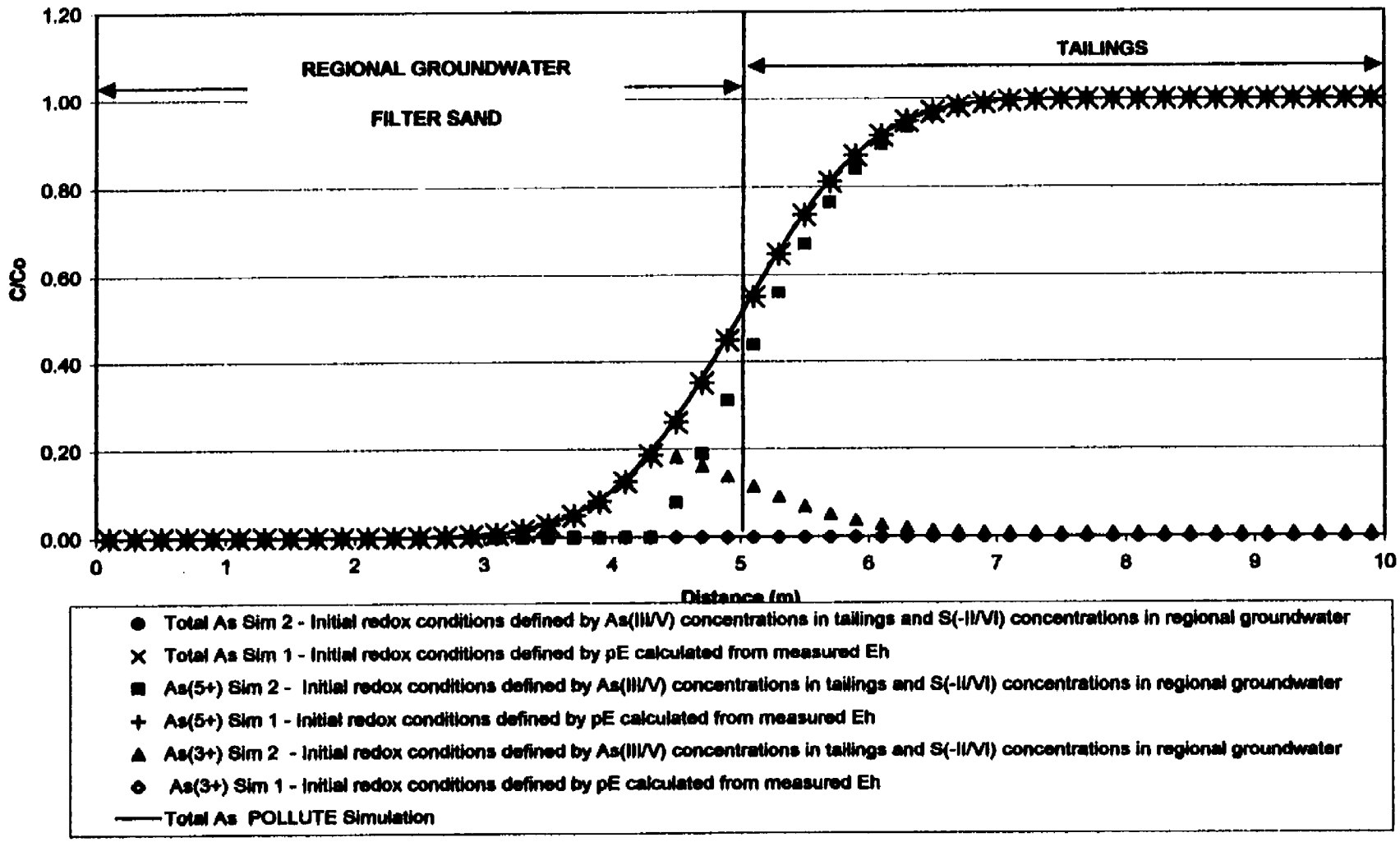

Figure 4.9 C/Co vs distance for arsenic after 100 years of diffusion.

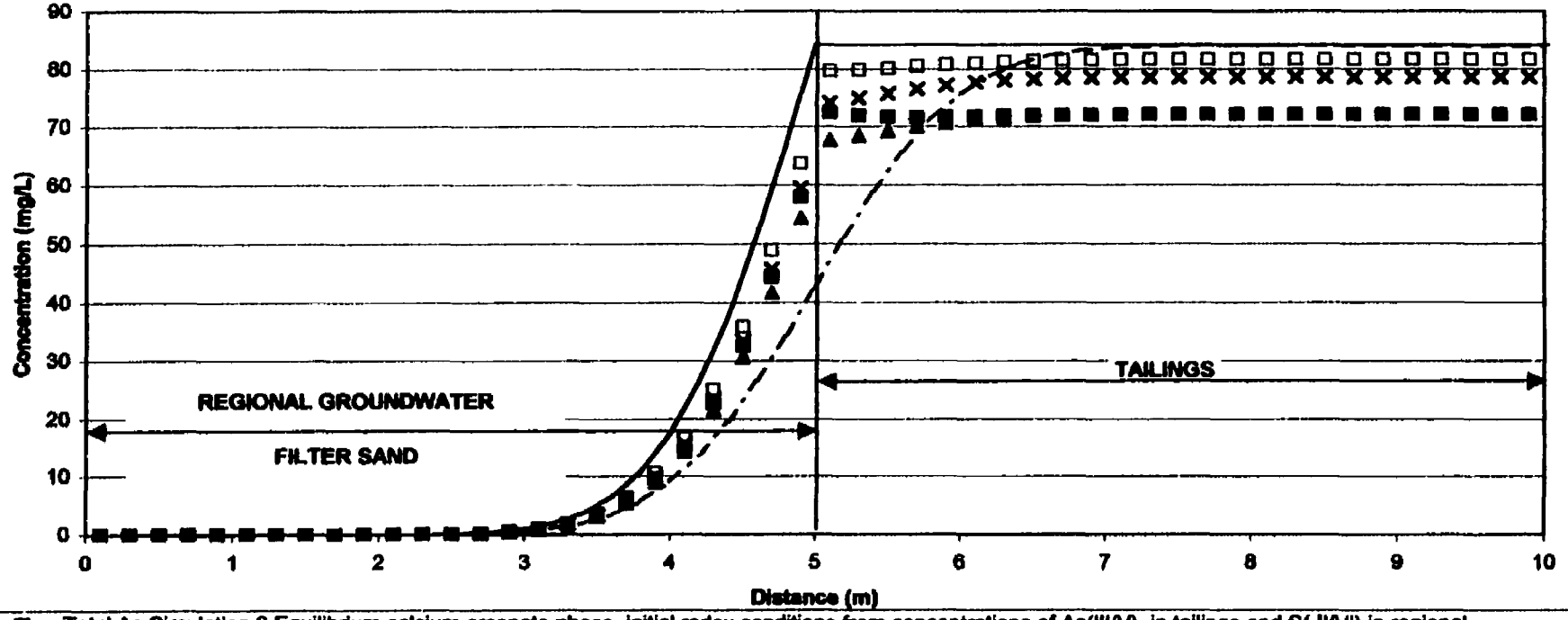

Figure 4.10 Arsenic concentrations versus distance after 100 years of diffusion for diffusive transport with equilibrium calcium arsenate phase present in tailings.

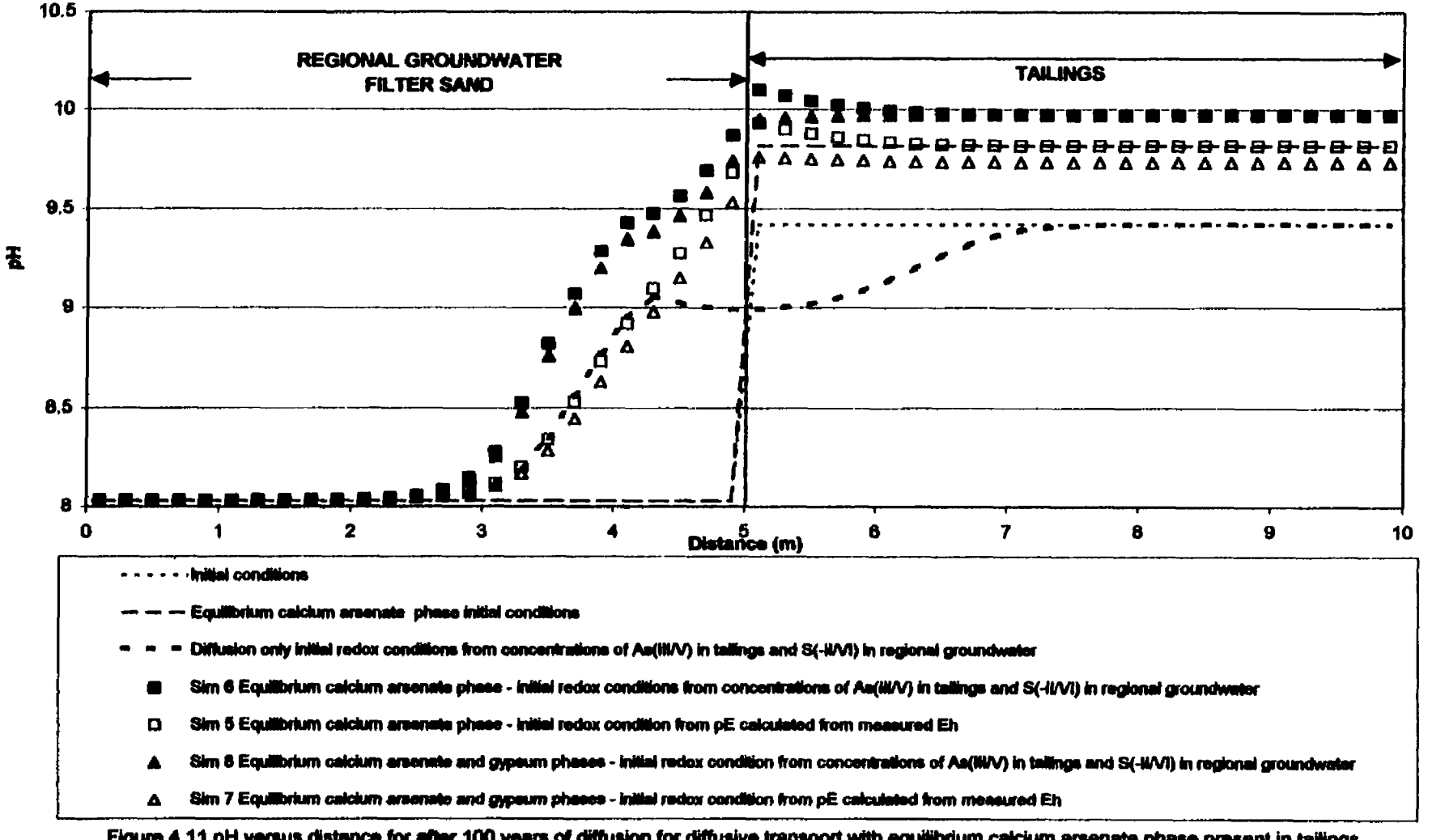

Figure 4.11 pH versus distance for after 100 years of diffusion for diffusive transport with equilibrium calcium arsenate phase present in tailings.

CHAPTER 5.0 SUMMARY AND RECOMMENDATIONS

The objectives of the research program were to characterize the source(s) of As in the Rabbit Lake in-pit tailings facility; measure insitu geochemical conditions in the Rabbit Lake in-pit tailings facility; determine primary and secondary As mineralization in the uranium tailings; determine the geochemical controls on dissolved As in the Rabbit Lake in-pit tailings, measure geochemical conditions in the regional groundwater surrounding the tailings facility; and investigate the potential for geochemical interaction between the tailings and the regional groundwater under diffusive mixing conditions.

The following sections review the key findings for the three papers (Chapters 2, 3, and 4) that describe the geochemistry of arsenic in the Rabbit Lake TMF and makes recommendations for future research.

5.1 DISTRIBUTION OF ARSENIC AND NICKEL IN THE RABBIT LAKE IN PIT TMF

Chapter 2 presents a description of the field investigation, details the stratigraphy of the tailings, summarizes the regional geology, describes the mineralogy of the ore bodies and tailings, and presents the distribution of arsenic and nickel in the TMF. The key issues were the distribution of arsenic within the Rabbit Lake TMF and the identification of primary and secondary arsenic, nickel, iron, and calcium minerals.

5.1.1 Key Findings

- The stratigraphy of the TMF consists of alternating layers of ice or frozen tailings, and tailings, which varied in consistency from a slurry to a firm silty sand.
- The age of tailings with depth in the Rabbit Lake TMF was estimated from historical tailings surface elevations and correlation with seasonal ice layer formation. Bore holes drilled as part of this investigation penetrated to a depth of 71 m corresponding to tailings deposited prior to June 1986.

- As a result of the milling process, the bulk of the tailings was present in the <45 μm grain size. The tailings solids are predominately composed of quartz (16 to 36%) and calcium sulphate (0.3 to 54%). Clay minerals are primarily illite (70 to 95%) and comprise between 3 and 14 % of the tailings mass.
- Arsenic and nickel concentrations show similar patterns with depth. Both concentrations increased from a range of 500 to 8,000 μg/g below 55 m depth to a range of 5,000 and 13,000 μg/g from 35 to 55 m depth. At 10 m depth the concentrations approached zero, then increased to 8,000 to 10,000 μg/g near surface. These patterns are strongly related to historical changes in arsenic and nickel concentrations in the mill feed.
- Mineralogy of the ore bodies indicated that arsenic and nickel in the mill feed occurred primarily as 1:1 molar ratio arsenides such as niccolite and gersdorffite. This assumption is supported by the observation that arsenic and nickel concentrations in the tailings were measured at a near 1:1 molar ratio.
- Monthly mill feed assays for arsenic were compared to monthly arsenic assays of leach residue solids. This comparison showed that an average of 71% of the arsenic in the mill feed was solubilized. EMP analysis suggested that solubilized arsenic is precipitated as Ca, Fe, and Ni arsenates during the neutralization process.
- Calcium arsenate was the most commonly observed arsenate during EMP analyses but Fe, Ni, and S were also detected in association with the Ca and As. Mill records indicated that as of September 1997, 17,000 tonnes of arsenic were discharged to the TMF of which approximately 15,000 tonnes (88%) was in the arsenate form and 2,000 tonnes (12%) was in the form of primary arsenides.
- Nickel solubilized in the leaching process likely precipitated as nickel hydroxide during tailings neutralization, but may have also formed nickel arsenates as indicated by Ni being detected in association with Ca and As in tailings precipitates. Nickel hydroxides were not observed during EMP analyses nor were they detected in XRD analysis.

5.1.2 Recommendations for Further Study

- A field investigation of the Rabbit Lake pit should be conducted to collect tailings samples from a depth of 50 m to the base of the Rabbit Lake TMF in order to complete the stratigraphic profile.
- Further subsurface investigations should be conducted in areas directly adjacent to the tailings discharge areas to investigate in detail the effects of grain size separation on the distribution of contaminants in the Rabbit Lake TMF.
- A subsurface investigation of the in-place pervious surround should be conducted to collect samples of filter sand, coarse rock drain material and the host rock of adjacent to the pervious surround. This investigation is required to determine whether the structure of the filter sand consists of a clear separation of the tailings and filter sand or whether the tailings solids have infiltrated into the filter sand. Filter sand and coarse rock drain material should also be analyzed to determine if arsenic or other solutes are sorbing to the media.
- More detailed mineralogical analysis of calcium arsenate and iron precipitates is required to determine their specific chemical and molecular structure. Analysis should be conducted on wet tailings samples to avoid potential dehydration and structural changes as a result of drying. Analysis of the wet secondary minerals will require EXAFS or other light source methods.

5.2 GEOCHEMISTRY OF ARSENIC IN URANIUM MINE MILL TAILINGS, SASKATCHEWAN, CANADA.

The objectives of Chapter 3 were to quantify the distribution of As forms in the tailings, and evaluate the present-day geochemical controls on dissolved As. These objectives were met by; analyzing pore fluid samples for dissolved constituents, measuring Eh, pH, and temperature of tailings core and pore fluid samples, conducting sequential extractions on solids samples, conducting geochemical modeling of pore fluid chemistry using available thermodynamic data, and by reviewing historical chemical mill process records. The key

issues were the insitu redox conditions within the tailings, the quantification of secondary arsenic, nickel, and iron minerals and equilibrium arsenic concentrations within the tailings.

5.2.1 Key Findings

- Dissolved arsenic concentrations in water samples from five monitoring wells installed within the tailing body ranged from 9.6 to 71 mg/L.
- The Eh, pH, and temperature measurements on tailings samples were within similar ranges in and between bore holes. The mean pH, Eh, and temperature of solid samples were 9.9, +174 mV and 3.1°C, respectively. Eh, pH, and temperature measurements on monitoring well fluids were within similar ranges with pH between 9.3 and 10.3, Eh between +58 and +213 mV, and temperature between 0.3 and –0.3°C. Eh measurements were still decreasing when monitoring was discontinued indicating that Eh conditions are less than +58 mV below 50 m depth in the tailings.
- Sequential extraction analysis of tailings samples indicated that the solid phase As changed composition at 34 m depth. Arsenic in tailings above 34 m depth was primarily associated with iron and other metal hydroxides. Arsenic in tailings below 34 m was primarily associated with amorphous, poorly ordered calcium arsenate precipitates. The change in As solid phases at this depth correlated to a change in the ratio of dissolved Fe to As in the associated raffinate. Tailings above 34 m depth had higher Fe to As ratios (>4) than tailings from below 34 m depths (<2).
- The partitioning of As between the metal organic and amorphous mineral colloid leaches suggested that the iron hydroxides absorbed As in a co-precipitation process. The sequential leaching further suggested that the As is adsorbed to the surface of iron hydroxides that in turn form clusters. Arsenic is held within the iron hydroxide clusters and was unavailable for desorption during the high pH metal-organic extractions. When the iron hydroxide clusters are solubilized in the amorphous mineral colloid leach, the As was released.

- Saturation index calculations indicated that tailings pore fluids are in equilibrium with respect to gypsum and oversaturated with respect to iron hydroxide. Although Ca-arsenates were observed with the EMP and were asscoited with amorphous masses of calcium sulphates, and iron hydroxides and as coatings of calcium sulphates and Ca-arsenates on gypsum crystals. their mineralogy could not be determined. Thus, the SI values of several potential calcium arsenate minerals were calculated using thermodynamic data obtained from the literature. These SI values ranged from under saturated to saturated.
- Based on the most likely calcium arsenate minerals present in the tailings. equilibrium As concentrations in the pore fluids should range between 13 and 81 mg/L. values that are very similar to those measured in the pore fluid samples.

5.2.2 Recommendation for Further Study

- Further tailings pore fluid sampling is required to determine insitu redox conditions. Specifically the. iron (Fe^{2+}/Fe^{+3}), sulfur (S^{2-}/S^{6+}), arsenic (As^{+3}/As^{+5}), oxygen. carbon (C^{+}/C^{4+}) and nitrogen (N^{+3}/N^{+5}) redox couples should be measured at 1 µg/L detection limits. Field alkalinity measurements (sulfuric acid titration method) resulted in the non-carbonate alkalinity being greater than the carbonate alkalinity and dissolved oxygen measurement were at the detection limits of the silver chloride membrane probes. The measurement of dissolved gases in the tailings should clarify insitu redox conditions.
- Insitu platinum electrode redox measurements in tailings monitoring wells needs to be conducted to determine steady state mV values in tailings below 50 m depth.
- The thermodynamic data in the WATEQ4F, PHREEQC, and calcium arsenate equilibrium constants by Bothe (1999) need to be assessed at low temperatures (0 – 4° C) to determine whether normal equilibrium chemistry applies.

- Sequential extraction analysis samples should be repeated on fresh tailings to determine the effects of sample drying on the results of sequential extraction analysis.
- Solubility kinetics for calcium arsenate minerals present in the Rabbit Lake tailings should be determined. Experiments should be conducted under controlled atmospheric conditions to reduce the influence of atmospheric gas on pH and redox conditions.
- Further studies are required on the formation of secondary minerals during the ore milling and tailings neutralization processes. These studies are needed for the optimization of the milling and tailings management processes to produce a tailings product that is geochemical stable and unlikely to release contaminants regardless of the hydrogeologic setting.

5.3 DIFFUSIVE REACTIVE TRANSPORT ANALYSIS OF AN IN-PIT TAILINGS MANAGEMENT FACILITY, SASKATCHEWAN CANADA

The objectives of Chapter 4 were to analyze the diffusive transport of arsenic from tailings pore fluids to regional groundwater in the filter sand using both multi species reactive transport and single species diffusion models. The analysis was conducted using insitu pore fluids measurements from the Rabbit Lake in-pit tailings facility and from the regional groundwater surrounding the TMF. The key issue was whether the sulphide-sulphate redox couple or the insitu Eh measurements made with the silver/silver chloride electrode were representative of the redox conditions present in the filter sand.

5.3.1 Key Findings

- Single solute diffusion models (POLLUTE) cannot be used to predict changes in pH, Eh, and As speciation as a result of diffusive mixing of tailings pore fluids and the regional groundwater.
- The sulphide–sulphate redox couple in the regional groundwater appears to control the redox conditions for diffusive mixing of the tailings pore fluids and regional groundwater.

- The sulphide–sulphate redox couple conditions present in the regional groundwater result in reducing conditions around the Rabbit Lake in-pit TMF. The reducing conditions cause As(V), the dominant species in the tailings, to be reduced to As(III) as arsenic diffuses from the tailings into the filter sand.
- The pH will decrease in the tailings as the protons in the low pH regional groundwater diffuse into the tailings. The solubility of calcium arsenate minerals present in the tailings are pH dependent. The decrease in pH in the tailings causes an increase in solubility of the calcium arsenate minerals.
- The assumption of a constant concentration source term results in higher mass flux of arsenic with time when compared to mineral-water equilibrium reactive transport models.
- Simulations using both calcium arsenate and calcium sulphate equilibrium mineral phases predicted lower As concentrations in the tailings pore fluid than for simulations using only calcium arsenate equilibrium mineral phases. Less calcium arsenate can dissolve because of the common (Ca^{2+}) ion effect.

5.3.2 Recommendation for Further Study

- A detailed geochemical study of the regional groundwater system around the Rabbit Lake pit should be conducted to determine appropriate geochemical conditions for reactive transport modeling.
- The model results predict conversion of arsenate to arsenite as the arsenic in the tailings diffuses and reacts with the regional groundwater. As there is a paucity of information on species-specific toxicity for arsenic. further research is recommended to assess of species-dependent differences upon predicted environmental impacts for arsenic.
- Further studies on the fate and transport of arsenic after it leaves the TMF are required to determine the speciation of arsenic as it impacts major receptors around the mine site.
- Further investigation of the Rabbit Lake TMF to determine the insitu structure of the pervious surround to better describe the interface between the

tailings and the regional groundwater system. Monitoring wells should be installed in the filter sand and rock drain in the filter sand and into the host rock adjacent to the in-pit TMF. The monitoring wells would be used to determine insitu geochemical conditions in the filter sand and to monitor the release of contaminants during the decommissioning of the TMF when natural groundwater conditions are restored.

- 2-dimensional and 3-dimensional reactive transport analysis of the Rabbit Lake in-pit TMF should be conducted to determine the effects of hydrodynamic dispersion on the release of contaminants from the TMF.

APPENDIX A BOREHOLE LOGS

97-R1

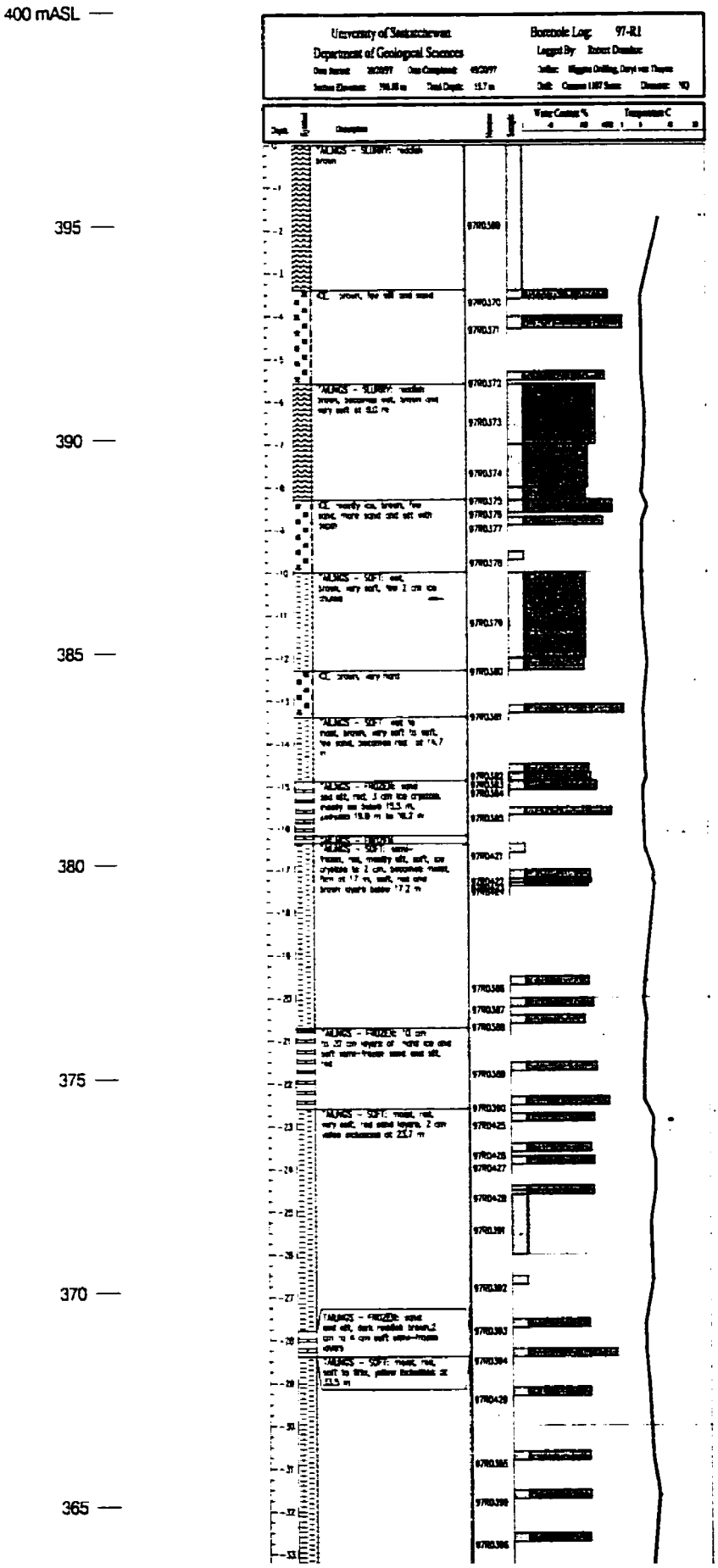
400 mASL
395
390
385
380
375
370
365
University of Saskatchewan
Department of Geological Sciences
Borehole Log: 97-R1

97-R2

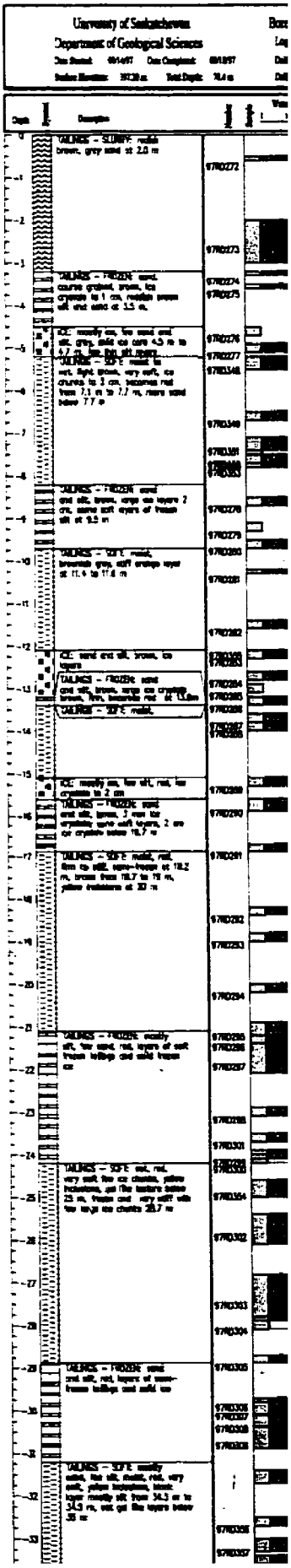

97-R2

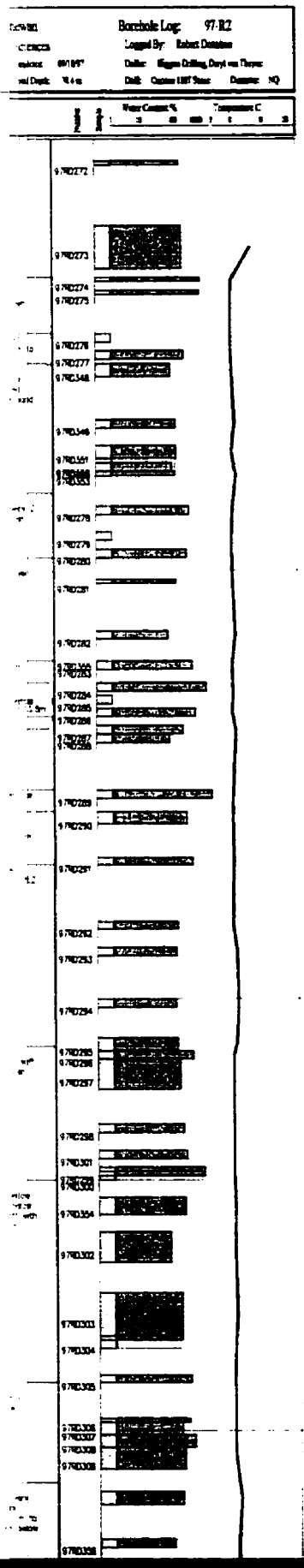
Borehole Log: 97-R2
Logged By: Robert Donahoe
Water Content %
Temperature C

97-R3

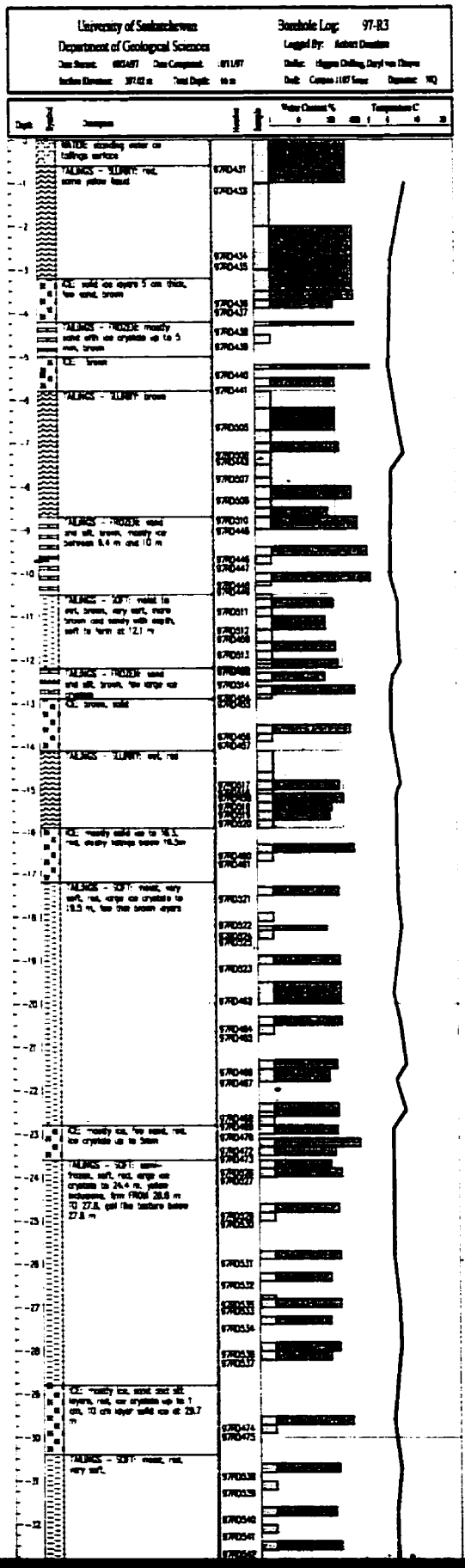
University of Saskatchewan
Department of Geological Sciences
Borehole Log: 97-R3
Logged By: Robert Donahoe
Water Content %
Temperature C
WATER: standing water on tailings surface
TAILINGS - SLIMY: red, some yellow layers
CL: solid ice layers 5 cm thick, fine sand, brown
TAILINGS - FROZEN: mostly sand with ice crystals up to 5 mm, brown
CL: brown
TAILINGS - SLIMY: brown
TAILINGS - FROZEN: sand and silt, brown, mostly ice between 9.4 m and 10 m
TAILINGS - SOFT: moist to wet, brown, very soft, more brown and sandy with depth, soft to firm at 12.1 m
TAILINGS - FROZEN: sand and silt, brown, few large ice crystals
CL: brown, solid
TAILINGS - SLIMY: red, red
CL: mostly solid ice to 16.3 m, clayey tailings below 16.3m
TAILINGS - SOFT: moist, very soft, red, large ice crystals to 18.5 m, few thin brown layers
CL: mostly ice, fine sand, red, ice crystals up to 5mm
TAILINGS - SOFT: semi-frozen, soft, red, large ice crystals to 24.4 m, yellow tailings/sand, firm FROM 26.8 m TO 27.8, gel like texture below 27.8 m
CL: mostly ice, sand, and silt layers, red, ice crystals up to 1 cm, 10 cm layer solid ice at 29.7 m
TAILINGS - SOFT: moist, red, very soft.

9

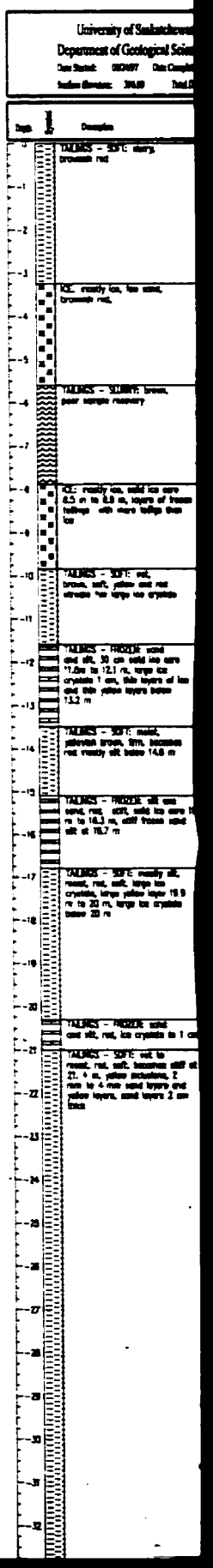
University of Saskatchewan
Department of Geological Sciences
TAILINGS - SOFT: slurry, brownish red
CL: mostly ice, fine sand, brownish red,
TAILINGS - SLIMY: brown, poor sample recovery
CL: mostly ice, solid ice core 6.5 m to 8.8 m, layers of frozen tailings with more tailings than ice
TAILINGS - SOFT: red, brown, soft, yellow and red streaks, few large ice crystals
TAILINGS - FROZEN: sand and silt, 30 cm solid ice core 11.5m to 12.1 m, large ice crystals 1 cm, thin layers of ice and thin yellow layers below 13.2 m
TAILINGS - SOFT: moist, yellowish brown, firm, becomes red mostly silt below 14.8 m
TAILINGS - FROZEN: silt and sand, red, soft, solid ice core 15 m to 16.3 m, stiff frozen sand silt at 16.7 m
TAILINGS - SOFT: mostly silt, moist, red, soft, large ice crystals, large yellow layer 19.9 m to 20 m, large ice crystals below 20 m
TAILINGS - FROZEN: sand and silt, red, ice crystals to 1 cm
TAILINGS - SOFT: wet to moist, red, soft, becomes stiff at 23. 4 m, yellow inclusions, 2 mm to 4 mm sand layers and yellow layers, sand layers 2 cm thick

97-R4

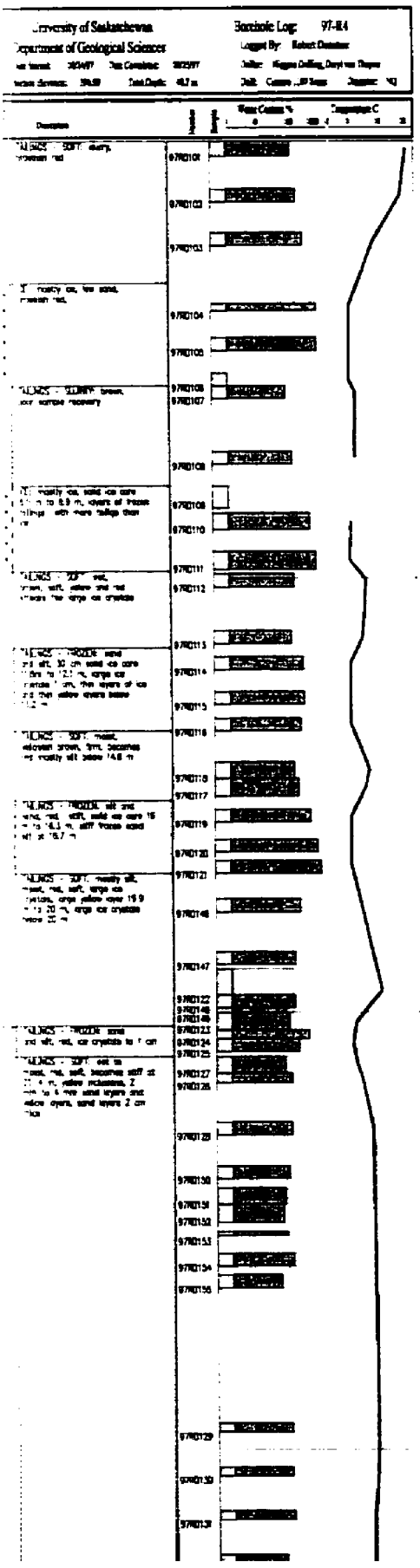

97-R5

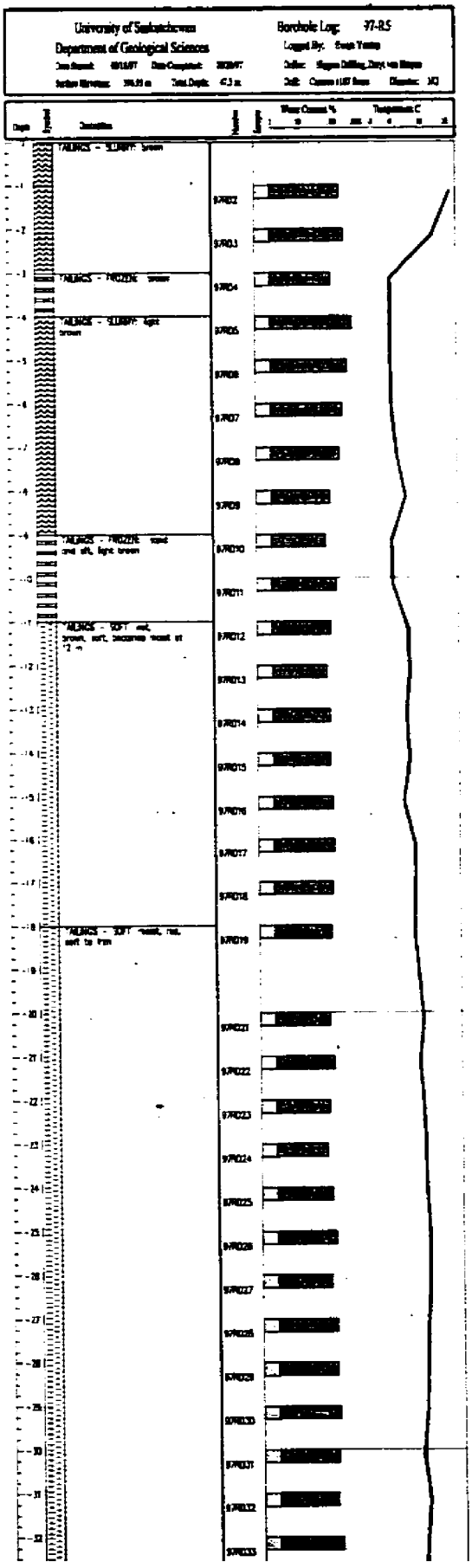

97-R6

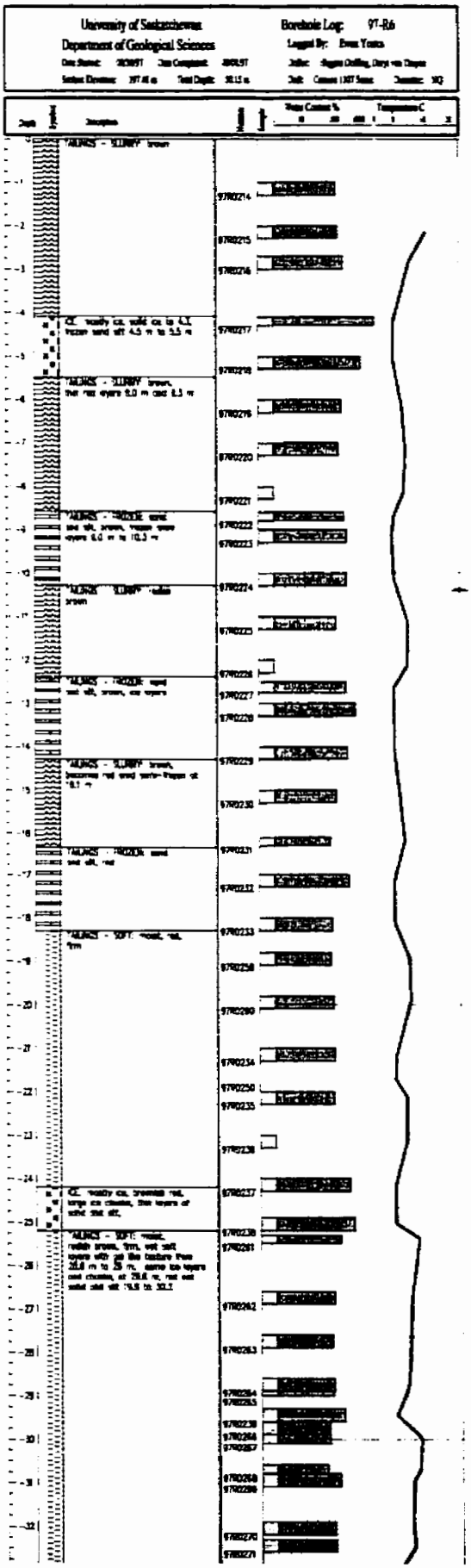
University of Saskatchewan
Department of Geological Sciences
Borehole Log: 97-R6

97-R7

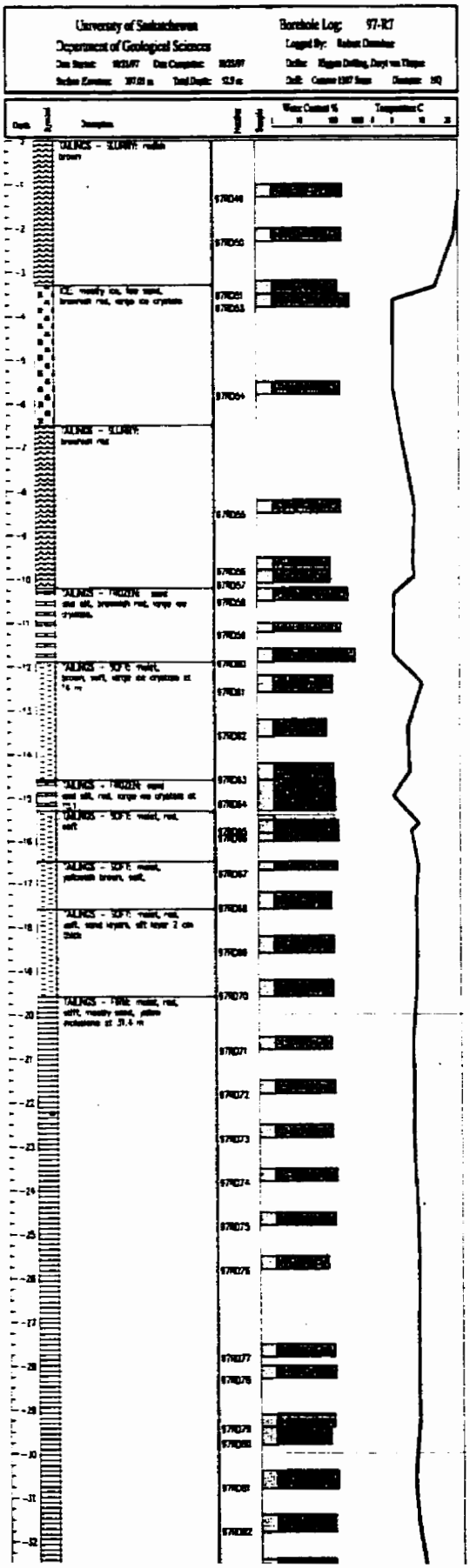
University of Saskatchewan
Department of Geological Sciences
Borehole Log: 97-R7

97-R7

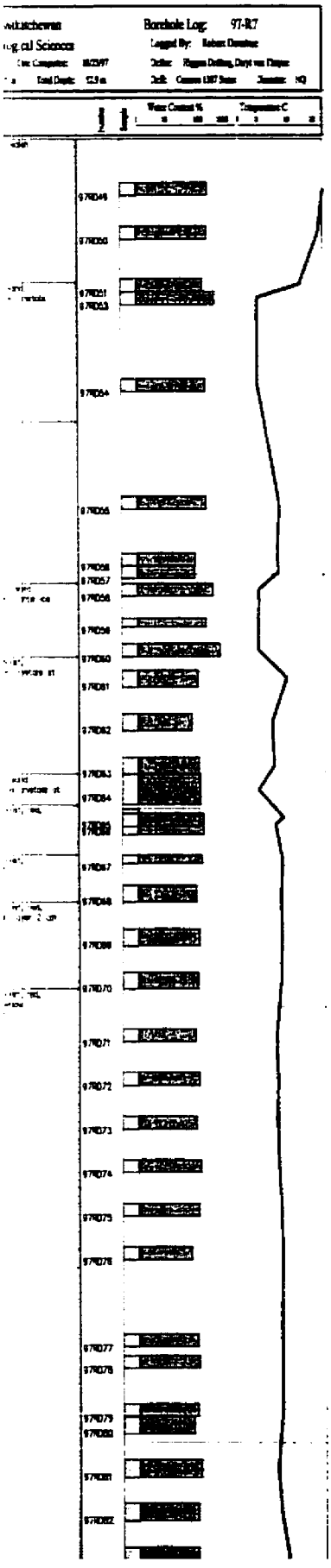

97-R8

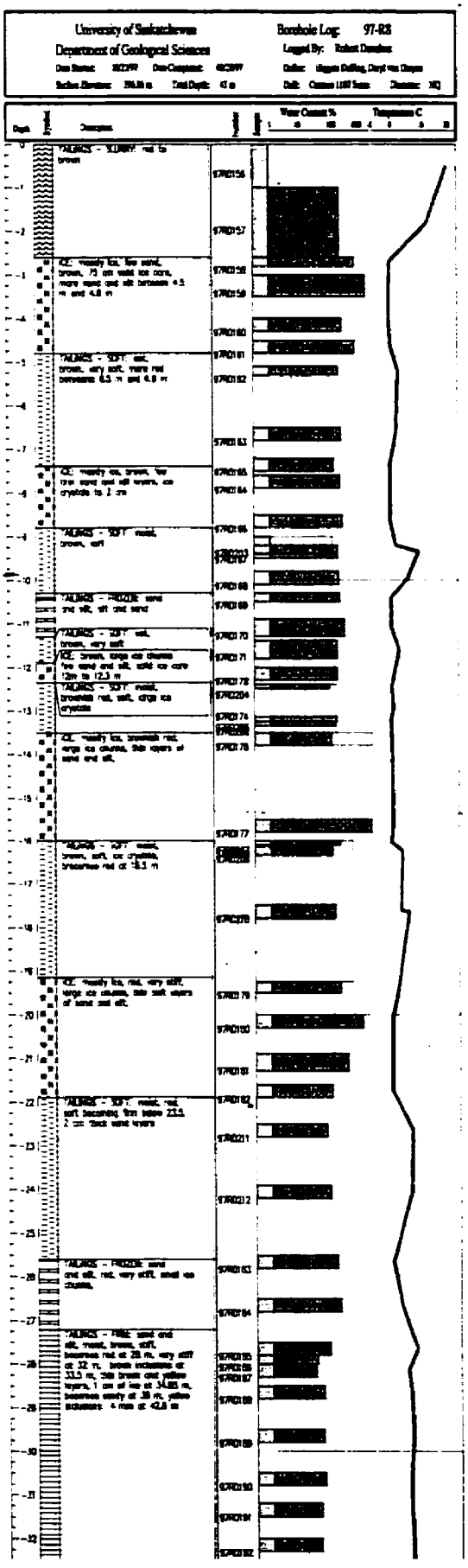

400 mASL

395

390

385

380

375

370

365

365

360

355

350

345

340

335

330

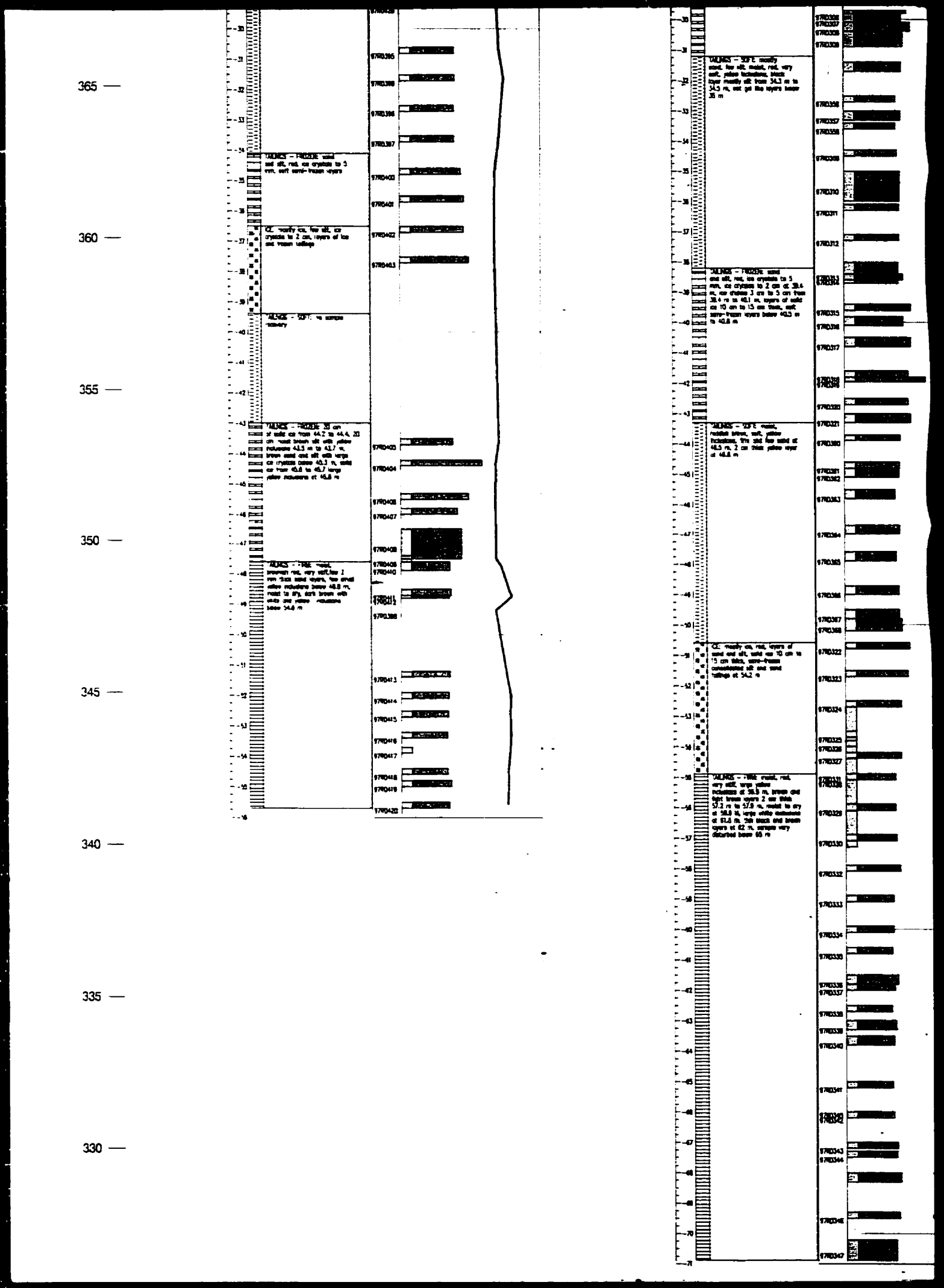

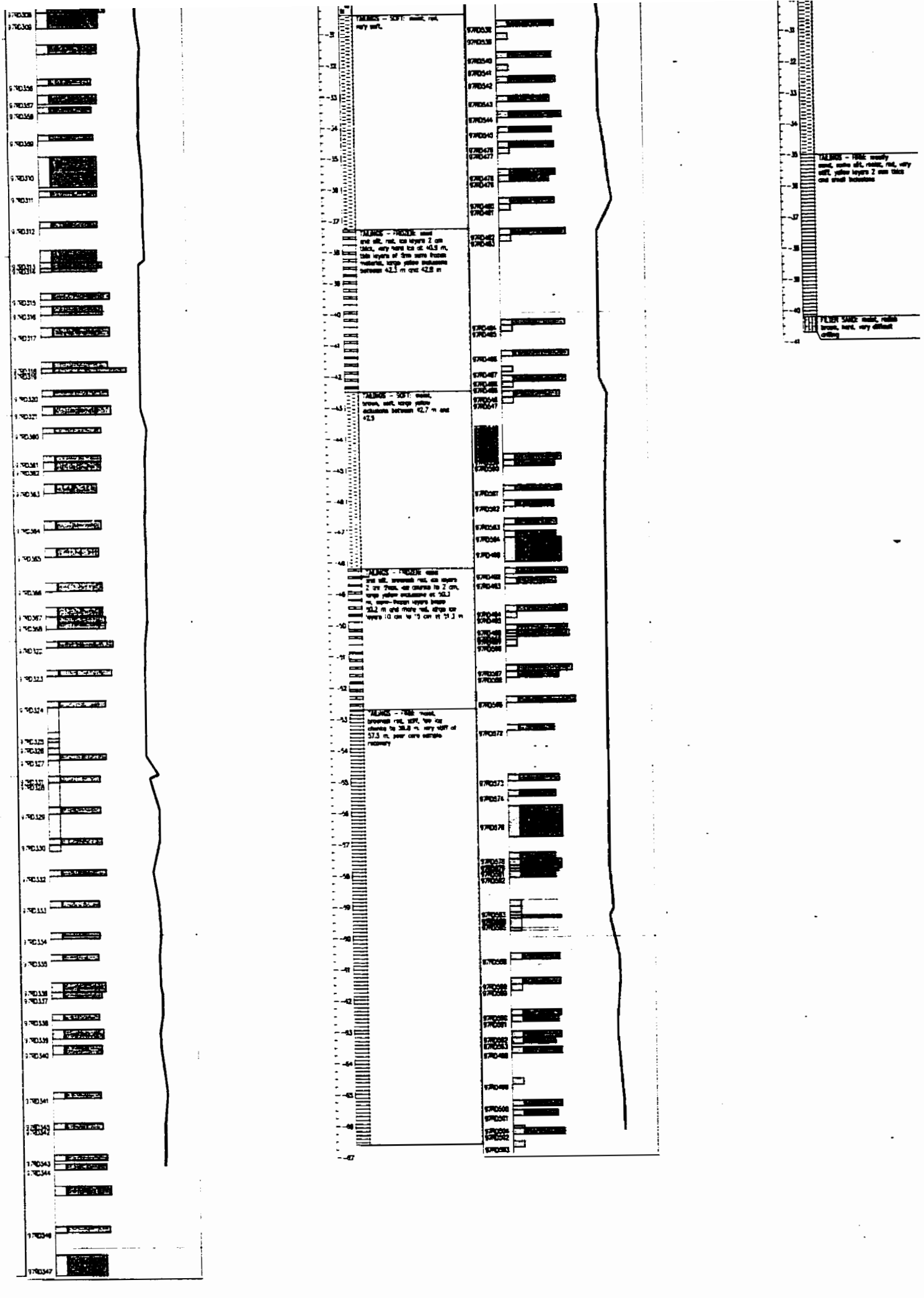

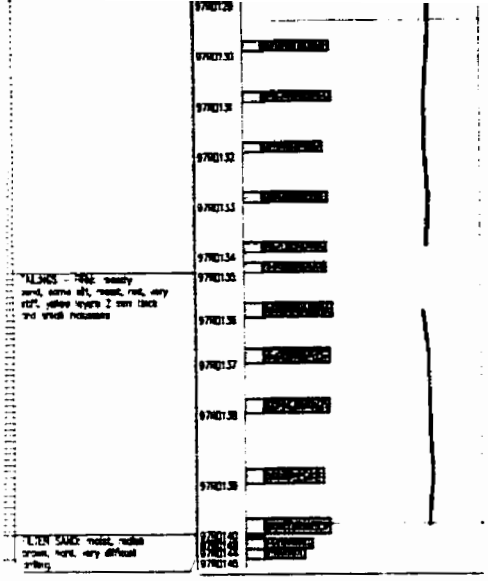

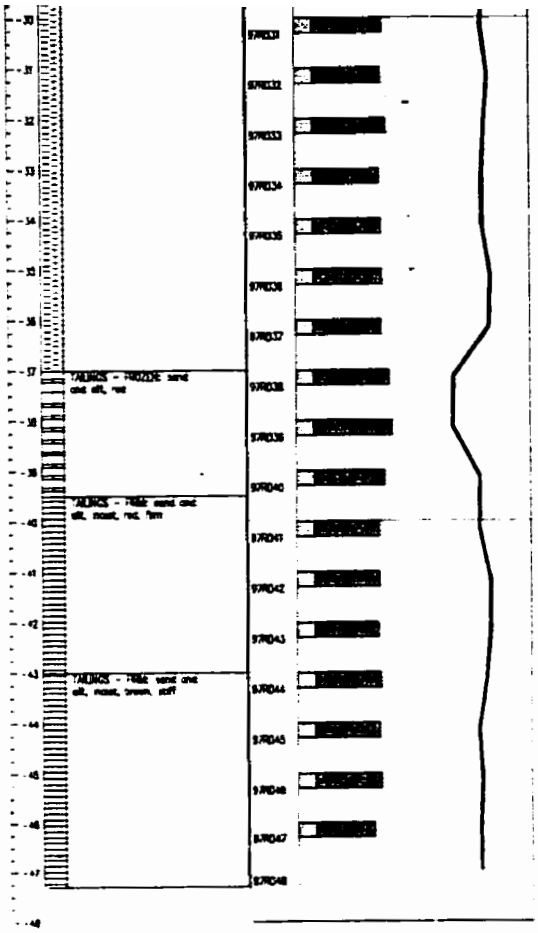

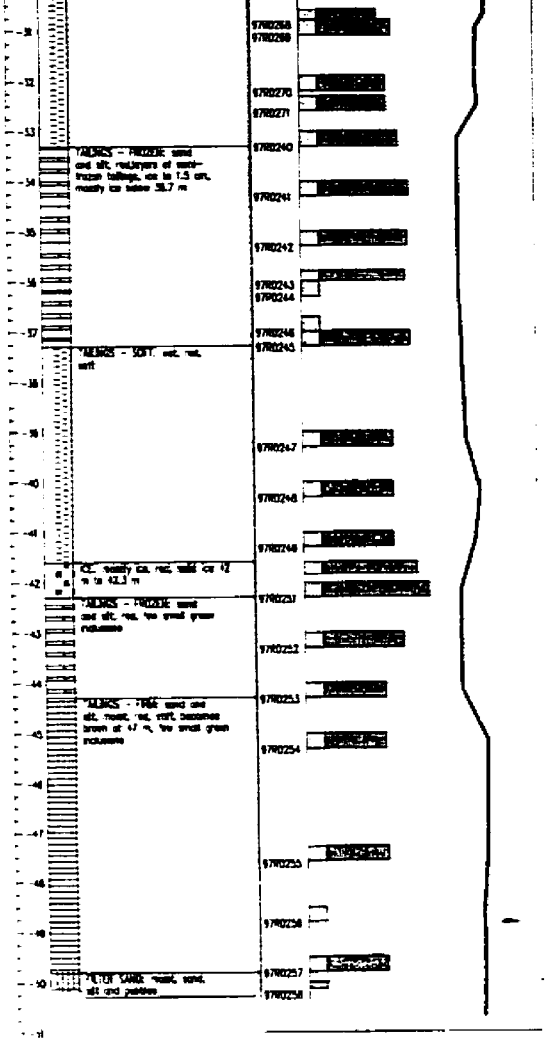

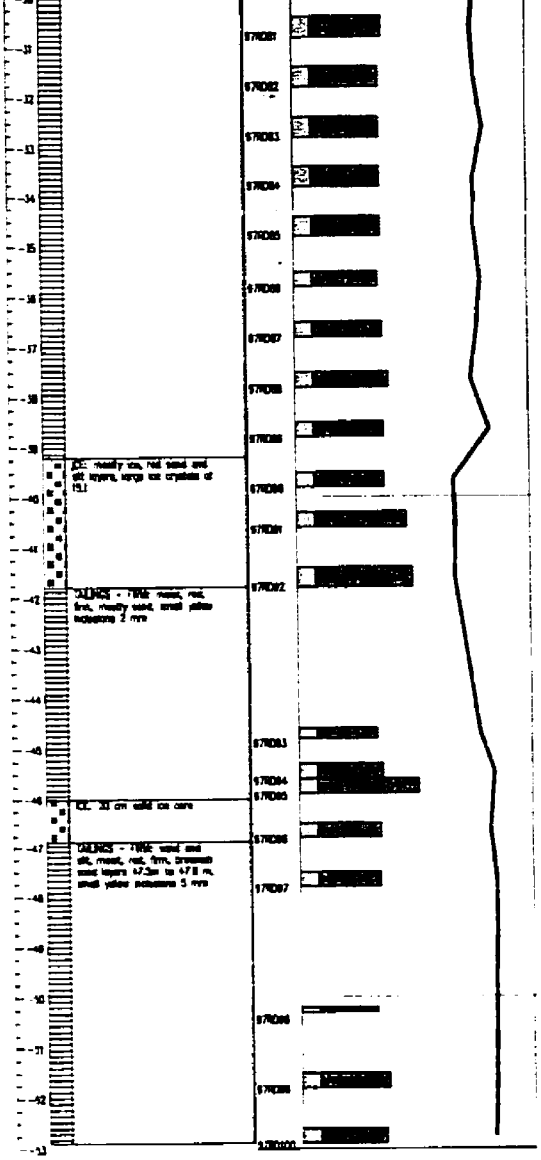

Legend

Water

Tailings - Soft

Tailings - Firm

Tailings - Frozen

Tailings - Slurry

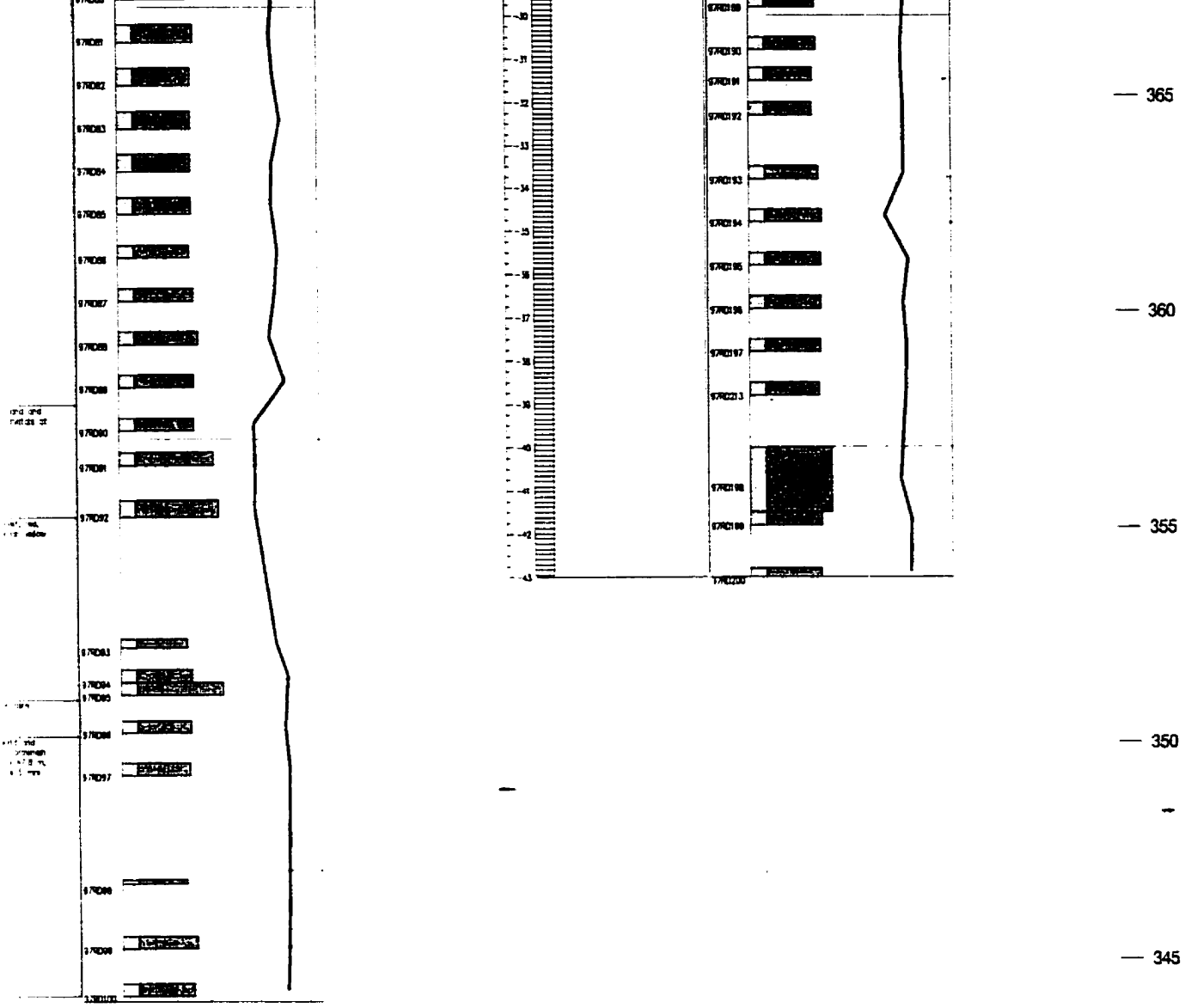

RABBIT LAKE

IN-PIT TAILINGS MANAGEMENT FACILITY

BOREHOLE LOGS

360

355

350

345

340

335

330

325

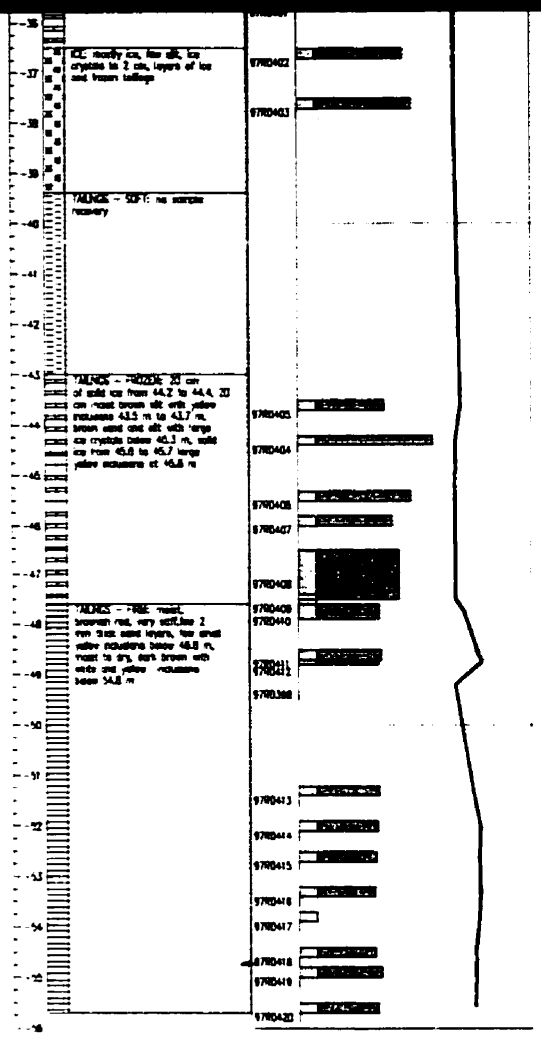

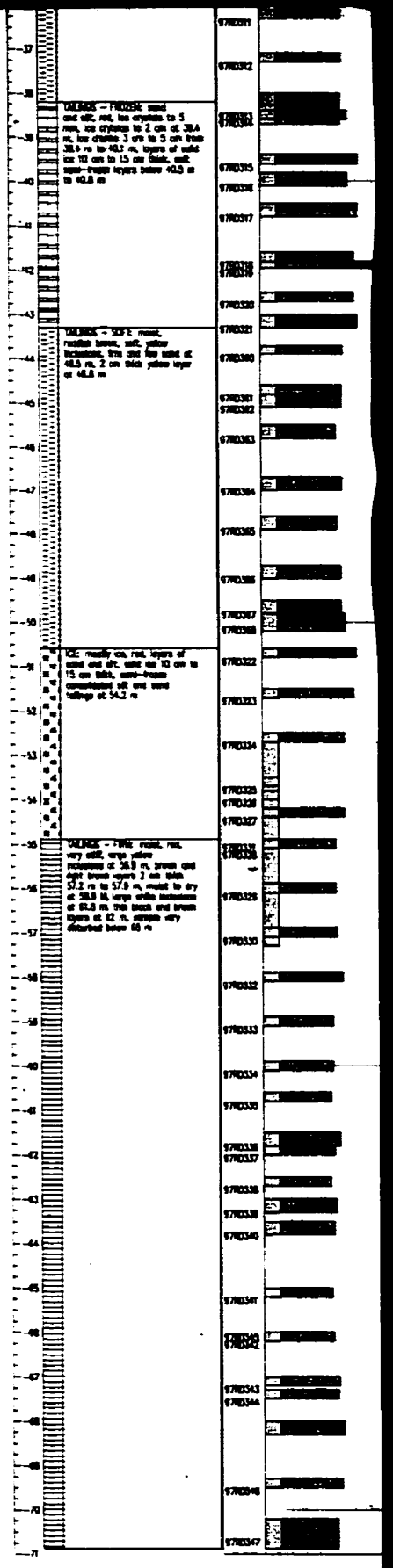

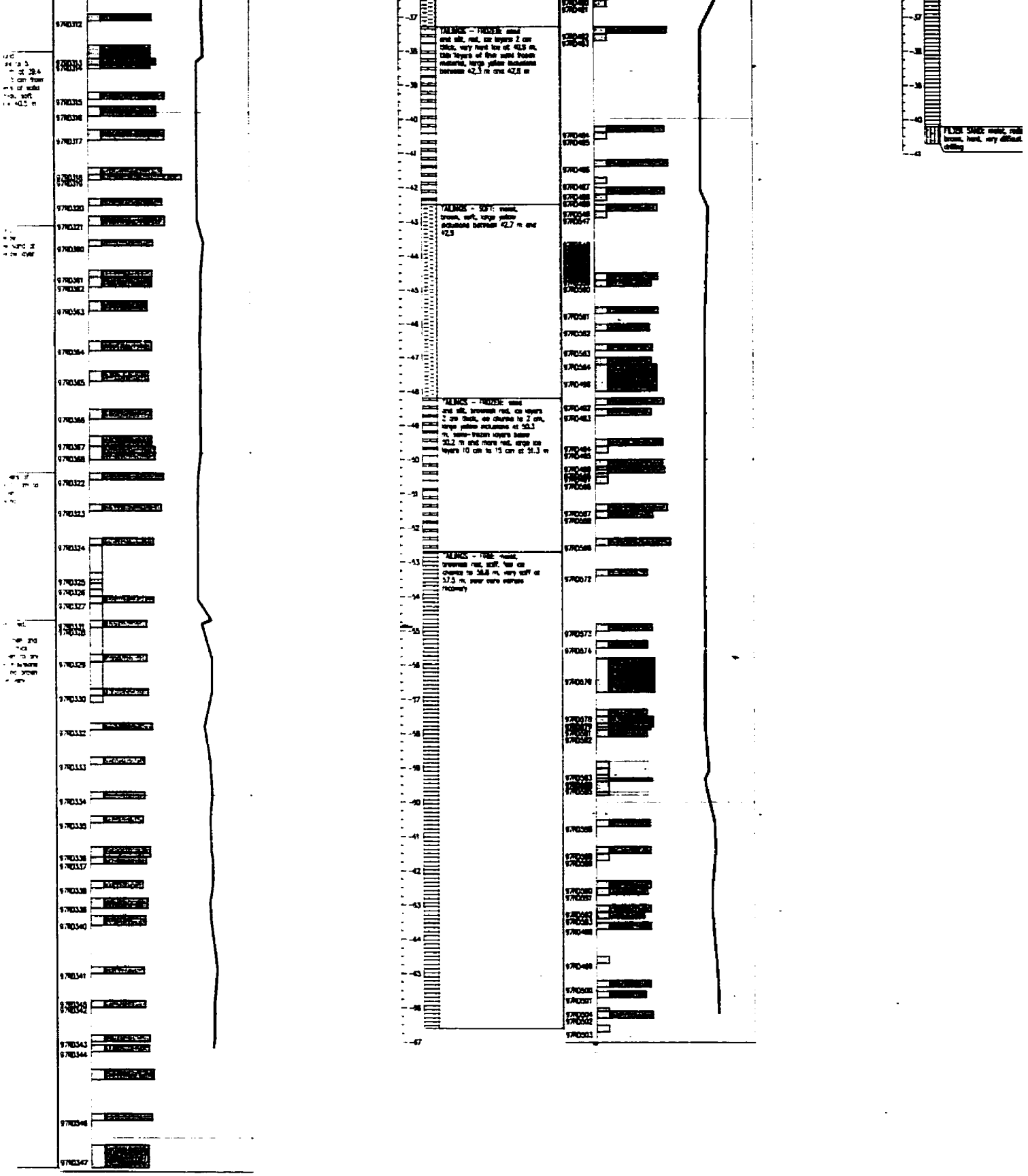

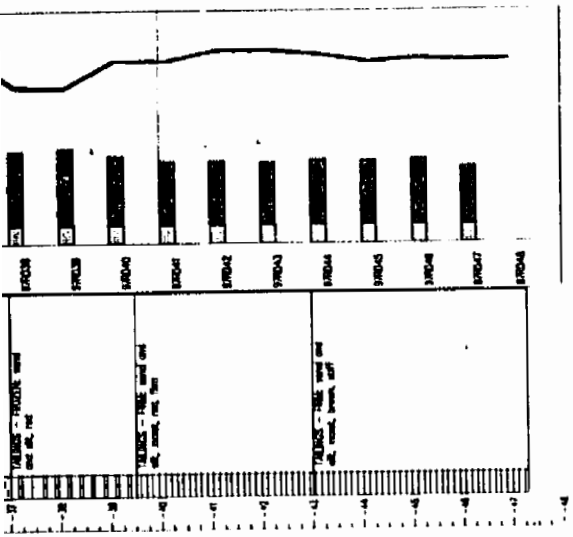

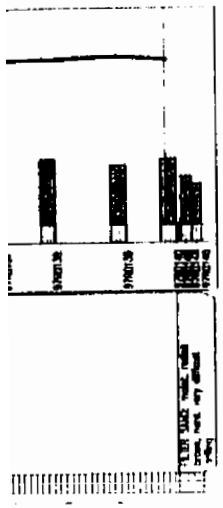

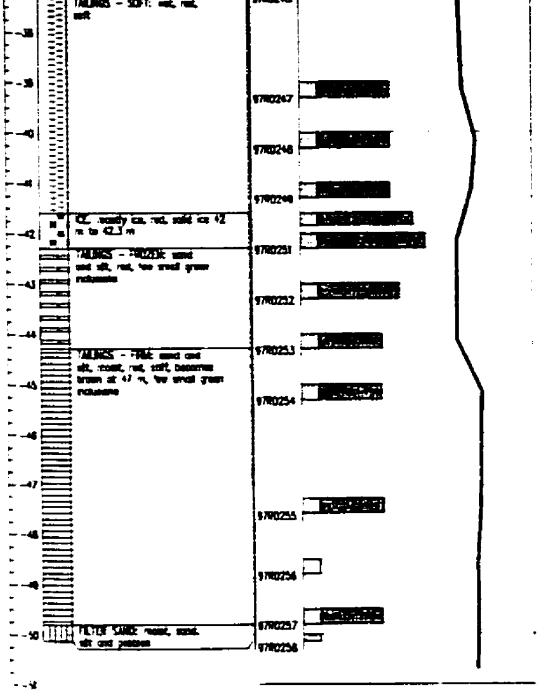

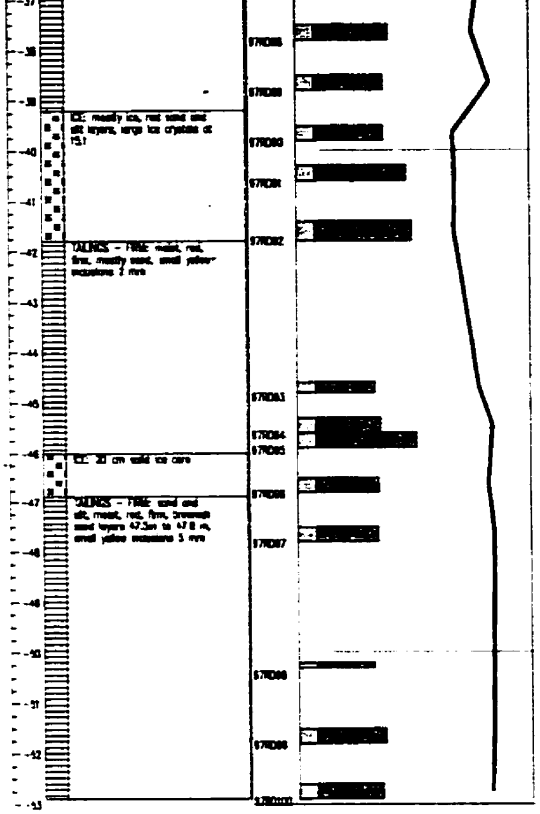

Legend

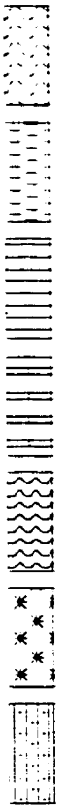

Water

Tailings - Soft

Tailings - Firm

Tailings - Frozen

Tailings - Slurry

Ice

Filter Sand

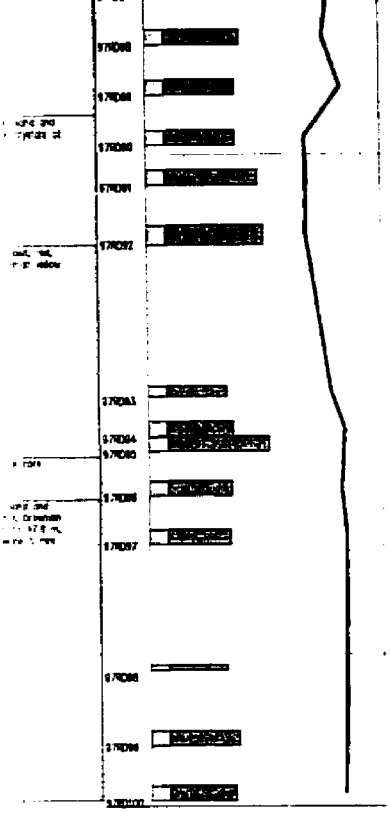

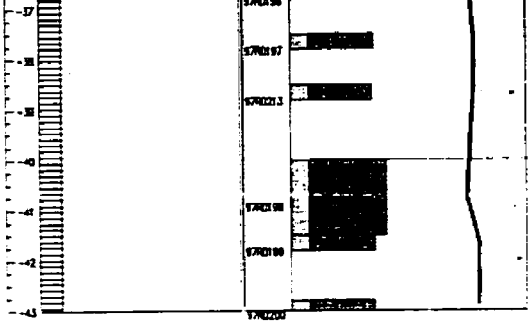

— 355

— 350

— 345

— 340

— 335

RABBIT LAKE

IN-PIT TAILINGS MANAGEMENT FACILITY BOREHOLE LOGS 97-R1 TO 97-R8

Compiled by: Rob Donahue
Drafted by: Wally Harildstad
Scale: 1:150

MIS00020

APPENDIX B SUMMARY OF SOLIDS FIELD MEASUREMENTS

Sample Number	Average Depth	pH	Temperature C	Eh mV
RD1	0.65			
RD2	1.15	9.44	17.4	257.3
RD3	2.15	9.65	14	238
RD4	3.15	9.54	4.5	267.9
RD5	4.15	9.67	3.3	251.3
RD6	5.15	9.62	1.2	253.8
RD7	6.15	9.19	3	-40
RD8	7.15	8.54	6.2	232.5
RD9	8.15	8.62	6.6	210.9
RD10	9.15	9.09	0.9	274.9
RD11	10.15	8.81	5.3	-300
RD12	11.15	9.18		229.4
RD13	12.15	9.27	5.3	245
RD14	13.15	9.85	5.4	154.7
RD15	14.15	9.65	5.4	115.2
RD16	15.15	10.65	5.3	132.7
RD17	16.15	10.74	7.1	151.4
RD18	17.15	10.52	7.2	185
RD19	18.15	10.32	8	175.9
RD20	19.15			200
RD21	20.15	10.16	10.5	152.2
RD22	21.15	10.36	8.7	149.7
RD23	22.15	9.93	9.1	199.8
RD24	23.15	9.91	9.2	168.5
RD25	24.15	10.2	10.4	155.1
RD26	25.15	10.32	9.8	90
RD27	26.15	9.38	10.4	132.1
RD28	27.15	9.69	9.8	170
RD29	28.15	9.48	9.4	172.5
RD30	29.15	10.41	8.8	148.9
RD31	30.15	9.5	8.5	163.4
RD32	31.15	9.61	9.7	182.5
RD33	32.15	9.15	8.1	67.5
RD34	33.15	9.8	8.1	48.8
RD35	34.15	9.66	8.7	187.2
RD36	35.15	9.24	9.5	145
RD37	36.15	8.57	10	138
RD38	37.15			200
RD39	38.15	8.14	1.5	17
RD40	39.15	8.68	9	176
RD41	40.15	9.76	8.7	197.4
RD42	41.15	8.84	10.5	190
RD43	42.15	9.81	10.7	170
RD44	43.15	10.24	11.6	193.7
RD45	44.15	10.24	10.7	147.1
RD46	45.15	9.17	8.3	190.4
RD47	46.15	8.7	9.3	245.2
RD48	47.00	9.38	10.1	219.3

Sample Number	Average Depth	pH	Temperature C	Eh mV
RD300	24.1	11.07	3.9	191.2
RD301	23.6	10.63	8.5	213.7
RD302	25.75	10.54	0.7	55
RD303	27.35	10.47	2.5	151.5
RD304	27.95	10.84	2.9	172.4
RD305	28.8	10.99	0.2	185.5
RD306	29.75	10.77	-0.1	179.9
RD307	29.95	10.47	-0.1	128.9
RD308	30.25	10.35	1.1	179.3
RD309	30.65	10.36	-0.2	167.9
RD310	35.5	10.61	2	95.6
RD311	36.2	9.46	2.6	132.8
RD312	37.2	9.72	2.6	132.8
RD313	38.35	9.74	3	189
RD314	38.5	9.49	-0.1	246.8
RD315	39.5	10.18	0.2	223.4
RD316	39.95	9.72	0	206.9
RD317	40.65	10.59	0.4	198.3
RD318	41.7	10.25	-0.3	222.5
RD319	41.875	9.83	8.2	232.3
RD320	42.6	9.66	-0.2	218.6
RD321	43.15	9.54	3.5	210.9
RD322	50.7	8.62	17.7	216.7
RD323	51.6	8.89	20.2	200.6
RD324	52.6	8.89	18.3	188.6
RD325	53.6	8.85	15.9	112
RD326	53.9	8.98	18.4	224
RD327	54.3	9.43	0.1	144.3
RD328	55	10.04	4.4	106.5
RD329	56	10.04	7.3	227.2
RD330	57	10.07	6.7	184.2
RD331	54.9	12.78	6.7	381.5
RD332	58	11.97	5.8	-168.9
RD333	59	10.07	6.9	155.1
RD334	60	10.16	7.2	196.9
RD335	60.7	9.73	7.3	216.1
RD336	61.65	10.7	4.5	-63.3
RD337	61.9	11.17	6.3	100.8
RD338	62.6	9.35	6.8	226.4
RD339	63.15	12.12	5.9	35.3
RD340	63.65	10.65	6.7	176.2
RD341	65.1	10.37	6.7	-305.9
RD342	66.1	10.43	7.2	149.5
RD343	67.1	9.61	6.7	172.8
RD344	67.4	10.29	7.1	87
RD345	68.15	10.33	5.7	171.2
RD346	69.4	9.46	5.4	181.7
RD347	70.55	9.77	5.2	160.8

Sample Number	Average Depth	pH	Temperature C	Eh mV
RD49	1.15	9.88	19.7	252.8
RD50	2.15	9.46	18.3	256.9
RD51	3.35	9.52	14.7	177
RD52	3.65	9.37	18	116.9
RD53	3.65	10.38	17.1	105.6
RD54	5.65	9.75	16.7	41.1
RD55	8.35	9.83	7.9	264
RD56	9.65	9.62	5.5	89.9
RD57	9.95	9.26	7.3	190
RD58	10.35	9.5	18.7	-160
RD59	11.10	8.95	18.8	-223
RD60	11.75	9	18.5	-283
RD61	12.40	9.27	7.4	224.2
RD62	13.40	9.26	7	258.3
RD63	14.40	9.38	4.6	172.4
RD64	14.95	11.12	6.3	120
RD65	15.60	11.14	7.5	100
RD66	15.75	10.52	8.4	177.6
RD67	16.60	10.01	11	172.7
RD68	17.40	10.67	7.6	224.9
RD69	18.40	10.53	8.3	161
RD70	19.40	10.07	8.4	216
RD71	20.65	10.3	6	159.5
RD72	21.65	10.6	6.4	114.5
RD73	22.65	10.26	8.4	154.5
RD74	23.65	9.95	5.9	135.2
RD75	24.65	10.16	7.3	174
RD76	25.65	10.26	8.4	154.5
RD77	27.65	10.27	8.2	170
RD78	28.15	9.68	9.5	179.3
RD79	29.25	9.61	9.7	180.4
RD80	29.60	9.72	7.8	207.5
RD81	30.60	10.11	9.4	174.5
RD82	31.60	10.45	9.2	155
RD83	32.60	9.96	8.6	197.1
RD84	33.60	9.19	7.8	290
RD85	34.60	9.24	8.6	180.2
RD86	35.65	9.98	9.3	187
RD87	36.65	10.03	8.8	210.8
RD88	37.65	10.63	8.8	131.6
RD89	38.65	9.31	9.8	202.8
RD90	39.65	9.49	12.4	120
RD91	40.45	9.5	13	50
RD92	41.60	9.19	14.6	190.6
RD93	44.70	9.23	11.9	195.4
RD94	45.45	9.17	14.7	62.8
RD95	45.75	8.72	17.2	260.3
RD96	46.65	8.81	14.4	222.9

Sample Number	Average Depth	pH	Temperature C	Eh mV
RD348	5.35	9.43	1.8	281
RD349	6.6	9.79	1.4	281.4
RD350	7.6	10.1	1.7	255.9
RD351	7.25	11.23	-0.1	291.1
RD352	7.55	10.89	1.2	156.4
RD353	7.75	10.94	2.5	162.5
RD354	24.8	10.94	1.2	198.2
RD355	31.55	9.99	2	255.5
RD356	32.6	10.46	2.4	229.5
RD357	33.15	10.31	2.9	257.9
RD358	33.5	10.38	2.8	233.5
RD359	34.4	9.87	1.5	-98.5
RD360	43.8	9.81	3	218.8
RD361	44.7	10.62	1.3	203.3
RD362	44.95	9.87	1.7	180.9
RD363	45.65	10.35	2	240
RD364	46.85	10.22	1.9	197.3
RD365	47.75	11.01	2.1	177.8
RD366	48.85	9.78	2.1	211.3
RD367	49.65	9.38	2.2	259.8
RD368	50	9.58	2.5	249.2
RD369	1.7	9.31	4.9	339
RD370	3.5	9.56	15.2	207.3
RD371	4.15	9.59	16.7	265.3
RD372	5.4	9.65	15.7	164.6
RD373	6.3	10.17	1.9	225.8
RD374	7.5	9.5	1.1	248.2
RD375	8.15	9.4	4.6	234.7
RD376	8.45	9.59	14.1	234.7
RD377	8.8	9.35	17.7	257.1
RD378	9.6	9.49	12.9	-171.5
RD379	11	9.33	1.1	217.5
RD380	12.15	9.48	1.3	150.5
RD381	13.2	9.77	15.7	198.1
RD382	14.6	10.02	1	107.2
RD383	14.8	10.64	2	142.8
RD384	15	10.76	9.6	98.5
RD385	15.6	10.79	11.88	188.9
RD421	16.5	11.09	2.4	258.3
RD422	17.1	10.79	3.7	145
RD423	17.25	11.31	3.6	119.1
RD424	17.35	10.82	6	182
RD386	19.6		2.2	218.6
RD387	20.1	10.85	0.1	114.4
RD388	20.5	11.32	0.5	164.1
RD389	21.6	10.32	17.6	186.2
RD390	22.4	10.12	14.7	193.5
RD425	22.8	10.98	3.4	230.4

Sample Number	Average Depth	pH	Temperature C	Eh mV
RD97	47.65	9.23	18.7	249.5
RD98	50.25	9.43	12.2	275
RD99	51.65	9.09	13	209.8
RD100	52.75	9.73	14.6	187.4
RD101	0.18	8.98	16.9	322.6
RD102	1.25	9.08	16	265.6
RD103	2.25	10.33	10.2	222.5
RD104	3.80	11.23	15.8	107.7
RD105	4.65	9.48	12.4	88.7
RD106	5.45	10.3	14	196.2
RD107	5.75	8.99	4.3	279.4
RD108	7.25	9.07	4.4	198.5
RD109	8.15	8.75	15.2	253.2
RD110	8.70	9.48	14.7	169.7
RD111	9.60	9.28	14.8	188.3
RD112	10.05	8.37	4.4	229.9
RD113	11.35	9.3	2.1	281.9
RD114	11.95	9.58	11.8	196.4
RD115	12.75	9.3	12.4	198.2
RD116	13.35	9.3	12.4	120
RD118	14.40	10.15	6.7	202.1
RD117	14.80	10.77	5.5	137.2
RD119	15.45	10.05	13.2	192.1
RD120	16.15	10.03	13.3	237.8
RD121	16.65	10.45	13.2	204.9
RD146	17.55	10.04	0.2	159.3
RD147	18.75	10	5.7	202.4
RD122	19.50	9.94	7.2	151.7
RD148	19.75	10.23	6.8	222.9
RD149	19.95	10.23	8.3	208.2
RD123	20.20	9.63	2.1	60
RD124	20.50	10.06	14.8	180
RD125	20.75	10.13	14.4	140
RD127	21.20	10.58	8.9	160
RD126	21.50	10.56	8.7	150
RD128	22.65	9.93	8.9	146.7
RD150	23.65	9.93	11.8	226.6
RD151	24.20	10.4	10.6	187.2
RD152	24.60	10.65	13.8	192.4
RD153	25.05	9.45	9.1	182.3
RD154	25.65	9.8	12.8	180.8
RD155	26.15	9.43	9.2	222.2
RD129	29.50	9.78	6.3	150
RD130	30.50	10.1	8.4	180
RD131	31.50	9.17	9.3	256.2
RD132	32.50	9.5	7.6	239.2
RD133	33.50	9.36	9.9	241.2
RD134	34.50	10.77	10.6	203

Sample Number	Average Depth	pH	Temperature C	Eh mV
RD426	23.5	10.81	4.1	206.2
RD427	23.8	10.22	4.3	211.1
RD428	24.5		3.3	163.6
RD391	25.25	10.51	0	115.5
RD392	26.6	10.94	2.9	147.4
RD393	27.6	6.64	20.9	134.8
RD394	28.3	10.73	3.4	212.3
RD429	29.2	10.18	3.4	212.2
RD395	30.7	10.29	1.7	217.2
RD399	31.6	10.35	5.4	134.3
RD396	32.6	9.71	4.9	231.4
RD397	33.6	9.23	3.3	225.8
RD400	34.7	9.9	3.9	222.7
RD401	35.6	9.56	-0.2	219.6
RD402	36.6	10.25	4.3	217.8
RD403	37.6	10.03	3.7	195.4
RD405	43.6	9.08	9	231.5
RD404	44.3	8.95	3.1	343.8
RD406	45.4	8.73	4.3	277.4
RD407	45.9	8.73	1.1	271.4
RD408	47	10.73	0	14.9
RD409	47.5	10.1	1.4	271.8
RD410	47.75	9.84	5.5	207.8
RD411	48.6	10.3	9	190.4
RD412	48.75	9.7	10.2	202.9
RD398	49.2	9.94	2.3	147.4
RD413	51.3	9.67	6.8	208.4
RD414	52	9.8	7.8	207.2
RD415	52.6	9.57	7.6	190.2
RD416	53.3	9.48	8.6	199.8
RD417	53.8	11.6	7.2	76
RD418	54.5	9.58	6.1	169.5
RD419	54.9	9.98	6.6	200.1
RD420	55.6	11.8	7.1	125.9
RD431	0.5	9.50	11.6	284.8
RD432	1	9.26	11.6	288.6
RD433	1	9.50	10.4	277.9
RD434	2.5	9.14	16.6	249.7
RD435	2.75	9.17	14.2	245.5
RD436	3.6	9.22	11.3	197.2
RD437	3.8	9.59	11	258.1
RD438	4.25	9.59	11	258.1
RD439	4.6	9.76	5.8	243.2
RD440	5.25	9.62	10.4	230.8
RD441	5.6	9.60	7.9	-121
RD505	6.45	8.84	1.2	321.8
RD508	7.1	8.86	2.6	294.2
RD442	7.25	8.81	3.8	286.6

Sample Number	Average Depth	pH	Temperature C	Eh mV
RD135	34.90	10.06	10.9	210
RD136	35.75	9.49	8.4	173
RD137	36.65	9.54	9.3	230
RD138	37.65	10.21	11.4	200
RD139	39.05	9.11	8.8	210.2
RD140	40.05	10.14	12.12	200
RD141	40.22	7.55	18.9	400
RD142	40.22	8.02	20.2	250
RD143	40.25	7.2	21.5	399.8
RD144	40.40	7.46	22.9	335
RD145	40.60	7.5	18.9	375
RD156	0.50	8.93	17.7	191.1
RD157	1.80	9.04	11.3	327.9
RD158	2.70	10.52	8.2	156.2
RD159	3.25	9.55	8.6	232.8
RD160	4.15	9.33	9.9	130
RD161	4.65	9.92	9.5	210.5
RD162	5.20	10.17	8.1	121.1
RD163	6.65	9.32	4.7	231.9
RD165	7.35	8.92	9.3	0
RD164	7.75	8.92	9.3	170
RD166	8.65	9.71	10.6	146.3
RD203	9.20	9.2	3.7	191.6
RD167	9.35	9.13	9.6	211.4
RD168	9.95	9.46	10.8	136.3
RD169	10.40	9.47	10.9	140
RD170	11.10	9.75	7	135
RD171	11.60	9.31	17.9	-125
RD172	12.15	10.86	0.2	178.3
RD173	12.15	9.91	7.7	205.8
RD204	12.45	10.96	4.5	111.1
RD174	12.95	10.21	3	150
RD205	13.20	10.45	6.4	110.9
RD206	13.30	10.62	6.1	188.6
RD175	13.65	9.75	14	313.4
RD176	13.65	10.92	4.1	120
RD177	15.65	10.57	14.5	183.3
RD207	16.05	11.13	1.1	146.3
RD208	16.13	10	19.8	266.5
RD209	16.25	10.68	7.8	167.6
RD178	17.63	10.14	8.8	-66.6
RD210	17.65	10.07	6.6	182.8
RD179	19.38	10.88	1.9	153.5
RD180	20.15	10.31	14.3	178.8
RD181	21.10	10.17	14.1	131.6
RD182	21.75	10.55	3.4	190
RD211	22.65	9.97	7.8	179
RD212	24.05	10.67	8.2	186
RD443	7.25	9.75	4.2	281.9
RD507	7.65	9.74	1.3	266.4
RD509	8.15	9.99	1.2	251.5
RD510	8.6	9.70	2	233
RD444	8.85	9.25	10.2	294.7
RD445	8.85	9.49	8.4	210.5
RD446	9.5	9.31	6.5	-173
RD447	9.7	9.04	8.6	-195.5
RD448	10.1	9.53	4.6	13.4
RD449	10.25	9.36	7.6	292.1
RD511	10.7	8.86	3.1	252.6
RD512	11.15	9.34	2.7	260.7
RD450	11.35	9.40	58	238.7
RD451	11.35	9.47	7.4	234.9
RD513	11.7	8.52	3.2	233.7
RD452	12.1	9.79	3.5	154.7
RD453	12.1	9.36	6.9	257.3
RD514	12.4	9.41	0.6	226.9
RD454	12.7	9.81	16.9	180.4
RD455	12.85	9.85	17.2	143.8
RD456	13.6	10.54	5	104.5
RD457	13.8	10.09	17.8	191.1
RD517	14.7	10.70	2.4	231.2
RD516	14.9	11.04	1.1	189.7
RD458	15	9.64	3.5	237.5
RD459	15	9.63	5.3	8.5
RD518	15.2	10.23	1.4	234.2
RD519	15.4	10 89	2	236.5
RD520	15.6	10.52	1.3	213.1
RD460	16.4	10.39	16.4	202
RD461	16.6	9.48	14.8	-62.7
RD521	17.4	10.53	1.7	216.8
RD522	18	10.57	3.3	205.5
RD524	18.25	10.40	2.8	209.5
RD525	18.4	10.72	2.2	218.7
RD523	19	11.08	2.2	226.8
RD462	19.75	10.53	0.7	219.6
RD463	19.75	10.50	5.1	234.4
RD464	20.4	10.77	5.7	182
RD465	20.6	10.61	6.8	153
RD466	21.4	9.78	7.8	311.2
RD467	21.65	10.84	5.3	232.3
RD468	22.45	10.59	6.3	233.6
RD469	22.65	10.44	5.4	215
RD470	22.9	10.62	0.8	220
RD471	22.9	10.72	0	204.3
RD472	23.2	10.16	7.2	126.8
RD473	23.4	10.14	10.8	-397.8

Sample Number	Average Depth	pH	Temperature C	Eh mV
RD183	25.65	10.2	0.4	194.8
RD184	26.65	9.79	13.8	230.4
RD185	27.65	10.01	10.4	173.6
RD186	27.90	8.82	10.6	100
RD187	28.15	8.82	12.6	200.8
RD188	28.65	9.31	12.2	210.7
RD189	29.65	8.97	12.6	257.4
RD190	30.65	9.33	6.3	239.7
RD191	31.35	8.77	12.1	268.6
RD192	32.15	9.49	6.5	140
RD193	33.65	9.82	9.2	183.5
RD194	34.65	9.4	5	184.9
RD195	35.65	9.6	9.2	189.4
RD196	36.65	9.98	8.2	176.6
RD197	37.65	9.92	9.4	187.6
RD213	38.65	9.69	8.7	207.2
RD198	40.75	9.55	7.5	-166.6
RD199	41.65	9.44	8.8	221.9
RD200	42.90	9.49	10.9	231.5
RD201	43.20	9.64	6.4	116.6
RD202	43.45	8.22	17.4	279.8
RD214	1.15	9.33	14	326.9
RD215	2.15	10.22	8.7	304
RD216	2.85	10.22	6	259.5
RD217	4.20	9.75	8.1	244.3
RD217	4.20	9.65	12.1	222.3
RD218	5.15	9.7	12.3	-150
RD219	6.15	9.69	3.5	281
RD220	7.15	9.93	3.8	232
RD221	8.15	9.24	5.7	195.4
RD222	8.70	9.24	11.9	236.9
RD223	9.15	9.45	-0.2	241
RD224	10.15	9.06	11.7	221
RD225	11.15	9.77	7.2	206.8
RD226	12.15	9.56	7.3	-270
RD227	12.63	9.4	17.1	97
RD228	13.15	9.61	13.8	35.5
RD229	14.15	9.82	15	160
RD230	15.15	9.7	6.3	-82
RD231	16.20	10.15	6.6	218.4
RD232	17.15	10.77	12.4	141.6
RD233	18.15	10.26	-0.2	188.1
RD259	18.95	10.54	4	134
RD260	19.95	10.54	5.9	150
RD234	21.15	10.5	4.8	122.6
RD250	21.73	8.88	5	241.7
RD235	22.15	10.24	5.5	139
RD236	23.15	10.34	5.5	173.4

Sample Number	Average Depth	pH	Temperature C	Eh mV
RD526	23.7	10.26	0.1	234.7
RD527	23.9	10.68	1	219.4
RD529	24.7	10.71	1.2	188.7
RD530	24.9	10.49	2.2	201.6
RD531	25.8	9.52	4	233.9
RD532	26.3	10.13	2.1	224.8
RD535	26.75	9.49	3.2	312
RD533	26.9	9.65	2.7	280.7
RD534	27.3	9.75	2.6	257.8
RD536	27.9	9.84	1.9	267.2
RD537	28.1	10.60	2	213.9
RD474	29.6	9.73	10.9	193.3
RD475	29.8	9.99	11.8	178.9
RD538	30.7	9.97	1.7	289.6
RD539	31.1	9.76	2.5	200
RD540	31.7	9.47	1.9	281.3
RD541	32.1	9.65	2.3	221.4
RD542	32.5	10.49	1.8	246.1
RD543	33.1	9.97	2.7	232.2
RD544	33.6	9.24	1.2	60.2
RD545	34.1	10.22	2.5	173.6
RD476	34.6	9.52	4.2	276.2
RD477	34.8	9.38	5.8	255
RD478	35.5	9.52	5.4	248
RD479	35.7	9.53	5.2	239
RD480	36.4	9.24	5.8	239
RD481	36.6	9.50	4.7	242.8
RD482	37.4	8.92	5.1	219.4
RD483	37.6	9.23	5.3	182.7
RD484	40.3	9.31	-0.2	256.9
RD485	40.5	9.27	-0.1	245.9
RD486	41.3	9.63	-0.2	67.9
RD486	41.3	9.42	4	194.9
RD487	41.8	9.21	6.6	70.6
RD488	42.1	9.30	8.2	180.3
RD489	42.3	9.54	5.5	147.6
RD546	42.6	9.27	1.7	293.5
RD547	42.8	10.65	1.8	206.6
RD548	43.5	10.60	3	169.6
RD549	43.6	10.73	3.5	187.7
RD550	43.7	10.83	5.5	192.4
RD551	43.8	10.96	6.2	192.4
RD552	43.9	10.87	6	126.5
RD553	44	10.98	5	158.9
RD554	44.1	10.98	5.2	106.8
RD555	44.2	11.01	4.8	97.9
RD556	44.3	10.97	4.2	98.3
RD557	44.4	10.94	4.2	168.8

Sample Number	Average Depth	pH	Temperature C	Eh mV
RD237	24.15	10.02	14.4	169.5
RD238	25.05	10.03	14.3	-88
RD261	25.40	10.43	0.3	-111
RD262	26.75	10.64	6.2	167
RD263	27.75	9.95	7.8	215
RD264	28.75	10.05	6.5	224.6
RD265	28.95	9.69	8.4	199
RD239	29.45	9.85	16	-104
RD266	29.75	9.47	5	234.7
RD267	30.00	9.76	6.3	214.6
RD268	30.70	9.95	8.4	239
RD269	30.95	10.61	6.6	210
RD270	32.05	9.42	7.9	200.7
RD271	32.45	9.16	7.7	221.8
RD240	33.15	9.09	15	-59
RD241	34.15	9.79	10.1	35
RD242	35.15	9.3	11.9	133
RD243	35.90	9.63	15.5	170
RD244	36.15	9.95	-0.3	28.5
RD246	36.85	9.23	13.2	-150
RD245	37.15	9.12	12.5	151
RD247	39.15	9.52	0.6	206.7
RD248	40.15	9.78	5.3	197.6
RD249	41.15	9.09	4.7	209.4
RD251	42.15	9.22	6	211.5
RD252	43.15	9.29	5.8	204
RD253	44.15	9.54	6.2	230.3
RD254	45.15	10.5	6.9	189.2
RD255	47.45	9.76	7.1	190.1
RD256	48.65	9.56	6.2	184
RD257	49.65	10.82	14.3	160
RD258	50.70			
RD272	0.55	9.28	8.1	358.1
RD273	2.5	10.09	5	317.8
RD274	3.25	9.55	4.1	283.3
RD275	3.55	9.66	3.5	161
RD276	4.6	9.71	3.6	253.5
RD277	5	9.69	6.4	69.3
RD278	8.6	9.69	11.5	143.2
RD279	9.2	9.59	2.4	79.6
RD280	9.6	9.46	9.6	158.9
RD281	10.25	9.42	0.6	251.3
RD282	11.5	9.64	1.1	214
RD283	12.2	10.06	8.5	212.2
RD284	12.7	9.64	5.2	196.7
RD285	13	9.93	3	260.3
RD286	13.3	10.38	5.4	192.2
RD287	13.7	10.62	1.1	129.2

Sample Number	Average Depth	pH	Temperature C	Eh mV
RD558	44.5	10.71	4.4	166.3
RD559	44.6	9.72	3.4	175.6
RD560	44.8	10.80	7.2	179.2
RD561	45.6	10.17	1.9	92.6
RD562	46.1	10.22	2.9	153.4
RD563	46.7	10.69	1.9	183.9
RD564	47.1	10.42	3.1	179.6
RD490	47.6	10.09	5.5	229.8
RD491	47.6		5.3	240.3
RD492	48.3	8.72	6.4	245.4
RD493	48.6	9.05	6.9	219.3
RD494	49.5	8.77	9.4	248.9
RD495	49.7	8.90	2.3	200
RD496	50.1	8.67	10.4	186.5
RD565	50.3	8.43	0	166.9
RD497	50.4	8.85	7.2	-297.4
RD566	50.6	8.47	-0.2	160.8
RD567	51.4	9.23	0.1	216.1
RD568	51.6	8.77	0	233.4
RD569	52.4	8.80	10.9	117.5
RD572	53.3	9.49	1.9	154.2
RD573	54.9	10.26	1.1	38.2
RD574	55.4	9.73	2.2	174.4
RD575	56.3	9.61	1.1	114.8
RD576	56.3	10.45	1.5	237.7
RD578	57.4	9.37	2.2	98.1
RD579	57.6	9.30	10.7	195.8
RD577	57.65	9.68	4.2	148.2
RD581	57.8	9.94	2.1	-36.8
RD582	58	10.79	3.2	-38.6
RD583	59.1	9.60	3.3	169
RD580	59.3	9.63	2.6	-408.8
RD584	59.35	9.58	5	200.9
RD585	59.5	9.83	2.3	233.1
RD586	60.6	9.57	5.4	208.9
RD587	60.6	9.62	5.7	136.6
RD588	61.4	9.81	6	39.6
RD589	61.6	9.89	6.3	202.9
RD590	62.4	9.86	4.5	191
RD591	62.6	10.20	4.6	92.3
RD592	63.1	12.51	4.9	94.3
RD593	63.3	12.01	5	-355.5
RD498	63.6	9.66	9.4	183.8
RD499	64.6	9.75	9.3	121.6
RD500	65.3	9.36	9.4	134.1
RD501	65.6	9.68	4.3	183
RD502	66.2	10.13	7.1	143.1
RD503	66.6	10.25	7.2	131.3

Sample Number	Average Depth	pH	Temperature C	Eh mV
RD288	13.9	10.83	1.8	150.9
RD289	15.2	10.46	1.9	248.5
RD290	15.75	10.63	11.3	196.7
RD291	16.8	10.74	6.5	178.2
RD292	18.3	10.72	-0.2	102
RD293	18.9	11.01	1.5	151.4
RD294	20.1	10.48	1.9	172.8
RD295	21.05	10.76	-0.2	232.3
RD296	21.3	10.47	9.4	186.2
RD297	21.75	10.54	-0.1	178.3
RD298	23	10.47	7.4	210.7
RD299	24	10.45	6	229.9

Sample Number	Average Depth	pH	Temperature C	Eh mV

APPENDIX C SUMMARY OF CHEMICAL ANALYSIS OF SOLIDS SAMPLES

Sample Number	Average Depth (m)	Al ug/g	As ug/g	Ba ug/g	Be ug/g	Bi ug/g	B ug/g	C ug/g	Ca ug/g	Cd ug/g	Cl ug/g	Co ug/g
97RD10	9.15	34600	16	56	2.8	14	190	0.11	19400	0.5	100	11
97RD106	5.45	29600	1500	29	3.1	50	170	0.95	161000	0.5	300	44
97RD107	5.75	45900	230	64	2.7	17	190	0.28	47400	0.5	1200	13
97RD109	8.15	65800	980	110	4.2	40	320	0.54	35400	0.5	100	40
97RD123	20.2	35200	4000	66	1.9	38	140	0.15	42900	0.5	590	54
97RD127	21.2	29600	3100	49	1.4	33	110	0.12	40800	0.5	200	41
97RD132	32.5	24000	12400	87	1.3	55	100	0.11	49300	0.6	480	95
97RD134	34.5	20300	7100	33	1.5	34	82	0.13	66800	0.5	490	38
97RD135	34.9	22600	4000	35	1.3	27	80	0.1	61800	0.5	490	26
97RD139	39.05	23200	7900	44	0.6	32	96	0.1	50700	0.5	480	44
97RD149	19.95	33900	3900	80	1.7	29	190	0.11	36600	0.5	200	61
97RD165	7.35	48000	130	100	3.6	31	270	0.73	68700	0.5	200	21
97RD173	12.15	43700	240	49	2.4	6.6	200	0.18	13400	0.5	100	8.7
97RD182	21.75	30300	3800	57	1.2	28	150	0.1	47100	0.5	490	41
97RD192	32.15	18500	7400	97	1	33	89	0.04	28500	0.5	300	46
97RD202	43.45	6600	580	21	0.5	2.7	13	0.01	3100	0.5	100	6.5
97RD204	12.45	49000	95	74	3.3	30	240	0.92	58500	0.5	340	16
97RD208	16.125	53300	1000	85	2.9	29	220	0.16	49900	0.5	100	23
97RD211	22.65	31100	9400	58	1.7	46	160	0.14	46700	0.5	580	75
97RD221	8.15	34600	790	58	0.0027	18	170	0.13	21500	0.5	200	12
97RD226	12.15	25500	2400	52	0.0022	23	140	0.18	24800	0.5	300	29
97RD23	22.15	22700	6100	90	1.1	38	120	0.17	43900	0.5	490	49
97RD235	22.15	17600	4000	49	0.0005	19	99	0.14	39200	0.5	380	29
97RD236	23.15	25300	2900	67	0.0015	18	150	0.13	40300	0.8	300	45
97RD244	36.15	27700	8100	97	0.0021	37	160	0.28	55400	0.8	800	62
97RD246	36.85	26800	12000	68	0.0019	48	150	0.1	44900	0.9	300	82
97RD254	45.15	21500	8200	54	0.0005	59	98	0.17	52100	0.5	190	76
97RD256	48.65	29500	5700	61	0.0015	24	140	0.18	45500	0.5	200	41
97RD258	50.7	20100	1600	39	0.0009	14	87	0.12	23200	0.5	200	23
97RD261	25.4	26800	3900	84	0.0005	48	150	0.18	42900	0.5	286	56
97RD266	29.75	22800	3300	56	0.0005	15	78	0.11	16000	0.5	187	41
97RD271	32.45	27400	11500	64	0.0005	67	120	0.17	52500	0.5	488	94
97RD276	4.6	48200	8300	140	0.5	76	290	0.43	39600	0.5	200	57
97RD279	9.2	42900	46	76	0.5	38	250	0.31	51000	0.5	100	21
97RD282	11.5	53200	37	77	0.5	40	290	0.22	47000	0.5	200	20
97RD285	13	70400	770	160	0.5	45	390	0.52	17300	0.5	380	30
97RD288	13.9	38200	1100	87	0.5	41	190	0.16	53200	0.5	500	31
97RD291	16.8	30000	3600	70	0.0005	15	160	0.23	41400	0.5	286	38
97RD293	18.9	41300	430	380	0.0018	24	180	0.49	52800	0.5	487	22
97RD298	23	34400	3000	88	0.0005	26	180	0.18	36000	0.5	279	36
97RD302	25.75	29700	5300	75	0.5	43	160	0.26	44800	0.5	490	43
97RD304	27.95	33600	5100	74	0.0005	21	180	0.18	48400	0.5	677	58
97RD308	30.25	37800	11200	100	0.0008	51	220	0.22	61300	0.5	461	95
97RD314	38.5	14600	12800	36	0.0005	60	89	0.09	51400	0.5	611	62
97RD316	39.95	20200	13700	77	0.0005	51	120	0.18	74400	0.5	1139	85
97RD325	53.6	47400	11200	110	0.5	64	240	0.22	59800	0.5	200	38
97RD326	53.9	49800	7800	120	0.5	48	200	0.33	58000	0.5	300	32
97RD338	62.6	19200	8100	48	0.0005	28	93	0.09	33400	0.5	278	150
97RD341	65.1	31600	7000	53	0.5	39	130	0.17	57000	0.5	370	61
97RD346	69.4	19300	8200	58	0.0005	32	110	0.2	48000	0.5	461	38
97RD347	70.55	31000	12900	110	0.5	64	160	0.2	61600	0.5	500	61

Sample Number	Average Depth (m)	Cr ug/g	Cu ug/g	Fe ug/g	IC ug/g	K ug/g	Mg ug/g	Mn ug/g	Mo ug/g	Na ug/g	Ni ug/g	OC ug/g
97RD10	9.15	24	160	10400	0.054	10400	8400	110	90	330	22	0.06
97RD106	5.45	56	670	21400	0.19	7200	36700	620	270	40	830	0.76
97RD107	5.75	27	140	11200	0.074	13700	12400	170	110	1100	170	0.21
97RD109	8.15	56	370	22300	0.12	21100	15300	300	220	230	540	0.42
97RD123	20.2	11	150	23200	0.09	11900	3100	110	64	850	2700	0.06
97RD127	21.2	11	93	27500	0.056	10100	3000	98	47	570	2000	0.06
97RD132	32.5	15	340	14500	0.022	6100	2100	190	41	100	8800	0.09
97RD134	34.5	20	180	14200	0.08	5800	12400	130	94	320	5200	0.05
97RD135	34.9	19	110	15800	0.1	8200	10300	110	67	330	2600	0.01
97RD139	39.05	17	200	13700	0.034	6700	5600	100	40	350	5700	0.07
97RD149	19.95	22	100	24200	0.09	16700	2400	130	57	550	2600	0.02
97RD165	7.35	43	310	15000	0.54	15100	12500	250	160	580	54	0.19
97RD173	12.15	110	68	9800	0.05	16500	16600	95	37	150	240	0.13
97RD182	21.75	27	100	25400	0.086	10100	3200	110	75	500	2500	0.01
97RD192	32.15	13	280	16000	0.028	6000	1900	84	41	350	5400	0.01
97RD202	43.45	13	30	5700	0.004	1400	1800	51	9.8	140	340	0.01
97RD204	12.45	33	280	15400	0.36	15500	14000	200	81	560	69	0.56
97RD208	16.125	26	140	29200	0.11	23400	12000	120	45	250	620	0.05
97RD211	22.65	26	250	27800	0.066	12100	2500	130	57	790	6800	0.07
97RD221	8.15	22	160	9300	0.035	10800	7900	120	73	460	400	0.1
97RD226	12.15	21	130	10400	0.044	7000	6500	120	81	590	1500	0.14
97RD23	22.15	24	150	17900	0.13	7400	5600	110	140	1300	4500	0.04
97RD235	22.15	19	130	25900	0.042	5900	1400	95	67	1400	2800	0.16
97RD236	23.15	18	95	24500	0.049	8800	1800	110	60	1300	2000	0.08
97RD244	36.15	28	290	25100	0.024	9900	3000	150	62	590	7200	0.26
97RD246	36.85	81	360	17700	0.024	9800	2700	150	36	240	9700	0.08
97RD254	45.15	17	310	14100	0.03	6400	5500	220	61	590	5900	0.14
97RD256	48.65	24	150	12600	0.025	9000	8000	160	56	640	3800	0.16
97RD258	50.7	24	61	10800	0.06	6000	3100	98	39	400	1100	0.06
97RD261	25.4	28	150	26400	0.053	9600	2600	120	65	1500	2800	0.09
97RD266	29.75	18	130	15800	0.011	7200	2100	85	31	440	2400	0.1
97RD271	32.45	15	470	17100	0.012	9400	2300	180	46	760	8400	0.16
97RD276	4.6	40	240	24600	0.092	14600	9500	290	200	630	6100	0.34
97RD279	9.2	34	350	13200	0.11	12600	11700	250	140	490	42	0.2
97RD282	11.5	44	470	14200	0.084	16600	13800	280	120	450	38	0.14
97RD285	13	46	290	21600	0.15	20800	16700	300	140	530	440	0.37
97RD288	13.9	15	320	17500	0.064	11800	5100	99	54	670	670	0.1
97RD291	16.8	23	98	29400	0.071	11600	2600	98	49	1300	2600	0.16
97RD293	18.9	19	300	12800	0.22	12900	10000	150	120	1800	280	0.27
97RD298	23	22	93	28900	0.035	12700	2500	99	59	1200	2100	0.14
97RD302	25.75	22	170	24800	0.068	10600	4200	120	97	1300	3700	0.17
97RD304	27.95	25	140	30800	0.037	12800	2600	150	64	1600	3600	0.14
97RD308	30.25	43	280	36600	0.047	14900	3300	220	94	1500	8200	0.17
97RD314	38.5	19	350	20600	0.024	4900	1900	130	47	780	9700	0.07
97RD316	39.95	24	390	23900	0.026	6600	3600	200	72	1300	10600	0.15
97RD325	53.6	43	230	11000	0.028	15800	5600	130	73	570	8500	0.19
97RD326	53.9	31	210	18800	0.036	17100	3200	150	59	610	6300	0.29
97RD338	62.6	17	370	13400	0.008	5600	3100	150	26	330	4600	0.08
97RD341	65.1	22	200	16300	0.052	8100	18800	190	76	430	4700	0.12
97RD346	69.4	20	200	18300	0.023	6300	2100	100	59	1000	5700	0.18
97RD347	70.55	29	180	15200	0.084	9800	4900	160	77	720	9000	0.12

Sample Number	Average Depth (m)	Pb-210 ug/g	Pb ug/g	Po-210 ug/g	P ug/g	Ra-226 ug/g	S acid sol ug/g	Sb ug/g	Si ug/g	Sr ug/g	S ug/g
97RD10	8.15	94	1600	59	130	131	46400	0.2	32.9	57	1.39
97RD106	5.45	52	780	32	1800	52	379000	0.3	7.4	89	12
97RD107	5.75	0	1200	0	340	179	107000	0.2	25.4	87	3.37
97RD109	8.15	0	5100	0	360	0	70400	0.4	25	130	2.18
97RD123	20.2	0	780	0	200	99	91200	0.6	28.8	150	2.85
97RD127	21.2	0	420	0	200	55	90200	0.3	30	130	2.8
97RD132	32.5	41	600	31	150	66	106000	1.3	28.8	110	3.43
97RD134	34.5	0	310	0	200	56	158000	0.7	25.6	73	5.1
97RD135	34.9	0	280	0	180	69	130000	0.5	28.3	74	4.49
97RD139	39.05	71	410	44	180	71	106000	1.1	28.5	93	3.63
97RD149	19.95	44	270	22	240	53	86700	0.3	29.5	180	2.89
97RD165	7.35	0	2000	0	330	254	120000	0.7	22.9	86	3.77
97RD173	12.15	56	360	38	170	62	20800	0.2	34.1	100	0.7
97RD182	21.75	0	310	0	210	54	95500	0.5	29.6	150	3.09
97RD192	32.15	47	560	50	120	63	59800	1	34.9	86	1.86
97RD202	43.45	5.2	210	6.2	200	5.7	5800	0.2	38.6	26	0.23
97RD204	12.45	0	1900	0	240	196	95600	0.2	24	55	2.88
97RD208	16.125	10	760	61	230	126	87100	0.4	27.2	160	2.7
97RD211	22.65	0	510	0	210	80	93400	1.1	28.4	160	3.05
97RD221	8.15	104	1100	90	190	129	44300	0.2	33.7	130	1.35
97RD226	12.15	108	1100	82	170	106	49800	0.3	33	88	1.69
97RD23	22.15	0	350	0	200	56	91400	0.6	33	140	2.6
97RD235	22.15	0	320	0	190	0	76100	1	32.2	170	2.32
97RD236	23.15	46	280	41	210	56	87700	0.4	31.7	180	2.79
97RD244	36.15	86	570	82	170	106	127000	1.7	27.9	140	3.77
97RD246	36.85	84	740	62	170	82	93800	1.9	30.4	140	2.98
97RD254	45.15	0	590	0	170	0	10700	1.5	27.4	120	3.6
97RD256	48.65	62	460	53	230	67	94900	1.1	30.2	130	3.16
97RD258	50.7	30	230	26	150	37	42900	0.2	35.5	81	1.25
97RD261	25.4	0	300	0	230	0	84600	0.7	32.3	210	2.68
97RD266	29.75	0	270	0	140	0	27300	0.6	35.6	140	0.96
97RD271	32.45	0	600	0	180	0	112000	2	28.6	170	3.62
97RD276	4.6	0	2300	0	340	229	71200	0.7	25.7	130	2.29
97RD279	9.2	196	2400	177	250	257	97300	0.2	25.9	72	3.46
97RD282	11.5	0	1600	0	310	194	109000	0.2	24.7	68	3.53
97RD285	13	360	2200	266	310	320	22400	0.2	26.8	100	0.82
97RD288	13.9	157	2100	105	180	202	105000	0.2	27.5	130	3.32
97RD291	16.8	0	440	0	190	0	83800	0.6	30	170	2.6
97RD293	18.9	0	1200	0	230	0	95300	0.2	25	82	3.38
97RD298	23	0	390	0	200	0	70900	0.5	29.7	190	2.4
97RD302	25.75	74	560	39	220	78	89100	0.4	29.6	150	2.57
97RD304	27.95	0	320	0	210	0	96900	1	27.7	190	3.18
97RD308	30.25	0	600	0	250	0	122000	1.6	23.3	230	4.29
97RD314	38.5	0	580	0	130	0	118000	2.1	26.7	110	3.36
97RD316	39.95	0	600	0	180	0	156000	2.2	23.7	130	4.92
97RD325	53.6	0	500	0	290	83	103000	1	23.9	250	3.55
97RD326	53.9	90	460	82	260	95	116000	0.7	22.7	220	3.72
97RD338	62.6	0	420	0	140	0	62100	1.4	17.3	96	2.2
97RD341	65.1	54	580	52	240	65	107000	0.8	27.6	94	3.7
97RD346	69.4	0	500	0	170	0	99900	1.3	29.8	140	4.35
97RD347	70.55	93	830	75	250	85	113000	1.2	23	170	4.73

Sample Number	Average Depth (m)	Th-230 ug/g	Ti 240	U 215	V 74	Zn 11	Zr 15
97RD10	9.15	120	240	215	74	11	15
97RD106	5.45	86	99	468	300	62	20
97RD107	5.75	0	190	395	110	15	21
97RD109	8.15	0	520	0	180	170	64
97RD123	20.2	0	150	388	210	33	130
97RD127	21.2	0	160	253	180	25	120
97RD132	32.5	108	65	286	160	140	77
97RD134	34.5	0	68	176	120	30	69
97RD135	34.9	0	80	188	120	23	72
97RD139	39.05	67	88	194	160	33	80
97RD149	19.95	74	160	205	300	26	150
97RD165	7.35	0	400	663	110	26	35
97RD173	12.15	30	95	256	100	8.4	22
97RD182	21.75	0	130	269	240	27	130
97RD192	32.15	33	68	404	120	95	59
97RD202	43.45	5.1	150	34.8	19	28	9
97RD204	12.45	0	350	852	89	31	31
97RD208	16.125	78	220	304	240	28	83
97RD211	22.65	0	130	373	230	34	120
97RD221	8.15	115	180	322	92	9.8	30
97RD226	12.15	119	140	394	100	27	34
97RD23	22.15	0	89	519	200	22	110
97RD235	22.15	0	82	0	160	18	150
97RD236	23.15	43	130	264	210	24	150
97RD244	36.15	73	150	254	240	48	140
97RD246	36.85	70	120	236	220	97	140
97RD254	45.15	0	87	0	150	43	120
97RD256	48.65	90	140	317	260	24	93
97RD258	50.7	34	150	145	150	25	54
97RD261	25.4	0	110	0	250	28	150
97RD266	29.75	0	100	0	160	50	72
97RD271	32.45	0	110	0	220	66	140
97RD276	4.6	0	280	0	190	400	68
97RD279	9.2	167	340	301	110	19	32
97RD282	11.5	0	370	0	150	18	29
97RD285	13	286	320	669	210	350	44
97RD288	13.9	102	150	423	170	23	74
97RD291	16.8	0	170	0	250	39	150
97RD293	18.9	0	300	0	100	9.7	41
97RD298	23	0	180	0	280	21	160
97RD302	25.75	95	140	382	220	25	100
97RD304	27.95	0	150	0	260	37	170
97RD308	30.25	0	150	0	320	73	190
97RD314	38.5	0	80	0	150	65	100
97RD316	39.95	0	100	0	200	61	120
97RD325	53.6	0	98	0	440	36	81
97RD326	53.9	84	90	426	410	36	110
97RD338	62.6	0	61	0	180	49	100
97RD341	65.1	42	120	273	200	41	90
97RD346	69.4	0	72	0	170	41	150
97RD347	70.55	127	94	1380	300	83	110

Sample Number	Average Depth (m)	Al ug/g	As ug/g	Ba ug/g	Be ug/g	Bi ug/g	B ug/g	C ug/g	Ca ug/g	Cd ug/g	Cl ug/g	Co ug/g
97RD359	34.4	51800	4200	340	0.5	30	260	3.12	88600	0.5	1800	88
97RD363	45.65	25600	6800	65	0.5	34	120	0.17	53400	0.5	710	41
97RD368	50	27000	20400	160	0.0009	41	160	0.2	82400	0.5	572	81
97RD378	9.6	60300	280	110	0.5	44	270	0.62	42000	0.5	200	33
97RD388	20.5	21900	4900	59	0.0005	30	140	0.17	45000	0.5	698	58
97RD392	26.6	36800	6600	82	0.5	37	160	0.21	51800	0.5	680	93
97RD400	34.7	26400	18700	50	0.5	66	120	0.1	89700	0.5	580	66
97RD403	37.6	33700	4300	96	0.0005	38	240	0.16	63400	0.5	365	41
97RD409	47.5	35200	7600	130	0.5	32	210	0.91	69000	0.5	190	35
97RD417	53.8	46800	1100	37	0.5	42	130	0.29	82900	0.5	300	29
97RD421	16.5	28600	3100	59	0.5	14	150	0.14	45100	0.5	380	51
97RD437	3.8	46200	13300	67	3.5	70	180	0.28	72900	0.5	2000	75
97RD441	5.6	66100	1500	69	3.4	22	260	0.25	58100	0.5	700	24
97RD461	16.6	35300	3400	88	1.9	5.7	170	0.12	58800	0.5	200	40
97RD467	21.65	38500	3000	83	1.7	18	170	0.08	36400	0.5	800	24
97RD47	46.15	28400	12000	68	1.4	27	140	0.03	45800	0.5	190	38
97RD473	23.4	40700	4500	60	1.8	25	150	0.17	60600	0.5	500	110
97RD474	29.6	35300	6700	87	0.0023	38	190	0.17	51800	0.5	590	72
97RD475	29.8	29000	5100	80	2	16	150	0.12	43600	0.5	300	61
97RD479	35.7	39200	11400	72	1.8	36	170	0.1	61900	0.5	600	78
97RD482	37.4	29300	17300	54	0.0018	19	130	0.16	74900	0.5	990	160
97RD483	37.6	35800	11300	76	2.2	19	170	0.12	66300	0.5	600	62
97RD484	40.3	26800	11800	73	0.0017	25	150	0.15	60800	0.5	880	63
97RD485	40.5	21600	5800	95	1.4	25	120	0.11	27600	0.5	500	43
97RD493	46.6	20300	11300	150	1	14	110	0.02	29200	0.5	600	30
97RD496	50.1	21500	10400	46	0.0009	46	100	0.12	45800	0.5	760	32
97RD497	50.4	26500	8600	81	0.9	30	110	0.06	50600	0.5	500	27
97RD500	65.3	18800	5700	40	0.0014	26	100	0.15	34400	0.5	270	120
97RD501	65.6	18700	4400	44	1	19	100	0.05	31800	0.5	400	85
97RD504	66.025	40200	560	30	3.8	5.8	98	0.42	82000	0.5	200	27
97RD508	7.1	55200	610	86	0.0034	15	270	0.23	54200	0.5	1000	18
97RD510	8.6	49500	200	85	3.5	20	220	0.38	55300	0.5	300	19
97RD512	11.15	45800	32	82	3.5	9.6	260	0.07	40500	0.5	200	11
97RD514	12.4	43000	34	87	3.7	14	250	0.21	40000	0.5	200	15
97RD515	12.05	37800	46	61	3.3	19	190	0.2	78600	0.5	200	21
97RD518	15.2	42700	570	27	0.0036	21	260	0.39	104000	0.5	990	24
97RD519	15.4	45500	520	12	3.8	33	240	0.96	122000	0.5	800	32
97RD520	15.6	49900	2000	75	3	27	240	0.14	86300	0.5	800	57
97RD524	18.25	31500	1100	62	2	13	140	0.13	42400	0.5	700	22
97RD526	23.7	40600	4800	57	1.9	24	140	0.16	63100	0.5	700	110
97RD531	25.8	27700	7300	71	0.0017	40	120	0.2	47900	0.5	580	63
97RD532	26.3	39700	8100	82	1.6	32	140	0.21	55400	0.5	1000	65
97RD534	27.3	37200	7200	61	1.7	25	150	0.2	51100	0.5	900	90
97RD537	28.1	36000	5500	65	1.8	20	140	0.2	70500	0.5	900	78
97RD543	33.1	52800	1800	120	2.9	20	260	0.06	31200	0.5	600	41
97RD544	33.6	79000	1500	330	0.0058	15	440	0.61	17800	1.2	500	65
97RD545	34.1	54900	9400	200	2.6	26	230	0.77	67900	0.5	1300	76
97RD546	42.6	23000	13000	54	0.0015	35	100	0.12	54000	0.5	590	84
97RD547	42.8	22000	6200	47	1.4	19	73	0.16	71600	0.5	500	40
97RD555	44.2	24500	5300	46	1.4	22	96	0.21	91200	0.5	1200	35
97RD560	44.8	24300	6900	55	1.3	19	94	0.11	47700	0.5	700	52

Sample Number	Average Depth (m)	Cr ug/g	Cu ug/g	Fe ug/g	IC ug/g	K ug/g	Mg ug/g	Mn ug/g	Mo ug/g	Na ug/g	Ni ug/g	OC ug/g
97RD359	34.4	42	77	42800	2.46	20300	13600	810	170	1000	3200	0.66
97RD363	45.65	27	160	16600	0.054	7600	7300	140	110	1300	5000	0.12
97RD368	50	37	170	19000	0.065	9600	2900	240	110	1700	15000	0.14
97RD378	9.6	26	560	20400	0.15	18200	15500	330	240	320	200	0.47
97RD388	20.5	20	140	23200	0.047	7700	1800	120	110	2400	3500	0.12
97RD392	26.6	13	200	29700	0.067	13100	3500	200	81	950	4800	0.14
97RD400	34.7	21	410	32400	0.043	9600	2200	160	47	430	14000	0.06
97RD403	37.6	30	130	34800	0.016	12200	2800	130	63	1000	2800	0.14
97RD409	47.5	27	240	19400	0.078	12400	2500	170	65	380	5700	0.83
97RD417	53.8	33	130	18900	0.14	5200	65100	210	170	400	730	0.15
97RD421	16.5	22	87	32300	0.062	9200	3200	110	47	490	2100	0.08
97RD437	3.8	25	89	20500	0.071	15000	5100	160	160	2100	9000	0.21
97RD441	5.6	36	210	10800	0.049	22800	10100	180	140	1100	920	0.2
97RD461	16.6	17	90	38900	0.06	13000	2600	110	69	510	2200	0.06
97RD467	21.65	9.6	93	30500	0.058	13500	2300	97	97	1200	1900	0.02
97RD47	46.15	21	59	17700	0.008	9300	2000	95	54	310	8500	0.02
97RD473	23.4	13	240	30100	0.041	14200	2400	170	57	460	3000	0.13
97RD474	29.6	15	190	33500	0.063	13000	2800	170	72	880	4900	0.11
97RD475	29.8	18	130	35100	0.067	15300	2100	150	56	830	3500	0.05
97RD479	35.7	23	360	19800	0.033	12900	3100	160	69	450	8400	0.07
97RD482	37.4	15	770	15200	0.034	10800	2600	280	72	770	13500	0.13
97RD483	37.6	28	160	16400	0.027	12000	3400	120	63	780	8300	0.09
97RD484	40.3	12	250	22700	0.041	9500	2600	150	60	740	8800	0.11
97RD485	40.5	16	300	17400	0.025	6600	2400	92	38	670	4200	0.08
97RD493	48.6	18	110	13400	0.009	5300	1700	79	57	640	7300	0.01
97RD496	50.1	7.5	440	13000	0.034	6800	1600	90	70	720	7700	0.09
97RD497	50.4	16	300	10900	0.035	8800	1700	94	60	590	6400	0.02
97RD500	65.3	8.2	280	11400	0.017	5600	8400	170	32	200	3300	0.13
97RD501	65.6	15	260	11300	0.017	5500	4300	170	31	160	2600	0.03
97RD504	66.025	39	110	12300	0.19	730	73800	260	170	140	370	0.23
97RD508	7.1	22	210	12700	0.039	19300	13600	190	120	1200	430	0.19
97RD510	8.6	28	390	10000	0.11	14500	12100	220	130	650	150	0.27
97RD512	11.15	21	120	7100	0.032	13100	7800	170	77	560	37	0.04
97RD514	12.4	32	260	10300	0.069	11900	11200	160	110	320	34	0.14
97RD515	12.05	40	570	12400	0.12	9900	12600	320	79	270	50	0.08
97RD518	15.2	19	460	13200	0.24	12400	12600	240	100	990	370	0.15
97RD519	15.4	29	650	17500	0.3	11700	11800	310	130	1100	430	0.66
97RD520	15.6	33	320	32400	0.053	18000	4200	130	81	800	1300	0.09
97RD524	18.25	22	84	23400	0.047	9300	7700	93	45	930	720	0.08
97RD526	23.7	8.7	250	29100	0.044	13300	2600	170	59	480	3200	0.12
97RD531	25.8	5.8	230	24800	0.14	9900	5400	120	100	1600	5400	0.06
97RD532	26.3	8.7	210	27200	0.1	13300	3700	120	110	1300	5400	0.11
97RD534	27.3	23	200	25900	0.047	12500	3600	150	75	1000	5000	0.15
97RD537	28.1	15	160	32900	0.12	12500	2700	190	80	970	3800	0.08
97RD543	33.1	26	74	36300	0.048	19500	3300	120	85	440	1000	0.03
97RD544	33.6	38	46	63200	0.45	33400	8100	220	54	1000	1100	0.16
97RD545	34.1	36	380	30700	0.51	19200	6700	290	170	910	7400	0.26
97RD546	42.6	11	380	14100	0.036	8000	3600	160	43	460	9900	0.08
97RD547	42.8	21	190	17200	0.084	6200	8000	130	68	620	4400	0.08
97RD555	44.2	20	160	16400	0.17	6500	5700	130	240	860	3600	0.04
97RD560	44.8	19	210	11700	0.059	6800	4100	110	66	810	4900	0.05

Sample Number	Average Depth (m)	Pb-210 ug/g	Pb ug/g	Po-210 ug/g	P ug/g	Ra-226 ug/g	S acid sol ug/g	Sb ug/g	Si ug/g	Sr ug/g	S ug/g
97RD359	34.4	30	50	33	1200	46	12800	0.4	15.2	550	1.01
97RD363	45.65	61	460	37	260	64	102000	0.7	29.8	120	3.33
97RD368	50	0	620	0	220	0	155000	3	25.8	210	4.85
97RD378	9.6	0	2400	0	380	319	86600	0.2	23.8	100	2.86
97RD388	20.5	0	370	0	200	0	90700	1	30.5	170	2.95
97RD392	26.6	0	450	0	250	71	103000	0.9	27.3	200	3.37
97RD400	34.7	0	560	0	190	97	164000	1.9	23.5	120	5.32
97RD403	37.6	0	490	0	220	0	138000	0.9	20.3	190	4.6
97RD409	47.5	0	370	0	220	77	143000	0.8	23.9	170	4.54
97RD417	53.8	0	250	0	470	37	140000	0.3	21.4	54	4.71
97RD421	16.5	0	370	0	200	54	83200	0.5	31.3	170	2.68
97RD437	3.8	0	1900	0	330	266	133000	1.4	21.2	170	4.07
97RD441	5.6	0	1700	0	280	207	121000	0.2	24.5	130	3.35
97RD461	16.6	0	430	0	200	76	118000	0.3	26.1	230	3.4
97RD467	21.65	0	400	0	240	81	80100	0.3	29.7	240	2.15
97RD47	46.15	0	950	0	160	121	98900	0.9	33.6	140	2.8
97RD473	23.4	0	250	0	210	39	112000	0.6	27.3	160	3.49
97RD474	29.6	0	480	0	220	0	118000	0.7	40.6	200	3.07
97RD475	29.8	0	390	0	210	74	79700	0.5	30.2	200	2.37
97RD479	35.7	0	580	0	190	97	97400	1.2	27.7	150	3.39
97RD482	37.4	0	810	0	160	0	178000	1.4	26.2	150	4.44
97RD483	37.6	0	630	0	210	87	126000	0.9	25.7	230	3.91
97RD484	40.3	0	390	0	160	0	138000	1	27.4	120	3.75
97RD485	40.5	0	360	0	140	49	53600	0.6	34.3	140	1.66
97RD493	48.6	0	470	0	150	58	60900	0.9	34.7	91	1.82
97RD496	50.1	0	500	0	160	0	93300	1	33.3	130	2.76
97RD497	50.4	0	570	0	180	104	99500	0.9	28.7	160	2.94
97RD500	65.3	0	800	0	180	0	80100	0.7	39.7	71	2.53
97RD501	65.6	0	1000	0	130	39	62500	0.9	34	59	2.18
97RD504	66.025	0	140	0	610	17	186000	0.2	16.4	30	5.84
97RD508	7.1	0	1400	0	260	0	114000	0.2	28.4	93	3.06
97RD510	8.6	0	1700	0	350	225	110000	0.2	23.7	110	3.25
97RD512	11.15	0	1100	0	280	142	95000	0.2	27.5	170	2.76
97RD514	12.4	0	1600	0	250	170	91400	0.2	26.2	84	2.64
97RD515	12.05	0	1100	0	500	113	178000	0.2	20.2	77	5.11
97RD518	15.2	0	2100	0	210	0	206000	0.2	20.9	79	6.13
97RD519	15.4	0	1900	0	290	291	236000	0.2	16.4	69	6.89
97RD520	15.6	0	1800	0	210	193	134000	0.3	25.1	160	3.95
97RD524	18.25	0	430	0	200	69	84100	0.2	30.3	130	2.51
97RD526	23.7	0	230	0	220	33	115000	0.5	27.6	170	3.56
97RD531	25.8	0	500	0	220	0	103000	0.7	34.1	170	2.66
97RD532	26.3	0	530	0	220	92	103000	0.9	26	180	3.37
97RD534	27.3	0	350	0	210	63	100000	1	27.1	150	3.05
97RD537	28.1	0	290	0	210	66	120000	0.6	26.1	160	3.63
97RD543	33.1	0	610	0	260	117	61800	0.4	27.6	260	1.92
97RD544	33.6	0	210	0	470	0	2400	0.2	21.1	620	0.14
97RD545	34.1	0	320	0	320	78	86600	1.1	21.6	250	2.46
97RD546	42.6	0	520	0	160	0	121000	1.1	27.4	100	3.43
97RD547	42.8	0	380	0	190	56	136000	0.8	27.1	84	4.13
97RD555	44.2	0	310	0	180	67	144000	0.6	25.1	69	4.52
97RD560	44.8	0	380	0	170	78	84500	1	30.8	110	2.96

Sample Number	Average Depth (m)	Th-230 ug/g	Ti 240	U 215	V 74	Zn 11	Zr 15
97RD359	34.4	16	190	3630	340	99	12
97RD363	45.65	85	98	563	200	41	110
97RD368	50	0	100	0	270	36	130
97RD378	9.6	0	440	0	150	150	34
97RD388	20.5	0	88	0	220	32	140
97RD392	26.6	0	200	0	280	52	130
97RD400	34.7	0	120	0	210	61	130
97RD403	37.6	0	160	0	340	41	240
97RD409	47.5	0	95	0	320	35	140
97RD417	53.8	0	100	0	160	29	61
97RD421	16.5	0	150	0	220	30	150
97RD437	3.8	0	230	0	210	44	90
97RD441	5.6	0	250	0	140	51	39
97RD461	16.6	0	180	0	290	38	130
97RD467	21.65	0	180	0	260	23	140
97RD47	46.15	0	100	304	260	24	100
97RD473	23.4	0	140	0	200	37	160
97RD474	29.6	0	130	0	270	49	0
97RD475	29.8	0	150	0	240	40	150
97RD479	35.7	0	130	0	270	54	130
97RD482	37.4	0	82	0	210	120	0
97RD483	37.6	0	91	0	290	31	100
97RD484	40.3	0	130	0	240	55	0
97RD485	40.5	0	96	0	190	35	100
97RD493	48.6	0	77	0	200	33	36
97RD496	50.1	0	68	0	230	25	0
97RD497	50.4	0	74	0	240	27	78
97RD500	65.3	0	71	0	170	72	0
97RD501	65.6	0	62	0	140	76	72
97RD504	66.025	0	120	0	120	17	40
97RD508	7.1	0	310	0	130	16	0
97RD510	8.6	0	260	0	120	16	28
97RD512	11.15	0	160	0	130	14	23
97RD514	12.4	0	300	0	120	14	24
97RD515	12.05	0	240	0	140	16	21
97RD518	15.2	0	330	0	110	15	0
97RD519	15.4	0	290	0	120	16	52
97RD520	15.6	0	220	0	250	30	140
97RD524	18.25	0	140	0	160	21	110
97RD526	23.7	0	170	0	210	28	150
97RD531	25.8	0	150	0	220	30	0
97RD532	26.3	0	180	0	250	32	100
97RD534	27.3	0	120	0	250	33	120
97RD537	28.1	0	150	0	220	55	150
97RD543	33.1	0	220	0	390	44	190
97RD544	33.6	0	120	0	550	52	0
97RD545	34.1	0	170	0	300	67	29
97RD546	42.6	0	86	0	170	76	0
97RD547	42.8	0	80	0	140	43	69
97RD555	44.2	0	97	0	150	24	84
97RD560	44.8	0	89	0	170	40	94

Sample Number	Average Depth (m)	Al ug/g	As ug/g	Ba ug/g	Be ug/g	Bi ug/g	B ug/g	C ug/g	Ca ug/g	Cd ug/g	Cl ug/g	Co ug/g
97RD561	45.6	24900	9500	70	0.0017	30	110	0.13	54400	0.5	500	47
97RD562	46.1	32600	5400	60	1.1	17	95	0.12	49200	0.5	800	28
97RD563	46.7	20800	5200	54	0.001	20	110	0.09	31800	0.5	400	28
97RD564	47.1	41900	13800	83	1.7	19	150	0.13	83300	0.5	700	56
97RD568	51.6	40300	8900	82	1.7	30	170	0.12	39400	0.5	600	44
97RD572	53.3	20400	7600	38	1.1	25	80	0.09	56300	0.5	700	46
97RD573	54.9	19200	9600	42	0.0011	35	80	0.23	46500	0.5	560	54
97RD574	55.4	18700	10300	57	1	22	89	0.14	47800	0.5	600	53
97RD578	57.4	34700	5300	69	1.7	25	150	0.12	47100	0.5	400	53
97RD580	59.3	46700	4100	51	1.4	17	140	0.14	51600	0.5	300	23
97RD582	58	29500	4000	41	1.2	17	100	0.16	42600	0.5	300	23
97RD584	59.35	41700	4700	85	0.002	17	210	0.19	48800	0.5	200	16
97RD585	59.5	27400	5500	37	0.7	25	85	0.13	54000	0.5	300	21
97RD587	60.6	23000	4700	32	1.1	13	86	0.06	33500	0.5	400	90
97RD590	62.4	26900	2600	52	0.0027	15	91	0.29	63700	0.5	200	47
97RD591	62.6	39200	380	25	3.5	5.8	70	0.39	80400	0.5	200	21
97RD593	63.3	25400	3700	42	1.3	24	97	0.06	24500	0.5	300	93
97RD62	13.4	48100	36	76	3.5	24	240	0.11	47300	0.5	200	20
97RD64	14.95	41900	240	70	3.1	22	260	0.21	39000	0.5	100	19
97RD80	29.6	36400	8000	74	2.2	46	170	0.59	41800	0.5	590	79
97RD90	39.65	28100	6400	55	1.6	33	130	0.11	54900	0.5	500	40
97RD93	44.7	29900	10100	57	1.8	37	140	0.07	49100	0.5	290	35
97RD98	50.25	20400	7700	53	1.2	41	97	0.16	45500	0.5	290	65

Sample Number	Average Depth (m)	Cr ug/g	Cu ug/g	Fe ug/g	IC ug/g	K ug/g	Mg ug/g	Mn ug/g	Mo ug/g	Na ug/g	Ni ug/g	OC ug/g
97RD561	45.6	13	210	14100	0.037	7100	5500	110	63	920	6800	0.09
97RD562	46.1	18	120	8700	0.077	7000	4900	83	63	750	3400	0.04
97RD563	46.7	9.1	93	10300	0.028	6500	1400	71	50	770	3800	0.06
97RD564	47.1	27	150	11100	0.068	15300	2700	120	91	960	9100	0.06
97RD568	51.6	30	260	16200	0.012	9700	2600	110	95	1100	6100	0.11
97RD572	53.3	20	230	9700	0.045	6800	4100	120	55	630	5300	0.05
97RD573	54.9	8.2	210	12600	0.044	5600	5300	130	63	640	6900	0.19
97RD574	55.4	20	210	12200	0.069	5100	4900	140	64	200	7400	0.07
97RD578	57.4	27	150	13600	0.033	10700	7000	210	65	370	3600	0.09
97RD580	59.3	24	92	10100	0.038	9800	9400	50	50	228	2800	0.1
97RD582	58	22	87	9600	0.049	7300	8200	100	56	380	2600	0.11
97RD584	59.35	21	27	10000	0.049	16400	4200	130	44	560	3600	0.14
97RD585	59.5	26	110	7000	0.033	8600	4300	83	59	270	3700	0.1
97RD587	60.6	17	210	9000	0.024	5200	7800	120	41	310	2500	0.04
97RD590	62.4	17	240	13300	0.11	4300	39600	230	140	230	1700	0.18
97RD591	62.6	31	87	11000	0.015	580	69800	210	99	40	280	0.37
97RD593	63.3	16	310	21000	0.019	7900	1700	240	24	220	2400	0.04
97RD62	13.4	35	340	14000	0.026	15800	11600	250	110	420	37	0.08
97RD64	14.95	30	180	11900	0.16	13000	9000	205	100	250	140	0.05
97RD80	29.6	33	210	26600	0.072	13100	4000	160	1200	1300	5400	0.52
97RD90	39.65	20	140	22400	0.032	9700	2300	120	43	480	4700	0.08
97RD93	44.7	12	75	14600	0.028	10400	2300	150	55	460	6900	0.04
97RD98	50.25	20	270	16700	0.028	6200	2500	160	58	500	5400	0.13

Sample Number	Average Depth (m)	Pb-210 ug/g	Pb ug/g	Po-210 ug/g	P ug/g	Ra-226 ug/g	S acid sol ug/g	Sb ug/g	Si ug/g	Sr ug/g	S ug/g
97RD561	45.6	0	550	0	200	0	114000	0.8	28.9	140	3.37
97RD562	46.1	0	390	0	200	48	75800	0.7	31.4	100	2.39
97RD563	46.7	0	550	0	150	0	66700	0.6	37.6	140	2.02
97RD564	47.1	0	700	0	250	74	117000	1.2	24.8	170	3.7
97RD568	51.6	0	580	0	220	90	90000	1.3	26.6	180	2.83
97RD572	53.3	0	390	0	180	63	122000	1.1	27.6	88	3.49
97RD573	54.9	0	600	0	170	0	94800	0.9	31.9	83	2.95
97RD574	55.4	0	560	0	210	76	101000	1.2	29.1	85	3
97RD578	57.4	0	440	0	210	66	90200	0.8	29.8	120	2.73
97RD580	59.3	0	470	0	200	74	84100	0.6	29.1	120	2.56
97RD582	58	0	390	0	190	60	85100	0.6	29.1	100	2.5
97RD584	59.35	0	280	0	250	0	104000	0.5	27.7	220	2.92
97RD585	59.5	0	290	0	170	48	117000	0.8	26.7	80	3.72
97RD587	60.6	0	370	0	180	37	72000	0.7	33.2	60	2.38
97RD590	62.4	0	1000	0	450	0	135000	0.4	29.5	52	4.35
97RD591	62.6	0	120	0	550	17	171000	0.2	17.8	27	5.59
97RD593	63.3	0	500	0	100	58	50800	0.8	33.6	55	1.85
97RD62	13.4	132	1700	72	230	138	107000	0.2	29.6	61	3.5
97RD64	14.95	0	1100	0	170	177	71200	0.2	27.9	78	2.34
97RD80	29.6	0	500	0	250	92	81400	1	29	190	2.74
97RD90	39.65	0	420	0	150	90	121000	0.8	26.1	100	4.03
97RD93	44.7	57	520	33	170	81	104000	1	29.6	150	3.3
97RD98	50.25	0	490	0	170	67	97800	0.9	29.9	99	3.21

Sample Number	Average Depth (m)	Th-230 ug/g	Ti 240	U 215	V 74	Zn 11	Zr 15
97RD561	45.6	0	93	0	220	48	0
97RD562	46.1	0	85	0	160	34	68
97RD563	46.7	0	72	0	210	25	0
97RD564	47.1	0	71	0	280	29	110
97RD568	51.6	0	73	0	350	35	110
97RD572	53.3	0	76	0	160	32	72
97RD573	54.9	0	120	0	160	30	0
97RD574	55.4	0	150	0	200	30	76
97RD578	57.4	0	110	0	250	28	100
97RD580	59.3	0	130	0	260	22	75
97RD582	58	0	83	0	200	15	61
97RD584	59.35	0	72	0	390	14	0
97RD585	59.5	0	87	0	160	14	52
97RD587	60.6	0	59	0	150	45	65
97RD590	62.4	0	110	0	140	50	0
97RD591	62.6	0	100	0	100	17	29
97RD593	63.3	0	84	0	190	49	110
97RD62	13.4	220	390	262	110	13	28
97RD64	14.95	0	130	296	150	11	39
97RD80	29.6	0	130	626	260	36	140
97RD90	39.65	0	110	303	210	30	95
97RD93	44.7	72	110	452	210	20	110
97RD98	50.25	0	78	329	160	37	93

APPENDIX D SUMMARY OF CHEMICAL ANALYSIS OF WATER SAMPLES

Analyte	Method	units	MDL	Borehole 97-R5 97RD0001	Borehole 97-R5 97RD0002	Borehole 97-R5 97RD0003	Borehole 97-R4 97RD106	Borehole 97-R4 97RD109	Borehole 97-R8 97RD173	Borehole 97-R8 97RD208	Borehole 97-R6 97RD244	Borehole 97-R6 97RD246	Borehole 97-R2 97RD276	Borehole 97-R2 97RD279
Aluminum	Al, ICP-AES	mg/l	0 005	0 23	0 42	0 18	0 053	0 005	0 006	0 014	0.19	0 038	0 005	0.035
Antimony	Sb, hydride gen	mg/l	0 001								0 006	0 02	0 005	0 005
Arsenic	As, ICP-AES	µg/l	0 002	2640	13000	20800	310	780	1500	1200	40000	220000	20000	90
Arsenic	Arsenic inorganic	µg/l	0 001											
Arsenic	Arsenic 3+	µg/l	0 001											
Arsenic	Arsenic monomethyl	µg/l	0 25											
Arsenic	Arsenic dimethyl	µg/l	0 25											
Arsenic	Arsenic 5+	µg/l	0 001											
Barium	Ba, ICP-AES	mg/l	0.001	0 03	0 034	0 023	0 086	0 1	0 21	0 21	0 065	0 045	0 048	0.042
Beryllium	Be, ICP-AES	mg/l	0 001				0 001	0 001	0 001	0 001	0 001	0 001	0 001	0 001
Boron	B, ICP-AES	mg/l	0.002	0 12	0 17	0 1	0 37	0 081	0 058	0 046	0 19	0 2	0 09	0 16
Cadmium	Cd, ICP-AES	mg/l	0 001	0 001	0 001	0 001	0 001	0 001	0 001	0 001	0 001	0 001	0 001	0 001
Calcium	Ca, ICP-SEQ	mg/l	0 1	573	677	655	550	520	520	350	730	730	480	580
Chloride	Cl, color	mg/l	1	545	355	224	115	14	19	83	648	85	211	125
Chromium	Cr, ICP-AES	mg/l	0 001	0 001	0 004	0 001	0 003	0 001	0 001	0 001	0 001	0 001	0 002	0 002
Cobalt	Co, ICP-AES	mg/l	0 001	0 001	0 001	0 001	0 001	0 001	0 001	0 001	0 001	0 001	0 001	0 001
Copper	Cu, ICP-AES	mg/l	0 001	0.012	0 024	0 007	0 005	0 001	0 003	0 006	0 004	0 001	0.001	0.013
Inorganic carbon	C, total inorganic	mg/l	1				6	7	8	6	24	51	19	15
Iron	Fe, ICP-AES	mg/l	0 001	0 09	0 005	0.001	0 002	0 001	0.001	0.001	0 001	0.001	0.007	0.012
Lead	Pb, ICP-AES	mg/l	0 002	0 005	0 004	0 016	0 002	0 002	0 002	0 002	0 002	0 002	0 002	0 005
Magnesium	Mg, ICP-SEQ	mg/l	0 1	40	38	39	4 5	11	3	0 32	5 7	14	18	170
Manganese	Mn, ICP-AES	mg/l	0 001	0 19	0 95	0 39	0 001	0 021	0 001	0 001	0 017	0 014	0 01	0.085
Molybdenum	Mo, ICP-AES	mg/l	0 001	22	37	22	3 5	0 56	3 3	3 4	31	6.4	4.5	1 1
Nickel	Ni, ICP-AES	mg/l	0 001	0 02	0 067	0 039	0 003	0 034	0 005	0 004	0 21	0 61	0 28	0.008
Organic carbon	C, total organic	mg/l	0 2				19	11	19	27	21	3 3	19	28
pH	pH		0	6 76	6 76	7 24	6 35	7 38	7 86	7 36	8 08	8 17	8 23	8 31
Phosphorus	P, ICP-AES	mg/l	0 05				0 05	0 05	0 05	0 05	0 1	0 05	0 1	0 19
Potassium	K, ICP-SEQ	mg/l	0 2	17	24	16	58	3 7	7 6	4 6	21	12	9.4	13
Radium-226	Ra 226, total	Bq/l	0 005	22	0 78	0 73	35	27	19	12	71	26	51	21
Silicon soluble	Si, ICP-AES(sol)	mg/l	0 01				1 1	2 9	5 5	5 4	11	17	4 6	8 4
Sodium	Na, ICP-SEQ	mg/l	0 1	563	366	251	110	20	27	90	390	87	180	330
Strontium	Sr, ICP-AES	mg/l	0 001				0 6	0 45	0.56	0 43	0.88	0.8	0.63	2.2
Sulfate	SO4, ICP-AES	mg/l	0 1	1810	1920	1750	1490	1320	1310	960	1420	1500	1520	2190
Titanium	Ti, unknown	mg/l	0 1				0 001	0 001	0 001	0 001	0 001	0 001	0 001	0 001
Uranium-Water	U, total	mg/l	0 5	685	576	2000	12	174	58	17	0 144	0 104		426
Vanadium	V, ICP-AES	mg/l	0 001	0 001	0 001	0 001	0 041	0 002	0 011	0 012	0 002	0 015	0 003	0 009
Zinc	Zn, ICP-AES	mg/l	0 005	0 008	0 015	0 009	0 005	0 008	0 012	0 018	0 006	0 005	0.01	0 022
Zirconium	Zr, Unknown	mg/l	0 005				0 001	0 001	0 001	0 001	0 003	0 001	0 001	0 001

Analyte	Method	units	MDL	Borehole 97-R2 97RD285	Borehole 97-R2 97RD325	Borehole 97-R2 97RD326	Borehole 97-R1 97RD378	Borehole 97-R1 97RD392	Borehole 97-R1 97RD400	Borehole 97-R1 97RD421	Borehole 97-R3 97RD461	Borehole 97-R3 97RD475	Borehole 97-R3 97RD483	Borehole 97-R3 97RD485	Borehole 97-R3 97RD497
Aluminum	Al, ICP-AES	mg/l	0.005	0.03	0.12	0.072	0.028	0.33	0.25	0.25	0.12	0.23	0.18	0.1	0.18
Antimony	Sb, hydride gen	mg/l	0.001	0.002	0.008	0.007	0.002	0.001	0.005		0.004	0.007	0.008	0.009	0.013
Arsenic	As, ICP-AES	µg/l	0.002	780	85000	85000	58	5000	37000	8000	9300	13000	75000	110000	150000
Arsenic	Arsenic inorganic	µg/l	0.001												
Arsenic	Arsenic 3+	µg/l	0.001												
Arsenic	Arsenic monomethyl	µg/l	0.25												
Arsenic	Arsenic dimethyl	µg/l	0.25												
Arsenic	Arsenic 5+	µg/l	0.001												
Barium	Ba, ICP-AES	mg/l	0.001	0.047	0.036	0.041	0.034	0.031	0.041	0.031	0.024	0.022	0.031	0.034	0.022
Beryllium	Be, ICP-AES	mg/l	0.001	0.001	0.001	0.001	0.001	0.001	0.001	0.001	0.001	0.001	0.001	0.001	0.001
Boron	B, ICP-AES	mg/l	0.002	0.085	0.15	0.12	0.096	0.047	0.23	0.046	0.074	0.13	0.11	0.067	0.057
Cadmium	Cd, ICP-AES	mg/l	0.001	0.001	0.001	0.001	0.001	0.001	0.001	0.001	0.001	0.001	0.001	0.001	0.001
Calcium	Ca, ICP-SEQ	mg/l	0.1	590	480	650	620	590	670	580	590	540	720	680	640
Chloride	Cl, color.	mg/l	1	30	122	63	64	500	443	472	166	216	594	560	500
Chromium	Cr, ICP-AES	mg/l	0.001	0.002	0.003	0.002	0.001	0.001	0.007	0.001	0.001	0.007	0.001	0.001	0.003
Cobalt	Co, ICP-AES	mg/l	0.001	0.001	0.001	0.001	0.002	0.001	0.008	0.001	0.001	0.001	0.001	0.001	0.001
Copper	Cu, ICP-AES	mg/l	0.001	0.004	0.013	0.01	0.006	0.023	0.043	0.017	0.01	0.029	0.011	0.007	0.022
Inorganic carbon	C, total inorganic	mg/l	1	8	34	33	9	7	13	9	8	11	16	27	31
Iron	Fe, ICP-AES	mg/l	0.001	0.007	0.009	0.001	0.003	0.001	0.002	0.001	0.001	0.001	0.001	0.001	0.001
Lead	Pb, ICP-AES	mg/l	0.002	0.002	0.002	0.002	0.002	0.002	0.002	0.002	0.002	0.002	0.002	0.002	0.002
Magnesium	Mg, ICP-SEQ	mg/l	0.1	3.5	18	17	48	0.47	9.2	0.72	1.8	1.7	8.5	5.9	10
Manganese	Mn, ICP-AES	mg/l	0.001	0.006	0.007	0.008	0.11	0.001	0.012	0.001	0.001	0.002	0.002	0.005	0.006
Molybdenum	Mo, ICP-AES	mg/l	0.001	2.5	20	10	2.2	33	20	28	13	18	24	21	20
Nickel	Ni, ICP-AES	mg/l	0.001	0.015	0.14	0.2	0.017	0.014	0.098	0.03	0.012	0.03	0.11	0.21	0.23
Organic carbon	C, total organic	mg/l	0.2	17	40	31	20	21	21	13	8	16	6.5	33	53
pH	pH		0	8.1	8.39	8.42	7.87	9.42	8.49	9.36	7.94	8.18	7.65	7.57	7.93
Phosphorus	P, ICP-AES	mg/l	0.05	0.05	0.07	0.05	0.05	0.05	0.14	0.25	0.08	0.14	0.1	0.15	0.07
Potassium	K, ICP-SEQ	mg/l	0.2	5.2	9.2	4.8	11	22	21	17	9.2	11	8.3	11	12
Radium-226	Ra 226, total	Bq/l	0.005	27	10	7.1	23	22	22	32	20	17	26	26	45
Silicon soluble	Si, ICP-AES(sol)	mg/l	0.01	4.1	7.4	6.7	2.7	3.3	4.7	13	7.6	5.4	4.7	9.8	5.6
Sodium	Na, ICP-SEQ	mg/l	0.1	47	180	100	110	610	260	550	220	440	320	430	460
Strontium	Sr, ICP-AES	mg/l	0.001	0.75	1	0.9	0.87	0.76	0.83	0.9	0.68	0.48	1	0.5	0.7
Sulfate	SO4, ICP-AES	mg/l	0.1	1400	1480	1540	1780	2010	1600	1990	1610	1680	1470	1670	1730
Titanium	Ti, unknown	mg/l	0.1	0.001	0.001	0.001	0.001	0.001	0.002	0.001	0.001	0.004	0.001	0.001	0.002
Uranium-Water	U, total	mg/l	0.5	192		1410									
Vanadium	V, ICP-AES	mg/l	0.001	0.004	0.025	0.066	0.001	0.048	0.031	0.068	0.026	0.057	0.009	0.01	0.004
Zinc	Zn, ICP-AES	mg/l	0.005	0.04	0.009	0.01	0.016	0.007	0.014	0.008	0.005	0.006	0.005	0.005	0.005
Zirconium	Zr, Unknown	mg/l	0.005	0.001	0.007	0.003	0.001	0.001	0.008	0.001	0.001	0.009	0.001	0.001	0.005

Analyte	Method	units	MDL	Borehole 97-R3 97RD547	Well 97-R1 RD1,RD2,RD3,RD4	Well 97-R1 RD8,RD9	Well 97-R2 RD14,RD15,RD16,RD17	Well 97-R2 RD21,RD23,RD24	Well 97-R2 RD26,RD27,RD28,RD29
Aluminum	Al, ICP-AES	mg/l	0 005	0 039	0 36	0 23	0 46	0 31	0.28
Antimony	Sb, hydride gen	mg/l	0 001	0 003					
Arsenic	As, ICP-AES	µg/l	0 002	3200	22400	20200	71000	60000	71000
Arsenic	Arsenic Inorganic	µg/l	0 001		18631	15819	55523		58695
Arsenic	Arsenic 3+	µg/l	0 001		131	123	611		512
Arsenic	Arsenic monomethyl	µg/l	0 25		250	250	250		250
Arsenic	Arsenic dimethyl	µg/l	0 25		250	250	250		250
Arsenic	Arenic 5+	µg/l	0 001		18500	15498	54912		58183
Barium	Ba, ICP-AES	mg/l	0 001	0 026	0 032	0 021	0 036	0 032	0 029
Beryllium	Be, ICP-AES	mg/l	*0 001*	*0 001*	*0 001*	*0 001*	*0 001*	0 001	*0 001*
Boron	B, ICP-AES	mg/l	0 002	0 09	0 11	0 054	0 08	0 082	0 079
Cadmium	Cd, ICP-AES	mg/l	0 001	0 001	0 001	0 001	0 001	0 001	0 001
Calcium	Ca, ICP-SEQ	mg/l	0.1	570	530	533	571	547	508
Chloride	Cl, color.	mg/l	1	482	626	545	702	610	625
Chromium	Cr, ICP-AES	mg/l	0 001	0 001	0 005	0 001	0 001	0 001	0 001
Cobalt	Co, ICP-AES	mg/l	0 001	0 001	0 001	0 001	0 001	0 001	0 001
Copper	Cu, ICP-AES	mg/l	0 001	0 001	0 031	0 012	0 033	0 022	0 019
Inorganic carbon	C, total inorganic	mg/l	1	10	15	12	22	19	20
Iron	Fe, ICP-AES	mg/l	0 001	0 001	0 19	0 21	0 48	0 001	0 004
Lead	Pb, ICP-AES	mg/l	*0 002*	*0 002*	*0 018*	*0 036*	*0 047*	*0 002*	*0 002*
Magnesium	Mg, ICP-SEQ	mg/l	0 1	0 28	14	14	18	19	15
Manganese	Mn, ICP-AES	mg/l	0 001	0 001	0 013	0 008	0 019	0 011	0 009
Molybdenum	Mo, ICP-AES	mg/l	0.001	14	47	45	43	37	35
Nickel	Ni, ICP-AES	mg/l	0 001	0 02	0 31	0 27	0 74	0 087	0.14
Organic carbon	C, total organic	mg/l	0 2	59	31	32	23	31	20
pH	pH		0	8 51	8 63	8 56	8 4	8.5	8.45
Phosphorus	P, ICP-AES	mg/l	0 05	0 05	0 09	0 07	0.08	0 07	0 05
Potassium	K, ICP-SEQ	mg/l	0 2	18	12	12	8 3	10	11
Radium-226	Ra 226, total	Bq/l	0 005		38	35	35	30	34
Silicon soluble	Si, ICP-AES(sol)	mg/l	0 01	5 8	3	2 8	4 6	4	3.8
Sodium	Na, ICP-SEQ	mg/l	0 1	550	763	625	639	553	756
Strontium	Sr, ICP-AES	mg/l	0 001	0 39	0 69	0 6	1 1	1	0 95
Sulfate	SO4, ICP-AES	mg/l	0 1	1840	1880	1800	1820	1630	1920
Titanium	Ti, unknown	mg/l	0.1	0 001	0 004	0 001	0 004	0 001	0.001
Uranium-Water	U, total	mg/l	0.5		46	82	270	224	201
Vanadium	V, ICP-AES	mg/l	0 001	0 005	0 001	0 001	0 001	0 001	0 001
Zinc	Zn, ICP-AES	mg/l	0 005	0.005	0 011	0 007	0 01	0 007	0 007
Zirconium	Zr, Unknown	mg/l	0 005	0.001	0.013	0.003	0.012	0.006	0.008

Analyte	Method	units	MDL	Well 97-R3 RD31,RD32,RD33	Well 97-R3 RD37,RD38,RD39,RD40	Well 97-R3 RD41,RD42,RD43,RD44	Well 97-R4 RD46,RD47,RD48	Well 97-R4 RD51,RD52,RD53,RD54
Aluminum	Al, ICP-AES	mg/l	0.005	0.32	0.2	0.22	0.27	0.21
Antimony	Sb, hydride gen	mg/l	0.001					
Arsenic	As, ICP-AES	µg/l	0.002	24000	16000	15000	13000	12000
Arsenic	Arsenic Inorganic	µg/l	0.001		12185	11736		13178
Arsenic	Arsenic 3+	µg/l	0.001		131	138		319
Arsenic	Arsenic monomethyl	µg/l	0.25		250	250		250
Arsenic	Arsenic dimethyl	µg/l	0.25		250	250		250
Arsenic	Arsenic 5+	µg/l	0.001		12054	11598		12857
Barium	Ba, ICP-AES	mg/l	0.001	0.027	0.023	0.02	0.034	0.026
Beryllium	Be, ICP-AES	mg/l	0.001	0.001	0.001	0.001	0.001	0.001
Boron	B, ICP-AES	mg/l	0.002	0.084	0.083	0.044	0.13	0.093
Cadmium	Cd, ICP-AES	mg/l	0.001	0.001	0.001	0.001	0.001	0.002
Calcium	Ca, ICP-SEQ	mg/l	0.1	526	546	525	567	564
Chloride	Cl, color.	mg/l	1	745	690	718	462	508
Chromium	Cr, ICP-AES	mg/l	0.001	0.001	0.001	0.001	0.001	0.014
Cobalt	Co, ICP-AES	mg/l	0.001	0.001	0.001	0.001	0.001	0.001
Copper	Cu, ICP-AES	mg/l	0.001	0.021	0.007	0.007	0.016	0.03
Inorganic carbon	C, total inorganic	mg/l	1	12	10	9	8	8
Iron	Fe, ICP-AES	mg/l	0.001	0.075	0.001	0.12	0.29	0.001
Lead	Pb, ICP-AES	mg/l	0.002	0.002	0.002	0.002	0.004	0.002
Magnesium	Mg, ICP-SEQ	mg/l	0.1	4.8	4.9	2.9	9.1	9.2
Manganese	Mn, ICP-AES	mg/l	0.001	0.009	0.007	0.005	0.015	0.007
Molybdenum	Mo, ICP-AES	mg/l	0.001	42	38	50	29	20
Nickel	Ni, ICP-AES	mg/l	0.001	0.1	0.028	0.13	0.21	0.035
Organic carbon	C, total organic	mg/l	0.2	23	21	22	18	19
pH	pH		0	8.89	8.79	9.37	9.11	9.3
Phosphorus	P, ICP-AES	mg/l	0.05	0.05	0.05	0.05	0.12	0.11
Potassium	K, ICP-SEQ	mg/l	0.2	6.8	6	6.4	7.1	5.9
Radium-226	Ra 226, total	Bq/l	0.005	32	27	26	20	21
Silicon soluble	Si, ICP-AES(sol)	mg/l	0.01	2.9	2.9	2.4	3.5	2.5
Sodium	Na, ICP-SEQ	mg/l	0.1	601	680	730	314	321
Strontium	Sr, ICP-AES	mg/l	0.001	1	0.93	0.92	0.77	0.51
Sulfate	SO4, ICP-AES	mg/l	0.1	1950	1750	1770	1420	1440
Titanium	Ti, unknown	mg/l	0.1	0.001	0.001	0.001	0.003	0.005
Uranium-Water	U, total	mg/l	0.5	113	87	98	123	126
Vanadium	V, ICP-AES	mg/l	0.001	0.001	0.001	0.001	0.004	0.013
Zinc	Zn, ICP-AES	mg/l	0.005	0.01	0.008	0.008	0.009	0.007
Zirconium	Zr, Unknown	mg/l	0.005	0.008	0.001	0.002	0.009	0.014

Analyte	Method	units	MDL	Well 97-R4 RD56,RD57,RD58,RD59	Well 97-R5 RD61,RD62,RD63	Well 97-R5 RD66,RD67,RD68	Well 97-R5 RD71,RD72,RD73,RD74
Aluminum	Al, ICP-AES	mg/l	0 005	0 14	0 37	0.36	0.053
Antimony	Sb, hydride gen	mg/l	0 001				
Arsenic	As, ICP-AES	µg/l	0 002	15000	11000	13000	9600
Arsenic	Arsenic Inorganic	µg/l	0 001	13710		9207	9766
Arsenic	Arsenic 3+	µg/l	0 001	350		99 5	92 4
Arsenic	Arsenic monomethyl	µg/l	0 25	544		1228	281
Arsenic	Arsenic dimethyl	µg/l	0 25	250		250	250
Arsenic	Arenic 5+	µg/l	0 001	13360		9108	9674
Barium	Ba, ICP-AES	mg/l	0 001	0 033	0 02	0 02	0 001
Beryllium	Be, ICP-AES	mg/l	0 001	0 001	0 001	0 001	0.001
Boron	B, ICP-AES	mg/l	0 002	0 14	0 17	0 18	0.042
Cadmium	Cd, ICP-AES	mg/l	0 001	0 001	0 001	0 001	0.001
Calcium	Ca, ICP-SEQ	mg/l	0 1	608	504	495	500
Chloride	Cl, color	mg/l	1	488	745	750	710
Chromium	Cr, ICP-AES	mg/l	0.001	0 001	0 001	0.001	0.001
Cobalt	Co, ICP-AES	mg/l	0.001	0.001	0.001	0.001	0.001
Copper	Cu, ICP-AES	mg/l	0 001	0 01	0 02	0 018	0 006
Inorganic carbon	C, total inorganic	mg/l	1	9	9	9	10
Iron	Fe, ICP-AES	mg/l	0 001	0 008	0 047	0.001	0.001
Lead	Pb, ICP-AES	mg/l	0 002	0 002	0 002	0 002	0.009
Magnesium	Mg, ICP-SEQ	mg/l	0 1	8 5	1 7	1 6	1.9
Manganese	Mn, ICP-AES	mg/l	0 001	0 005	0 006	0 004	0.001
Molybdenum	Mo, ICP-AES	mg/l	0 001	24	56	58	16
Nickel	Ni, ICP-AES	mg/l	0 001	0 038	0 061	0 03	0 011
Organic carbon	C, total organic	mg/l	0 2	19	30	27	36
pH	pH		0	9 15	9 7	9 67	9 25
Phosphorus	P, ICP-AES	mg/l	0.05	0 09	0 14	0 15	0 16
Potassium	K, ICP-SEQ	mg/l	0 2	5 7	12	11	11
Radium-228	Ra 226, total	Bq/l	0 005	20	17	18	19
Silicon soluble	Si, ICP-AES(sol)	mg/l	0 01	2 7	3 8	4	1.7
Sodium	Na, ICP-SEQ	mg/l	0.1	343	927	864	854
Strontium	Sr, ICP-AES	mg/l	0.001	0 62	0.77	0 78	0 14
Sulfate	SO4, ICP-AES	mg/l	0.1	1500	2250	2010	2010
Titanium	Ti, unknown	mg/l	0.1	0.001	0.001	0.001	0.001
Uranium-Water	U, total	mg/l	0.5	131	21	26	33
Vanadium	V, ICP-AES	mg/l	0.001	0.001	0.029	0.031	0.007
Zinc	Zn, ICP-AES	mg/l	0.005	0.005	0.011	0.011	0.005
Zirconium	Zr, Unknown	mg/l	0 005	0.005	0 012	0 009	0.002

APPENDIX E SUMMARY OF CHEMICAL ANALYSIS OF REGIONAL GROUNDWATER

SRC ANALYTICAL

Cameco Corporation

Date Samples Received: 22-May-98 Client P.O.:

SAMPLE	CLIENT DESCRIPTION
10633	STN8.6.1 20-05-98 RD36,37,35,39 *WATER*

ANALYTE	UNITS	10633
INORGANICS		
P. alkalinity	mg/L	<1
Carbonate	mg/L	<1
Calcium	mg/L	37±2
Chloride	mg/L	3±1
Bicarbonate	mg/L	200±4
Potassium	mg/L	3.0±0.2
Magnesium	mg/L	18±0.9
Sodium	mg/L	7.3±0.4
Hydroxide	mg/L	<1
Sulfate	mg/L	8.1±0.4
Total alkalinity	mg/L	164±3
Total hardness	mg/L	166±3
Inorganic carbon	mg/L	39±2
Organic carbon	mg/L	1.8±0.2
Ammonia as nitrogen	mg/L	0.10±0.01
Nitrate	mg/L	<0.04
Boron	mg/L	0.043±0.02
Phosphorus	mg/L	<0.05
Silver	mg/L	<0.001
Aluminum	mg/L	<0.005
Arsenic	ug/L	<0.5
Barium	mg/L	0.016±0.004
Beryllium	mg/L	<0.001
Cadmium	mg/L	<0.001
Cobalt	mg/L	<0.001
Chromium	mg/L	<0.001
Copper	mg/L	<0.001
Iron	mg/L	0.13±0.01
Manganese	mg/L	0.039±0.01
Molybdenum	mg/L	<0.001
Nickel	mg/L	<0.001
Lead	mg/L	<0.002
Silicon, soluble	mg/L	4.4±0.2
Strontium	mg/L	0.30±0.02
Titanium	mg/L	<0.001
Vanadium	mg/L	<0.001
Zinc	mg/L	<0.005
Zirconium	mg/L	<0.001

SRC ANALYTICAL

Cameco Corporation

Date Samples Received: 22-May-98 Client P.O.:

ANALYTE	UNITS	10633
Total dissolved solids	mg/L	192±4
pH	pH units	7.90±0.05
RADIONUCLIDES		
Lead-210	Bq/L	0.04±0.03
Radium-226	Bq/L	0.13±0.04
Thorium-230	Bq/L	0.04±0.01
Uranium	ug/L	20±2

"<": not detected at level stated above.
cc Robert Donahue.

SRC ANALYTICAL

Cameco Corporation

Date Samples Received: 22-May-98 Client P.O.:

SAMPLE	CLIENT DESCRIPTION	
10632	STN8.6.2 20-05-98 RD29,30,31,32	*WATER*

ANALYTE	UNITS	10632
INORGANICS		
P. alkalinity	mg/L	<1
Carbonate	mg/L	<1
Calcium	mg/L	13±0.6
Chloride	mg/L	5.2±0.3
Bicarbonate	mg/L	142±3
Potassium	mg/L	4.5±0.2
Magnesium	mg/L	10±0.5
Sodium	mg/L	30±2
Hydroxide	mg/L	<1
Sulfate	mg/L	11±0.6
Total alkalinity	mg/L	116±2
Total hardness	mg/L	74±1
Inorganic carbon	mg/L	28±1
Organic carbon	mg/L	8.0±0.4
Ammonia as nitrogen	mg/L	0.23±0.01
Nitrate	mg/L	<0.04
Boron	mg/L	0.21±0.05
Phosphorus	mg/L	<0.05
Silver	mg/L	<0.001
Aluminum	mg/L	0.014±0.005
Arsenic	ug/L	2.5±0.5
Barium	mg/L	0.018±0.004
Beryllium	mg/L	<0.001
Cadmium	mg/L	<0.001
Cobalt	mg/L	<0.001
Chromium	mg/L	<0.001
Copper	mg/L	<0.001
Iron	mg/L	0.037±0.009
Manganese	mg/L	0.039±0.01
Molybdenum	mg/L	0.034±0.008
Nickel	mg/L	<0.001
Lead	mg/L	<0.002
Silicon, soluble	mg/L	4.6±0.2
Strontium	mg/L	0.24±0.01
Titanium	mg/L	<0.001
Vanadium	mg/L	<0.001
Zinc	mg/L	<0.005
Zirconium	mg/L	<0.001

SRC ANALYTICAL

Cameco Corporation

Date Samples Received: 22-May-98 Client P.O.:

ANALYTE	UNITS	10632
Total dissolved solids	mg/L	164±3
pH	pH units	8.12±0.05
RADIONUCLIDES		
Lead-210	Bq/L	<0.03
Radium-226	Bq/L	0.09±0.03
Thorium-230	Bq/L	<0.01
Uranium	ug/L	25±2

"<": not detected at level stated above.
cc Robert Donahue.

SRC ANALYTICAL

Cameco Corporation

Date Samples Received: 22-May-98 Client P.O.:

SAMPLE	CLIENT DESCRIPTION	
10631	STN8.6.3 19-05-98 RD22,23,24,25	*WATER*

ANALYTE	UNITS	10631
INORGANICS		
P. alkalinity	mg/L	7±1
Carbonate	mg/L	8±1
Calcium	mg/L	8.5±0.4
Chloride	mg/L	44±2
Bicarbonate	mg/L	121±2
Potassium	mg/L	5.4±0.3
Magnesium	mg/L	3.7±0.2
Sodium	mg/L	71±4
Hydroxide	mg/L	<1
Sulfate	mg/L	24±1
Total alkalinity	mg/L	113±2
Total hardness	mg/L	36±1
Inorganic carbon	mg/L	26±1
Organic carbon	mg/L	1.5±0.2
Ammonia as nitrogen	mg/L	0.31±0.02
Nitrate	mg/L	<0.04
Boron	mg/L	0.34±0.08
Phosphorus	mg/L	<0.05
Silver	mg/L	<0.001
Aluminum	mg/L	0.014±0.005
Arsenic	ug/L	<0.5
Barium	mg/L	0.012±0.003
Beryllium	mg/L	<0.001
Cadmium	mg/L	<0.001
Cobalt	mg/L	<0.001
Chromium	mg/L	<0.001
Copper	mg/L	<0.001
Iron	mg/L	0.022±0.006
Manganese	mg/L	0.013±0.003
Molybdenum	mg/L	0.008±0.004
Nickel	mg/L	<0.001
Lead	mg/L	<0.002
Silicon, soluble	mg/L	2.6±0.1
Strontium	mg/L	0.16±0.02
Titanium	mg/L	<0.001
Vanadium	mg/L	<0.001
Zinc	mg/L	<0.005
Zirconium	mg/L	<0.001

SRC ANALYTICAL

Cameco Corporation

Date Samples Received: 22-May-98 Client P.O.:

ANALYTE	UNITS	10631
Total dissolved solids	mg/L	234±5
pH	pH units	8.61±0.05
RADIONUCLIDES		
Lead-210	Bq/L	0.03±0.03
Radium-226	Bq/L	<0.007
Thorium-230	Bq/L	0.08±0.03
Uranium	ug/L	<0.5

"<": not detected at level stated above.
cc Robert Donahue.